Engineered Fc Gamma Receptor Ligands for Affinity Separation of Monoclonal Antibody Glycovariants

Thesis presented for the degree of Doctor of Philosophy

Elizabeth Jessica Edwards

Department of Biochemical Engineering

University College London

September 2023

I, Elizabeth Edwards, confirm that the work presented in this thesis is my own. Where information has been derived from other sources, I confirm that this has been indicated in the thesis.

Abstract

Monoclonal antibodies (mAbs) are one of the greatest revenue generators in the pharmaceutical sector. Therapeutic mAbs are primarily of the IgG1 subclass and carry two *N*-linked glycans in their fragment crystallisable (Fc) region. The presence or absence of a core fucose on these *N*-glycans has a huge impact on antibody-dependent cellular cytotoxicity (ADCC), a common effector function for IgG1 mAbs. This is due to afucosylated IgG1 having a stronger affinity for the Fc gamma receptor 3a (FcγRIIIa), the immune cell receptor which mediates ADCC. This results in upregulated ADCC activity of afucosylated compared to fucosylated IgG1. Since this discovery, FcγRIIIa has been developed as a chromatographic affinity ligand for the separation of fucosylated and afucosylated IgG1.

This thesis presents novel affinity ligands based on the FcγRIIIa for the separation of fucosylated and afucosylated IgG1, termed FcγR ligands. These engineered ligands comprise only the binding domain of FcγRIIIa and a single glycosylation site. This results in the FcγR ligands being smaller and less complex than FcγRIIIa, with the aim of improving the ligand density and commercial viability of a column with these ligands compared to FcγRIIIa. The results presented show that the FcγR ligands have the expected primary structure and a similar *N*-glycosylation pattern to what was designed. The K_D obtained for the FcγRIIIa-IgG1 interaction was 1.4μM, whilst the K_D values for the FcγR ligand-IgG1 interactions were ~100-fold lower at 20-60nM. The FcγR ligands show an opposite differential affinity for fucosylated and afucosylated IgG1 compared to FcγRIIIa, with a K_D for the FcγRIIIa-low-fucose IgG1 interaction of 0.34μM and no observable interaction between the FcγR ligands and low-fucose IgG1. This gives a larger differential affinity of the FcγR ligands for these two glycovariants compared to FcγRIIIa. Suggestions are made for future FcγRIIIa-based ligands, along with future research needed to further understand the FcγRIIIa differential affinity for fucosylated and afucosylated IgG1.

Impact Statement

This thesis is focused on the development of chromatographic FcγRIIIa-based affinity ligands for the separation of fucosylated and afucosylated IgG1 mAbs. FcγRIIIa is a receptor present on immune cells that mediates the antibody effector function ADCC. IgG1 which does not possess a core fucose on the Fc *N*-glycan, afucosylated IgG1, has a higher affinity for FcγRIIIa than fucosylated IgG1, resulting in upregulated ADCC activity of afucosylated compared to fucosylated IgG1.

Regulators therefore require manufacturers to characterise and monitor fucosylation levels throughout the development of new mAbs or mAb biosimilars. Fucose does not have an associated charge and is too small to create an observable band shift on an electrophoretic gel, making gel-based techniques unviable options for detecting fucosylation. Mass spectrometry is an effective strategy; however, it is often time-consuming and expensive.

A chromatographic column immobilised with FcγRIIIa has proven to be an effective separation method for fucosylated and afucosylated glycoforms, allowing approximate quantification of fucosylated species in an antibody sample using a relatively fast separation. However, the capacity of the FcγRIIIa column is very low at approximately 2mg/mL afucosylated IgG (Application Notes: Glycap-3A™ Version 1.2, Zepteon™), and its production costs are high due to the need for a mammalian expression system for FcγRIIIa production. The FcγRIIIa itself is also a large and complex molecule, introducing significant potential for heterogeneity in these ligands.

The FcγR ligands used in this work were based on the FcγRIIIa but engineered to be smaller, less complex and cheaper to produce. Various protein analysis techniques have confirmed that the FcγR ligands have the desired primary structure and a lower molecular weight than FcγRIIIa, as well as a glycomic profile similar to what was intended. The yeast expression system used to produce the FcγR ligands was cheaper and took less time than a mammalian system would have for the production of FcγRIIIa.

Our results show that the FcγR ligands separate fucosylated and afucosylated IgG1, with the differential affinity of the ligands for these glycoforms being switched around compared to FcγRIIIa. In fact, the affinity of the FcγR ligands for fucosylated IgG1 has increased compared to FcγRIIIa's affinity for the same IgG1 species, and there is seemingly now no interaction of

the FcγR ligands with afucosylated IgG1. This could mean a more effective separation using the FcγR ligands compared to FcγRIIIa due to the more distinct difference in affinity.

The FcγR ligands would have very similar commercial applications to the FcγRIIIa-immobilised column, namely in mAb or biosimilar development when demonstrating lot-to-lot variability and characterising fucosylation levels. If the production of the FcγR ligands were to be scaled up, they could be used as a polishing step in afucosylated mAb manufacturing. Academically, this work has also raised questions about our current understanding of the FcγRIIIa structure and its impact on the differential affinity for fucosylated and afucosylated IgG1, which has created opportunity for further research in this area. A deeper understanding of this topic could lead to improved FcγRIIIa-based affinity ligands, or even improved mAbs and mAb-based therapeutics.

UCL Research Paper Declaration Form

referencing the doctoral candidate's own published work(s)

Please use this form to declare if parts of your thesis are already available in another format, e.g. if data, text, or figures:

- *have been uploaded to a preprint server*
- *are in submission to a peer-reviewed publication*
- *have been published in a peer-reviewed publication, e.g. journal, textbook.*

This form should be completed as many times as necessary. For instance, if you have seven thesis chapters, two of which containing material that has already been published, you would complete this form twice.

1. **For a research manuscript that has already been published** (if not yet published, please skip to section 2)

   a) **What is the title of the manuscript?**

   Strategies to control therapeutic antibody glycosylation during bioprocessing: synthesis and separation

   b) **Please include a link to or doi for the work**

   https://onlinelibrary.wiley.com/doi/10.1002/bit.28066

   c) **Where was the work published?**

   Biotechnology and Bioengineering

   d) **Who published the work?** (e.g. OUP)

   Wiley

   e) **When was the work published?**

   19th February 2022

   f) **List the manuscript's authors in the order they appear on the publication**

   Elizabeth Edwards, Maria Livanos, Anja Krueger, Anne Dell, Stuart M. Haslam, C. Mark Smales, Daniel G. Bracewell

   g) **Was the work peer reviewed?**

   Yes

   h) **Have you retained the copyright?**

   Open access as per funder requirements

   i) **Was an earlier form of the manuscript uploaded to a preprint server?** (e.g. medRxiv). If 'Yes', please give a link or doi)

   No

   If 'No', please seek permission from the relevant publisher and check the box next to the below statement:

   ☒

*I acknowledge permission of the publisher named under **1d** to include in this thesis portions of the publication named as included in **1c**.*

2. **For a research manuscript prepared for publication but that has not yet been published** (if already published, please skip to section 3)
   a) **What is the current title of the manuscript?**

   Engineered Fc gamma receptor ligands for affinity separation of monoclonal antibody glycovariants

   b) **Has the manuscript been uploaded to a preprint server?** (e.g. medRxiv; if 'Yes', please give a link or doi)

   No

   c) **Where is the work intended to be published?** (e.g. journal names)

   Biotechnology and Bioengineering, Biotechnology Progress or MAbs

   d) **List the manuscript's authors in the intended authorship order**

   Elizabeth Edwards, Anja Krueger, Maria Livanos, Stuart Haslam, Daniel Bracewell (corresponding author)

   e) **Stage of publication** (e.g. in submission)

   Drafting

3. **For multi-authored work, please give a statement of contribution covering all authors** (if single-author, please skip to section 4)

   Daniel Bracewell and Maria Livanos conceived the original idea. Elizabeth Edwards and Anja Krueger planned and conducted the experiments and wrote the paper. Daniel Bracewell and Stuart Haslam supervised the project.

4. **In which chapter(s) of your thesis can this material be found?**

   Chapters 5 and 6

5. **e-Signatures confirming that the information above is accurate** (this form should be co-signed by the supervisor/ senior author unless this is not appropriate, e.g. if the paper was a single-author work)

   Candidate
   E. Edwards
   Date:
   04/09/23

   Supervisor/ Senior Author (where appropriate)
   D. G. Bracewell
   Date
   08/09/23

Acknowledgements

Firstly, I would like to thank Dan for his support, guidance and expertise throughout this project. Dan has always struck the right balance between allowing me to formulate my own ideas and still keeping me on track. He has been immensely helpful throughout my time at UCL.

I would also like to thank Maria, Lourdes, Mike and Steve, who have all helped me tremendously. Maria's knowledge and guidance helped me considerably, particularly at the very start of my PhD, and Lourdes has rescued many of my fermentations and shake flask cultures, never failing to provide sound reasoning for why something may have happened. If my incessant pestering of Steve with yet more results or another possible explanation ever got on his nerves, he never showed it.

The encouragement of my peers has been a huge help. In particular I would like to thank Annabel, Georgia, Jordan, Matt, Hannah, Gyorgy, Julian, Ciara, Delphine, Ferdi and the rest of the third-floor office for making me laugh every day and providing welcome relief from the stresses of experiments. In addition, the Bioseparations group has provided much-needed support, both technical and otherwise, over the course of my time in the department.

Finally, I would like to thank my Mum and Dad for always having such unwavering faith in me, and both Pablo and my sister for the countless pep talks, without which I would not have reached this stage. Louis has provided endless reassurance and proof-reading expertise, for which I am very grateful. This thesis would not have been possible if it weren't for you all.

Engineered Fc Gamma Receptor Ligands for Affinity Separation of Monoclonal Antibody Glycovariants

List of Figures

List of Tables

Abbreviations and Notation

3D	Three-dimensional
A_{260}	Absorbance at 260nm
A_{280}	Absorbance at 280nm
AAL	Aleuria Aurantia Lectin
AC	Affinity chromatography
ADC	Antibody-drug conjugate
AMBIC	Ammonium biocarbonate
AOX1	Alcohol oxidase 1
αMF	α-mating factor
BCN	Bicyclo[6.1.0]nonyne
BleoR	Bleomycin resistance gene
BLI	Biolayer interferometry
BMGY	Buffered complex glycerol medium
BMMY	Buffered complex methanol medium
BSM	Basal salts medium
CCR4	Chemokine C receptor 4
CDC	Complement-dependent cytotoxicity
C_H	Constant heavy
CHO	Chinese hamster ovary
CIP	Cleaning in-place
CLL	Chronic lymphocytic leukaemia
CM5	Carboxymethylated 5
CNBr	Cyanogen bromide
COG	Cost of goods
ConA	Concanavalin A
CQA	Critical quality attribute
CV	Column volumes
DBC	Dynamic binding capacity
DCW	Dry cell weight
D_I	Impeller diameter
DMSO	Dimethylsulfoxide
DNA	Deoxyribonucleic acid
DO	Dissolved oxygen
DoE	Design of experiments

DSP	Downstream processing
D_T	Tank diameter
DTT	Dithiothreitol
ECD	Extracellular domain
EDC/NHS	1-ethyl-3-(dimethylaminopropyl)carbodiimide/*N*-hydroxysuccinimide
ELISA	Enzyme-linked immunosorbent assay
EMA	European Medicines Agency
Endo-CC	Endo-β-*N*-acetylglucosaminidase from *Coprinopsis cinerea*
Endo D	Endo-β-*N*-acetylglucosaminidase D
Endo H	Endo-β-*N*-acetylglucosaminidase H
Endo Hf	Endoglycosidase and mannose binding protein, *E. coli* expressed
Endo M	Endo-β-*N*-acetylglucosaminidase M
Endo S	Endo-β-*N*-acetylglucosaminidase S
ER	Endoplasmic reticulum
ESI-LC-MS	Electrospray ionisation-liquid chromatography-mass spectrometry
EU	European Union
Fab	Fragment antigen binding
Fast DDA	Fast data-dependent acquisition
Fc	Fragment crystallisable
Fc 1	Flow channel 1
Fc 2	Flow channel 2
FcγR	Fc gamma receptor
FcγRIIIa	Fc gamma receptor 3a
FcRn	Neonatal Fc receptor
FDA	Food and Drug Administration
FT	Flow-through
GMII	Golgi α-mannosidase II
GMD	GDP-mannose 4,6-dehydratase
GnTI	β1,2-*N*-acetylglucosaminyltransferase I
GnTIII	β1,4-*N*-acetylglucosaminyltransferase III
HCPs	Host cell proteins
HEK-293	Human embryonic kidney 293
HER2	Human epidermal growth factor receptor 2
HER2 ECD	Human epidermal growth factor receptor 2 extracellular domain
HRP	Horseradish peroxidase
HRP-SA	Horseradish peroxidase-streptavidin

H_T	Tank height
IAA	Iodoacetic acid
ICH	International Council for Harmonisation
IDT	Integrated DNA Technologies
IgA	Immunoglobulin A
IgD	Immunoglobulin D
IgE	Immunoglobulin E
IgG	Immunoglobulin G
IgM	Immunoglobulin M
IL-6	Interleukin-6
IMAC	Immobilised metal ion affinity chromatography
ITAM	Immunoreceptor tyrosine-based activation motif
IVIg	Intravenous immunoglobulin
K_A	Association constant
K_D	Dissociation constant
LAC	Lectin affinity chromatography
mAb	Monoclonal antibody
MAC	Membrane attack complex
MALDI-TOF	Matrix-assisted laser desorption/ionisation-time-of-flight
MALDI-TOF/TOF	Matrix-assisted laser desorption/ionisation-time-of-flight/time-of-flight
ManNAc	N-acetyl-mannosamine
MES	2-(N-morpholino)ethanesulfonic acid
MHC	Major histocompatibility complex
$MnCl_2$	Manganese chloride
MOE	Molecular Operating Environment
MS	Mass spectrometry
MS/MS	Tandem mass spectrometry
Mut^+	Methanol utilisation plus
Mut^S	Methanol utilisation slow
MWCO	Molecular weight cut-off
m/z	Mass-to-charge
NHS	N-hydroxysuccinimide
Ni-NTA	Nickel-nitrilotriacetic acid
OD_{280}	Optical density at 280nm
OD_{600}	Optical density at 600nm
ORF	Open reading frame
pAb	Polyclonal antibody

PDB	Protein Data Bank
PBS	Phosphate-buffered saline
PBS-P+	Phosphate-buffered saline with added detergent
PEG	Polyethylene glycol
pH	Potential of hydrogen
pI	Isoelectric point
PI	Point of induction
pKa	Acid dissociation constant
PNGase F	Peptide-N4-(*N*-acetyl-beta-glucosaminyl)asparagine amidase F
PPG	Polypropylene glycol
PTM1	*Pichia* trace metal 1
R_{max}	Analyte binding capacity of the surface
RMD	GDP-6-deoxy-D-lyxo-4-hexulose reductase
RO	Reverse osmosis
RU	Resonance units
SA	Streptavidin
SDS-PAGE	Sodium dodecyl sulfate-polyacrylamide gel electrophoresis
SE	Standard error
s.f	Significant figures
sFcγRIIIa	Soluble Fc gamma receptor 3a
SGP	Sialylglycopeptide
SIP	Sterilisation in-place
SNP	Single nucleotide polymorphism
SPA	Staphylococcal Protein A
SPAAC	Strain-promoted azide-alkyne cycloaddition
SPR	Surface plasmon resonance
Tris-HCl	Tris-hydrochloride
UCL	University College London
UK	United Kingdom
US	United States
USD	United States Dollar
UV	Ultraviolet
V_H	Variable heavy
V_L	Variable light
(v/v)	Volume per volume
WCW	Wet cell weight
WT	Wild-type

(w/v)	Weight per volume
YPD	Yeast extract-peptone-dextrose
YNB	Yeast nitrogen base

Amino Acid Abbreviations

Alanine	Ala	A
Arginine	Arg	R
Asparagine	Asn	N
Aspartic acid	Asp	D
Cysteine	Cys	C
Glutamic acid	Glu	E
Glutamine	Gln	Q
Glycine	Gly	G
Histidine	His	H
Isoleucine	Ile	I
Leucine	Leu	L
Lysine	Lys	K
Methionine	Met	M
Phenylalanine	Phe	F
Proline	Pro	P
Serine	Ser	S
Threonine	Thr	T
Tryptophan	Trp	W
Tyrosine	Tyr	Y
Valine	Val	V

Monosaccharide Abbreviations and Symbols

Table 1.1 – names, abbreviations and symbols for the monosaccharides commonly referred to in this work. These abbreviations and symbols are derived from the Symbol Nomenclature for Glycans, which is described as "a community-curated standard for the depiction of monosaccharides and glycans using various colour-coded, geometric shapes, along with defined text additions" (Neelamegham et al., 2019).

Name	Abbreviation	Symbol
Fucose	Fuc	▲
Galactose	Gal	●
Mannose	Man	●
N-acetylglucosamine	GlcNAc	■
N-acetylneuraminic acid/sialic acid	Neu5Ac	◆

Units

A	Amperes
Å	Angstroms
AU	Absorbance units
cm	Centimetres
CV	Column volumes
Da	Daltons
°C	Degrees Celsius
fmol	Femtomole
g	Grams
g/L	Grams per litre
g/mol	Grams per mole
kDa	Kilodaltons
L	Litres
μF	Microfarads
μg	Micrograms
μg/mL	Micrograms per millilitre
μL	Microlitres
μm	Micrometres
μM	Micromolar
mL	Millilitres
M	Molar
mL/hr	Millilitres per hour
mL/L	Millilitres per litre
mm	Millimetres
mM	Millimolar
ng	Nanograms
nm	Nanometres
nM	Nanomolar
Ω	Ohms
psi	Pounds per square inch
%	Percent
M^{-1}	Per mole
$M^{-1}\ cm^{-1}$	Per mole per centimetre
rcf	Relative centrifugal force

rpm	Revolutions per minute
RU	Response units
s	Seconds
×g	Times gravity
V	Volts
vvm	Volume of gas sparged per unit volume of culture per minute

List of Publications

Review article

Edwards, E., Livanos, M., Krueger, A., Dell, A., Haslam, Stuart M., Smales, C. Mark., Bracewell, Daniel G. (2022) Strategies to control therapeutic antibody glycosylation during bioprocessing: Synthesis and separation. Biotechnology and Bioengineering. [Online] Available from: doi:10.1002/bit.28066.

Planned original research article

Engineered Fc gamma receptor ligands for affinity separation of monoclonal antibody glycovariants. Estimated journals: Biotechnology and Bioengineering, Biotechnology Progress or mAbs. (Relates to Chapter 6).

Conference presentation (oral)

Development of affinity ligands for antibody glycovariant separations based on the Fc gamma receptor. ACS Spring 2022. San Diego, CA, USA. (Relates to Chapter 6).

Patent application

GB2204016.6: affinity chromatography ligands for antibody glycovariant separation.

Chapter 1 – Introduction

1.1 Monoclonal Antibodies

In this section, some general background and details about monoclonal antibodies (mAbs) are provided, including their structure, effector functions and glycosylation.

1.1.1 Monoclonal Antibodies Background

Antibodies play an integral role in the human adaptive immune system (Alberts et al., 2002). Antibodies were first discovered in the 1890s by Emil von Behring and Shibasabura Kitasato, who showed that the transfer of serum from animals that had been immunised against diptheria could prove curative for other animals suffering from the disease (von Behring & Kitasato, 1890). This was the first published demonstration of what is now known as passive immunity and showed the potential that this type of treatment could have in humans. In 1901, Behring was awarded the Nobel Prize for Medicine or Physiology as a result of this discovery.

The therapeutic potential of manufactured antibodies was not harnessed until much later. In 1959, both Gerald Edelman and Rodney Porter independently determined the antibody chemical structure (Edelman, 1959; Porter, 1959) for which they shared the Nobel Prize in Physiology and Medicine in 1972. Shortly after, the first atomic resolution structure of an antibody was published (Inbar, Hochman & Givol, 1972), which was swiftly followed by the introduction of mAbs by Georges Köhler and César Milstein (Köhler & Milstein, 1975). This marked a new age of antibody-based therapeutics, with the first mAb, muromonab-CD3, commercially known as Orthoclone OKT3®, being approved by the United States (US) Food and Drug Administration (FDA) in 1983 (Lu et al., 2020). Forty years on, there are 150 antibody-based therapeutics that have either been approved or are pending approval in the European Union (EU) or the US (Reichert, 2023). As of 2023, the mAbs market is expected to be worth $237.61 billion USD (GrandViewResearch.com, 2021).

mAbs are produced by identical B cells from a single parent clone. Firstly, an animal (usually a mouse) is injected with the antigen against which the mAb to be produced will act. The animal will mount an immune response against the antigen, at which point the spleen of the animal is removed and the B cells are isolated. These are fused with immortalised B cell cancer cells, a myeloma, to create a hybrid cell line called a hybridoma. This cell line possesses the antibody-producing capabilities of the B cell and the proliferative properties of the myeloma cells, meaning these cells can grow continuously in culture while producing the antibody of choice. While mAbs bind the same epitope on a particular antigen, polyclonal

antibodies (pAbs) bind multiple epitopes, meaning they are more likely to cross-react with other targets. pAbs are also produced at different times in different animals, which gives rise to batch-to-batch variability. For these reasons, it was the advent of mAbs and the hybridoma technology used to produce them that allowed these molecules to be used as therapeutics (Zaroff & Tan, 2019).

1.1.2 General Antibody Structure

An antibody or immunoglobulin (Ig) has a general structure (see Figure 1.1). Ig is a macromolecule with a molecular weight of approximately 150kDa and consists of four polypeptide chains, two heavy (50kDa each) and two light (25kDa each), which are arranged into a Y shape. There are two main functional parts to an Ig molecule; the fragment antigen binding (Fab) and fragment crystallisable (Fc) regions. The Fab region binds the target antigen and is made up of variable and constant regions. The variable regions determine the binding specificity of the antibody for a particular antigen. The Fc region is attached to the Fab via a hinge region, a flexible polypeptide linker, and interchain disulfide bonds which link each chain of the Fc region to each other. The Fc region is known as the constant region and is responsible for engaging immune cells, such as phagocytes and natural killer cells (Janeway Jr. et al., 2001). The cross-linking of the antigen and the immune cells by the antibody results in removal of the antigen by the body's immune system (see Section 1.1.3).
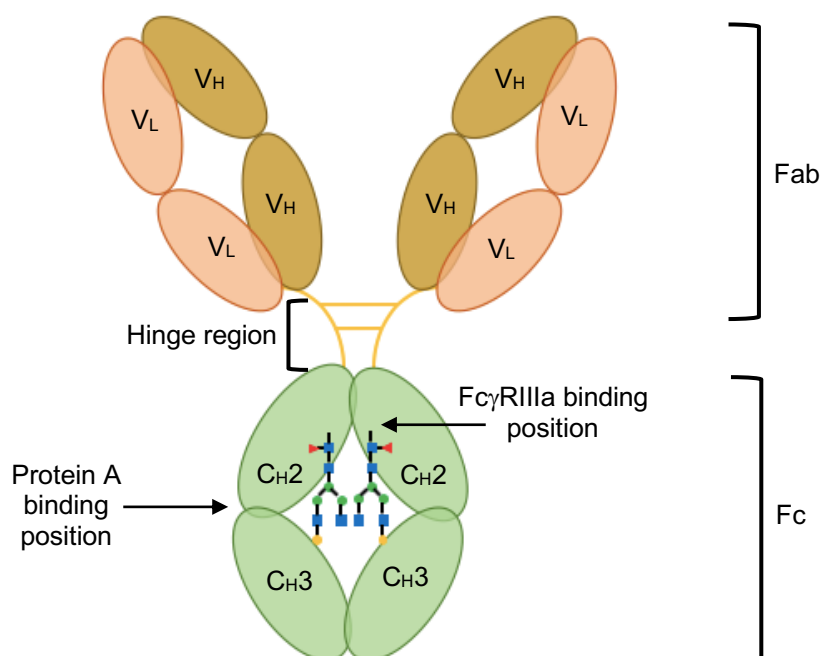
Figure 1.1 – general immunoglobulin structure. The Fab region, which is the region of the molecule that binds the target antigen, consists of variable heavy (V_H) and variable light (V_L) chains. The Fab is joined to the Fc by the hinge region. The Fc region is made up of four constant heavy (C_H) regions, with

each C_H2 and C_H3 chain connected to each other by disulfide bridges. One *N*-glycan is attached to each C_H2 chain. The FcγRIIIa and Protein A binding positions are labelled.

There are five different classes of antibodies; IgA, IgD, IgE, IgG and IgM. Within the IgA and IgG classes, there exists subclasses. Each class and subclass of antibody possess different properties, including mechanisms of action, half-life and distribution (see Table 1.2).

Table 1.2 – classes, subclasses and properties of immunoglobulins. Text in bold refers to properties of the antibody class as a whole, i.e. IgA total serum distribution is 15% (Liu et al., 2019; Schroeder & Cavacini, 2010).

Class	Subclass	Molecular Weight (kDa)	Structure	Half-life (days)	Distribution in Serum (%)	Complement Fixation	Opsonisation	Fc Receptor Engagement
IgA	IgA1	160	**Monomer, dimer**	**6**	**15**	**–**	**–**	**FcαR**
	IgA2	160						
IgD	N/A	184	Monomer	3	<0.5	–	–	FcδR
IgE	N/A	188	Monomer	2	<0.01	–	–	FcεR I,II
IgG			**Monomer**		**75**	**+**	**+++**	**FcγR**
	IgG1	146		21	67% of IgG	Yes	Yes	I,II,III
	IgG2	146		20	22% of IgG	Yes	Yes	II
	IgG3	170		7	7% of IgG	Yes	Yes	I,II,III
	IgG4	146		21	4% of IgG	No	No	I,II
IgM	N/A	970	Pentamer	10	10	+++	+	FcμR

The most abundant mAb isotype in human serum is IgG1. This mAb is present in the form of a monomer, i.e. each molecule is composed of one Ig molecule (see Figure 1.1). As well as being the most common, IgG1 is also the most well-characterised and understood out of all mAb isotypes. IgG1 engages all Fc gamma receptor (FcγR) subforms and acts by way of complement-dependent cytotoxicity (CDC) and antibody-dependent cellular cytotoxicity (ADCC) to eliminate target antigens and particles (see Section 1.1.3). For these reasons, IgG1 has always been an obvious choice for therapeutic antibody development and continues to be the dominant isotype for mAb therapeutics. IgG1 is also a practical choice for therapeutic antibody development due to its relatively high thermostability, its monomeric structure and the fact that it only has two disulfide bonds, meaning fewer issues with aberrant protein folding and aggregation than other isotypes, such as the pentameric IgM (Thomson, 2016). The activity profile of IgG1 was well-suited to the initial targets of antibody development; out of the first 14 chimeric, human or humanised antibodies or Fc-fusion proteins, 13 of them had an IgG1 Fc (Strohl & Strohl, 2012).

1.1.3 Mechanisms of Action

When the immune system is threatened by an infectious agent such as a bacterium, fungus or virus, both the innate and adaptive immune responses are stimulated. Although the innate immune response is the first line of defence against potential pathogens, the adaptive immune response is able to mount a more specific and long-lasting attack on an infective agent. Within adaptive immunity, there exists humoral and cellular immunity. Humoral immunity is mediated by antibodies and targets circulating, extracellular antigens, whereas cellular immunity is mediated by T cells which bind antigens presented on cell surfaces via the major histocompatibility complex (MHC) (Alberts et al., 2002). As the focus of this project is not T cell-mediated immunity, only the role of B cells in antibody production will be outlined here.

B cells possess over 10^5 different cell surface receptors which each bind different antigens. When one of these receptors on a naïve or memory B cell recognises an antigen, the cell is activated with the aid of a helper T cell. The activated B cell will then divide and differentiate into an antibody-producing effector cell called a plasma cell, secreting antibodies which have the same binding site as the B cell-surface receptor that initially bound the antigen, ensuring specificity for the target. These target-specific antibodies go on to act by way of their effector functions to clear the infection. These effector functions include blocking ligand-receptor interactions, opsonisation and phagocytosis, CDC and ADCC (Alberts et al., 2002). It is by way of these mechanisms that manufactured mAbs also exert their therapeutic activity. The blocking of ligand-receptor interactions is a fairly self-explanatory mechanism; antibodies will either compete directly with the antigen for the receptor, create steric hindrance or interfere with the conformation of the receptor in such a way that an antigen cannot bind the receptor (List et al., 1999). The other effector functions will be explained in more detail in this section.

1.1.3.1 Opsonisation and Phagocytosis

The process of phagocytosis can be divided into four steps: 1) antigen or target recognition, 2) stimulation of the internalisation pathway, 3) phagosome creation and 4) phagolysosome maturation. Antigen recognition either occurs through direct binding of the antigen with receptors on the surface of a phagocyte, or indirectly through opsonins. Opsonins are soluble molecules that bind antigen, coating them and tagging them for phagocytosis. IgG antibodies are opsonins which bind antigen via their Fab regions, leaving the Fc region available for binding FcγRs on the surface of phagocytes such as natural killer (NK) cells. The binding of the Fc region of IgG bound to an antigen with one of the FcγRs induces phagocytosis, and the cross-linked antigen is internalised by the phagocyte. Upon engagement of an FcγR, phagocytosis is stimulated using immunoreceptor tyrosine-based activation motif (ITAM)-

mediated signalling. This pathway culminates in actin polymerisation and the reorganisation of the phospholipid membrane, enabling the cell to extend the membrane around the antigen and form a phagosome which internalises the antigen. An endosome then fuses with the phagosome to form a phagolysosome, releasing lytic enzymes which degrade the antigen (Rosales & Uribe-Querol, 2017). Antibodies play a crucial role in opsonisation by tagging foreign particles and potential pathogens for phagocytosis.

1.1.3.2 Complement-Dependent Cytotoxicity

IgG and IgM antibodies can exert their therapeutic activity by way of CDC. When these antibody classes bind antigen on a target cell, such as a bacterial cell, the classical complement pathway is initiated. This occurs when the protein C1q along with the serine proteases C1r and C1s together form the C1 complex, which binds the Fc region of IgG or IgM antibodies and cross-links the target antigen with the C1 complex via the antibody. This cross-linking elicits a biochemical cascade which culminates in the tagging of the bound antigen as foreign, which leads to opsonisation, additional complement activation and eventual formation of the membrane attack complex (MAC) (Dunkelberger & Song, 2010). The MAC is made up of complement proteins which form pores in the membrane of the pathogenic target cell, leading to lysis of the target cell (Xie, Jane-Wit & Pober, 2020). A huge number of IgG1 therapeutic mAbs use CDC as an effector function, in particular anti-CD20 mAbs such as rituximab (Marshall, Stopforth & Cragg, 2017).

1.1.3.3 Antibody-Dependent Cellular Cytotoxicity

ADCC is an effector function that involves the cross-linking of a target antigen with an immune cell via an activating FcγR (FcγRI, FcγRIIa/c and FcγRIIIa) on the surface of the immune cell membrane (Li et al., 2009). Antibody subclasses IgA, IgE and IgG are capable of mediating ADCC, although it is usually IgG antibodies which are involved in ADCC due to their high prevalence in human serum (Zahavi et al., 2018). The first step in ADCC involves the binding of the target antigen to the antibody via the antibody Fab region, and the concomitant binding of the antibody's Fc region to an activating FcγR on the surface of an NK cell. This stimulates the phosphorylation of the ITAM of the activating FcγR bound to the antibody, which is present on the intracellular region of the FcγR chain associated with the activating FcγR. This phosphorylation, mediated by src kinases within the NK cell, elicits biochemical cellular cascades within the NK cell which result in the release of perforin and granzyme by the cell, causing apoptosis of the target cell (Gómez Román, Murray & Weiner, 2014). ADCC is an important effector function for many IgG1-based therapeutic antibodies, including trastuzumab (Petricevic et al., 2013) and cetuximab (Seo et al., 2014).

1.1.4 Monoclonal Antibody Fc Glycosylation and Impacts on Effector Functions

Much of the work in this section is taken from Edwards et al., 2022.

IgG antibodies are mainly biantennary *N*-glycosylated in their Fc region at a single site (Asn297) on each C_H2 domain (see Figure 1.1). The overall diversity of *N*-glycosylation lies primarily in the antennae of the glycan and in the presence or absence of a fucose residue on the core of the *N*-glycan. Glycosylation in the Fc region affects IgG affinity for FcγRs, which mediate effector functions such as ADCC, phagocytosis and cytokine secretion (Junker, Gordon & Qureshi, 2020).

Out of all known post-translational modifications, glycosylation has one of the most significant impacts on therapeutic antibody pharmacokinetics (Boune et al., 2020). Glycosylation is known to have effects on the biological activity, solubility, serum half-life and safety of therapeutic antibodies (Bas et al., 2019; Narhi et al., 1991; Varki, 1993). Glycans have an important role in immunity and self-recognition during common immune events, and ultimately can impact the therapeutic efficacy of biopharmaceuticals (Gagneux & Varki, 1999; van Kooyk & Rabinovich, 2008). Therefore, controlling glycosylation in antibody biotherapeutics is of critical importance. As glycosylation is diverse and challenging to control during bioprocessing, most FDA- or European Medicines Agency (EMA)-approved IgG-type biotherapeutics contain *N*-glycosylation in the Fc region only. As glycosylation heterogeneity substantially impacts mAb immunogenicity and therapeutic efficacy, the control and characterisation of mAb glycosylation profiles is specified in International Council for Harmonisation (ICH) guideline Q6B (EMA, 1999). The EMA also state that "particular attention should be paid to the degree of sialylation, galactosylation, mannosylation and fucosylation" (Carillo et al., 2020; Edwards et al., 2022). The impact that each of these glycans have on IgG effector functions is detailed in the following sections.

1.1.4.1 Sialylation

IgG serum half-life is primarily governed by its interaction with the neonatal Fc receptor (FcRn). The FcRn is expressed on endothelial cells and other immune cells such as dendritic cells and macrophages. The FcRn acts as a salvage pathway for IgG in the bloodstream. When IgG binds the FcRn, the IgG-receptor complex is endocytosed into the cell and then recycled back to the cell surface where the IgG is released back into the serum at neutral pH. IgG with increased affinity for the FcRn have a longer serum half-life as they more readily enter this salvage pathway. It has been found that sialylation of the *N*-glycan in the IgG Fc region

enhances the IgG's affinity for the FcRn, resulting in increased serum half-life of sialylated and hypersialylated IgG compared to nonsialylated IgG (Bas et al., 2019).

Intravenous immunoglobulin (IVIg) is the treatment of choice for patients with immunodeficiencies and inflammatory diseases such as Kawasaki disease, dermatomyositis and lupus. It is prepared from pools of plasma-derived IgG, which are harvested from tens of thousands of donors in order to capture a diverse antibody repertoire (Jolles, Sewell & Misbah, 2005). Despite IVIg being a standard treatment for several different diseases, and these preparations having been used for over 30 years, their precise mechanism of action is yet to be elucidated. However, it has been concluded that the presence of terminal sialic acid residues on the Fc *N*-glycan of IgG is crucial to the clinical efficacy of IVIg in the context of many different disease models (Anthony et al., 2008; Anthony & Ravetch, 2010; Brückner, Lehmann, Dudziak, & Nimmerjahn, 2017; Schwab et al., 2014). Amongst other observations, desialylation of the Fc fragment reduces the anti-inflammatory activity of IVIg. Conversely, the enrichment of these preparations with sialic acid results in improved *in vivo* efficacy in a mouse model of rheumatoid arthritis (Käsermann et al., 2012) (Edwards et al., 2022).

1.1.4.2 Galactosylation

Galactosylation of the IgG Fc *N*-glycan has an impact on CDC activity. One study found that CD-20 targeting IgG1 and IgG3 antibodies with terminal *N*-glycan galactosylation showed increased binding to C1q, the protein involved in forming the C1 complex in the classical complement pathway, resulting in enhanced complement-mediated tumour cell lysis. This effect was not seen for IgG2 and IgG4 (Peschke et al., 2017). It is also thought that terminal galactosylation of the IgG Fc *N*-glycan has an effect on ADCC activity, but that this effect relies on the glycan not containing a core fucose. One particular study found that terminal galactose only enhances ADCC activity on afucosylated IgG1, but when the fucose is present there is minimal effect of terminal galactosylation on ADCC activity (Zhang et al., 2020).

1.1.4.3 Mannosylation

IgG that possess high-mannose structures at the *N*-glycan site in the Fc region have been shown to have improved ADCC activity due to an increased affinity for the FcγRIIIa, but a reduced CDC activity due to a decreased affinity for C1q (Zhou et al., 2008). It is not known, however, whether the increased affinity of high-mannose IgG for the FcγRIIIa is just due to the fact that these glycans do not possess core fucose, which is the predominant factor that confers increased FcγRIIIa binding (Boune et al., 2020). This could also be the case for the effect of terminal galactosylation on ADCC activity described above. High-mannose structures

in the Fc region of IgG are also associated with a reduced serum half-life compared to other glycosylation structures in this region (Goetze et al., 2011; Yu et al., 2012).

1.1.4.4 Fucosylation

The glycan pattern which yields the greatest impact on ADCC effector function is core fucosylation in the IgG Fc. The removal of a core fucose residue from the *N*-glycan attached to the conserved Asn297 of the Fc region of IgG is known to increase the affinity of IgG for the FcγRIIIa, resulting in enhancement of ADCC activity *in vivo* by up to 40-fold (Shields et al., 2002; Shinkawa et al., 2003). This discovery stimulated research focused around generating cell lines yielding afucosylated mAbs, as well as investigations into upstream control strategies to direct mAb glycosylation towards particular glycan profiles. As a result, afucosylated mAbs are now licensed as therapeutics in their own right, with examples of such mAbs currently on the market or in clinical trials including obinutuzumab, mogamulizumab, MEDI-551, DI-B4, ublituximab, imgatuzumab and tomuzotuximab (Zahavi et al., 2018).

Rituximab is a CD20-targeting mAb that was first approved by the FDA for the treatment of relapsed or refractory non-Hodgkin's lymphoma. It is now a standard treatment for the majority of B cell neoplasms either in combination with chemotherapy or as a standalone therapy. Although it has shown good clinical efficacy, evidence that some tumours develop resistance to rituximab has been reported. In an attempt to mitigate this, obinutuzumab was developed. Amongst other modifications, obinutuzumab has reduced core fucosylation and therefore increased ADCC activity compared to rituximab. In the context of chronic lymphocytic leukaemia (CLL), obinutuzumab demonstrates strong clinical advantages over rituximab and enhanced progression-free survival of patients receiving obinutuzumab therapy compared to rituximab (Freeman & Sehn, 2018). Another afucosylated mAb that targets CD20 is ublituximab, which has recently been granted Fast Track Designation by the FDA for the treatment of CLL in combination with umbralisib.

Efforts towards the production of afucosylated IgG have mainly focused on cell line engineering for a number of reasons. Fucosidases aimed at hydrolysing the core fucose are usually not successful due to steric hindrance. It is also not possible to use size-, charge- or hydrophobicity-based separation methods to separated fucosylated and afucosylated mAbs due to the fucose having a very low molecular weight and no associated charge. Finally, the use of lectin affinity chromatography is not feasible for the isolation of afucosylated mAbs due to specificity issues and potential lectin-induced toxicity (Edwards et al., 2022).

1.2 Affinity Chromatography and Protein A Development

In this section, some background on affinity chromatography (AC) and Protein A development is provided.

1.2.1 Affinity Chromatography Background

The concept of AC was first laid out in a paper published in 1968 (Cuatrecasas, Wilchek & Anfinsen, 1968). These three scientists purified three enzymes using non-competitive enzyme inhibitors immobilised to cyanogen bromide (CNBr)-activated Sepharose® beads. This paved the way for AC's use as a commonplace protein separation and purification technique. In 1971, Pharmacia Fine Chemicals introduced the CNBr-activated Sepharose® 4B resin to the market. The success of this resin led to the development of other ligands for protein purification during the 1970s, one of the first of which was concanavalin A (ConA) immobilised onto Sepharose® beads. This was used for the separation of glucose- and mannose-containing glycoproteins (Lloyd, 1970).

AC is known for achieving high purity levels without generating the need for a large number of processing steps, meaning that a high yield and a relatively low processing time can be achieved. AC has been in use as a purification step in large-scale manufacturing processes for over 40 years and is now used as the primary capture step in the vast majority of biopharmaceutical manufacturing processes (Łacki & Riske, 2019). An AC primary capture step is very common in the downstream processing (DSP) chain of a mAb bioprocess due to its high selectivity and therefore ability to achieve high yields and purity levels (Hober, Nord & Linhult, 2007). By far the most successful development in the field of AC to date has been Protein A chromatography, which has evolved to become the gold-standard for mAb purification within the bioprocessing industry (Janson & Jönsson, 2011).

1.2.2 Protein A Development

Staphylococcal Protein A (SPA) is a protein exposed on the outer surface of the cell wall of *Staphylococcus aureus*, a Gram-positive bacterium. SPA consists of three regions; S is the signal sequence that contains the localisation signal for the protein, the XM region anchors the protein to the cell wall, and the IgG binding region consists of five homologous binding domains E, D, A, B and C (see Figure 1.2) (Hober, Nord & Linhult, 2007).
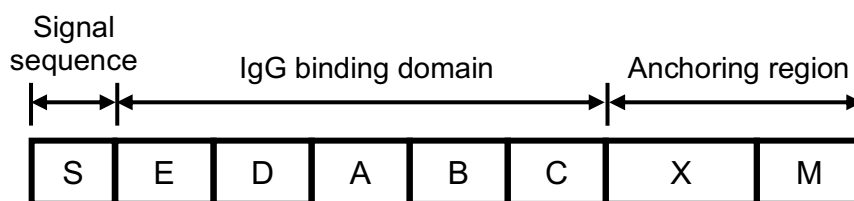
Figure 1.2 – Staphylococcal protein A (SPA) structure. S contains the signal sequence, the IgG binding domain is made up of homologous binding domains E, D, A, B and C, and the anchoring region is made up of domains X and M which anchor the protein to the *S. aureus* cell wall. Adapted from Figure 1 of Hober, S., Nord, K. & Linhult, M. (2007) Protein A chromatography for antibody purification. *Journal of Chromatography B*.

The ability of SPA to bind human antibodies was first discovered in the 1950s (Jensen, 1958). This binding was then further characterised to be between SPA and the Fc region of IgG1, IgG2 and IgG4 (Forsgren & Sjöquist, 1966), with the association constant (K_A) of this binding being approximately 10^8 M^{-1} (Hober, Nord & Linhult, 2007). Shortly after this discovery, interest quickly mounted surrounding the potential use of SPA as an affinity ligand for mAb purification. In 1972, the first paper reporting the immobilisation of SPA on a Sepharose® column and its ability to purify IgG was published (Hjelm, Hjelm & Sjöquist, 1972). In 1975, Pharmacia Fine Chemicals introduced the first Protein A resin to the market, and it quickly became their best-selling product (Janson & Jönsson, 2011). Since then, the ligand structure was improved and refined so that the resin became more practical for large-scale bioprocessing.

Since 1978, the productivity, capacity and overall practicality of Protein A resins have improved almost year on year. Reflecting their nearly-exclusive usage as mAb purification technologies, Protein A resin sales growth has closely mirrored that of mAb therapeutics (Bolton & Mehta, 2016). It could even be argued that the huge success of mAbs as therapeutics could be partly due to the concurrent development of Protein A chromatography, meaning that effective and economically practical purification of mAbs was achievable and the manufacturing processes were robust and highly optimised (Łacki & Riske, 2019). As Protein A chromatography has proven it can perform well in large-scale DSP chains, it has now become the benchmark for mAb purification techniques, particularly as a primary capture step. The concerns with SPA that were associated with the earlier technology, including lack of pH stability during product elution and cleaning and the high resin cost, have been improved upon significantly over the years (Ramos de la Peña, González-Valdez & Aguilar, 2019).

Due to the early SPA ligands being unstable at extreme pH conditions, which are the conditions used for elution and cleaning in-place (CIP), Protein A resins previously had much shorter lifetimes compared to other resins, for example ion exchange resins. Considerable efforts were therefore made to develop Protein A resins with extended lifetimes by employing a protein engineering strategy.

In the B domain of SPA (see Figure 1.2), there is an Asn-Gly dipeptide. These dipeptide sequences are notoriously prone to deamidation (Meinwald, Stimson & Scheraga, 1986), so this site was mutated by site-directed mutagenesis to Asn-Ala to improve the chemical stability of the ligand. This mutation was successful in enhancing SPA's resistance to chemical cleavage yet still maintained the affinity of the SPA for IgG Fc. The engineered form of the B domain is referred to as the Z domain. Novel binding specificities of the Z domain have been achieved through the use of a combinatorial protein engineering approach (Hober, Nord & Linhult, 2007). Additionally, in the late 1990s it was found that by modifying the loop region between helices two and three of the Z domain, variants of Z have been generated which allow for milder elution conditions of IgG. This loop region is not involved in binding IgG but has a role in the stability of the protein. By reducing the stability of the Z region through the modification of this loop region, the Z-IgG interaction can be broken at a higher pH due to SPA having a reduced stability and therefore changing its tertiary structure at milder pH conditions. This development meant that IgG could be eluted from Protein A columns at a pH of 4.5 rather than the previously used 3.3, which is a condition that some mAbs cannot withstand (Gulich, Uhlen & Hober, 2000). In addition to the primary structure manipulations of SPA and in order to make the large-scale manufacture of these ligands feasible, recombinant *Escherichia coli* or *S. aureus* strains began to be used for the production of the SPA affinity ligands instead of native *S. aureus* to mitigate containment issues. Ligand coupling through a C-terminal cysteine instead of through free amines on lysine residues was also carried out. This reduced ligand leaching and improved IgG accessibility, meaning that Protein A resins could achieve a higher binding capacity (Łacki & Riske, 2019).

Whilst Protein A chromatography is undoubtedly now the gold standard for mAb primary capture in the DSP chain, Protein A resins are not able to distinguish between different IgG Fc glycosylation patterns which may be more or less clinically efficacious, or even immunogenic in some cases. Efforts to control mAb glycosylation have primarily been focused on upstream rather than downstream processing, as will be discussed in the following section.

1.3 Strategies to Control Monoclonal Antibody Glycosylation

Attempts to control and direct biologic glycosylation towards certain profiles have primarily focused on cell line engineering and bioprocess control, including process parameter alterations such as pH shifts and the addition of supplements to cell culture media during mAb production. The work in this section is taken from Edwards et al., 2022.

1.3.1 Cell Line Engineering Strategies

Various developments in cell line engineering for mAb manufacturing have aimed to reduce the core fucosylation of the *N*-glycan at Asn297 in the Fc region of IgG, as this is known to confer the most significant increase in ADCC activity of IgG mAbs compared to galactosylation, mannosylation, sialylation and *N*-acetyl-glucosamine (GlcNAc) levels. The Potelligent® technology was first developed by Kyowa Hakko Kogyo Co. Ltd. in 2004 to address this issue. After the discovery was made that reduced core fucosylation of IgG mAbs results in enhanced ADCC *in vivo*, the group at Kyowa Hakko Kogyo focused on generating a mammalian cell line that was capable of yielding IgG with reduced core fucosylation to enhance its therapeutic efficacy. The group generated a Chinese hamster ovary (CHO) cell line which had the gene encoding the fucosyltransferase (α1,6-FucT) responsible for adding the fucose to the core GlcNAc, *FUT8*, knocked out. This was achieved by disrupting both *FUT8* alleles using sequential homologous recombination (Yamane-Ohnuki et al., 2004). These *FUT8*$^{-/-}$ cells produce IgG which does not possess core fucose and therefore elicits a greater level of ADCC compared to fucosylated mAbs. An example of a current therapy manufactured using the Potelligent® CHO *FUT8*$^{-/-}$ cell line is mogamulizumab, commercially known as Poteligeo®. This mAb was originally approved for the treatment of chemokine C receptor 4 (CCR4)-expressing T cell leukaemia-lymphoma and peripheral T cell lymphoma (Evans & Syed, 2014). The EMA now list Poteligeo® as a treatment for mycosis fungoides and Sézary syndrome.

Another technique which has been used to yield afucosylated IgG mAbs is interference with the synthetic pathway that gives rise to the fucose precursor or substrate for α1,6-FucT, GDP-fucose. One such approach has been to disrupt the gene that encodes the enzyme GDP-mannose 4,6-dehydratase (GMD). GMD is involved in catalysing the conversion of D-glucose to GDP-fucose and is therefore crucial for the activity of α1,6-FucT in carrying out fucosylation downstream in this pathway. CHO cells deficient for GMD reportedly completely lack GDP-fucose, and when not provided with sources of L-fucose in the growth media these cells yield 100% afucosylated IgG (Kanda et al., 2007).

Genetic engineering approaches to achieve afucosylation have been developed which yield glycans with bisecting GlcNAc. GlcNAc bisection creates steric hindrance for α1,6-FucT, thereby preventing core fucosylation on resulting glycan structures. This has been achieved using different approaches, one of which has been to engineer cells to overexpress the enzyme β1,4-*N*-acetylglucosaminyltransferase III (GnTIII), which adds a bisecting GlcNAc residue onto the βMan of the *N*-glycan core structure (Hossler, Khattak & Li, 2009). This technology, commercially known as GlycoMAb®, was developed by Glycart (Evans & Syed, 2014). GlycoMAb® technology has since been optimised so that the localisation motif of the Golgi α-mannosidase II (GMII) is incorporated into the expressed GnTIII. This results in the GnTIII enzyme out-competing α1,6-FucT more effectively (Ferrara et al., 2006), possibly due to the fact that the addition of the localisation motif means that the GnTIII is more likely to act earlier in the glycosylation pathway when core fucosylation has not yet occurred, therefore preventing fucosylation more successfully. This particular platform is used to produce obinutuzumab (Yu, Marshall, Cragg, & Crispin, 2017).

Alternatively, reduction in the level of core fucosylation can be achieved by engineering CHO cells to heterologously express the enzyme GDP-6-deoxy-D-lyxo-4-hexulose reductase (RMD). As described above, this mechanism also affects the GDP-fucose synthesis pathway, but this time indirectly. RMD is responsible for the production of GDP-D-rhamnose, which negatively inhibits the GMD enzyme. By inhibiting GMD, the production of GDP-fucose is downregulated and the pool of substrate for the α1,6-FucT enzyme is depleted. This approach has shown remarkable success, yielding 98% afucosylated IgG (von Horsten et al., 2010). The platform was developed by ProBioGen™ and is commercially known as GlymaxX® technology, which was licensed to Bayer in 2019. Bayer stated that they would "leverage the technology to further increase the potency of an undisclosed antibody candidate for oncological indications" (BioSpace, 2019).

The humanisation of the yeast *N*-glycosylation pathway was a significant breakthrough in cell line engineering. A review of early efforts in this space is provided by Wildt & Gerngross, which covers the first attempts to engineer *Saccharomyces cerevisiae* in the 1990s and some of the studies carried out in the early 2000s (Wildt & Gerngross, 2005). In 2003, Choi et. al reported engineering of the *Pichia pastoris* glycosylation pathway so that it could perform some early human *N*-glycan processing steps. Firstly, the gene encoding α1,6-mannosyltransferase, the initiating enzyme in the *P. pastoris* glycosylation pathway, was deleted. Several combinatorial genetic libraries were then constructed using fungal type II membrane proteins and the catalytic domains of enzymes from mammals, insects, amphibians, worms and fungi with the aim of generating α1,2-mannosidase and human β1,2-*N*-acetylglucosaminyltransferase I

(GnTI) (Choi et al., 2003). Further investigation has revealed more enzymes within the yeast glycosylation pathway that must be targeted and deleted in order to reduce hypermannosylation, as well as how best to localise active forms of enzymes downstream in this pathway required for converting the $Man_8GlcNAc_2$ to $Man_5GlcNAc_2$, then to $GlcNAcMan_5GlcNAc_2$ and so on. A review of these efforts is provided by Laukens, Visscher, & Callewaert (2015). Another recent study used CRISPR/Cas9 to humanise the yeast *Kluyveromyces marxianus* (Lee et al., 2020). The success of these efforts suggests that some IgG biotherapeutics could eventually be produced using yeast expression systems.

The degree and type of sialylation of mAbs can also be altered by engineering the host expression system. In one study in CHO cells, the enzyme which attaches sialic acid in an $\alpha2,6$ linkage was overexpressed to increase the amount of $\alpha2,6$ sialylation, and CRISPR/Cas9 was used to disrupt the genes encoding the enzymes responsible for $\alpha2,3$ sialylation, thus reducing levels of $\alpha2,3$ sialylation. This is favourable as $\alpha2,6$ sialylation in the Fc region of IgG has been reported to increase ADCC activity compared to $\alpha2,3$ sialylation (Chung et al., 2017).

Despite the success of cell line engineering strategies for altering the glycosylation of IgGs, development has been arduous and expensive. There are often significant regulatory hurdles that must be overcome when gaining approval for the use of a new cell line for biologics manufacturing, such as demonstrating the required product quality. Combining this with the fact that not all genetic engineering strategies have yielded overwhelming levels of success, research efforts have also focused on fermentation process parameter alterations, media supplementation and enzymatic glycoengineering (Edwards et al., 2022).

1.3.2 Upstream Processing Conditions

Manipulating fermentation process conditions is arguably a cheaper and possibly less time-consuming approach to controlling mAb glycosylation than cell line engineering and can be applied during a bioprocess to tune glycan patterns. A number of groups have experimented with pH changes in particular; low pH has commonly been found to enhance galactosylation and sialylation, but concomitantly decreases specific productivity (Aghamohseni et al., 2014). Galactosylation is generally associated with an increase in CDC activity, whilst sialylation is known to result in increased serum half-life and ADCC (St. Amand et al., 2014). In a study investigating the effect of temperature shifts on glycosylation macroheterogeneity, a reduction in culture temperature from 37ºC to 33ºC increased glycosylation site occupancy of recombinant human tissue plasminogen activator by up to 4%, and an increase in culture pH resulted in a decrease in site occupancy (Gawlitzek et al., 2009). Temperature reductions in fermentation have had differing effects on glycan structures depending on the system that is

being experimented with; in some cases, more processed glycan structures are generated, and in other cases less so (Villiger et al., 2016).

1.3.3 Media Supplementation

Media supplementation approaches have shown great utility in yielding different glycoforms. This approach can be useful for directing glycosylation towards certain profiles, for example increasing sialylation through the addition of *N*-acetyl-mannosamine (ManNAc) (Yin et al., 2017) or manganese, galactose and uridine (Villacrés, Tayi & Butler, 2021) to the culture medium. As with cell line engineering, many media supplementation approaches have focused on reducing IgG Fc core fucosylation due to this having the most significant impact on ADCC activity out of all known oligosaccharide variations. A common addition to cell culture media when attempting to yield afucosylated IgG is kifunensine, an inhibitor of α1,2-mannosidase I. This enzyme is responsible for trimming the *N*-glycan to a form that can be subsequently fucosylated. Other additions to cell culture media which have been investigated for preventing fucosylation are 2-deoxy-2-fluorofucose and 5-alkynylfucose, which are both inhibitors of the fucosyltransferase α1,6-FucT. Whilst addition of these inhibitors to cell culture media have been shown to reduce IgG Fc core fucosylation, results from one study showed that there was significant incorporation of these analogues into the resulting IgG glycans, and 2-deoxy-d-fluorofucose in particular is known to be toxic. The group stated that they had not investigated the effect of incorporation of these analogues into mAb glycans on the mAb's potency and safety (Zimmermann et al., 2019).

Other media supplementation approaches have been studied with the aim of targeting biologic glycosylation more generally, including degrees of mannosylation, galactosylation GlcNAcylation and sialylation. The addition of manganese chloride (MnCl$_2$) can direct glycosylation towards more highly mannosylated and galactosylated structures, which is likely to enhance mAb ADCC activity. MnCl$_2$, uridine and galactose supplementation has been shown to increase galactosylation levels, as does the addition of glutamate (but not glutamine) to cell cultures (St. Amand et al., 2014). The effect of differing levels of ammonia has been investigated by several groups, with the consensus being that in the case of mAbs, higher ammonia concentrations reduce glycosylation overall. However, many reports are contradictory and depend on other factors such as the cell line, glucose, lactate and amino acid concentrations, dissolved oxygen and shear rate (Aghamohseni et al., 2014). This is yet another reflection of how sensitive glycosylation pathways are to process factors and the difficulty in its control.

Due to its impact on ADCC activity, the levels of mannosylation of IgG biosimilars must be monitored carefully. High mannose structures (Man5 and higher) have been reported to increase as a result of the addition of alternative sugars and amino sugars to the culture medium when producing a mAb using a CHO cell line, although upon scale-up this supplementation caused a secondary interaction with osmolality in a study by Rameez et. al (2021). Mannose and glucosamine in combination with either fructose, galactosamine or both fructose and galactosamine resulted in increased high-mannose levels of the biosimilar compared to the innovator molecule in the region of 140-160%, which correlated with an increased ADCC activity (>100%) compared to the innovator molecule (Rameez et al., 2021). As well as increasing ADCC activity, high mannose structures in the Fc region of IgG are also commonly associated with a faster serum clearance rate compared to other glycosylation structures in this region (Goetze et al., 2011; Yu et al., 2012), making mannosylation an important process to control during antibody production. Ornithine, spermine and copper in fermentation media have been found to correlate with levels of high mannose, which is postulated to be via the polyamine pathway and cellular redox (Kang et al., 2015). Kang et al. also noted that conditions of low osmolality resulted in decreased levels of high mannose, which had been found in previous studies (Pacis et al., 2011). Conversely to the effect of increasing manganese concentration, which results in reduced mannosylation, depriving the culture of copper has been found to reduce levels of high mannose glycans. When high mannose levels are elevated, ornithine accumulates in the culture medium. Supplementation of the media with ornithine also results in increased levels of high mannose, and reduction of spermine in the media results in reduced high mannose levels. Spermine is an inhibitor of the enzyme that converts ornithine into putrescine in the polyamine pathway; by lowering the amount of spermine, ornithine accumulates, and therefore the levels of high mannose increase (Kang et al., 2015). These results suggest a link between the polyamine pathway and glycosylation, although this has not been studied extensively.

A design of experiments (DoE) approach was used by Loebrich et al. (2019) to evaluate the effect of commonly used media additives to control glycosylation of an IgG1 produced in a CHO-K1 cell line. They found that 12.5mM glucosamine decreased galactosylation levels, 5.0mM uridine increased galactosylation and 1.0mM copper decreased levels of Man5 glycan structures. The degrees to which these supplements achieved these effects varied, with some having concomitant effects on other glycan structures; 1.0mM copper, for example, also increased levels of G0, G0F and G1F (glycans with no galactosylation, no galactosylation and one fucose, and one galactose and one fucose respectively). The effect of other supplements, such as glycerol, cytidine and ManNAc, was also investigated, the latter of which at lower

concentrations increased levels of G0F specifically but did not affect the levels of other glycan structures (Loebrich et al., 2019).

1.3.4 Enzymatic Remodelling

A number of studies have investigated the use of endoglycosidases for antibody glycan remodelling. Endo-β-*N*-acetylglucosaminidase S (Endo S) is an endoglycosidase which cleaves between the two GlcNAc residues of the *N*-glycan core. It is specific for IgG and has been used for the remodelling of IgG Fc *N*-glycans in a number of studies (Li et al., 2018; Kurogochi et al., 2015; Sjögren, Lood, & Nägeli, 2020). The discovery of this enzyme sparked interest in this area, including the immobilisation of wild-type (WT) Endo S and its glycosynthase mutant D184M with gained transglycosylation activity for the enzymatic glycoengineering of IgG (Li et al., 2018). Other endoglycosidases are specific for different oligosaccharide structures. Endo-β-*N*-acetylglucosaminidase H (Endo H), for instance, cleaves high-mannose and hybrid *N*-glycans and has been used for glycoprotein remodelling, whilst endo-β-*N*-acetylglucosaminidase D (Endo D) cleaves the GlcNAc-β1-4-GlcNAc-linkage in the chitobiose core region of *N*-glycans, resulting in a truncated β-GlcNAc-α1,6-Fuc on a glycoprotein (Sjögren, Lood & Nägeli, 2020). Enzymatic remodelling techniques have shown significant potential *in vivo* for generating IgG with more homogenous glycoprofiles. However, when it comes to yielding afucosylated IgG, enzymatic techniques have their limitations. As mentioned in Section 1.1.4.4, fucosidases are not efficient at removing fucosylated structures from IgG due to steric hindrance.

During glycan remodelling reactions, many endoglycosidases utilise sugar oxazoline transition state analogues which act as the glycan donor substrates for transglycosidases (Yang & Wang, 2017). However, oxazoline compounds can undergo side reactions if conditions are not controlled within strict limits; the carbon between the nitrogen and oxygen of oxazoline can undergo nucleophilic attack from a reactive amino group, such as a lysine side chain. These side reactions are undesirable, particularly when manufacturing clinical-grade material, as they can make downstream operations more complex and alter product function (Manabe et al., 2018).

For these reasons, developments have been made in order to negate the need for the sugar oxazoline donor substrate for glycan remodelling. Many of these efforts have focused on engineering endoglycosidases and using alternative glycan donors (Boune et al., 2020). The glycosylation state of trastuzumab has been remodelled using mutant forms of Endo S, endo-

β-*N*-acetylglucosaminidase M (Endo M) and endo-β-*N*-acetylglucosaminidase from *Coprinopsis cinerea* (endo-CC). In one study, an Endo M mutant was used to remove a fully sialylated glycan from sialylglycopeptide (SGP), and an Endo S mutant with transglycosylation activity then catalysed the addition of this glycan to the Fc region of deglycosylated trastuzumab (Iwamoto et al., 2018). In another study, the use of an oxazoline donor substrate was successfully negated by using SGP as the donor and Endo S to deglycosylate an anti-CCR4 antibody followed by a mutant endoglycosidase, endo-CC N180H, to transfer the glycan from SGP to the antibody (Manabe et al., 2018). Whilst particular mutants of these endoglycosidases achieved high efficiency in these studies and this method would likely increase the glycosylation heterogeneity of other IgG mAbs, the addition of further steps during larger scale mAb processing is likely to be unattractive to manufacturers due to the inevitable reduction in yield that these extra processing steps would cause. Additionally, this method requires the presence of a donor glycoprotein; in the case of the work carried out by Manabe et al. (2018), it was noted that a particularly large amount of SGP donor substrate was required for the successful transglycosylation reaction. This adds cost to a process and can complicate downstream processing.

1.3.5 Chromatographic Separations

Whilst enzymatic remodelling efforts have yielded success, their use is rarely reported at larger scales. Developments have been made in the area of chromatography which focus on glycoform separations, such as the use of anion or cation exchange chromatography to separate out sialylated species. This is possible due to the negative charge on terminal sialic acid residues and is a technique that has primarily been used at an analytical scale (Hurum & Rohrer, 2011; Rohrer, 2000). This section focuses on affinity ligand development that has been made towards separating differentially glycosylated recombinant proteins.

1.3.5.1 Lectins

One chromatographic technique that has gained interest over the past decade has been lectin affinity chromatography (LAC). Lectins are proteins or glycoproteins often derived from plants which have the ability to bind specific carbohydrate moieties, making them useful ligands for separating different glycoforms of glycopeptides, glycoproteins or glycolipids. Whilst monomeric binding affinities of lectins can be low, multivalent interactions can increase binding affinities into the nanomolar range and the binding is reversible, which are characteristics consistent with properties that make for suitable affinity ligands. Lectins do not react with or modify their targets and generally remain stable at conditions of variable pH and

ionic strength, meaning that their three-dimensional (3D) structure and binding affinity for their target is unlikely to alter after elution or after several chromatographic cycles. Lectins have been successfully immobilised onto Sepharose®, silica beads and some monolithic supports, with no significant perturbations in binding affinity reported (Hage et al., 2012).

Despite the suitability of lectins for use as affinity ligands and their ability to separate different product glycoforms, they are not widely used, particularly in industrial-scale processing. This is likely due to difficulties in consistent manufacturing, as lectins are often multimeric with many of their own glycosylation sites, making them difficult to produce recombinantly. This results in batch-to-batch variation, which compromises their effectiveness as affinity ligands (O'Connor, Monaghan & Cawley, 2017). There is also the potential for these resins to leach toxic lectins (Bolton, Ackerman & Boesch, 2013). In addition, eukaryotic lectins often require post-translational modification, which not only increases their structural complexity but also renders them unsuitable for recombinant production in a bacterial host. Attempts have been made to synthesise plant lectins recombinantly, but these efforts have normally resulted in very low yields of insoluble protein. These issues have made lectin production almost impossible to scale up, and has constrained their use to analytical scale applications (Keogh et al., 2014). Additionally, in the context of enriching for afucosylated IgG, the use of lectins is not suitable. Although one study did identify the ability of Aleuria Aurantia Lectin (AAL) to specifically bind fucose moieties on IgG, this lectin is only capable of doing so if the antibody is denatured or treated with a glycosidase (Chen et al., 2012).

1.3.5.2 Fc Gamma Receptors

Affinity ligands based on the FcγRIIIa have been developed and patented in various economic areas for the separation of fucosylated and afucosylated IgG (EP 2 768 845 B1, US 10221210 B2, US 2016/0222081 A1). The first company to do this was Zepteon™, who obtained their patent covering the US in 2019. This group transiently expressed WT FcγRIIIa in human embryonic kidney 293 (HEK-293) cells and immobilised it to an activated *N*-hydroxysuccinimide (NHS) Sepharose® resin using amine chemistry. These ligands have been successfully used in different settings to enrich for afucosylated IgG (Boesch et al., 2018; Freimoser–Grundschober et al., 2020; Lippold et al., 2019). In particular, they are used during IgG-type mAb biosimilar development to match fucosylation levels of the biosimilar with the innovator molecule, which is key to obtaining regulatory approval, and during lot-to-lot comparisons.

Despite the proven capability of these ligands for enriching afucosylated IgG, the capacity of the column is low and would not be viable in industrial-scale processing (Bolton, Ackerman & Boesch, 2013). Reasons for this are likely to be due to WT FcγRIIIa possessing up to five glycosylation sites, giving the ligands a large hydrodynamic radius; a variety of highly complex glycans at these sites could affect the overall shape of the ligands, and consequently their hydrodynamic properties that may influence their separation capabilities. It could also be related to the immobilisation chemistry used, as there are a number of lysine residues in the binding site of WT FcγRIIIa. The biocompatible 1-ethyl-3-(dimethylaminopropyl)carbodiimide/N-hydroxysuccinimide (EDC/NHS) method is neither an orthogonal nor a specifically targeted labelling strategy, so multiple surface-exposed lysine residues of the WT FcγRIIIa are conjugated for immobilisation (see Figure 6.8). The IgG binding of the WT FcγRIIIa may therefore be compromised, resulting in a lower separation efficacy. The Japanese company Tosoh have developed aglycosylated FcγRIIIa-based affinity ligands with enhanced pH and/or temperature stability compared to WT FcγRIIIa. Whilst these ligands are not capable of discriminating between fucosylated and afucosylated IgG due to their own lack of glycosylation, they do seem to be able to separate IgG based on galactosylation levels (Kiyoshi et al., 2018) (Edwards et al., 2022).

1.4 Summary

MAb-based therapeutics remain one of the biggest players in the biopharmaceutical sector and show consistent growth year on year. The effector functions that IgG1-based mAbs use to exert their therapeutic activity are largely impacted by the glycosylation pattern in the Fc region. In particular, ADCC, often mediated by the FcγRIIIa, is significantly impacted by the presence or absence of a core fucose on the *N*-glycans linked to the two C_H2 domains in the Fc region of IgG1. When one or both of these glycans are afucosylated, the affinity of IgG1 for the FcγRIIIa is increased, resulting in upregulation of ADCC activity of afucosylated IgG1 compared to fucosylated IgG1 (Zahavi et al., 2018).

There are many opportunities for further engineering, optimisation and development of mAb-based drugs, and with the impending mAb 'patent cliff' effect whereby many mAbs are reaching the end of their patent lifetimes in the coming years, there is a wealth of investment currently going into mAb biosimilar manufacturing. As our understanding of glycosylation pathways and the effects of glycosylation on biologic immunogenicity and pharmacokinetics deepens, and indeed as time goes on, the stringency of regulations surrounding mAb glycosylation and the importance of controlling and monitoring it are likely to increase. The

upstream approaches to controlling mAb glycosylation have not proved infallible, and it is therefore necessary for downstream approaches to be employed in conjunction with upstream technologies to yield products within a desired glycosylation specification. Advancements have been made in the field of chromatographic affinity ligand development, primarily for the separation of fucosylated and afucosylated IgG, but there is ample opportunity for further research in this area to enhance our ability to produce IgGs with more defined glycosylation profiles (Edwards et al., 2022).

Table 1.3 – summary of approaches for manipulating biologic glycosylation mentioned Section 1.3, including their advantages and disadvantages.

Strategy	Specific Approach	Desired Outcome	Advantages	Disadvantages
Cell line engineering	Knocking out gene encoding the transferase which adds fucose to the core GlcNAc, α1,6-FucT (*FUT8* knockout)	Reducing core fucosylation	Effective and safe, now used in commercial therapeutic antibody manufacturing	Required a significant amount of time and resources to achieve
	Disruption of fucose precursor production (disruption of gene encoding GMD)	Reducing core fucosylation	Highly effective	Required a significant amount of time and resources to achieve
	Overexpression of enzyme which creates bisecting GlcNAc, which causes steric hindrance for α1,6-FucT (overexpression of GnTIII)	Reducing core fucosylation	Effective and safe, now used in commercial therapeutic antibody manufacturing	Required a significant amount of time and resources to achieve
	Heterologous expression of RMD, which inhibits GMD and prevents the production of the precursor for α1,6-FucT	Reducing core fucosylation	Effective, now used in commercial protein manufacturing	Required a significant amount of time and resources to achieve
	Deletion and introduction of certain transferase enzymes into *P. pastoris* in order to yield complex-type glycosylation	Humanisation of the yeast *N*-glycosylation pathway	Aim is to produce cell lines which could generate therapeutic proteins, which would mean shorter, cheaper and less complex production processes	Still a work in progress, unknown at this stage if there will be other off-target effects or immunogenic glycovariants formed. Also would require change to currently established commercial

				platform cell line development and production processes
	Overexpression of transferase adding sialic acid in α2,6 linkage and disruption of transferase adding sialic acid in α2,3 linkage	Reduction in α2,3 sialylation and increase in α2,6 sialylation	α2,6 sialylation linkage has been reported to increase ADCC activity	A lot of resource and time invested for potentially not a huge amount of gain, as more effective approaches for yielding afucosylated glycans exist
Upstream processing	Reduction in pH	Increase in galactosylation and sialylation	In some cases, increased galactosylation can enhance ADCC and increased sialylation can extend serum half-life	The decrease in pH was found to decrease productivity
	Reduction in temperature	Increase in glycan site occupancy for human tissue plasminogen activator. Also potential changes in glycan structure in some cases	A relatively simple and inexpensive way to manipulate the glycan profile	Likely to decrease cell growth rate and therefore reduce productivity
Media supplementation	Addition of kifunensine to inhibit α1,2-mannosidase I, the enzyme which trims the IgG *N*-glycan to a form which can be fucosylated	Reducing core fucosylation	A cheaper way of reducing core fucosylation than cell line engineering	Unknown if the addition of kifunensine has an impact on therapeutic activity or safety
	Addition of 2-deoxy-2-fluorofucose and 5-alkynylfucose, inhibitors of α1,6-FucT	Reducing core fucosylation	A cheaper way of reducing core fucosylation than cell line engineering	Shown that there was incorporation of these compounds into the final product, and that 2-deoxy-2-fluorfucose in particular is toxic
	Addition of MnCl$_2$, uridine, galactose and glutamate	Increasing galactosylation levels	Increased galactosylation can increase ADCC activity for some IgG	Unknown if the addition of these molecules have an impact on

				therapeutic activity or safety
	Addition of mannose and glucosamine in combination with either fructose, galactosamine or both fructose and galactosamine	Increasing high-mannose levels	High-mannose structures cannot be fucosylated, meaning increased ADCC activity for IgG	Unknown if the addition of these molecules have an impact on therapeutic activity or safety
	Addition of ornithine, spermine and copper	Increasing high-mannose levels	High-mannose structures cannot be fucosylated, meaning increased ADCC activity for IgG	Unknown if the addition of these molecules have an impact on therapeutic activity or safety
Enzymatic remodelling	Engineering of Endo S, Endo M and endo-CC	Removing need for oxazoline transition state analogue, which can undergo side reactions and yield toxic by-products	Results in a much more defined glycosylation profile than other approaches, such as altering upstream processing parameters	Unsuitable for large-scale production as traduceses more processing steps and therefore reduces process efficiency
Chromatographic separations	Lectins	Separations of various glycoforms	Relatively cheap to produce, can target different glycoforms	Scale-up has been challenging and there have been issues with the leaching of toxic lectins
	Fc gamma receptors	Separation of fucosylated and afucosylated IgG	A more efficient way of analysing fucosylation levels than mass spectrometry	Currently unsuitable for large-scale production as column capacities are low

1.5 Thesis Aims and Objectives

In the following three subsections, the aims and objectives of this thesis are detailed. These will be referred to again in Section 7.1 of this document to discuss whether and how these aims were met.

1.5.1 FcγR Ligand Design and Construction

The affinity ligands used in this work were designed by Dr. Maria Livanos, previously of University College London (UCL). The ligands are engineered forms of the FcγRIIIa and have been designed with the aim of reducing the size, complexity and cost of manufacturing compared to the FcγRIIIa ligands whilst still maintaining a differential affinity for fucosylated

and afucosylated IgG1. These ligands will be referred to as 'FcγR ligands' throughout this document and more details behind their design rationale are detailed in Chapter 3.

1.5.2 FcγR Ligand Production, Purification and Analysis

The engineered FcγR ligands are intended to be produced in yeast expression systems, with one construct being produced in an engineered yeast system to minimise the extent of hypermannosylation on the construct. The aim is that the ligands will be produced at large-scale, although shake flask production would suffice for this project. It is anticipated that the ligands will be purified using His-tag affinity chromatography and analysed using gel electrophoresis and/or Western blot analysis. We plan to conduct mass spectrometry analysis of both the proteomic and glycomic profiles of the ligands to confirm that both the primary structure and the glycosylation patterns of the ligands are as expected, or at least similar to what we expect.

1.5.3 Measuring FcγR Ligand Affinities for IgG1 Glycovariants

The affinities of the FcγR ligands for IgG1 glycovariants will be tested using surface plasmon resonance (SPR). These glycovariants will include natively- or heterogeneously-glycosylated IgG1, deglycosylated IgG1 and afucosylated or reductively-fucosylated IgG1. If enough of the FcγR ligands are produced, they will be immobilised to agarose beads, either using amide or thiol linkages via lysine or cysteine side chains, respectively. A separation of heterogeneously-glycosylated IgG1 would then be carried out using this resin to analyse the separative properties of the FcγR ligands.

1.6 Organisation of Thesis

In this chapter, an introduction to mAbs, mAb effector function and glycosylation, chromatography, Protein A development and strategies to control mAb glycosylation has been provided. Chapter 2 details the materials and methods used throughout this work.

Chapter 3 presents the design rationale behind the FcγR ligands and other constructs used in this work. This chapter explains why the ligands were designed the way they were and gives context to the following results chapters. Chapter 4 delineates the fermentation attempts that were made to produce large amounts of the FcγR ligands and some of the challenges that were encountered with this work. This primarily involved proteolytic degradation, with this chapter also outlining the mitigation strategies that were employed to reduce the effect of proteolytic activity on the product. Chapter 5 details the shake flask production and purification processes, as well as the mass spectrometry analysis of the proteomic and glycomic profiles

of the FcγR ligands. Chapter 6 describes the binding studies that were carried out between the ligands and various glycovariants of IgG1. Finally, Chapter 7 summarises what was learned in each of the results chapters and outlines possible avenues of future work in this area. This is followed by Chapters 8 and 9 which give the references and supplementary information in the form of an appendix, respectively.

Chapter 2 – Materials and Methods

2.1 Molecular Modelling

Molecular modelling was carried out using PyMOL (Schrödinger LLC). Crystal structures were downloaded from the Protein Data Bank (PDB); the PDB code for each structure is stated in the corresponding figure caption. Proteins were either shown as Cartoon or Surface representations and glycans were shown as Sticks. Where an amino acid residue is of interest, it is shown using the Sticks representation. Distances between atoms were measured using the Measurement Wizard.

2.2 Cell Lines, Cloning and Transformation

All plasmid construction and transformation for the production of FcγRIIIa D2 Man5 (Man5) and FcγRIIIa D2 Man9 (Man9) were carried out by BioGrammatics™ (Carlsbad, CA, USA). Open reading frames (ORFs) for both Man9 and Man5 were codon-optimised and the deoxyribonucleic acid (DNA) was synthesised and cloned into the pPICZαB expression vector which had an α-mating factor (αMF) secretion signal and the bleomycin resistance gene (BleoR) for antibiotic selection. The entire ORF and cloning junctions were sequence verified and plasmid DNA was linearised at the PmeI site in the alcohol oxidase 1 (AOX1) promoter for insertion into the *P. pastoris* genome. Transformation was carried out by electroporation (600Ω, 10μF, 1150V) and transformed cells were selected on yeast extract-peptone-dextrose (YPD) plates with 500μg/ml of Zeocin™. Strains transformed: Bg10 (wild type *P. pastoris*), Bg11(*AOX1$^-$*, Mut^S) and the protease-deficient Bg25(*PEP4$^-$*, *SUB2$^-$*, Mut$^+$).

Man5 was produced in the protease-deficient Mut$^+$ GlycoSwitch® SuperMan5-10 strain (*PEP4$^-$*, *SUB2$^-$*). The same pPICZαB plasmid was transformed into the GlycoSwitch® SuperMan5-10 strain using the electroporation protocol described above using ~250ng of the expression vector. Protein sequences are given in Section 3.5 and plasmid maps are shown in Appendix 9.1.

The following work was carried out by evitrea™ (Schlieren, Switzerland). FcγRIIIa, referred to as refFcγRIIIa as it was used as the reference to establish whether our kinetics/affinity assays were working, was recombinantly and transiently expressed in the CHO cell line CHO-S using 250mL shake flask cultures, followed by purification using His-tag affinity chromatography. The sequence is shown in Section 3.5 (Sequence 2). Two trastuzumab samples were purchased; one which was natively- or heterogeneously-glycosylated, and another which was afucosylated. The heterogenously-glycosylated trastuzumab was produced in CHO cells and

purified using Protein A chromatography. The afucosylated trastuzumab was produced in CHO cells using GlymaxX® technology from ProBioGen™ and was also purified using Protein A chromatography. refFcγRIIIa and both trastuzumab batches were stored at -80°C prior to use and thawed at room temperature. The samples did not undergo more than two freeze/thaw cycles.

Tocilizumab was produced at UCL in 50L bioreactor fed-batch CHO cell culture and purified using Protein A chromatography. It was stored at -80°C prior to use and thawed at room temperature. The samples did not undergo more than two freeze/thaw cycles.

2.3 Media Preparation

All media and salt solutions were prepared in-house using Milli-Q water and were either autoclaved or sterile-filtered prior to use. The autoclave cycle used steam heated to 121°C with a holding time of 15 minutes. Buffered complex glycerol medium (BMGY) was composed of 10g/L yeast extract, 20g/L peptone, 1% glycerol, 100mM potassium phosphate buffer pH 6.0, 1.34% yeast nitrogen base (YNB) and 4×10^{-5}% biotin. Buffered complex methanol medium (BMMY) was composed of 10g/L yeast extract, 20g/L peptone, 0.5% methanol, 100mM potassium phosphate buffer pH 6.0, 1.34% YNB and 4×10^{-5}% biotin. Fermentation basal salts medium (BSM) was composed of 26.7% phosphoric acid (85%), 0.93g/L calcium sulfate, 18.2g/L potassium sulfate, 14.9g/L magnesium sulfate heptahydrate, 4% (w/v) glycerol and 0.1% polypropylene glycol (PPG) and pH-adjusted to pH 3.0 using 25% ammonium hydroxide. All pH measurement was carried out using a SevenCompact™ pH/Ion meter S220 from Mettler Toledo™ (Ohio, USA). *Pichia* trace metal 1 (PTM1) salts were composed of 6g/L cupric sulfate pentahydrate, 0.08g/L sodium iodide, 3g/L manganese sulfate monohydrate, 0.2g/L sodium molybdate dihydrate, 0.02g/L boric acid, 0.5g/L cobalt chloride, 20g/L zinc chloride, 65g/L ferrous sulfate heptahydrate, 0.2g/L biotin and 0.005% sulfuric acid.

2.4 Shake Flask Cultures

Specific growth conditions, where they vary from the following protocol, are stated in the results chapters.

Glycerol stocks of the cell lines described in Section 2.2 were initially provided by Dr. Maria Livanos and were subsequently made up from shake flask cultures which were grown using the protocol described below. Once the cultures reached an optical density at 600nm (OD_{600})

8-18AU, 1-2mL stocks were made in cryovials using a ratio of 80% cells and 20% glycerol (undiluted and autoclaved). These were stored at -80°C.

Cell stocks were thawed at room temperature prior to shake flask inoculation. To produce both the FcγRIIIa D2 Man5 and Man9 constructs, 1L sterile, baffled shake flasks were initially used to grow the cultures in 100mL of BMGY with initial inoculum volumes of 0.5mL from glycerol cell stocks that were made with OD_{600} 11-18AU. This is referred to as the first BMGY growth phase. These cultures were grown at 28°C in a Kuhner ISF-1-V Incubator Shaker at 180rpm until an OD_{600} reading of 2-6AU was reached (~16-24 hours post-inoculation). ~5-20mL of these cultures was used to inoculate 1L sterile, baffled shake flasks containing 200mL BMGY. This is referred to as the second BMGY growth phase. These cultures were grown at 28°C, 180rpm until OD_{600} ≥18AU was reached. The cultures were then pooled and centrifuged in a Beckman Coulter Avanti® J-E Centrifuge (Wycombe, UK) at 3000×g for 5 minutes. The supernatants were discarded and the cell pellets were resuspended in 100mL BMMY for induction. 10-20mL of this resuspension was added to each of 1L sterile, baffled flasks containing BMMY to give a total culture volume of 200mL in each flask at an OD_{600} of ~2.5-5AU. This is referred to as the BMMY growth phase. Antifoam, which was sterile 100% PPG, was added to a final concentration of 0.05mL/L (0.01mL per flask). The cultures were incubated at 30°C in shaking incubators at 150-200rpm. If the cultures grew for longer than 24 hours on methanol, 100% methanol was added at 24 hours post-induction to a final concentration of 0.5%. Optimal protein expression was seen once the cultures reached OD_{600} 11-18AU. The specific growth conditions and media/flask volumes are given in the figure captions of each respective growth curve.

Samples were analysed for OD_{600}. 3 x 1mL samples were taken from the cultures and diluted if needed (either 1 in 10 or 1 in 100). The media were used as blanks (either BMGY or BMMY depending on the growth phase) and OD_{600} of the sample was read at each time point using 1mL total sample volume placed in a cuvette. Measurements were obtained using an Amersham Biosciences Ultraspec 500 pro spectrophotometer (Amersham Biosciences, Slough, UK). If the samples were diluted, the value was corrected using the dilution factor.

Harvesting took place once the cultures reached OD_{600} ~11-18AU. Cultures were harvested by centrifuging in a Beckman Coulter Avanti® J-E Centrifuge at 3000×g for 5 minutes at 4°C. The cell pellets were discarded and the supernatants were filtered through a 0.2μm pore-size filter. The filtered supernatants were then stored at either -80°C or -20°C prior to chromatographic purification.

2.5 Small-Scale 250mL Fermentation

During the early stages of the project, the affinity ligands were produced in small-scale *P. pastoris* fermentations in 250mL bioreactors.

2.5.1 Inoculum Preparation

Cell stocks were stored at -80°C and thawed at room temperature prior to shake flask inoculation. 3 x 1L sterile, baffled shake flasks containing 100mL BMGY each were inoculated with either 0.1mL, 0.2mL or 0.5mL initial cell stock volume. These cultures were incubated overnight in a Kuhner ISF-1-V Incubator Shaker at 180rpm at 28°C. Samples were analysed for OD_{600} using the procedure described in Section 2.4. Once OD_{600} 10-15AU had been reached, 10mL of the culture was used to inoculate each 250mL bioreactor.

2.5.2 Reactor Set-Up and Operation

Small-scale fermentation was run using the Dasgip® Parallel Bioreactor System (Eppendorf™, Hamburg, Germany) consisting of 4 benchtop 250mL bioreactors (reactor geometry shown in Figure 2.1). The control software used was DASware® control software. A two-point pH calibration was used to calibrate the pH probes in each vessel (pH 4.0 and 7.0). The pumps were calibrated using the pre-set pump calibration procedure in the DASware control software; this procedure pumps reverse osmosis (RO) water through each of the pumps for a set amount of time and the user inputs the weights of water collected at the end of this cycle. The system then calibrates the pumps based on this information. The dissolved oxygen (DO) probes for each vessel were calibrated before each fermentation using a two-point calibration (100% and 0% oxygen). The feed lines for the acid, base, glycerol and methanol were primed manually by running 2mL of each feed through the lines until the feed emerged from the outlet of each line.

100mL of BSM was poured into each vessel and the lid, pH and DO probes were secured. The vessels and media were autoclaved. 12mL PTM1 salts per L glycerol (12mL/L) and 0.1mL/L autoclaved 100% PPG (antifoam) were added to autoclaved 50% (w/v) glycerol under sterile conditions to be used for the glycerol fed-batch phase (>200mL glycerol for one fermentation run using all four vessels). 12mL PTM1 salts per L methanol were added to 100% methanol to be used for the methanol fed-batch phase (>500mL methanol for one fermentation run using all four vessels). The acid used was 8% (v/v) phosphoric acid and the base used was 10% (v/v) ammonium hydroxide; the pH was controlled automatically by the system adding in acid or base when required to maintain the pH setpoint. Inoculum volume was 10mL and at time of inoculation (timepoint zero), 0.43mL PTM1 salts were syringed into each vessel.

A sample was taken at timepoint zero and at various timepoints throughout the fermentations thereafter. Where casamino acids were used, 10g of casamino acids (OmniPur® Casamino Acids, Merck, New Jersey, USA) were dissolved in 100mL Milli-Q water and then autoclaved. A 3mL bolus addition of this casamino acid solution was added to the vessels at 5 hours post-induction.

The fermentation procedure was run from a script, with a different script being used for growth of Mut$^+$ and Mut^S *P. pastoris*. The temperature was set to 30°C and the pH pre-induction was set to 5.0. Once methanol feeding commenced, the pH setpoint was raised to 6.5. The DO setpoint was 30% and the agitation rate was controlled by a cascade system in order to keep the DO below this setpoint; the agitation rate was initially set to 400rpm and maxed out at 1200rpm. Oxygen was sparged into the vessels at a rate of 0.5-6.0vvm, but the percentage of oxygen varied depending on the growth requirements of the cells in each vessel. The impeller in each vessel was a Rushton turbine.

The fermentation protocol was based on the standard *P. pastoris* fermentation protocol provided by Invitrogen™ ('Pichia Fermentation Process Guidelines', Version B). There was an initial glycerol batch phase, which lasted 18-24 hours, and at the end of this batch phase there was a DO spike, signifying that the cells had consumed all of the glycerol in the media within the vessel. When this spike in DO occurred, the glycerol fed-batch phase commenced and 50% (w/v) glycerol with 12mL/L PTM1 salts began being fed to each vessel at a rate of 1.82mL/hr. The glycerol fed-batch phase duration was 4 hours. Once the glycerol fed-batch phase was complete, the methanol fed-batch phase (induction) commenced.

The methanol feeding regime differs between Mut$^+$ and Mut^S strains of *P. pastoris*. Once glycerol had been fed to each vessel for 4 hours, the glycerol feed was switched off and 100% methanol containing 12mL/L PTM1 salts began being fed to each reactor. For Mut^S strains, the feed rate was 0.1mL/hr for the first two hours. The rate was increased in 10% increments every 30 minutes until a feed rate of 0.3mL/hr was reached, which was sustained for the remainder of the fermentation. For Mut$^+$ strains, methanol was fed at a rate of 0.36mL/hr to each vessel for the first 5 hours. The feed rate was then increased to 0.73mL/hr for a further 2 hours, followed by increasing again to 1.09mL/hr, which was maintained for the remainder of the fermentation.

Samples were analysed off-line for OD$_{600}$ (see Section 2.4), wet cell weight (WCW) and dry cell weight (DCW). For the WCW measurements, the weights of individual 1mL Eppendorf™ tubes were recorded and 3 x 0.5mL samples were taken from the cultures and placed in each

of these 1mL Eppendorf™ tubes. These samples were centrifuged in an Eppendorf™ Centrifuge 5424 R (Eppendorf™, Hamburg, Germany) at 15,000g for 10 minutes. For samples taken pre-induction the supernatant was discarded, and for samples taken post-induction the supernatant was collected and stored at -20°C. The total weight of the tube and the cell pellet was recorded, and the weight of the tube was subtracted to give the weight of the cells in the original 0.5mL sample. This was multiplied by two to get the weight of cells (g) in 1mL, and multiplied by 1000 to get a value for WCW in g/L. For the DCW measurements, the cell pellet and tube were placed at 100°C for 24 hours to dehydrate the pellet. The tube lids were opened so that water could evaporate from the pellet. The total weight of the dehydrated pellet and the tube was measured and the weight of the tube was subtracted, giving the weight of the dehydrated pellet alone from a 0.5mL sample. This was again converted to get a value for DCW in g/L.
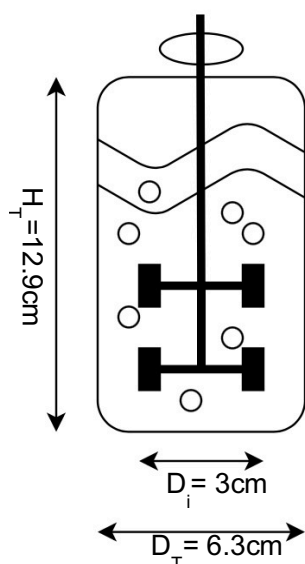
Figure 2.1 – reactor geometry of the 250mL Dasgip® Parallel Bioreactor. The vessel height is 12.9cm, width is 6.3cm, radius is 3.15cm and impeller diameter is 3cm. The H_T:D_T ratio of the vessel is ~2:1 and the D_I:D_T ratio is ~0.5:1. The total vessel volume is ~400mL and the maximum working volume is 250mL.

2.5.3 Harvest

The contents of each vessel were decanted into separate centrifuge bottles and centrifuged using the Beckman Coulter Avanti® J-E Centrifuge at 10,000×g for 20 minutes at 4°C. The supernatant from each vessel/centrifuge bottle was filtered through a 2μm filter followed by a 0.45μm pore-size filter. The filtrate was labelled appropriately and stored at -20°C prior to chromatographic purification.

2.6 Large-Scale 30L Fermentation

2.6.1 Inoculum Preparation

Cell stocks were stored at -80°C and thawed at room temperature prior to shake flask inoculation. 3 x 2L sterile, baffled shake flasks containing 400mL BMGY each were inoculated with 1mL initial cell volume. These cultures were incubated overnight in a Kuhner ISF-1-V Incubator Shaker at 180rpm at 30°C. Samples were analysed for OD_{600} using the procedure described in Section 2.4. Once OD_{600} 10-15AU had been reached, 1L of the culture was used to inoculate the 30L bioreactor.

2.6.2 Reactor Set-Up and Operation

Large-scale fermentations were run using a Sartorius Stedim Biostat® Cplus 30L bioreactor (Göttingen, Germany) (reactor geometry shown in Figure 2.2). The pH probe was calibrated using a two-point calibration (pH 4.0 and 7.0). 10L of BSM was poured into the reactor and both the vessel and the media were sterilised using the system's pre-set sterilisation in-place (SIP) function, which involved heating the media to 121°C and maintaining this temperature for 15 minutes. The DO probes for each vessel were calibrated before each fermentation using a two-point calibration (100% and 0% oxygen). The feed lines for the acid, base, glycerol and methanol were primed manually by running feed through each of the lines until the feed emerged from the outlet of each line.

The acid used was 8% (v/v) phosphoric acid and the base used was 10% (v/v) ammonium hydroxide. For the glycerol fed-batch phase, 50% (w/v) autoclaved glycerol containing 12mL/L PTM1 salts and 0.1mL/L antifoam (PPG) was used (>1L glycerol feed required per fermentation). For the methanol fed-batch phase, 100% methanol containing 12mL/L PTM1 salts was used (>500mL per fermentation). Inoculum volume was 1L and at time of inoculation, 43mL PTM1 salts were added to the vessel. A sample was taken at the point of inoculation and at various timepoints throughout the fermentation thereafter. Samples were analysed off-line for OD_{600} (see Section 2.4), WCW and DCW (see Section 2.5.2).

The temperature was set to 30°C and the pH pre-induction was set to 5.0. Once methanol feeding commenced, the pH setpoint was raised to 6.5. The DO setpoint was 30% and the agitation was controlled by a cascade system in order to keep the DO below this setpoint; the agitation rate was initially set to 300rpm and maxed out at 800rpm. Oxygen was sparged into the vessels at a rate of 0.5vvm, but the percentage of oxygen varied depending on the growth requirements of the cells in the vessel. The impeller used was a Rushton turbine.

The fermentation protocol was based on the standard *P. pastoris* fermentation protocol provided by Invitrogen™. The pH and temperature were controlled by the system according to the setpoints, the DO was maintained below 30% by alterations in agitation rate and the feeding regime was controlled manually. The glycerol batch phase lasted approximately 16 hours, and when the DO spike occurred the 50% (w/v) glycerol feed containing 12mL/L PTM1 salts was started at a rate of 181.5mL/hr. The glycerol fed-batch phase duration was 4 hours. Once the glycerol fed-batch phase was complete, the methanol fed-batch phase commenced. Only a Mut$^+$ strain was grown at large-scale with a maximum induction period of 6 hours. For the first 5 hours methanol was fed at a rate of 36mL/hr, and the feed rate was increased to 73mL/hr for the remainder of the fermentation. The glycerol fed-batch, methanol fed-batch and pH increase post-induction were all controlled manually and did not run from a script.
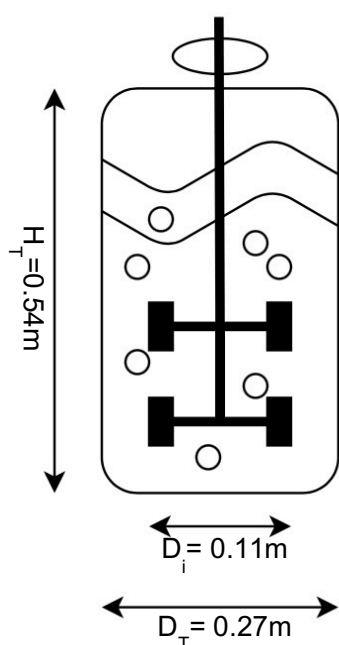
Figure 2.2 – vessel geometry of 30L Biostat® Cplus reactor. The vessel height is 0.54m, width is 0.27m, radius is 0.14m and impeller diameter is 0.11m. The H_T:D_T ratio of the vessel is 2:1 and the D_I:D_T ratio is 0.4:1. The total vessel volume is 30L.

2.6.3 Harvest

Harvesting was carried out according to the procedure given in Section 2.5.3. On the occasion when protease inhibitors were added to the supernatant, Pierce™ EDTA-free Protease Inhibitor Tablets (Thermo Fisher Scientific™, Massachusetts, USA) were used. These target serine, cysteine and aspartic acid proteases. 2 tablets were dissolved in 4mL of 1X phosphate-buffered saline with added detergent (PBS-P$^+$) by vortex mixing, which was added to 20mL of harvest. The composition of 1X PBS-P$^+$ is given in Section 2.9.1.

2.7 Chromatographic Purification

Both His-tag affinity purification using a nickel-nitrilotriacetic acid (Ni-NTA) resin and protein (FcγRIIIa) affinity chromatography techniques were used for protein purification.

2.7.1 His-Tag Affinity Purification

The filtered supernatant from a shake flask or reactor harvest was thawed in a room temperature water bath and then filtered through a 0.2μm pore-size filter. The supernatant was pH-adjusted to pH 7.2-7.8 using 25% ammonium hydroxide to allow for the 6xHis tag to interact with the nickel on the resin. The sample was then filtered again through a 0.2μm pore-size filter to remove any precipitates that may have formed during pH adjustment. The sample was kept at 4°C before and during purification.

Purification was carried out on either an ÄKTA avant™ 150 or an ÄKTA go™ purification system. The system was maintained with all lines filled with 20% ethanol, and all lines and pumps were washed with 20% ethanol and Milli-Q water prior to the purification run. The lines and pumps were then washed and filled with their respective buffers to be used during the run. All buffers were prepared in 50mM sodium phosphate (10.107g/L sodium phosphate dibasic heptahydrate, 1.697g/L sodium phosphate monobasic heptahydrate) using Milli-Q water and were sterile-filtered prior to use. The equilibration buffer was made up of 10mM imidazole (0.68g/L), the wash buffer 20mM imidazole (1.36g/L) and the elution buffer 300mM imidazole (20.4g/L).

A 5mL HisPur™ Ni-NTA Chromatography Cartridge from Thermo Fisher Scientific™ was attached drop-to-drop to the ÄKTA system and equilibrated with 10 column volumes (CV) of equilibration buffer (not collected). All sample was loaded onto the column (maximum 350mL at a time) and the flow-through was collected in 10mL fractions. The column was washed with 20CV of wash buffer which was also collected in 10mL fractions. A gradient elution was used starting at 4% elution buffer (diluted with equilibration buffer) and ending at 100% elution buffer over 10CV, and 2mL fractions were collected. The column was re-equilibrated at the end of the run with 5CV equilibration buffer. The flow rate at all stages of the run was 5mL/min, the temperature of the ÄKTA was maintained at 25°C and the A_{280} (absorbance at 280nm) and A_{260} were monitored throughout the run. Column pressure was also monitored and the system was set up so that the flow rate would reduce automatically should the column pressure exceed the limits specified by the manufacturer, which was 43.5psi.

For the CIP procedure, all pumps used were washed with Milli-Q water. The column was also washed with 10CV Milli-Q water. The sample pump was washed with 1M sodium hydroxide and the column was also washed with 10CV 1M sodium hydroxide. Again, the sample pump was washed with Milli-Q water and the column was washed with 10CV Milli-Q water. All pumps and lines were then washed with 20% ethanol and the column was washed with 10CV 20%

ethanol. The column was filled with 20% ethanol, removed from the ÄKTA drop-to-drop and stored upright at 4°C. All collected fractions were stored at -20°C prior to analysis.

2.7.2 FcγRIIIa Affinity Chromatography

To separate tocilizumab for fucosylated and afucosylated glycovariants, a 1mL Glycap-3A™ affinity column was purchased from Zepteon™ (Boston, MA, USA) which binds afucosylated IgG1. This column is comprised of an NHS-Sepharose® 4 Fast Flow resin with FcγRIIIa-176V (transiently expressed in HEK-293 cells) immobilised via EDC/NHS chemistry.

Purification was carried out on either an ÄKTA avant™ 150 or an ÄKTA go™ purification system. The system was maintained with all lines filled with 20% ethanol, and all lines and pumps were washed with 20% ethanol and Milli-Q water prior to the purification run. The lines and pumps were then washed and filled with their respective buffers to be used during the run. The equilibration and wash buffer used for this separation was PBS (Thermo Fisher Scientific™, MA, USA). 5 PBS tablets were dissolved in 1L of Milli-Q water to give pH 7.4 and the following salt concentrations: 10mM phosphate, 2.7mM potassium chloride, 13.7mM sodium chloride. The elution buffer used was 100mM glycine pH 3.2. All buffers were sterile-filtered prior to use.

The Glycap-3A™ column was attached drop-to-drop to the ÄKTA and equilibrated with 10CV of equilibration buffer (not collected). 6mg total of antibody was loaded onto the column at a concentration of 1.1mg/mL via a sample pump (5.5mL sample volume). The flow-through was collected in 2mL fractions. The column was washed with 20CV of wash buffer which was collected in 5mL fractions. A gradient elution was used starting at 4% elution buffer (diluted with equilibration buffer) and ending at 100% elution buffer over 20CV, and 1mL fractions were collected. 2-(N-morpholino)ethanesulfonic acid (MES) pH 8.5 was used as neutralisation buffer in the tubes which were predicted to contain the elution fractions. Tubes 1-9 of the elution tubes contained 110μL MES pH 8.5 (10% volume neutralisation buffer) and tubes 10-22 contained 1mL MES pH 8.5 (50% volume neutralisation buffer), which allowed for an extra 2 elution tubes. The column was re-equilibrated at the end of the run with 5CV equilibration buffer. The flow rate at all stages of the run was 0.5mL/min, the ÄKTA temperature was maintained at 25°C and the A_{280} was monitored throughout the run. Pre- and delta-column pressure were also monitored and the system was set up so that the flow rate would reduce automatically should the column pressures exceed the limits specified by the manufacturer; the pre-column pressure limit was 25psi and the delta-column pressure limit was 30psi.

For the CIP procedure, all lines and pumps used during the run were washed with Milli-Q water followed by 20% ethanol. The column was washed with 5CV of a mixture of PBS and 20% ethanol (50% v/v) followed by backflushing with 5CV of the same solution. A final column wash of 10CV of this solution was carried out before filling the column with the PBS and 20% ethanol solution and detaching it drop-to-drop from the ÄKTA. The column was stored upright at 4°C. All collected fractions were stored at -20°C or -80°C prior to analysis.

2.8 Protein Analysis and Characterisation

Samples from the fermentation, shake flask studies and purification runs were analysed along with commercially-sourced proteins using mainly sodium dodecyl sulfate-polyacrylamide gel electrophoresis (SDS-PAGE) and Western blot analysis. Mass spectrometry was used to confirm the primary sequence and identify the glycosylation profile of the antibodies and ligand constructs. A zymogram was used to confirm the presence of enzymatic activity within harvest samples from both small- and large-scale fermentations, along with shake flask harvest samples.

2.8.1 Gel Electrophoresis

Samples were diluted in Laemmli SDS reducing sample buffer (4X) from Thermo Fisher Scientific™ in a buffer to sample ratio of 1:3 and the sample and buffer mixture was placed at 95°C for 5 minutes to denature the proteins. The samples, along with 7µL of PageRuler™ Prestained Protein Ladder (10-180kDa) from Thermo Fisher Scientific™, were loaded onto Invitrogen™ Novex™ 16% Tris-Glycine Mini Gels (WedgeWell format, 15 wells). The buffer used was Pierce™ 10X Tris-Glycine SDS running buffer from Thermo Fisher Scientific™ (~800mL), which was diluted to 1X using Milli-Q water and used to fill both chambers of the gel tank. The gel tanks were attached to a Bio-Rad™ PowerPac™ Basic (California, USA) and the gel was run at 200V for 50 minutes. After running, gels were incubated in 20mL of Abcam InstantBlue® Coomassie Protein Stain (Cambridge, UK) for at least 2 hours. The gels were imaged under blue light at 460nm using an Amersham Imager 600 from Cytiva™ (Massachusetts, USA).

2.8.2 Western Blot Analysis

Gels were run using the method described in Section 2.8.1. Instead of staining, gels were transferred to Bio-Rad™ Trans-Blot® Turbo™ Mini 0.2µm Nitrocellulose membranes (7 x 8.5cm). The transfers were carried out using a Bio-Rad™ Trans-Blot Turbo Transfer System on the machine's Low Molecular Weight pre-programmed protocol, which is optimised for

proteins below 30kDa. The transfer protocol ran for 4.5 minutes at 1.3A up to 25V using 1 mini gel per cassette.

The nitrocellulose membranes with the protein transferred from the gel were placed in 50mL of blocking solution, which was 5% milk powder (AppliChem© non-fat dried milk powder) dissolved in PBS. This was incubated on a rocking shaker for 1 hour. At the end of the blocking phase, the membrane was incubated with antibody. For this, the blocking solution was decanted and replaced with 10mL 1% milk dissolved in PBS, to which anti-His antibody was added in a 1 in 100 dilution. The anti-His antibody used was Bio-Techne polyHis HRP mAb clone AD.1.1.10 (Minnesota, USA). This was incubated on a rocking incubator for 1 hour. Only one antibody incubation step was required as the anti-His antibody used was conjugated to horseradish peroxidase (HRP) for chemiluminescent imaging.

The antibody solution was decanted and three 5-minute washes of the membrane with PBS were carried out to remove any remaining unbound antibody from the membrane. SuperSignal™ West Femto Maximum Sensitivity Substrate from Thermo Fisher Scientific™ was used to visualise the membranes. In darkness, 2mL of the luminol/enhancer was mixed with 2mL of the stable peroxide buffer and poured over the membranes, followed by incubation on a rocking shaker for 1 minute. The membranes were imaged in an Amersham Imager 600 from Cytiva™ using the chemiluminescence option on the Automatic setting.

2.8.3 Mass Spectrometry

This section was completed with the help of Dr. Anja Krueger, Imperial College London.

2.8.3.1 Proteomics

All samples, including the FcγR ligands, refFcγRIIIa and antibody samples, were dried into an Eppendorf™ vial prior to application (total mass of each sample: 20-30µg). For reduction, 10μL of 8M guanidine hydrochloride and 1µL of 10 mM dithiothreitol (DTT) in 55mM ammonium bicarbonate (AMBIC) buffer pH 8.4 was added and the samples were heated to 56°C for 30 minutes. For carboxymethylation, the samples were cooled to room temperature and 1µL of 55mM iodoacetic acid (IAA) in AMBIC was added. The samples were then incubated in the dark for 30 minutes at room temperature. Prior to protease digestion, 30μL of AMBIC was added and sequencing grade proteases (1:20, enzyme:protein) were individually applied on aliquots of the proteins, i.e. endoproteinase Glu-C, trypsin and chymotrypsin (New England Biolabs®, Massachusetts, USA). Digestions were run overnight in a water bath at 30-37°C according to the manufacturer's recommendations. For targeted tandem mass

spectrometry (MS/MS) only, chymotrypsin and Glu-C (both sequencing grade) were used consecutively followed by Sep-Pak® C18 cartridge purification after the enzymatic digest. Endoglycosidase and mannose binding protein, *E. coli* expressed (Endo Hf) digestion was carried out according to the New England Biolabs® manufacturer recommendations. Samples were run on the Synapt G2 instrument (Waters™, Massachussetts, USA) for electrospray ionisation-liquid chromatography-mass spectrometry (ESI-LC-MS) analysis as survey run or targeted fast data-dependent analysis (DDA). A gradient of 15-45% acetonitrile in 0.1% formic acid (solvent B) was used with 0.1% formic acid as baseline solvent A. The samples were injected as 200fmol per µL in 0.1% formic acid. Data analysis was carried out manually supported by BiopharmaLynx and MassLynx software for peptide mapping (Waters™).

2.8.3.2 Glycomics

For glycomic analysis, the 30-50µg protein samples (antibody samples, refFcγRIIIa and the FcγR ligands) were reduced using 10mM DTT in 0.6M Tris buffer pH 8.5 at 56°C for 1 hour. Carboxymethylation was carried out using IAA in 50mM AMBIC pH 8.4 for 30 minutes at room temperature in the dark. Samples were dialysed using a Slide-A-Lyzer™ Mini Dialysis Device (molecular weight cut-off (MWCO) 3.5K) for 2 days in 50mM AMBIC buffer and subsequently freeze-dried overnight. The protein samples were digested with trypsin (porcine) in a 1:20 enzyme:protein ratio in 200µL AMBIC buffer at 37°C overnight. The digest was purified using Sep-Pak® C18 cartridges (Waters™) according to the manufacturer's recommendations. Protein fractions were merged and deglycosylated using deglycosylases dependent on the sample protein expression system.

Dried antibody samples were digested with 5µL of peptide-N4-(*N*-acetyl-beta-glucosaminyl)asparagine amidase F (PNGase F) in 200µL AMBIC buffer at 37°C. Deglycosylation with Endo Hf for the yeast-expressed FcγR ligands was carried out according to New England Biolabs® recommendations. Briefly, 20µL of 10x digestion buffer was added and diluted with Milli-Q water so that 1x buffer concentration was reached, followed by the addition of 5µL of Endo Hf. The enzyme was left overnight in a water bath at 37 °C. Samples were purified via Sep-Pak® C18 cartridges (Waters™) and the watery glycan fraction was collected. The volume was reduced in a SpeedVac™ system (Thermo Fisher Scientific™) and freeze-dried overnight. Cleaved glycan samples were permethylated with dimethylsulfoxide (DMSO)/iodomethane, extracted using a chloroform-water solvent system and argon dried. Glycans were Sep-Pak® purified via a standard water/acetonitrile solvent system. The purified permethylated glycan samples were embedded into a 3,4-diaminobenzophenone matrix and

analysed using an Applied Biosystems™ 4800 MALDI TOF/TOF™ Analyser (California, USA). Mass spectra were analysed and processed using GlycoWorkbench software.

2.8.4 Zymography

The protocol described in Section 2.8.1 for running SDS-PAGE gels was largely followed. The differences compared to this protocol and the zymogram protocol are described hereafter. The positive control used was thermolysin (molecular weight: 34.6kDa) and the gels used were Invitrogen™ Novex™ 10% Gelatin Zymogram Gels. The gel was run at 125V for 90 minutes. Once the gel run was complete, the gel was incubated in 100mL of 1X Invitrogen™ Novex™ Zymogram Renaturing Buffer for 30 minutes. This buffer was decanted and the gel was incubated in 100mL of 1X Invitrogen™ Novex™ Zymogram Developing buffer for 30 minutes. At the end of this incubation step, this buffer was decanted and replaced with fresh developing buffer and incubated overnight. The gel was stained by incubation with Thermo Fisher Scientific™ SimplyBlue™ SafeStain for 1 hour, which was rinsed and destained with Milli-Q water for 90 minutes. The gel was then imaged in the same manner as the SDS-PAGE gels described in Section 2.8.1.

2.8.5 Sample Dialysis and Concentration

To dialyse sample from one buffer into another, either Slide-A-Lyzer™ Mini Dialysis Devices (2mL, 3.5K MWCO) from Thermo Fisher Scientific™ or SpectraPor® Float-A-Lyzer® Dialysis Devices (5mL, 3.5-5K MWCO) from Repligen™ were used (Massachusetts, USA).

The Slide-A-Lyzer™ protocol was used for the buffer exchange of samples with a volume of 0.2-2mL. Firstly, the device was removed from the 50mL conical tube and placed upside down on a clean surface to prevent membrane contamination. To the conical tube, 44.5mL of dialysis buffer was added and set aside. 4mL of dialysis buffer was then added to the device to wet the membrane, then decanted. Immediately, to prevent the membrane becoming dry, 0.2-2mL of sample to be dialysed was added to the device. This was then placed slowly into the conical tube containing dialysis buffer, ensuring that the membrane was fully in contact with the buffer in the conical tube and there were no air bubbles on the surface of the membrane that would prevent diffusion. The cap was placed onto the conical tube and the device was then placed either at 4°C or on an orbital shaker at room temperature, 100rpm, depending on the temperature stability of the sample. The dialysis buffer was changed after 2 hours at these conditions, and the sample was left to dialyse overnight at the appropriate conditions. For a 0.2mL sample, the dialysis ratio was ~1:225 (sample volume to dialysis buffer volume). For a 2mL sample, the ratio was ~1:25. For a ratio smaller than ~1:45, i.e. a sample

volume larger than 1mL, a third buffer change was performed, which was left to dialyse for a further 2 hours minimum.

For the buffer exchange of samples which were between 2-5mL in volume, a Float-A-Lyzer® device was used. The packaging and cap were removed from the Float-A-Lyzer®, the tubing was filled with 20% ethanol and the device was submerged in 20% ethanol for 10 minutes. The ethanol was decanted and the device was filled and submerged with Milli-Q water for 20 minutes. This was decanted and the device was rinsed with Milli-Q water a further three times to ensure all the ethanol had been removed. The sample to be dialysed was then pipetted into the tubing and the cap was replaced. A flotation ring was fitted to the tubing and the device was placed in a dialysis reservoir of ~650mL with a magnetic stirrer. Dialysis was carried out with gentle stirring at 4°C for 4 hours before the dialysis buffer was replaced. The second and final dialysis step was carried out overnight. For a 2mL sample, the dialysis ratio was 1:325, and for a 5mL sample the ratio was 1:130. After the dialysis procedure, the sample was retrieved from the device using a long pipette.

To concentrate sample, either the MilliporeSigma™ Amicon™ Ultra Centrifugal Filter Units (0.5mL, 3K MWCO, Thermo Fisher™ Scientific) or Pall Microsep™ Advance Spin Filters (5mL, 3K MWCO) were used (New York, USA). To the 0.5mL devices, a maximum of 0.2mL of sample was pipetted into the device, and to the 5mL devices a maximum of 5mL was pipetted into the device. The spin filters were centrifuged in an Eppendorf™ Centrifuge 5424 R at 10,000rcf for 10 minutes at 4°C. The filtrate was discarded and the retentate was collected and stored either at 4°C, -20°C or -80°C depending on subsequent processing steps.

To quantify protein concentrations, a NanoDrop™ One Spectrophotometer from Thermo Fisher Scientific™ was used. When measuring antibody sample concentrations, the setting used was Protein – Protein A_{280} – Immunoglobulin. For all other proteins, the setting used was Protein – Protein A_{280} – Type: other protein ε and molecular weight. The ε (extinction coefficient) was set to the appropriate value depending on the protein being measured, and if this was not known a value of $0.01M^{-1}$ cm^{-1} was used. The molecular weight was entered and the baseline correction was set to 340nm. The slide was first wiped with a Kimtech™ wipe and $2\mu L$ of the buffer that the protein was solubilised in was loaded onto the slide as a blank. Once the blank had been measured, another sample of PBS was measured to ensure the A_{280} reading was 0AU. Three sample measurements were tested for A_{280} and $\frac{A_{260}}{A_{280}}$, and afterwards the blank was tested again to ensure that it read 0. The average A_{280} and $\frac{A_{260}}{A_{280}}$ values for the

sample measurements were taken. The protein molecular weight and extinction coefficient were obtained using the online ExPASy ProtParam tool. The sample concentration was computed using these values and the A_{280} measurements from the NanoDrop™.

Using the A_{280} values obtained and assuming that all A_{280} absorbance is from FcγR ligand protein only:

$$\text{Concentration (mg/mL)} = \frac{A_{280}}{\varepsilon \times l} \times \text{MW (1)}$$

where A_{280} = absorbance at 280nm (AU)

ε = extinction coefficient ($M^{-1} cm^{-1}$)

l = path length (1cm)

MW = molecular weight (g/mol)

The computed molecular weight of the FcγR ligand protein backbone was 11,410g/mol and the extinction coefficient was 22550M^{-1} cm^{-1}, both to 4 significant figures (s.f). For details regarding the FcγRIIIa D2 Man9 and Man5 ligand constructs, see Section 3.4.

FcγRIIIa D2 Man9:

$$\text{Concentration (mg/mL)} = \frac{0.16\text{AU}}{22,550\text{M}^{-1}\text{cm}^{-1} \times 1\text{cm}} \times 11,410\text{g/mol}$$

Concentration = 0.0810mg/mL to 3 s.f

FcγRIIIa D2 Man5:

$$\text{Concentration (mg/mL)} = \frac{0.23\text{AU}}{22,550\text{M}^{-1}\text{cm}^{-1} \times 1\text{cm}} \times 11,410\text{g/mol}$$

Concentration = 0.116mg/mL to 3 s.f

These stock solutions were used for subsequent analysis and binding studies.

2.9 Surface Plasmon Resonance

Proteins used in SPR studies included Man9, Man5, refFcγRIIIa, trastuzumab and afucosylated trastuzumab and tocilizumab. The materials and protocols used for immobilisation and kinetics/affinity assays are detailed in this section.

2.9.1 Protein Immobilisation Techniques

The running buffer used for all experiments (immobilisation and kinetics/affinity assays) was 1X PBS-P$^+$. The composition of this buffer was 20mM phosphate, 2.7mM potassium chloride, 137mM sodium chloride and 0.05% Surfactant P20 (Tween 20). The buffer was diluted in Milli-Q water from a stock solution of 10X PBS-P$^+$ and sterile-filtered prior to use.

2.9.1.1 EDC/NHS

The EDC/NHS immobilisation chemistry utilises a carboxymethylated 5 (CM5) chip. Throughout the immobilisation procedure, the flow rate varied between 5-10μL/min.

Antibody samples were dialysed into 10mM sodium acetate pH 6.5 using the Slide-A-Lyzer™ protocol described in Section 2.8.5. A new CM5 chip was equilibrated by passing running buffer over the chip at a flow rate of 10μL/min for a minimum of 4 hours. After this, a baseline for the active channel, flow channel 2 (Fc 2) was first established using running buffer. Next was the pre-concentration step, which injected 10μL of sample to be immobilised over the inactivated chip. The chip surface was then washed with either 30μL 50mM sodium hydroxide or 10mM sodium acetate pH 3.5 to remove any unbound protein from the pre-conditioning step. EDC and NHS were mixed and 70μL of the mixture was passed over the chip, activating the channel surface by modifying the carboxymethyl groups on the dextran chains to NHS esters. A baseline was established with running buffer before the next step. The sample for immobilisation was then injected over the chip according to the amount that would be approximately required to reach the desired immobilisation level based on the system's calculations in the pre-conditioning step. Running buffer was again passed over the chip to establish a baseline. Remaining unbound NHS-esters were inactivated by passing 70μL of 1M ethanolamine over the chip surface. The final immobilised ligand level was calculated by subtracting the baseline after EDC/NHS activation from the final response level in this step.

2.9.1.2 Streptavidin-Biotin

Biotinylation was carried out using either the EZ-Link™ Maleimide-PEG$_2$-Biotin (No-Weigh Format, 10x2mg vials) kit or EZ-Link™ Sulfo-NHS-LC-Biotin (sulfosuccinimidyl-6-[biotin-amido]hexanoate), both from Thermo Fisher Scientific™.

First, the protocol for biotinylation using the maleimide-PEG$_2$-biotin tag is described. This tag has a total molecular weight of 525.62Da. It is composed of a biotin group linked to two polyethylene glycol (PEG) moieties, which is then linked to a maleimide group. When sulfhydryl groups on cysteine residues are in their reduced state, they react with the maleimide group to form a stable thioether bond with the biotin tag.

As recommended by the manufacturer, a 20-fold molar excess was used for biotinylation:

$$\text{mL protein} \times \frac{\text{mg protein}}{\text{mL protein}} \times \frac{\text{mmol protein}}{\text{MW protein}} \times \frac{20\text{mmol biotin}}{\text{mmol protein}} = \text{mmol biotin to be added (2)}$$

This equation can be rearranged to equation 3:

$$\text{mg protein} \times \frac{20\text{mmol biotin}}{\text{MW protein}} = \text{mmol biotin to be added (3)}$$

The protein to be biotinylated in this case was trastuzumab at a concentration of 5.4mg/mL (36.5μM) with a molecular weight of 148kDa:

$$5.4\text{mg protein} \times \frac{20\text{mmol biotin}}{148,000\text{mg}} = 0.000730\text{mmol biotin reagent}$$

Volume of 20mM stock solution to be added to 1mL of 36.5μM trastuzumab sample:

$$0.000730\text{mmol} \times \frac{1,000,000\mu\text{L}}{20\text{mmol}} = 36.5\mu\text{L of 20mM biotin stock solution}$$

The protein to be biotinylated was already solubilised in sulfhydryl-free buffer (PBS) which was between pH 6.5-7.5, as specified in the manufacturer's protocol. A 20mM biotin stock solution was prepared by adding 190μL of PBS to 2mg of EZ-Link™ Maleimide-PEG$_2$-Biotin and resuspending. Next, 36.5μL of biotin stock solution was added to the sample of protein to be immobilised and resuspended. This mixture was incubated at 4°C overnight. To remove remaining free unbound biotin, the sample was dialysed into 1X PBS-P$^+$ using a Slide-A-Lyzer™ Mini Dialysis Device according to the procedure described in Section 2.8.5.

Next, the protocol for biotinylation using sulfo-NHS-LC-biotin is described. The sulfo-NHS-LC-biotin tag has a total molecular weight of 556.59Da. This tag is composed of the biotin group

and a spacer arm with a length of 22.4Å linked to a sulfosuccinimidyl group which reacts with activated lysine residues on the protein to be tagged.

As recommended by the manufacturer, a 20-fold molar excess was used for biotinylation:

$$\text{mL protein} \times \frac{\text{mg protein}}{\text{mL protein}} \times \frac{\text{mmol protein}}{\text{MW protein}} \times \frac{20\text{mmol biotin}}{\text{mmol protein}} = \text{mmol biotin to be added (2)}$$

This can be rearranged to equation 3:

$$\text{mg protein} \times \frac{20\text{mmol biotin}}{\text{MW protein}} = \text{mmol biotin to be added (3)}$$

Again, the protein to be biotinylated was trastuzumab at a concentration of 5.4mg/mL (36.5μM) with a molecular weight of 148kDa:

$$5.4\text{mg protein} \times \frac{20\text{mmol biotin}}{148,000\text{mg}} = 0.000730\text{mmol biotin reagent}$$

Volume of 10mM stock solution to be added to 1mL of 36.5μM trastuzumab sample:

$$0.000730\text{mmol} \times \frac{1,000,000\mu\text{L}}{10\text{mmol}} = 73.0\mu\text{L of 10mM biotin stock solution}$$

The protein to be biotinylated was already solubilised in PBS between pH 7.2-8.0, as specified in the manufacturer's protocol. A 10mM biotin stock solution was prepared by adding 360μL of Milli-Q water to 2mg of sulfo-NHS-LC-biotin and resuspending. Next, 73μL of biotin stock solution was added to the sample of protein to be immobilised and resuspended. This mixture was incubated at 4°C for 2 hours. To remove remaining free unbound biotin, the sample was dialysed into 1X PBS-P$^+$ using a Slide-A-Lyzer™ Mini Dialysis Device according to the procedure described in Section 2.8.5.

Protein biotinylation was confirmed using a Western blot and probing the membrane with streptavidin conjugated to HRP (HRP-SA) according to the Western blot protocol described in Section 2.8.2.

The streptavidin (SA) chip was first washed with 3 x 10μL injections of 1M sodium chloride 50mM sodium hydroxide. The sample containing the biotinylated trastuzumab to be

immobilised was then injected in a 2μL pulse to see if the desired immobilisation level or higher was reached. If the desired immobilisation level was not reached, a larger pulse was injected over the chip. This process was repeated until the desired immobilisation level was achieved. The surface was washed with running buffer to remove any unbound protein. The final immobilisation level was the response at the end of the final wash minus the baseline before the first immobilisation pulse.

2.9.1.3 Protein L

A sensor chip with recombinant Protein L pre-immobilised via EDC/NHS chemistry to a carboxymethylated dextran-coated surface was used. Tocilizumab at a concentration of 4mg/mL (27μM) was passed over the surface of the equilibrated Protein L chip at a flow rate of 5μL/min and injection was stopped manually after 25 seconds. The initial capture response level on Fc 2 was ~54,000RU. A ~1-hour wash of running buffer at a flow rate of 10μL/min was then carried out, after which the response level was ~52,000RU.

2.9.1.4 Human Epidermal Growth Factor Receptor 2

Human epidermal growth factor receptor 2 (HER2)/ERBB2 Protein, Human, Recombinant (extracellular domain, domain IV, His tag) from Sino Biological Inc. (Bejing, China) was dialysed into 10mM sodium acetate at pH 4.5 using the Slide-A-Lyzer™ protocol described in Section 2.8.5. The sample concentration of HER2 in 10mM sodium acetate pH 4.5 was 16.7μg/mL or 0.98μM. Immobilisation to a CM5 chip was achieved using the protocol described in Section 2.9.1.1, with a final immobilisation level of ~3200RU.

A 20μM sample of afucosylated trastuzumab was passed over the HER2-immobilised surface at a flow rate of 5μL/min for 180 seconds. The baseline in the Fc 2 channel before capture was 26,213RU and during the injection of afucosylated trastuzumab the response was 27,124RU. Once the injection of afucosylated trastuzumab was stopped, the response returned to 26,263RU.

2.9.1.5 Click Chemistry

3 x 500μL samples of heterogeneously-glycosylated trastuzumab and afucosylated trastuzumab were both diluted to 20μM in PBS (pH 7.4). An 8mL stock solution of 600μM bicyclo[6.1.0]nonyne (BCN) was made up in PBS. For both trastuzumab and afucosylated trastuzumab, 5, 10 and 15 molar equivalents of BCN (100μM, 200μM and 300μM respectively) were made up from the 600μM BCN stock solution and mixed with each of the 20μM antibody

74

samples. These mixtures were incubated at room temperature for 1 hour for conjugation of the BCN to the antibody.

Two PD-10 Desalting Columns from Cytiva™ (Massachusetts, USA) were used to remove excess unconjugated BCN from the samples (separate columns were used for trastuzumab and afucosylated trastuzumab samples). The same procedure was used for each column. Firstly, the cap was removed and the ethanol in the column was discarded. The column outlet tip was removed and the remaining liquid in the column was allowed to elute. The column was washed with 3 x 5mL washes of PBS, and then the 0.5mL sample was loaded onto the column. The lowest molar equivalent sample was loaded first. Once the sample had fully entered the bed, 1.5mL of PBS was applied to the column to push the sample to the bottom of the bed. Next, 1mL of PBS was applied to the column to elute the sample. The concentration of the eluted sample was measured by measuring A_{280} using an Amersham Biosciences Ultraspec 500 pro spectrophotometer (Slough, UK). The calculated sample concentrations based on the A_{280} readings equated to 3.3-3.8μM.

10μL of each of the six samples were incubated with 1μL of PEGylated azide at 37°C for 30 minutes. 10μL of Laemmli SDS reducing sample buffer (4X) from Thermo Fisher Scientific™ was incubated with each of these samples at 90°C for 5 minutes. Each 20μL sample was then loaded onto a reducing gel and run and imaged according to the protocol given in Section 2.8.1.

2.9.2 Deglycosylation of Protein Samples

Deglycosylation of both antibody and ligand constructs was carried out enzymatically. For the IgG1 samples, PNGase F was used. This deglycosylation of IgG1 was performed in order to test the affinity of the FcγRIIIa ligand constructs for deglycosylated IgG1 as a negative control for the binding experiments; it has been established previously that deglycosylation of IgG1 results in no interaction with FcγRIIIa (Geuijen et al., 2017; Hanson & Barb, 2015). PNGase F was sourced from New England Biolabs® Inc. (Massachusetts, USA) and the deglycosylation protocol was linearly scaled up based on the protocol provided by the manufacturer, although the reaction was carried out under non-denaturing conditions so that the antibody remained intact and could be used in subsequent SPR experiments. 120μL of antibody at a concentration of 4mg/mL (480μg total) was incubated with 20μL PNGase F at 37°C for 7 hours. The reaction mixture was removed from these conditions and stored at 4°C. PNGase F was not removed from the reaction mixture.

To prepare the deglycosylated FcγRIIIa D2 ligand construct, Endo H was used, which cleaves the β1,4 linkage between the two core GlcNAcs in the chitobiose core leaving a single GlcNAc attached to the Asn. Endo H was sourced from New England Biolabs® Inc. and the protocol was linearly scaled up based on the protocol provided by the manufacturer, although the reaction was again carried out under non-denaturing conditions so that the protein remained intact. To 500μL of FcγRIIIa D2 Man5 at a concentration of 0.116mg/mL (58μg of Man5), 14μL of 10X Glycobuffer 3 and 20μL of Endo H was added. The reaction mixture was incubated at 37°C on an orbital shaker at 100rpm for 90 minutes. The reaction mixture was then stored at 4°C. The Endo H enzyme was not removed from the reaction mixture.

2.9.3 Kinetics/Affinity Assays and Dissociation Constant Derivation

All binding studies were carried out on a Biacore™ X100 from Cytiva™ (Massachusetts, USA). Three CM5 chips were used; one with immobilised tocilizumab, one with immobilised deglycosylated tocilizumab and one with immobilised low-fucose tocilizumab. The ligand immobilisation levels for the chips were ~5500RU, ~3300RU and ~1600RU respectively. The analyte concentrations used are stated in the respective sensorgrams and the running buffer used was 1X PBS-P$^+$ with the composition as stated previously in this section.

The flow rate was set to 5μL/min. The assays were run in multi-cycle mode which meant that the chip was regenerated after each cycle. The assays began with three cycles of running buffer before the analyte at the specified concentrations was injected over the chip. The analyte concentrations began with a buffer-only control cycle. There was then another buffer-only control cycle after the first three analyte cycles (including the buffer-only cycle) and another penultimate buffer-only cycle after the largest analyte concentration and before the repeat cycle. Ligand was injected over the chip for 120 seconds and the dissociation time was 600 seconds. The regeneration solution used was 10mM Tris-hydrochloride (Tris-HCl) which was injected over the chip for 120 seconds. Caps were placed onto the sample tubes to prevent evaporation of sample during the assay.

All dissociation constant (K_D) values were obtained using the Biacore™ X100 Evaluation Software Version 2.0.1 Plus Package. All concentrations used in the assay were used to derive K_D unless otherwise stated. The Affinity – Steady State 1:1 model in the Biacore™ Evaluation Software (Biacore™ X100 Handbook BR-1008-10 Edition AB, Cytiva™, Appendix D) was used to derive K_D for each interaction studied. This model assumes a 1:1 interaction and calculates K_D from a plot of steady state binding values (R_{eq}) against analyte concentration

(C). The equation includes an offset for the bulk refractive index contributions (RI), which is assumed to be the same for all samples:

$$R_{eq} = \frac{C\,R_{max}}{K_D + C} + RI \quad (4)$$

where R_{eq} = steady state binding level (RU)

C = analyte concentration (μM)

R_{max} = analyte binding capacity of the surface (RU)

K_D = dissociation constant (μM)

RI = bulk refractive index contribution (RU)

Chapter 3 – FcγR Ligand Design and Construction

3.1 Introduction

Characterising glycosylation profiles during mAb manufacturing is an essential step in gaining regulatory approval for a drug. Levels of mannosylation, galactosylation, sialylation and fucosylation are particularly important as specified by the EMA due to the often significant impacts on drug pharmacokinetics, immunogenicity, serum half-life and overall clinical efficacy (Carillo et al., 2020). During biosimilar development, a manufacturer must match as closely as possible the glycosylation profile seen on the innovator molecule with the biosimilar, including fucosylation levels if ADCC is an effector function. Mass spectrometry (MS) is a well-established method of carrying out this sort of analysis, but this is time-consuming as it usually takes a significant amount of optimising and often cannot be carried out in-house. A faster method is to use affinity chromatography columns with ligands that are specific for certain glycans to carry out a separation of the sample. In the case of fucosylation, the only known column available that can carry out this sort of separation is an FcγRIIIa column.

FcγRIIIa is known to have a higher affinity for afucosylated IgG1 than for fucosylated IgG1. The K_D can be up to 40-fold lower, i.e. stronger, between FcγRIIIa and afucosylated IgG1 compared to its fucosylated counterparts (Shields et al., 2002; Shinkawa et al., 2003). FcγRIIIa has therefore been developed for use as an affinity ligand for the separation of fucosylated and afucosylated IgG1 (Bolton, Ackerman & Boesch, 2013). These ligands have been patented (US10221210B2) and have been shown to be effective at binding afucosylated IgG1, both in the literature and in work shown in Chapter 6.4.1. This resin is commercially known as the Glycap-3A™ resin and is available from Zepteon™ as either a 1mL or 5mL column.

Whilst these ligands work effectively, the FcγRIIIa is a relatively large protein (apparent molecular weight ~40-60kDa) made up of two separate domains and has a total of 5 glycosylation sites (see Figure 3.1). The potential for heterogeneity that this high degree of glycosylation causes is not ideal for affinity ligands. In addition, the dual-domain structure creates a large hydrodynamic radius, which could result in a lower ligand density and therefore a reduced separation efficiency compared to ligands with a smaller hydrodynamic radius.
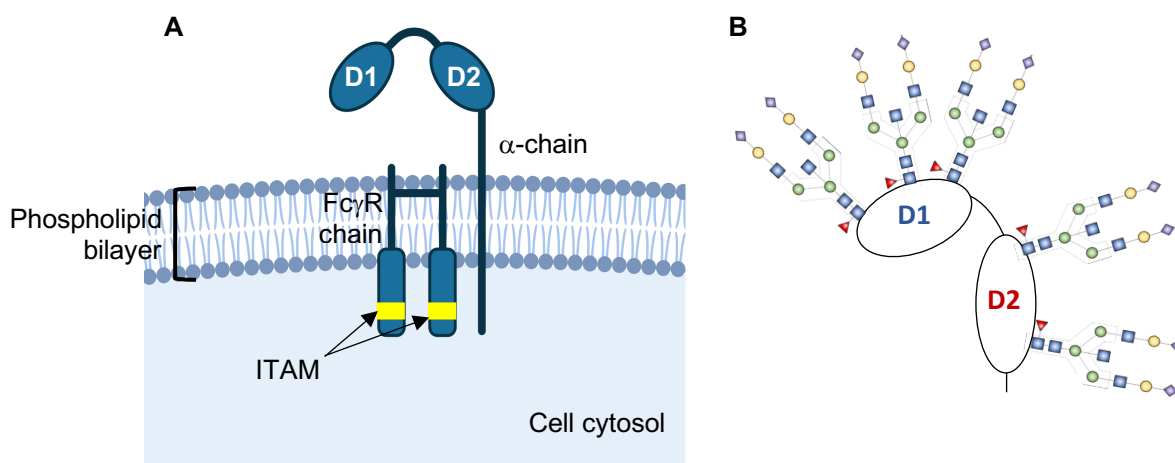
Figure 3.1 – FcγRIIIa. **A)** Depiction of FcγRIIIa embedded within the cell membrane. The receptor is made up of an α-chain containing two extracellular domains (D1 and D2) and the FcγR chain that interacts non-covalently with the α-chain and contains the ITAM. Figure created using Biorender.com. **B)** Schematic of the FcγRIIIa recombinantly expressed in mammalian cell culture showing the 5 glycosylation sites. The IgG binding site is on the D2 domain. This style of representation will be used to depict the FcγR ligands used in this work.

In an attempt to negate the heterogeneity issues caused by the high degree of glycosylation, FcγRIIIa has been recombinantly produced in an *E. coli* expression system. These ligands have a simpler and cheaper production process than the WT FcγRIIIa, which must be produced in mammalian cell culture. Due to the lack of cellular glycosylation machinery in *E. coli* cells, FcγRIIIa produced in this expression system is aglycosylated. Whilst this has the advantage of making the ligand structure less complex and more homogenous, it also removes the ability of the protein to differentiate between fucosylated forms of IgG1 (Kiyoshi et al., 2018). These aglycosylated ligands therefore do not perform the same separation of fucosylated and afucosylated IgG1 as an FcγRIIIa resin does.

Our aim was to design affinity ligands based on the FcγRIIIa which retain the ability of FcγRIIIa to differentiate between fucosylated and afucosylated IgG1 whilst removing the complexity of manufacturing these ligands in a mammalian system and reducing the potential for heterogeneity in their structure. This chapter will show the modelling work which has been carried out to explain current theories behind the differential affinity of FcγRIIIa for fucosylated and afucosylated IgG1 and the design of the engineered FcγR ligands, along with the rationale behind these design choices.

3.2 Hypotheses Behind Differential Affinity for Fucosylated and Afucosylated IgG1

The IgG1-FcγRIIIa interaction has been widely demonstrated to largely depend on the glycosylation patterns of both IgG1 and FcγRIIIa, with one of the most significant heterogeneities in glycosylation that gives rise to differential affinity of the receptor for the mAb being the removal of a core fucose on the glycan attached to Asn297 of the IgG1 Fc region (Zahavi et al., 2018). Not only does the presence of this core fucose have an effect on the affinity of the mAb for the receptor and on ADCC effector function, but it also affects the overall 3D structure of IgG1. Computational structural analyses of the IgG1-FcγRIIIa complex reveal that there are certain residues in the binding site of FcγRIIIa that are important for binding the mAb, and indeed one in particular (Lys128) which could be pivotal in differentiating between the binding of afucosylated and fucosylated IgG1 (see Figure 3.2).

3.2.1 FcγRIIIa Residues Involved in Binding IgG1

Investigation using the molecular visualisation software PyMOL reveals that the residues that comprise the binding site of FcγRIIIa for IgG1 Fc seem to be Lys120, Gly127, Lys128, Gly129, Arg130, Lys131, Tyr132, His134 and His135 (see Figure 3.2). One residue in particular that has been reported to be of interest when elucidating the discrepancy between the binding of afucosylated and fucosylated IgG1 is Lys128. When afucosylated IgG1 is bound to FcγRIIIa, a tyrosine residue in IgG1 (Tyr296) is angled more towards the FcγRIIIa binding site, in particular towards Lys128. The terminal amine group on Lys128 is likely to form a hydrogen bond or electrostatic interactions with the oxygen of the C=O (carbonyl group) on Tyr296. The pKa of a lysine side chain is normally around 10.5 (Oregioni et al., 2017), meaning that at any pH below this, which includes physiological pH, the terminal amine group is always protonated and so exists as NH_3^+ (protonated amine). According to PyMOL, the distance between the protonated amine of Lys128 and the carbonyl on Tyr296 is 2.8Å (see Figure 3.3A). Hydrogen bonds are typically strong and 2.7-3.2Å in length (Zhou & Wang, 2019), so this distance of 2.8Å is consistent with that of a hydrogen bond.
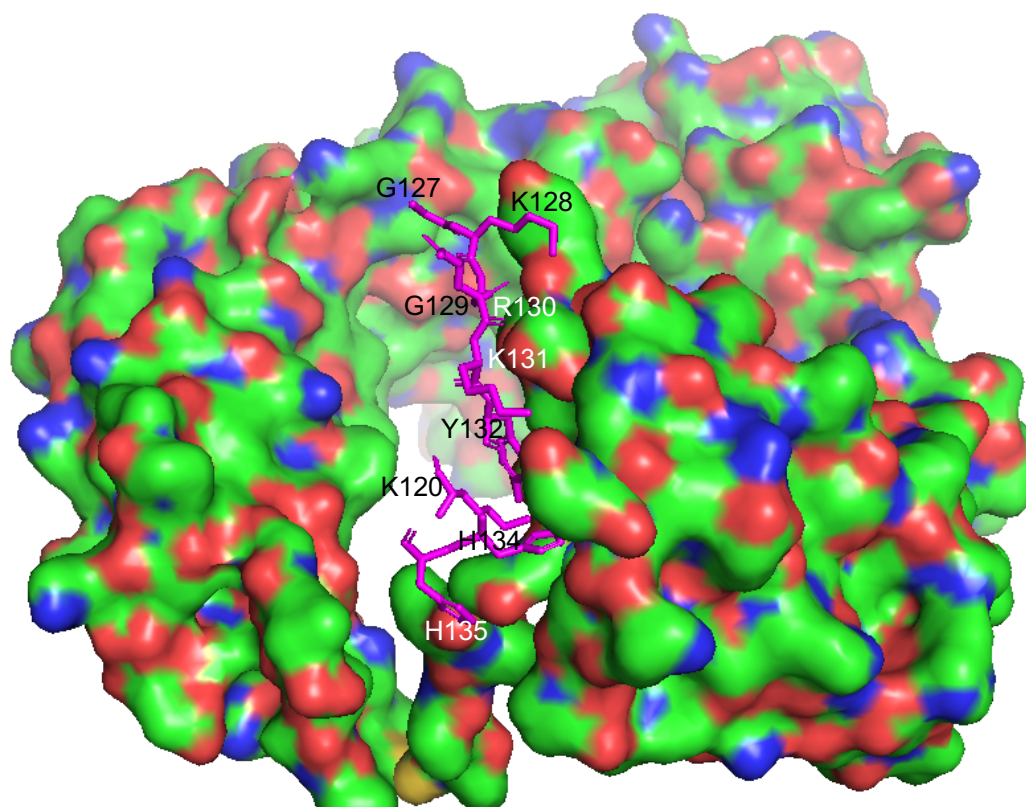
Figure 3.2 – residues from FcγRIIIa within the binding interface of IgG1 Fc and FcγRIIIa. FcγRIIIa residues are labelled and depicted in magenta, and the IgG Fc chains are shown in the Surface representation in green, red and blue (carbon, oxygen and nitrogen respectively). The rest of the FcγRIIIa peptide chain and the IgG glycans are not shown for clarity. Figures constructed using PyMOL (PDB code: 3AY4).

The presence of the core fucose has a profound effect not only on the 3D structure of IgG1, but also on the 3D structure of the entire IgG1-FcγRIIIa complex. It is thought that there are two main mechanisms which govern the differential affinity of the two mAb glycoforms for FcγRIIIa. These are the proximity of the interacting glycans (attached to Asn297 of the IgG1 Fc region and Asn162 of FcγRIIIa), and the flipping of a tyrosine residue (Tyr296) on IgG1.

3.2.2 IgG1 and FcγRIIIa Glycan Proximity

One of the main mechanisms that mediates the differential affinities of afucosylated and fucosylated IgG1 for FcγRIIIa is thought to be steric hindrance of the interacting glycans (Ferrara et al., 2006). This has only ever been postulated to be the case for IgG1 and WT FcγRIIIa with mammalian complex-type glycosylation. The glycans on Asn297 of the IgG1 Fc region and Asn162 of FcγRIIIa directly interact in the binding site of the IgG1-FcγRIIIa complex, and when IgG1 is fucosylated, the fucose residue protrudes into the space that the FcγRIIIa Asn162 glycan occupies. This creates steric clash between the two glycans and prevents the

two molecules from getting into close proximity with each other, which could result in the reduction in binding strength of fucosylated IgG1 to FcγRIIIa. When the fucose residue is not present on the glycan attached to Asn297 of the IgG1 Fc region, this steric hindrance is reduced and the two molecules can get closer together, which could increase the strength of the binding between afucosylated IgG1 and FcγRIIIa (see Figure 3.2).
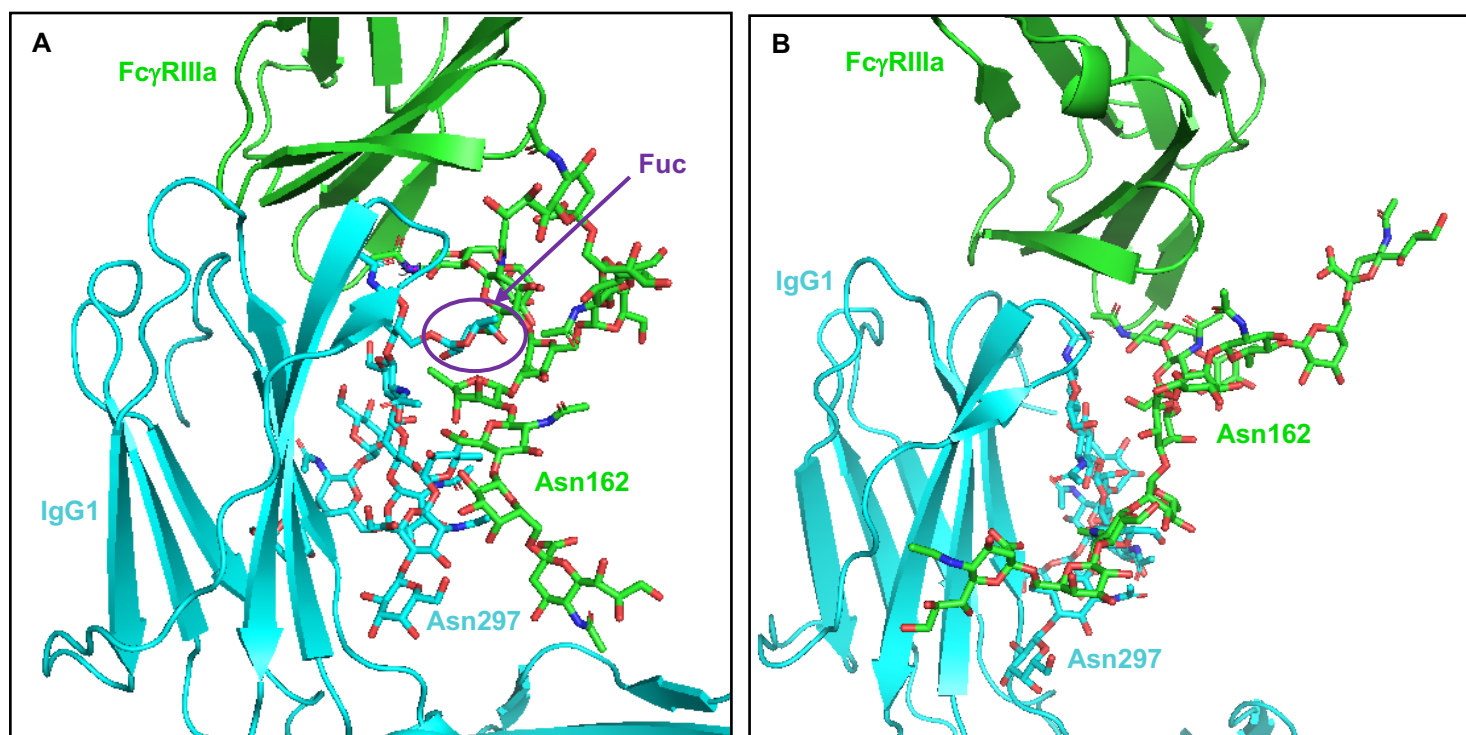
Figure 3.3 – **A)** comparison of the glycan interaction between fucosylated IgG1-FcγRIIIa and **B)** afucosylated IgG1-FcγRIIIa. IgG1 and its associated glycan attached to Asn297 of the Fc region are shown in cyan and FcγRIIIa and its associated glycan attached to Asn162 are shown in green. The fucose residue in Figure 3.2A is circled in purple. Figures constructed using PyMOL (PDB code for A: 5XJF, PDB code for B: 3AY4).

From Figure 3.3A, the distortion that the fucose creates in the IgG1-FcγRIIIa complex can be seen, particularly in terms of glycan steric hindrance. In Figure 3.2B, the glycan attached to FcγRIIIa is inclined more towards the IgG1 and is physically much closer than in Figure 3.3A. In the fucosylated structure, the fucose residue protrudes from the rest of the glycan and creates steric clash with the glycan on FcγRIIIa, angling it away from IgG1. This change is thought to be a significant contributing factor to the discrepancy in affinity between these two IgG1 glycoforms for FcγRIIIa.

3.2.3 Flipping of Tyr296 on IgG1

In the complex of fucosylated IgG1 with FcγRIIIa, molecular modelling suggests that there is a 'flipping' of Tyr296 of IgG1 when a core fucose residue is present in the glycan on Asn297 compared to when this glycan is afucosylated (Li et al., 2018). In the afucosylated IgG1-FcγRIIIa structure, Tyr296 of IgG1 is inclined much more towards FcγRIIIa, and a hydrogen bond could be formed between Lys128 and Tyr296 (see Figure 3.4A). In the fucosylated IgG1-FcγRIIIa structure, Tyr296 flips away from FcγRIIIa and the protonated amine of Lys128 is also angled away from Tyr296 (see Figure 3.4B).
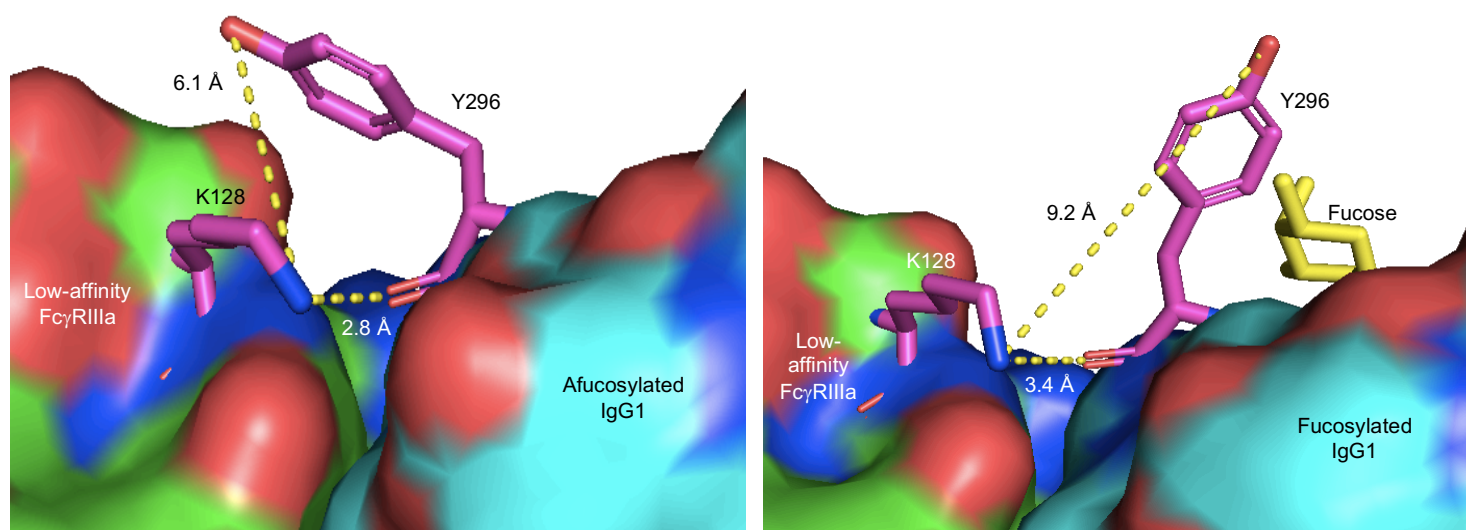
Figure 3.4 – **A)** Tyr296 (Y296) of afucosylated IgG1 interacting with Lys128 (K128) of FcγRIIIa low-affinity variant (F158). The two residues (shown in magenta) likely interact via a hydrogen bond between the terminal protonated amine of K128 and the carbonyl of Y296 (yellow dashed line, 2.8Å). The other labelled distance of 6.1Å, between the terminal protonated amine of K128 and the terminal hydroxyl group of Y296, has been included to illustrate the 'flipping' that Y296 undergoes between the fucosylated and afucosylated forms of IgG1 in complex with FcγRIIIa (see Figure 3.4B) Figure created using PyMOL (PDB: 3AY4). **B)** Y296 of fucosylated IgG1 interacting with K128 of FcγRIIIa F158 (low-affinity variant). The presence of the fucose on the glycan attached to Asn297 of IgG1 causes the side chain of Y296 to become angled away from K128 and the FcγRIIIa. The distance between the terminal protonated amine of K128 and the terminal hydroxyl group of Y296, which was 6.1Å in Figure 3.4A, increases to 9.2Å. The distance between the terminal protonated amine of K128 and the carbonyl group of Y296 increases from 2.8Å (see Figure 3.4A) to 3.4Å, which is outside of the range for a hydrogen bond (2.7Å – 3.2Å, Zhou & Wang, 2019). Figure created using PyMOL (PDB: 5XJF).

The loss of the hydrogen bond in the fucosylated IgG1-FcγRIIIa compared to the afucosylated complex could contribute to the reduction in affinity for FcγRIIIa of the fucosylated compared to the afucosylated IgG1. For the high-affinity variant of FcγRIIIa (V158), the distance between the terminal protonated amine of K128 and the terminal hydroxyl group of Y296 is 9.5Å for the

fucosylated IgG1, but all other measurements displayed on Figures 3.4A and B are the same distance for FcγRIIIa V158 (high-affinity variant) as they are for FcγRIIIa F158 (see Section 3.5 for explanation of variant differences).
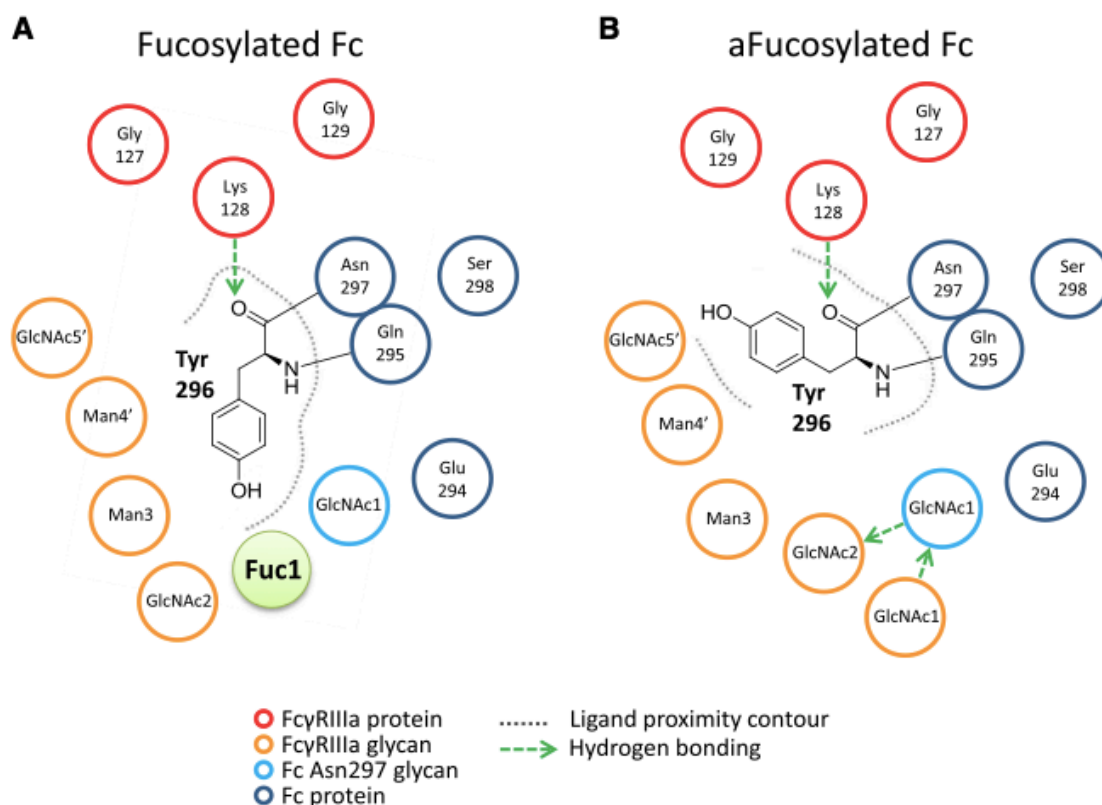
Figure 3.5 – schematic of interaction between **A)** fucosylated and **B)** afucosylated IgG1 Fc in the binding site of FcγRIIIa. When the fucose is not present, the flipping of Tyr296 towards the FcγRIIIa protein and away from the Fc, in particular the Fc Asn297 glycan, can be seen. Figure produced using Molecular Operating Environment (MOE) and taken from Li, J., Hsu, H.-C., Mountz, J. D., & Allen, J. G. (2018). Unmasking fucosylation: from cell adhesion to immune system regulation and diseases. *Cell Chemical Biology.*

3.3 Rationale for FcγR Ligand Design

The characteristics that have been engineered into the FcγR ligands used in this work and the reasons behind these design choices are detailed below.

3.3.1 Single Domain Structure

As shown in Figure 3.1, the FcγRIIIa α-chain has a dual-domain structure and is a relatively large protein. The binding site for IgG1 is on the D2 domain of FcγRIIIa (see Figure 3.6), meaning it is necessary for affinity ligands based on this protein to contain this domain. Our ligands are comprised of only the D2 binding domain, which makes for a ligand with a smaller

hydrodynamic radius compared to the dual-domain protein. This could allow for an increased ligand density on a resin, which would result in more available binding sites for IgG1 and therefore an improved separation efficiency compared to a WT FcγRIIIa resin. To our knowledge, the single-domain D2 FcγRIIIa has not yet been successfully expressed before in either mammalian, bacterial or yeast cell culture before this work.
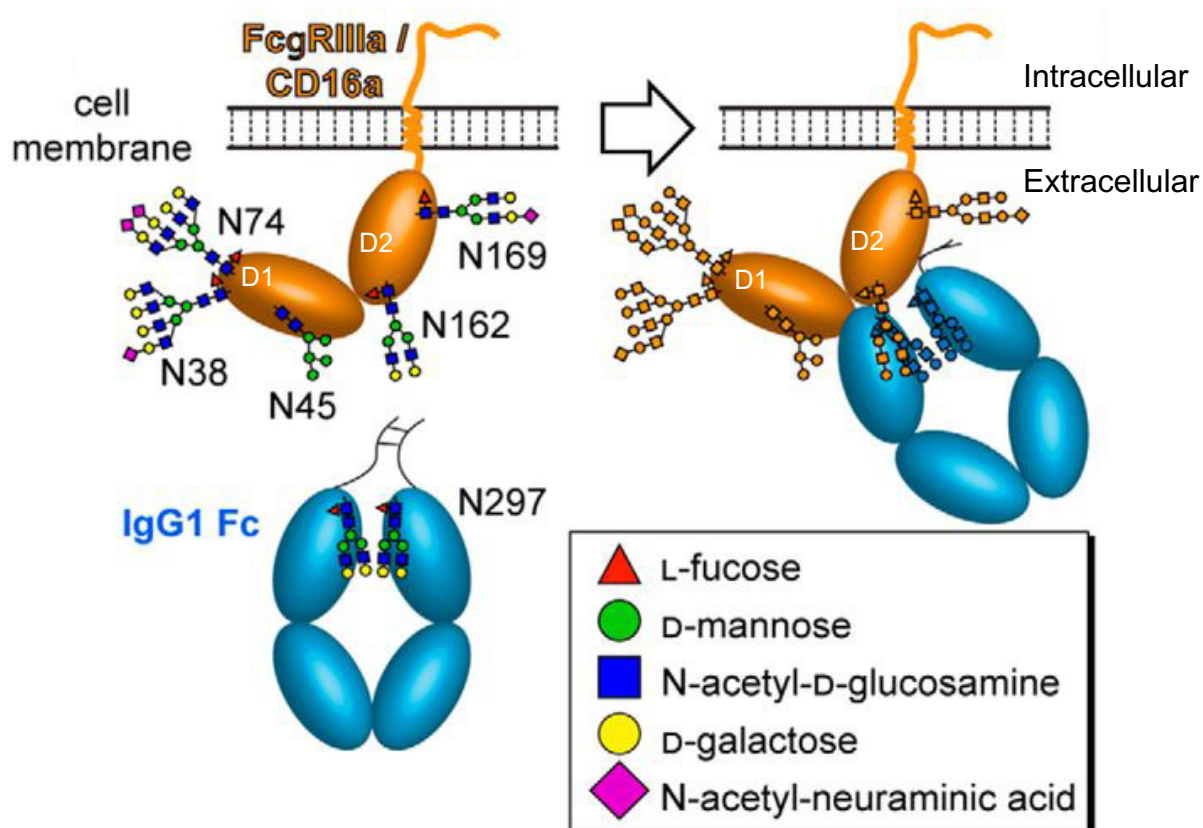
Figure 3.6 – membrane-bound FcγRIIIa, also known as CD16a, in complex with IgG1 Fc. The D2 domain interacts directly with the IgG1 Fc. Binding also directly involves the glycans at Asn162 on the D2 domain and Asn297 on the IgG1 Fc. Adapted from Subedi, G.P. & Barb, A.W. (2018) CD16a with oligomannose-type N-glycans is the only "low-affinity" Fc γ receptor that binds the IgG crystallizable fragment with high affinity *in vitro*. *Journal of Biological Chemistry*.

3.3.2 Monoglycosylation

The FcγRIIIa D2 domain possesses two glycosylation sites at Asn162 and Asn169 (see Figure 3.6). It has been reported by multiple sources that the glycan at Asn162 is directly involved in modulating affinity for fucosylated and afucosylated IgG1 (Falconer et al., 2018; Ferrara et al., 2011; Isoda et al., 2015; Mizushima et al., 2011). In order for our ligand constructs to retain the ability of the FcγRIIIa to differentiate between fucosylated and afucosylated IgG1, we assumed based on this knowledge that it would be necessary to retain the glycan at position Asn162 in the D2 domain. However, to reduce some of the complexity and potential for

heterogeneity in the ligand molecule, the glycan at position Asn169 has been removed so that the ligands are monoglycosylated.

3.3.3 Yeast Expression System

The dual-domain FcγRIIIa is recombinantly and transiently expressed in HEK-293 cells for the manufacture of the Glycap-3A™ resin (Bolton, Ackerman & Boesch, 2013). Our FcγR ligands are expressed in a *P. pastoris* expression system as it is cheaper and often simpler to carry out than mammalian cell culture. *P. pastoris* is still capable of carrying out post-translational modifications in a similar way to mammalian systems, including glycosylation, which is important for the functionality of these ligands, although *P. pastoris* creates mannose-based glycans rather than complex glycans. *P. pastoris* possesses a secretory pathway, meaning that our proteins of interest are secreted. This avoids a cell disruption step which would complicate the ligands' production and place a burden on subsequent downstream processing.

3.4 FcγR Ligand Constructs

Based on this design rationale, the following FcγR ligand constructs were designed. Sequence design and cloning was carried out by Dr. Maria Livanos.

3.4.1 FcγRIIIa D2 Man9

FcγRIIIa D2 Man9 was the first construct developed in this work. As mentioned above, it consists of the D2 binding domain of FcγRIIIa and possesses a single glycosylation site at Asn162, which directly interacts with IgG1 and is thought to be at least partially responsible for the protein's selectivity between fucosylated and afucosylated IgG1. The gene for FcγRIIIa D2 Man9 was cloned into a pPICZαB plasmid which was transfected into both Mut[+] and Mut[S] strains of *P. pastoris*, however the majority of the cell cultures in this work were conducted using the Mut[+] strain as this was the protease-deficient strain. The mass spectrometry characterisation of this construct is shown in Figures 5.14 and 5.15. As shown in Figure 5.14, there is extensive hypermannosylation seen on this construct, with branching up to Man16 at the *N*-glycan site. The most abundant glycan pattern at this site on this construct is Man9, hence the nomenclature.
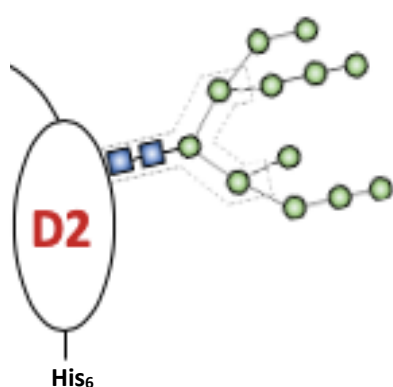
Figure 3.7 – pictorial representation of the FcγRIIIa D2 Man9 construct. The single domain structure (D2) is represented by the oval structure, which is normally linked to the D1 domain by the top black curved line in FcγRIIIa. The single *N*-glycan is represented using the Symbol Nomenclature for Glycans (see Table 1.1). The majority of *N*-glycans at this site are of the Man9 structure, although the degree of mannosylation varies between individual molecules. There is also *O*-glycosylation present on this protein.

3.4.2 FcγRIIIa D2 Man5

FcγRIIIa D2 Man5 was the second construct developed. The same pPICZαB plasmid was cloned into a strain of *P. pastoris* called GlycoSwitch™ SuperMan5-10 (BioGrammatics Inc., CA, United States). The maximum structure that can be produced in the SuperMan5-10 strain is Man10 (Pekarsky et al., 2018). The mass spectrometry characterisation of this construct is shown in Figure 5.18.
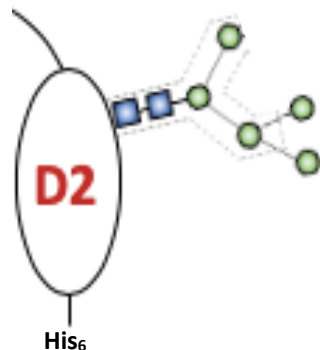
Figure 3.8 – pictorial representation of the FcγRIIIa D2 Man5 construct. Again, the D2 domain is represented by the oval structure and the single *N*-glycan is represented using the Symbol Nomenclature for Glycans. Glycans at this site will be of the Man10 structure or smaller due to the genetic modification in the glycosylation pathway of the host expression system. This protein is also expected to carry *O*-linked glycosylation, although a reduced degree compared to Man9.

3.4.3 FcγRIIIa D2

This construct is the single D2 domain with no *N*-glycosylation apart from a single GlcNAc at the *N*-glycan site. To prepare this construct, FcγRIIIa D2 Man5 was treated with Endo H. This enzyme cleaves the β1,4 glycosidic bond between the two GlcNAcs in the chitobiose core, removing the majority of the *N*-linked glycan on the D2 and leaving a single GlcNAc at this site. *O*-linked glycans are not cleaved and therefore remain attached to the protein.

Figure 3.9 – pictorial representation of the FcγRIIIa D2 construct. Again, the D2 domain is represented by the oval structure. At the site where the single *N*-glycan is normally present, a single GlcNAc residue is present. This is a result of the enzymatic digestion of FcγRIIIa D2 Man5 using EndoH.

3.5 Construct Sequences

Low-affinity WT Human FcγRIIIa

Below is the sequence provided in the UniProt database for the low-affinity human FcγRIIIa (accession number P08637) with the signal peptide highlighted in orange.

```
1          11         21         31         41
MWQLLLPTAL LLLVSAGMRT EDLPKAVVFL EPQWYRVLEK DSVTLKCQGA

51         61         71         81         91
YSPEDNSTQW FHNESLISSQ ASSYFIDAAT VDDSGEYRCQ TNLSTLSDPV

101        111        121        131        141
QLEVHIGWLL LQAPRWVFKE EDPIHLRCHS WKNTALHKVT YLQNGKGRKY

151        161        171        181        191
FHHNSDFYIP KATLKDSGSY FCRGLFGSKN VSSETVNITI TQGLAVSTIS

201        211        221        231        241        251
SFFPPGYQVS FCLVMVLLFA VDTGLYFSVK TNIRSSTRDW KDHKFKWRKD PQDK
```

Figure 3.10 – sequence 1, depicting the sequence provided in the UniProt database for the low-affinity variant of human FcγRIIIa. The signal peptide is highlighted in orange, the *N*-glycosylation sites are highlighted in purple, and the Phe/F residue, which makes this the low- rather than the high-affinity variant of FcγRIIIa, is highlighted in green. The high-affinity variant contains a Val/V residue instead of Phe/F at this site.

Theoretical molecular weight: 29.1kDa

Predicted isoelectric point (pI): 8.20

The low- and high-affinity FcγRIIIa variants are characterised by a single nucleotide polymorphism (SNP) from T to G at position 559 in the *FCGR3A* gene. This results in a substitution from phenylalanine (Phe, F) to a valine (Val, V) at position 158 in the primary sequence if excluding the signal peptide, 176 if including it (Amiah et al., 2020). In order to maintain consistency with the literature, sequence positions in the rest of this document will be referred to in terms of the protein sequence excluding all signal peptides, for example F158 or V158. This position is highlighted in green in Sequence 1. In the sequences for the ligand constructs provided below, any remaining amino acid residues from the signal peptide will be highlighted in orange, and the V or F will be highlighted in green at position 158.

There are 5 glycosylation sites on FcγRIIIa highlighted in magenta at Asn56, 63, 92, 180 and 187 according to the full sequence; these positions are 38, 45, 74, 162 and 169 without the signal peptide, which is how they are described throughout the literature. The molecular weights and pIs for all constructs were predicted using the online 'Compute pI/Mw' tool from Expasy and are therefore theoretical values.

FcγRIIIa Reference Ligand Construct (refFcγRIIIa)

```
1          11         21         31         41
GMRTEDLPKA VVFLEPQWYR VLEKDSVTLK CQGAYSPEDN STQWFHNESL

51         61         71         81         91
ISSQASSYFI DAATVDDSGE YRCQTNLSTL SDPVQLEVHI GWLLLQAPRW

101        111        121        131        141
VFKEEDPIHL RCHSWKNTAL HKVTYLQNGK GRKYFHHNSD FYIPKATLKD

151        161        171        181
SGSYFCRGLF GSKNVSSETV NITITQgggs HHHHHHC
```

Figure 3.11 – sequence 2, depicting the sequence of refFcγRIIIa, the recombinant version of FcγRIIIa produced in CHO-S used primarily for binding assay establishment. The remainder of the signal peptide is shown in orange, the *N*-glycosylation sites are highlighted in purple, and the Phe/F residue is highlighted in green.

Theoretical molecular weight: 21.4kDa

Predicted pI: 6.70

This construct was transiently expressed in CHO-S and used as the reference for binding assay establishment. The sequence starts at position 17 of Sequence 1, removing the majority of the signal peptide, and ends at position 192. The five glycosylation sites are highlighted in magenta and the F158 SNP is highlighted in green.

A 6xHis tag was added to the C-terminus of each of the four proteins used in this work to aid purification. The tags were attached to the C-termini via a Gly-Gly-Gly-Ser linker so that the activity of the protein was less likely to be affected by the addition of the tag. In addition, a cysteine residue was added to the end of the 6xHis tag.

FcγRIIIa D2, FcγRIIIa D2 Man9 and FcγRIIIa D2 Man5

```
1          11         21         31         41
HIGWLLLQAP RWVFKEEDPI HLRCHSWKNT ALHKVTYLQN GKGRKYFHHN

51         61         71         81         91
SDFYIPKATL KDSGSYFCRG LVGSKNVSSE TVQITITQgg gsHHHHHHC
```

Figure 3.12 – sequence 3, depicting the sequence for FcγRIIIa D2, FcγRIIIa D2 Man9 and FcγRIIIa D2 Man5. At the position in this sequence (72) that corresponds to 158 in the native FcγRIIIa sequence, there is a Val/V residue rather than a Phe/F, which is highlighted in green. The single *N*-glycan site is highlighted in purple and a substitution from N to Q has been made, which is highlighted in red at position 83 in this sequence.

Theoretical molecular weight: 11.4kDa
Predicted pI: 9.47
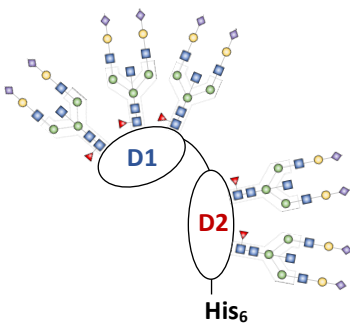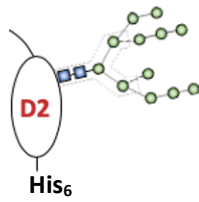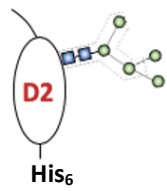
The primary sequence is the same for FcγRIIIa D2, FcγRIIIa D2 Man9 and FcγRIIIa D2 Man5; the constructs differ only in their *N*-glycan patterns at Asn162 and possibly also in their *O*-glycosylation patterns. This sequence starts at position 105 and ends at 192 of Sequence 1. Val158 (position 72 in Sequence 3) is highlighted in green. This amino acid substitution confers the high-affinity phenotype in WT FcγRIIIa. The glycosylation site at Asn162 (position 76 in Sequence 3) is highlighted in magenta, and a mutation has been made that substitutes Asn169 (Asn83 in Sequence 3) for a glutamine (Glu, Q). This is to remove the potential for *N*-linked glycosylation at this site, ensuring that the final proteins will only possess the one *N*-linked glycan at Asn76. The plasmid maps for these ligand constructs are shown in Appendix 9.1.

3.6 Summary of FcγR Ligands

A summary table of our novel FcγR ligands and their characteristics is provided below.

Table 3.1 – summary of the FcγR ligand constructs and their properties.

Construct	FcγRIIIa Reference	FcγRIIIa D2 Man9	FcγRIIIa D2 Man5	FcγRIIIa D2
Shorthand Name	refFcγRIIIa	Man9	Man5	D2
Structure				
Domain(s)	Dual domain (D1 and D2 domains)	Single (D2 binding domain only)	Single (D2 binding domain only)	Single (D2 binding domain only)
Glycosylation	Complex-type *N*-glycosylation at up to 5 sites (N38, N45, N74, N162, N169)	Monoglycosylated (*N*-linked) at N162, hypermannosylated. Also some *O*-linked	Monoglycosylated at N162, Man5-10. Also some *O*-linked	Deglycosylated (single GlcNAc remaining at N162). *O*-linked glycosylation pattern of Man5
Expression system	CHO-S transient expression	Bg25 *P. pastoris* (Mut⁺)	SuperMan5-10 *P. pastoris*	Bg25 *P. pastoris* (Mut⁺)

Chapter 4 – Attempts to Produce FcγR Ligands using Fermentation

4.1 Introduction

Yeast expression systems are widely used in the biotechnology sector to produce a variety of recombinant proteins for vaccine or biopharmaceutical production. *S. cerevisiae*, for instance, is used for the production of the hepatitis B and human papillomavirus vaccines (Bill, 2015). More recently, *P. pastoris* has become a popular choice for recombinant protein production for a range of applications. *P. pastoris* is a methylotrophic yeast, meaning it can survive solely on methanol as its carbon and energy source (Karbalaei, Rezaee & Farsiani, 2020). Its wide usage can be primarily attributed to three factors; the AOX1 promoter, which is induced by methanol and results in strong expression of recombinant proteins; its ability to grow to high cell densities during fermentative growth; and its similarity to *S. cerevisiae* in terms of molecular biology-based tools used for cloning (Cregg, 2022). In addition, *P. pastoris* is low cost, possesses a secretory pathway and is able to glycosylate proteins. *P. pastoris* can achieve high cell densities during fermentation using low-cost media, which makes it an ideal expression system for large scale fermentations (Liu et al., 2016).

However, despite the various merits of *P. pastoris* as an expression system for recombinant protein production, it is also known for producing a number of proteolytic enzymes which can degrade heterologous proteins. Whilst these proteases are still produced in shake flask cultures, their rate of production increases significantly in high cell density bioreactor cultures, which negatively impacts recombinant protein production. Various methods have been researched with the aim of mitigating this degradation, such as developing protease-deficient *P. pastoris* strains, manipulating pH conditions in the bioreactor and adding protease inhibitors to cultures (Zhang, Liu & Wu, 2007).

In the previous chapter, the design rationale behind the FcγR ligands was detailed and their characteristics were described. It was explained that a *P. pastoris* expression system was selected for FcγR ligand production due to its ability to glycosylate, its secretory pathway and its low cost and ease of culture compared to mammalian expression systems, such as CHO or HEK-293. In this chapter, attempts to produce the FcγR ligands using fermentation are detailed, as well as mitigation strategies used to try and reduce the effects of proteolytic degradation.

4.2 Results

The results from both the small- and large-scale fermentations are detailed in this section.

4.2.1 Small-Scale Fermentations

Initial shake flask cultures to produce the FcγRIIIa D2 Man9 and FcγRIIIa D2 Man5 (Man9 and Man5) constructs showed that the titre obtained from these cultures was low (see Figure 4.1). In order to generate enough product for mass spectrometric characterisation, binding studies and potentially immobilisation to a resin for chromatographic separation, upwards of ~10mg of each ligand construct would be needed. Logically, it was decided that fermentation would be used to produce this amount of protein.
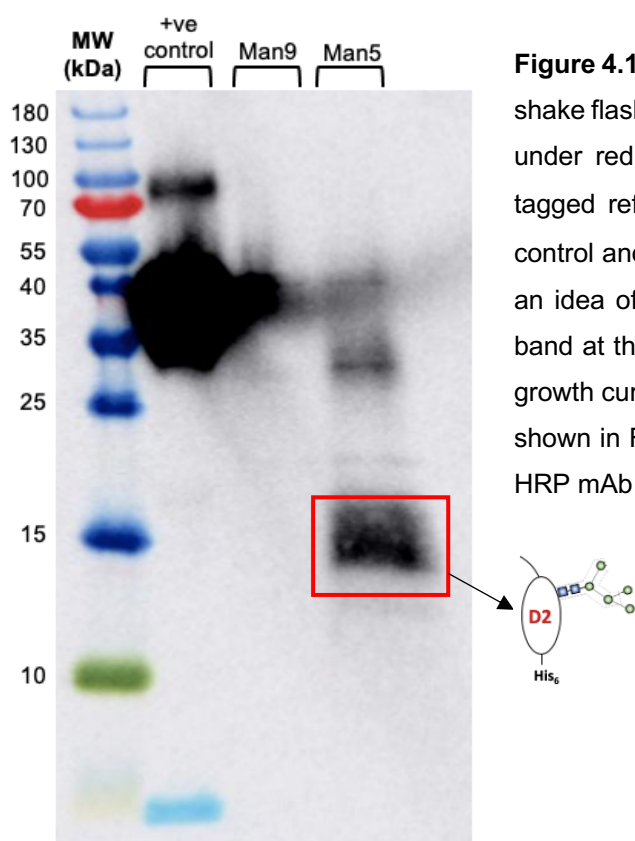
Figure 4.1 – Western blot analysis showing the harvest from initial shake flask studies to produce the Man9 and Man5 constructs, run under reducing conditions. The positive control used was His-tagged refFcγRIIIa at a concentration of 150μg/mL. 5μL of the control and 15μL of sample was loaded onto the gel, which gives an idea of the low titre obtained from shake flask cultures. The band at the expected molecular weight for Man5 is labelled. The growth curves for the cultures that gave rise to these samples are shown in Figure 4.2. The antibody used was Bio-Techne polyHis HRP mAb clone AD.1.1.10, an anti-His antibody.
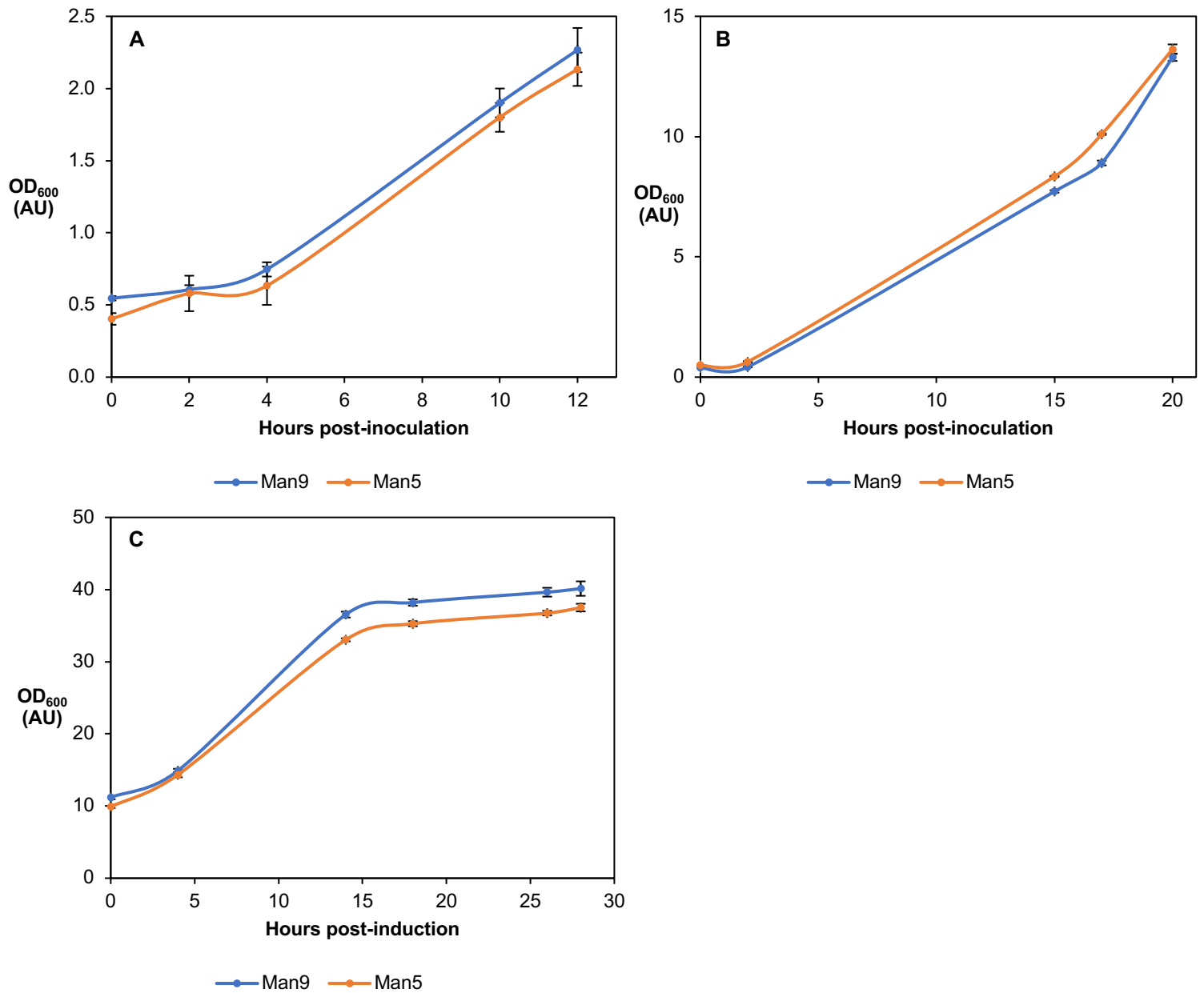
Figure 4.2 – growth curves of the shake flask cultures producing Man9 using Mut[+] Bg25 *P. pastoris* and Man5 using GlycoSwitch™ SuperMan5-10 (n = 3). The Western blot analysis of the harvest from these cultures is shown in Figure 4.1. **A)** The first BMGY growth phase (first glycerol batch phase), which inoculated 0.2mL of each cell glycerol stock (OD_{600} ~18AU) into 2 x 500mL baffled shake flasks containing 100mL BMGY. These were grown at 30°C in a shaking incubator at 180rpm. **B)** The second BMGY growth phase (second glycerol batch phase), which inoculated 10mL from the cultures in the 500mL flasks into 190mL BMGY in 2 x 1L baffled shake flasks. These were grown at 30°C, 180rpm. **C)** The BMMY growth phase (induction). The cultures from the 1L flasks were centrifuged and the pellet was resuspended in BMMY. 20mL of this resuspension was inoculated into 2 x 1L baffled shake flasks containing 180mL BMMY and the culture was grown until OD_{600} ~40AU was reached (28 hours, 30°C, 200rpm).

It is clear from Figure 4.1 that the titre from shake flask cultures would not be sufficient for production of protein in the region of ~10mg, despite high cell densities being reached according to the growth plot shown in Figure 4.2C. It was therefore decided, based on these results and other similar results, that scaling up to fermentation in bioreactors would be a good option to produce a larger amount of product.

For initial process characterisation, small-scale fermentations were carried out at the 250mL scale using the Dasgip® Parallel Bioreactor System. Initial fermentations were carried out based on the Invitrogen™ protocol ('Pichia Fermentation Process Guidelines', Version B). The conditions set out in the Invitrogen™ protocol and those that were used for the first fermentation study for initial process characterisation are shown in Table 4.1.

Table 4.1 – conditions and parameters recommended by Invitrogen™ for *P. pastoris* fermentation and those used in the first fermentation to produce Man9 using a Mut^S strain (see Figure 4.3 for traces and growth plot for this fermentation). The fermentation was carried out in 250mL Dasgip® bioreactors. The methanol fed-batch phase was initially planned to be ~100 hours as designated in the Invitrogen™ protocol, however there was a drop in agitation at ~62 hours post-induction, indicating cell death. The reactors were therefore harvested at ~75 hours post-induction. The pH was raised to 6.5 post-induction as the product is not stable at pH 5.0.

Parameter	Invitrogen™ Guidelines	First Fermentation Study
OD$_{600}$ of inoculum for fermenter inoculation (AU)	2-6	6
Inoculum volume	10% of initial media volume	10mL (10% of initial media volume)
Medium	Fermentation basal salts medium	Fermentation basal salts medium (100mL)
DO setpoint (%)	>20	30
pH pre-induction	5.0	5.0
Temperature (°C)	30	30
Agitation (rpm)	500-1500	400-1200 (cascade control)
Aeration (vvm)	0.1-1.0	0.5-6.0 (cascade control)
Length of glycerol batch phase (hrs)	18-24	20
Length of glycerol fed-batch phase (hrs)	~4	4
Length of methanol fed-batch phase (hrs)	~100	75
pH post-induction	5.0	6.5
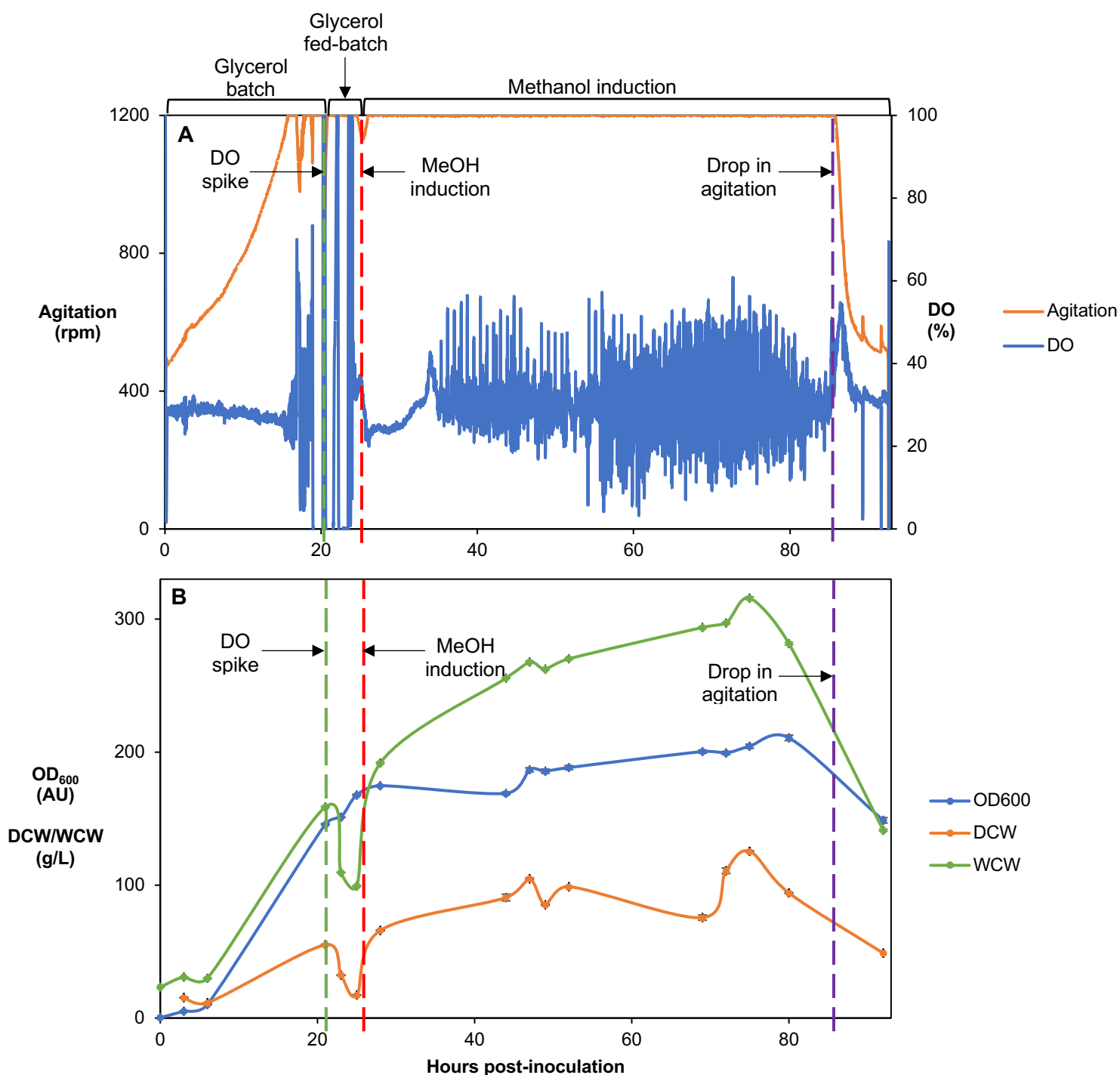
Figure 4.3 – **A)** fermentation trace from one 250mL vessel of a small-scale fermentation run using the Dasgip® Parallel Bioreactor to produce Man9 using Bg11 (Mut^S) *P. pastoris*. The glycerol batch phase lasted for 20 hours, followed by a 4-hour batch phase, meaning that methanol induction occurred at 24 hours post-inoculation. At 85 hours post-inoculation (62 hours post-induction), the agitation rate began to drop below 1200rpm. **B)** Growth plot from the fermentation shown in panel A (n = 3). A drop in WCW and DCW was seen at the 80-hour post-inoculation timepoint, 57 hours post-induction. Harvesting took place at 94 hours post-inoculation, after methanol had been fed for 70 hours.

The DO is maintained at or below the setpoint of 30% by controlling the agitation. The faster the cells are growing, the faster they consume oxygen, and therefore a faster oxygen transfer to the cells is required. A faster oxygen transfer is achieved by increasing the agitation rate. The drop in agitation at 62 hours post-induction seen in Figure 4.3A signifies that a lower agitation rate is required to maintain the DO setpoint, so oxygen is being consumed by the culture at a lower rate. This is indicative of cell death. Another fermentation study was carried out using the GlycoSwitch® SuperMan5-10 strain, a Mut$^+$ *P. pastoris* strain, to see if the same effect was seen with this cell line (see Figure 4.4).
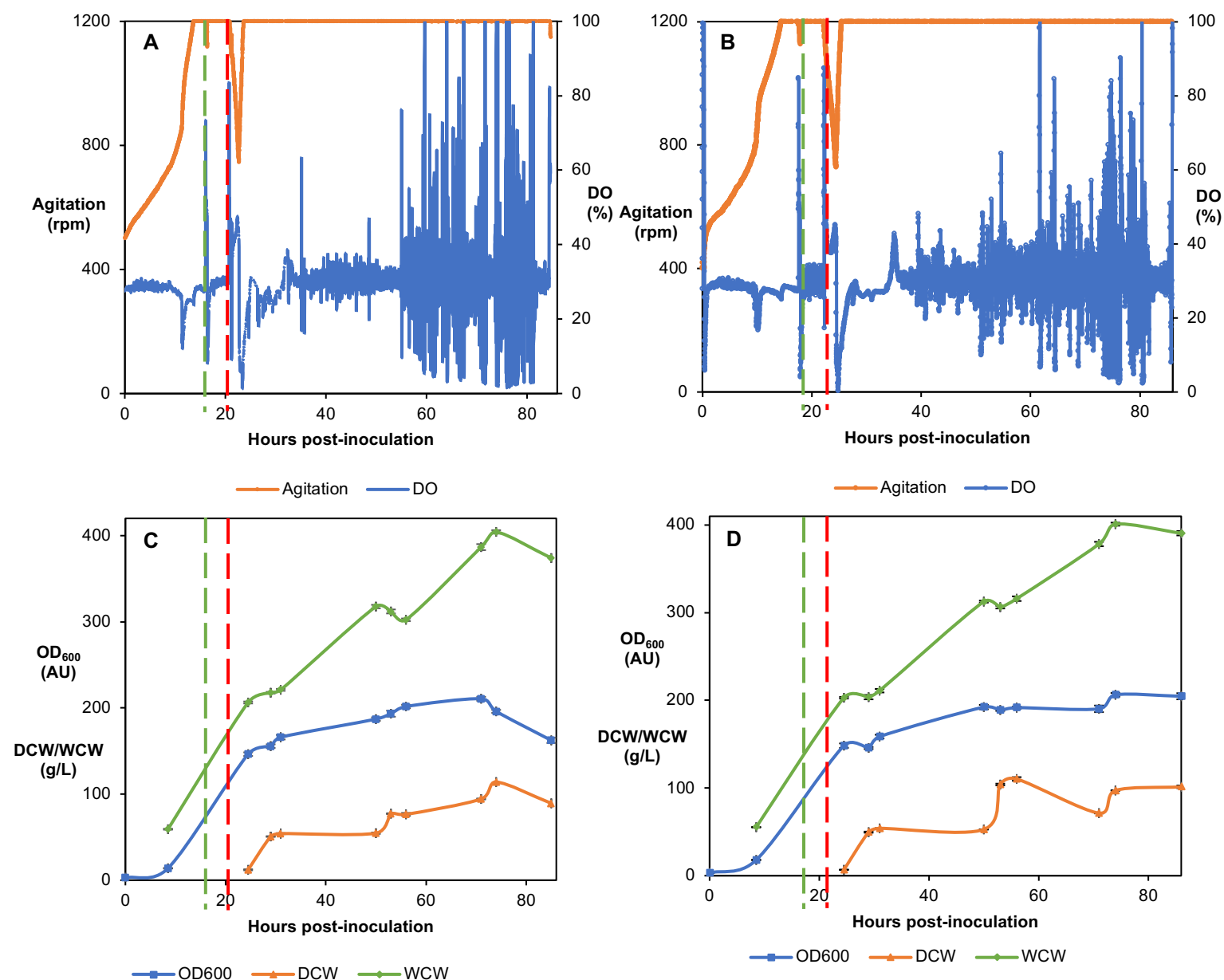
Figure 4.4 – fermentation traces and growth plots (n = 3) from Units 1 and 2 of the Dasgip® producing Man5 using the GlycoSwitch® SuperMan5-10 *P. pastoris* expression system. Panels **A** and **C** are from Unit 1 (U1), and **B** and **D** are from Unit 2 (U2) of the Dasgip® system. The end of the glycerol batch phase and the start of the glycerol fed-batch phase is indicated by the green dashed line, and the point of induction is indicated by the red dashed line. For U1, the glycerol batch phase lasted for 16 hours, so methanol induction occurred 20 hours post-inoculation. After 65 hours of methanol feeding, (85 hours post-inoculation), the agitation began to drop and so the reactor was harvested. For U2, the glycerol batch phase lasted for 17 hours and methanol induction occurred 21 hours post-inoculation. The reactor was harvested at the same time as U1 as the culture was 1 hour behind, so it was anticipated that the agitation would also drop for U2.
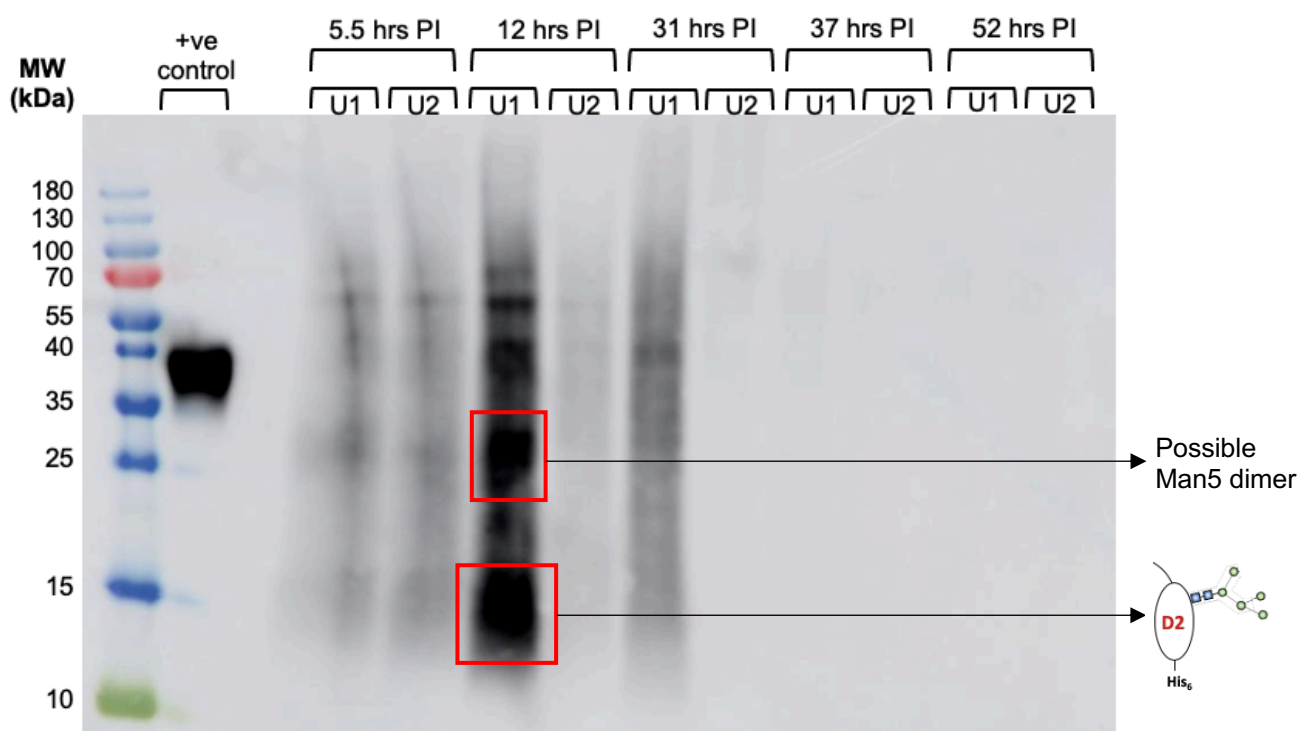
Figure 4.5 – timecourse Western blot analysis run under reducing conditions of the fermentation shown in Figure 4.4 (producing Man5 using GlycoSwitch® SuperMan5-10) in both units 1 and 2 (U1 and U2) of the Dasgip® Parallel Bioreactor System. Product is seen at 5.5, 12 and 31 hours post-induction (PI) in vessels 1 and 2, but thereafter no signal is shown. Some multimerisation and smearing is seen due to glycosylation heterogeneity in the product. The primary antibody used was an anti-His-tag antibody and no secondary antibody was used. The positive control was His-tagged refFcγRIIIa and the band of the expected molecular weight for Man5 is labelled, along with a possible Man5 dimer.

In Figure 4.4, the same effect can be seen as there was for the Mut^S fermentation where there is a drop in agitation at ~60 hours post-induction (PI). As there was for the Mut^S fermentation, the Mut$^+$ culture also showed a drop in growth before this event occurred. Additionally, the Western blot in Figure 4.5 shows that product was present at 12 hours PI, but levels of product decreased after this point and by 37 hours PI no product was present in the culture broth. The cell growth was still increasing at this point, so it is unlikely that cell death was causing this loss of product. It is more likely that decreasing levels of product is due to proteolytic degradation, which is relatively common in fermentative growth of *P. pastoris* and was confirmed by a zymogram (see Figure 4.18). Following these results, it was decided that strategies to mitigate protease degradation would be used for subsequent fermentations. These included adding casamino acids, using a mixed sorbitol and methanol feed during induction and shortening the induction period. Efforts were first directed towards production of the Man5 construct as this had shown more reliable production at a higher titre in shake flasks.

4.2.2 Mitigating Proteolytic Degradation

As mentioned, *P. pastoris* is known to release many proteases which readily degrade heterologous proteins. Despite both of our Mut$^+$ strains (one producing Man9 and one producing Man5) being knockouts for certain proteases (*PEP4*$^-$, *SUB2*$^-$), *P. pastoris* produce many different proteases, meaning it is difficult to target all of them by way of genetic manipulation. Timecourse Western blot analysis strongly suggested that proteolytic degradation was occurring in the small-scale fermentations that had been carried out so far (see Figure 4.5). This was characterised by the observation that product would be present at earlier timepoints but not later on during the induction phase. Zymography was also carried out, which confirmed the presence of enzymatic activity in samples (see Figure 4.18). This section will detail the mitigation strategies that were employed to minimise this degradation and the results from these studies.

4.2.2.1 Casamino Acid Addition

Previous work has used casamino acid pulsing to reduce degradation from proteases (Clare et al., 1991; Sinha et al., 2005; Velez-Suberbie et al., 2020). The idea behind this strategy is that the casamino acids provide an alternative substrate for the proteases, diverting degradation away from the protein of interest by offering a competing substrate.
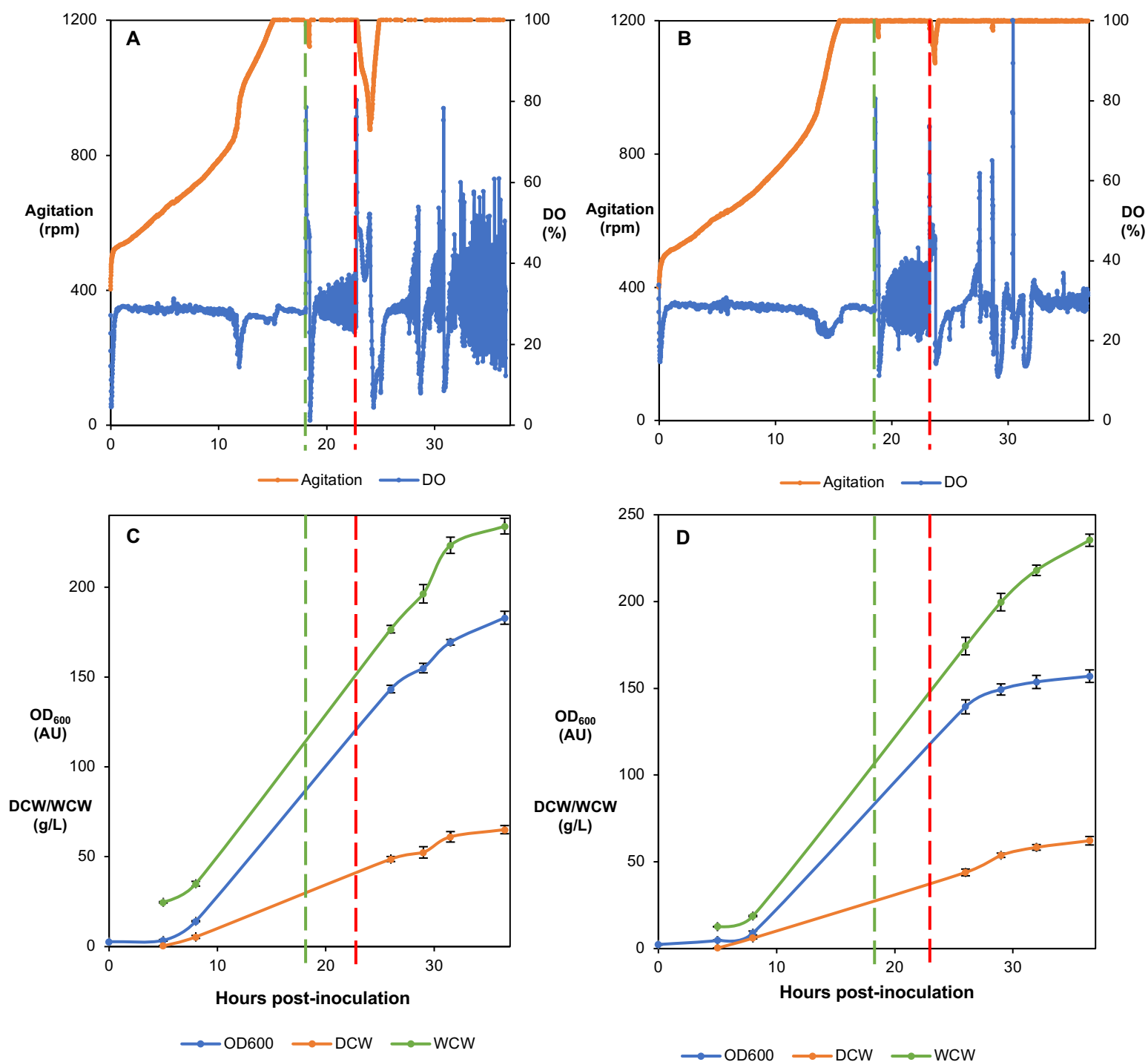
Figure 4.6 – fermentation traces and growth plots (n = 3) for Dasgip® fermentation producing Man5 using GlycoSwitch® SuperMan5-10 with casamino acid bolus addition (**A** and **C**) and without casamino acid addition (**B** and **D**). The green dashed line indicates the end of the glycerol batch phase and the start of the 4-hour glycerol fed-batch phase. The red dashed line indicates the point of methanol induction (~22-23 hours post-inoculation). The induction period was 12 hours.
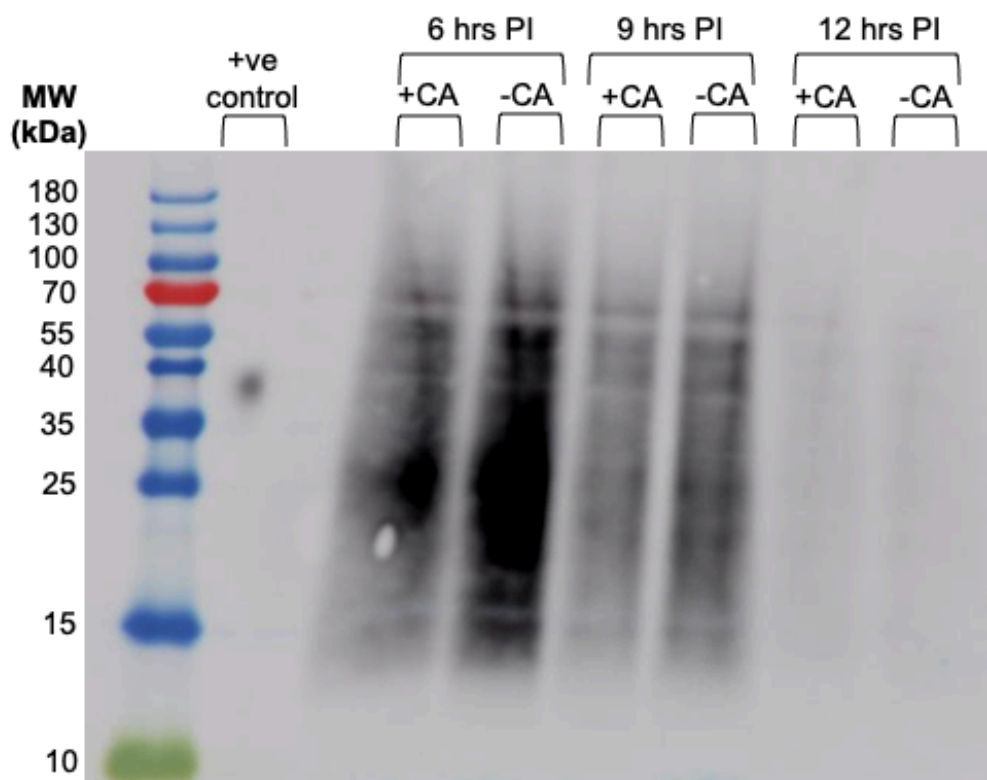
Figure 4.7 – timecourse Western blot analysis of fermentation producing Man5 for which the traces and growth plots are shown in Figure 4.6. Samples from 6, 9 and 12 hours PI (12 hours PI was when the reactors were harvested) are shown and the gel was run under reducing conditions. Some aggregation and smearing are seen. +CA indicates with casamino acid addition, -CA indicates without (negative control). The primary antibody used was an anti-His-tag antibody and no secondary antibody was used. The positive control was His-tagged refFcγRIIIa.

The methanol induction period was shortened due to the previous observations of limited product being seen after 12 hours of methanol feeding (see Figure 4.5). Casamino acids were added in a 3mL bolus 5 hours PI. According to the Western blot shown in Figure 4.7, there was no real impact on product yield by adding casamino acids. Some possible aggregation could be occurring, but it is unlikely that this is due to casamino acid addition as the effect is seen in both vessels which had and did not have a casamino acid bolus addition.

4.2.2.2 Co-Feeding Methanol and Sorbitol

The AOX1 promoter used in *P. pastoris* is induced by methanol. Whilst *P. pastoris* is able to use methanol as a carbon source, excess methanol in the culture medium is toxic to cells. Accumulation of methanol results in the production of toxic metabolites, such as formic acid and formaldehyde, which inhibit growth. For this reason, during the induction phase a fed-batch methanol feeding regime is used to prevent the accumulation of methanol in the culture medium. Additionally, studies into the effect of mixing methanol with other non-repressing

carbon sources, such as glycerol and sorbitol, have been carried out (Çalık et al., 2013). In particular, co-feeding methanol and sorbitol has been investigated with the aim of reducing proteolytic degradation in *P. pastoris*.
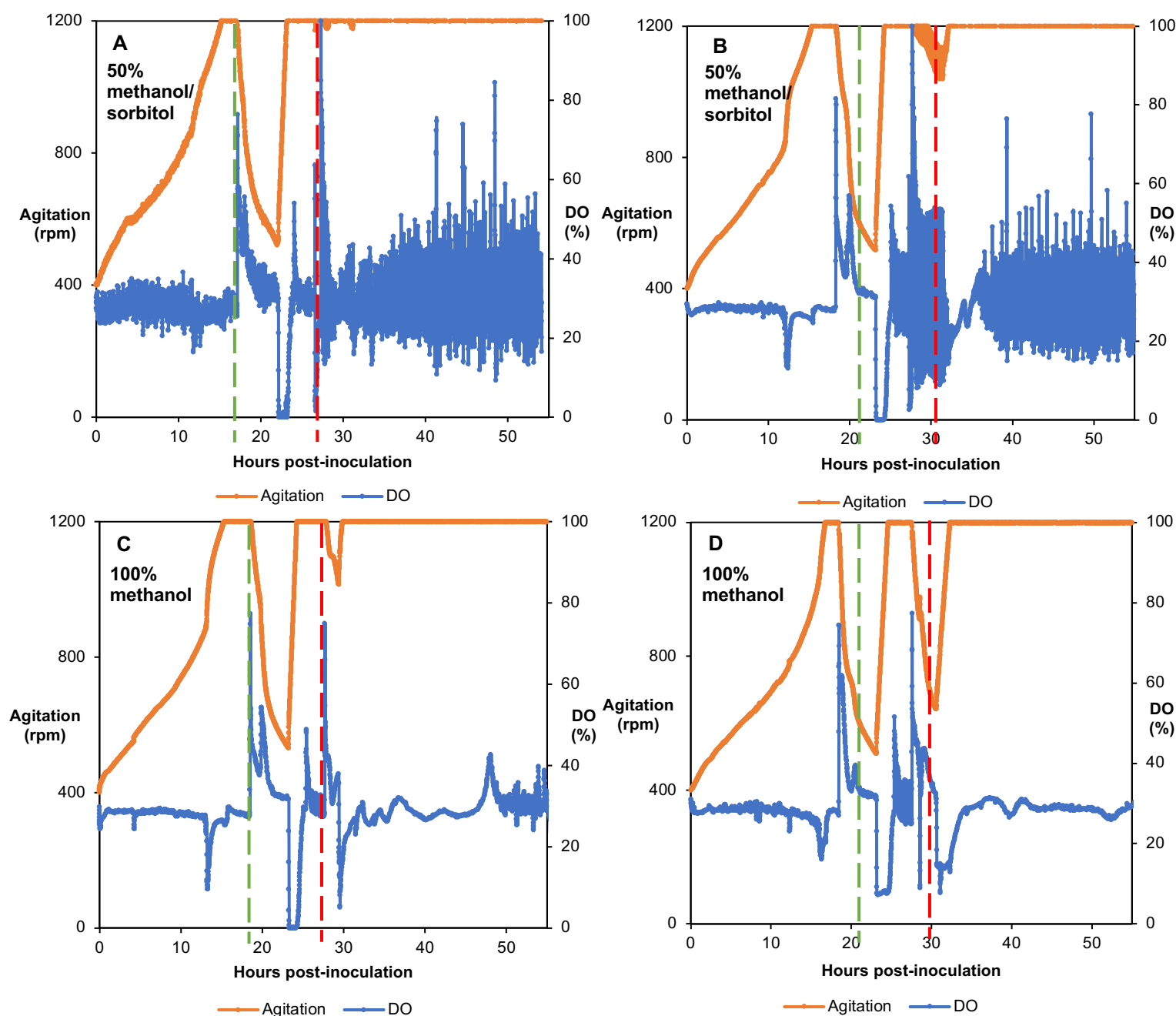
Figure 4.8 – fermentation traces of all four 250mL reactors from a Dasgip® fermentation run producing Man5 using GlycoSwitch® SuperMan5-10. Panels **A** and **B** are traces from the reactors that were fed a mixed methanol and sorbitol feed, panels **C** and **D** are traces from reactors that were fed only methanol during the induction period. The red dashed line indicates the point of induction (~27-28 hours post-inoculation); the induction period was 28 hours for each vessel. After the initial DO spike at the end of the glycerol batch phase (indicated by the green dashed line), there was a starvation phase due to a pump malfunction, so the agitation dropped. Once the pump malfunction was rectified, the 4-hour glycerol fed-batch phase was carried out, followed by induction.

The induction period was extended to 28 hours as the feed rates were kept the same, so less methanol was being fed to the cultures with the 50% methanol/sorbitol co-feed. This meant that by 12 hours PI, the culture would have only been fed half the amount of methanol it would have been fed if it was a 100% methanol feed. By inducing for longer, it also meant a more effective timecourse study could be carried out.
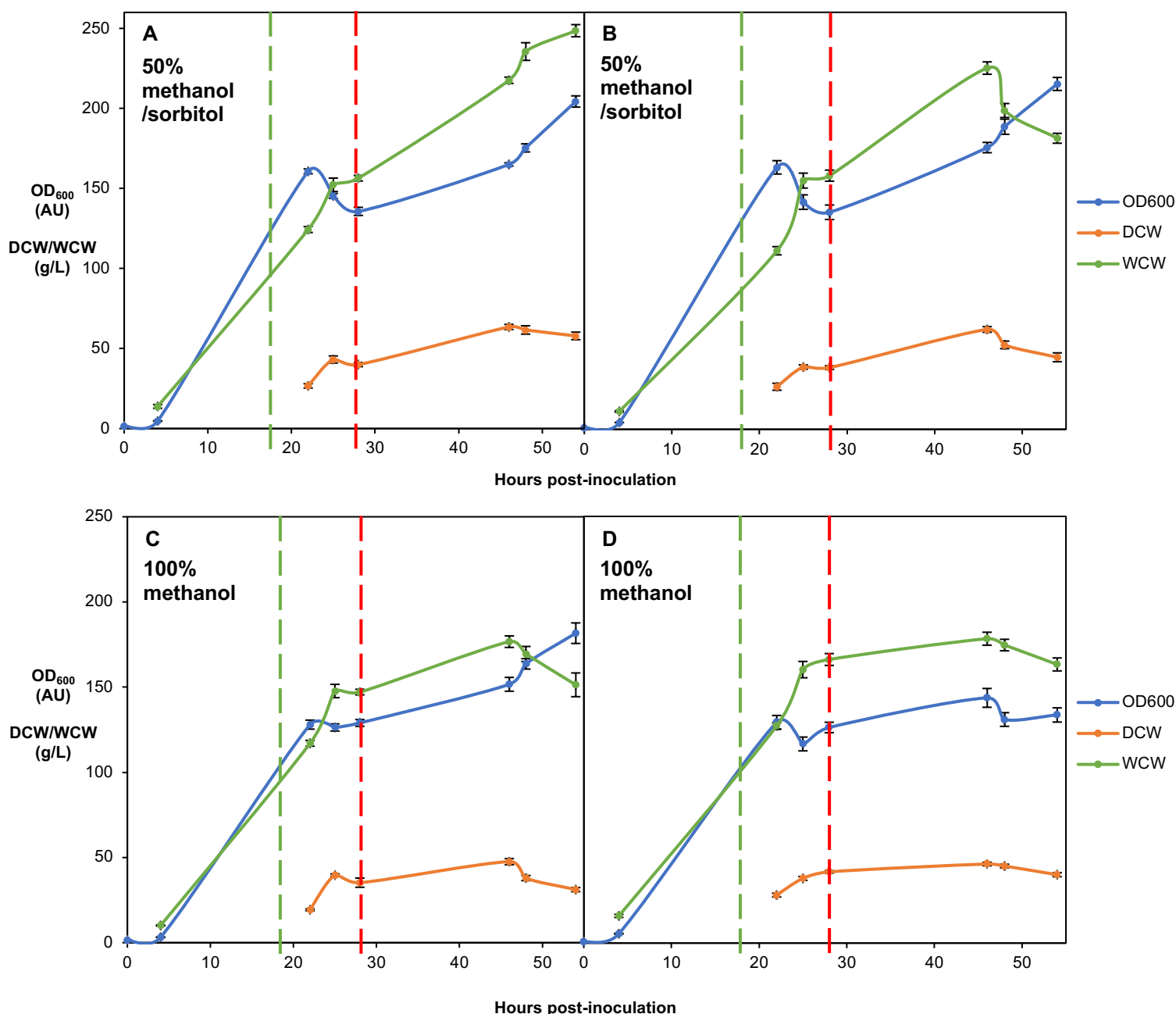
Figure 4.9 – growth plots from the vessels for which the fermentation traces are shown in Figure 4.8 (n = 3). Panels **A** and **B** are from the vessels which were fed a 50% methanol/sorbitol co-feed, panels **C** and **D** are from the reactors which were fed pure methanol throughout the induction period. The green dashed line indicates the start of the glycerol fed-batch phase and the red dashed line indicates the point of induction.

In Figure 4.8, the drop in agitation post-induction was more pronounced in panels C and D, which were the reactors being fed pure methanol rather than 50% methanol/sorbitol. Due to the higher concentration of methanol in reactors C and D, there was a higher level of methanol toxicity and growth slowed more in these vessels compared to reactors A and B that were fed methanol and sorbitol. Figure 4.9 shows that growth of the cultures in reactors C and D is noticeably lower than the growth from the cultures in the vessels that were fed methanol and sorbitol, which again reflects the effect of methanol toxicity on culture growth.
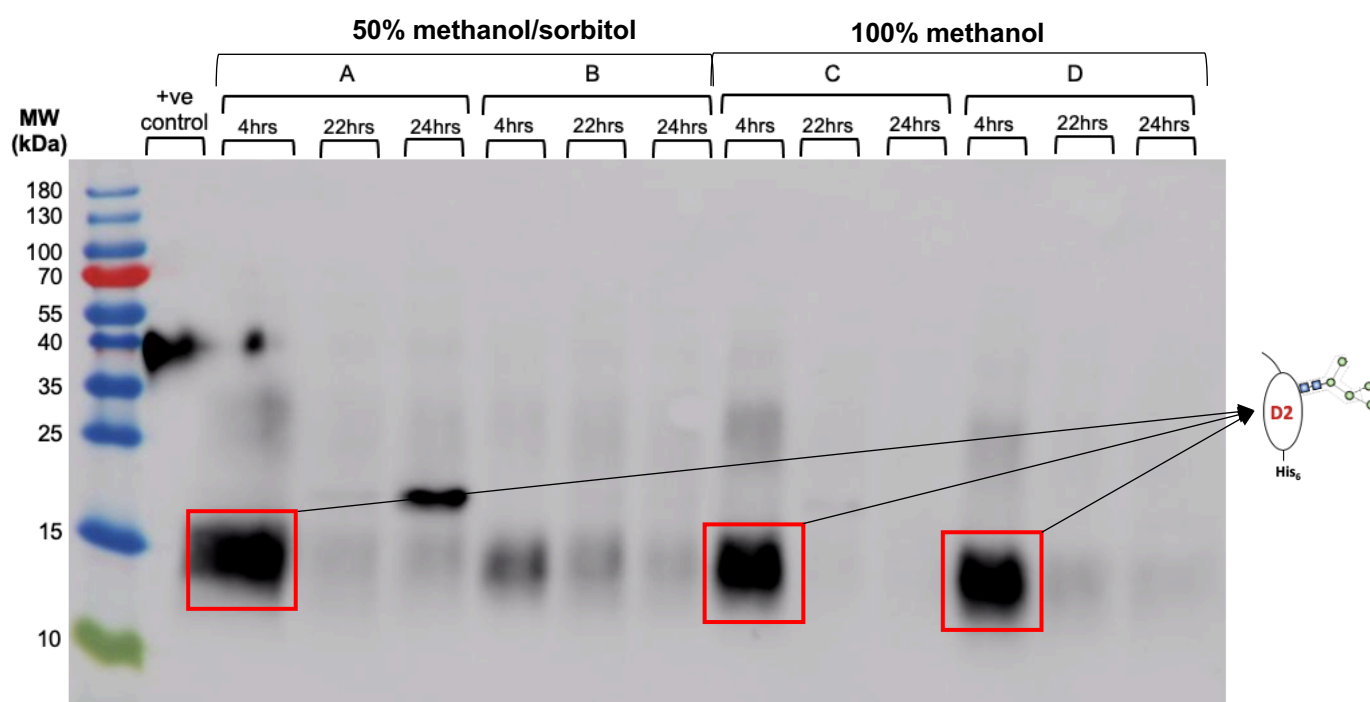
Figure 4.10 – timecourse Western blot analysis of the fermentation producing Man5 for which the traces and growth plots are shown in Figures 4.8 and 4.9, respectively. Vessels A and B were fed a 50% methanol/sorbitol feed, vessels C and D were fed pure methanol. All timepoints are hours post-induction (PI). The band at the expected molecular weight for Man5 is labelled. The primary antibody used was an anti-His-tag antibody and no secondary antibody was used. The positive control was His-tagged refFcγRIIIa.

The Western blot in Figure 4.10 showed that there was no significant positive effect of feeding methanol and sorbitol instead of pure methanol on protease degradation in the cultures. The protein expression appeared to be more aberrant and inconsistent compared to the cultures that were fed purely methanol. The best expression seemed to be at t = 4 (4 hours PI) from the methanol-only fed reactors. The conclusion therefore was that it was not worth pursuing this mitigation strategy in further fermentations. At t = 6 in vessel A, the signal is detected at ~17kDa, which is higher than expected. This could be non-specific binding of antibody on the

membrane, or it could be that the sorbitol co-feed has affected the product and caused it to run differently on the gel.

4.2.2.3 Shortening the Induction Period

As the other attempts to minimise proteolytic degradation had not been successful, it was decided that the induction period would be shortened in order to minimise the effect of the degradation.
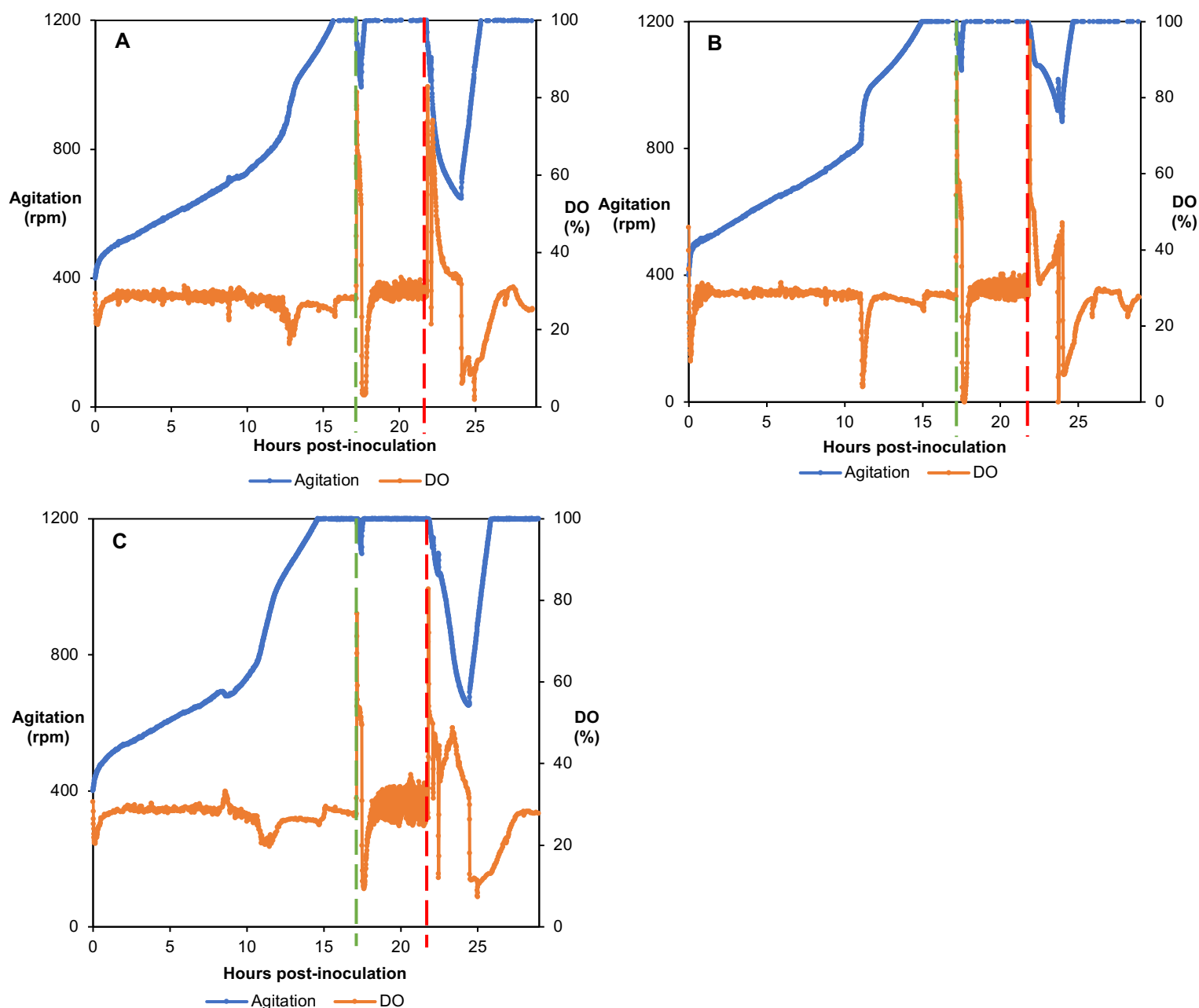
Figure 4.11 – fermentation traces from units 1, 2 and 4 of the 250mL Dasgip® vessels producing Man5 using GlycoSwitch™ SuperMan5-10. **A)** Unit 1, **B)** unit 2, **C)** unit 4. The glycerol batch phase lasted ~17 hours and the methanol induction period was 6 hours. Unit 3 was used, however the culture had a starvation period after the glycerol batch phase, which affected cell growth and therefore has not been

included. The green dashed line indicates the start of the glycerol fed-batch phase and the red dashed line indicates the start of the methanol fed-batch phase (induction).
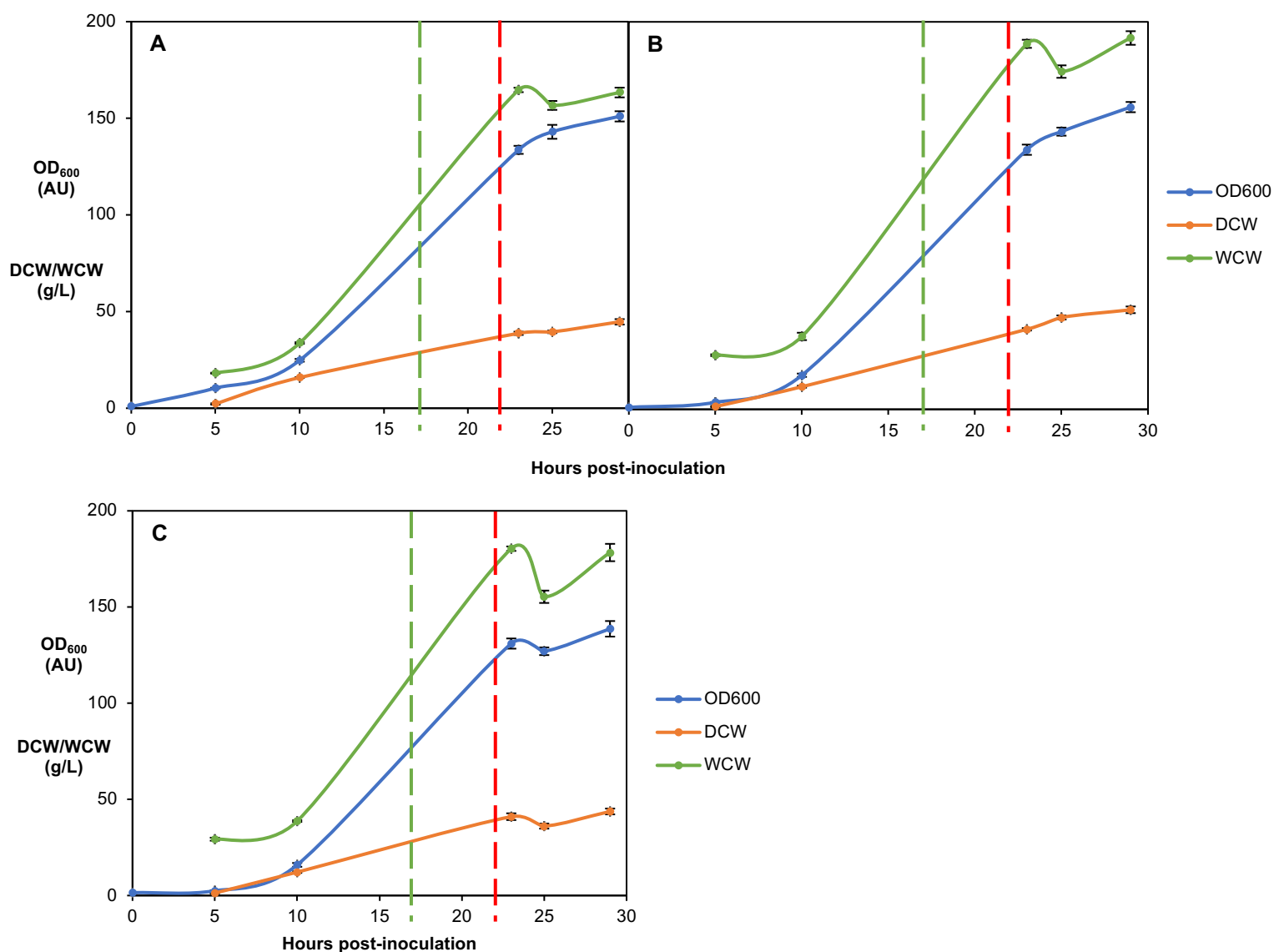
Figure 4.12 – growth plots from the reactors for which the fermentation traces are shown in Figure 4.11 (n = 3). **A)** Unit 1, **B)** unit 2, **C)** unit 4. The green dashed line indicates the start of the glycerol fed-batch phase and the red dashed line indicates the start of the methanol fed-batch phase (induction).
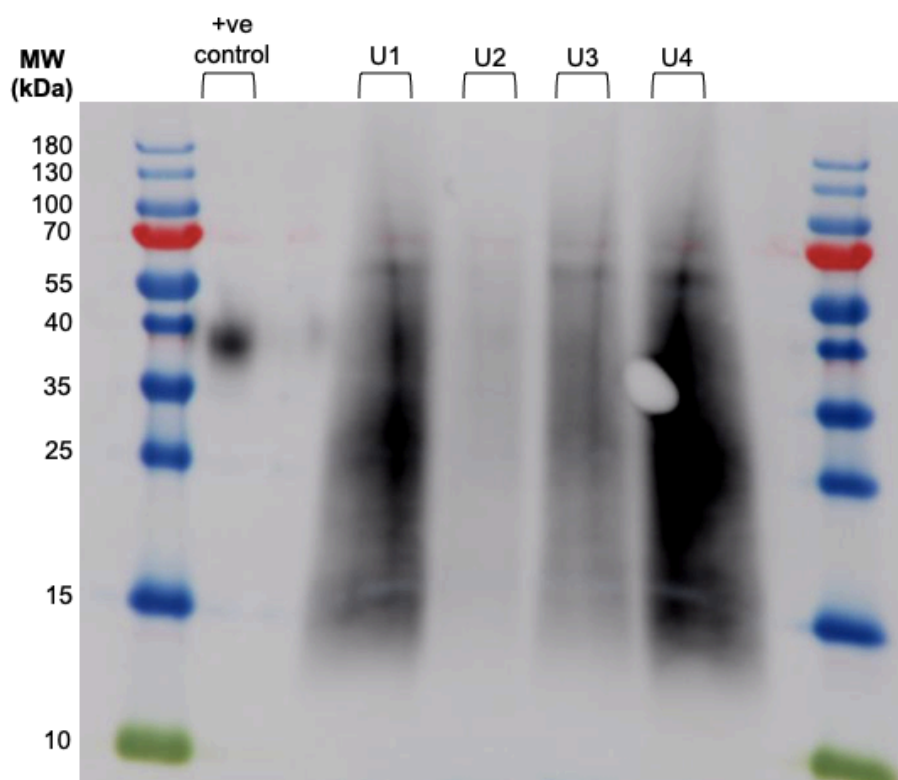
Figure 4.13 – Western blot of harvest from each reactor used for the fermentation producing Man5 shown in Figures 4.11 and 4.12, run under reducing conditions. These are endpoint samples taken from the harvest of each reactor. U1 = A, U2 = B, U4 = C. Despite the starvation period that occurred in Unit 3, there appeared to be some product, although the quality may have been affected. Some smearing is seen, possibly due to protein aggregation. The primary antibody used was an anti-His-tag antibody and no secondary antibody was used. The positive control was His-tagged refFcγRIIIa.

For the GlycoSwitch™ SuperMan5-10 strain producing the Man5 construct, the optimal induction period appeared to be around 6 hours before the levels of degradation exceeded expression and product began to disappear (see Figures 4.7, 4.10 and 4.13). Based on this observation, scale-up to a 30L vessel was carried out with the aim of producing a large enough volume of product that even if degradation did occur, there would be enough remaining product from such a large volume of harvest for subsequent binding studies.

4.2.3 Large-Scale Fermentation to Produce Man5

Despite the issues faced with proteolytic degradation, it was decided that the fermentation would be scaled up. The bioreactor used for the large-scale fermentations was a Biostat® Cplus 30L stainless steel bioreactor from Sartorius Stedim.

Studies were carried out using the GlycoSwitch™ SuperMan5-10 strain to produce the Man5 ligand construct. Based on previous fermentations and subsequent Western blot analyses,

the optimal induction period at the 250mL scale seemed to be 6 hours, so this was used as the induction period for the first large-scale fermentation attempt.

Table 4.2 – conditions and parameters used for the first 30L-scale fermentation compared to the 250mL-scale protocol for the production of Man5 using GlycoSwitch™ SuperMan5-10. The inoculum and fermentation medium volumes were scaled up 100x and allowed for headspace in the reactor. The DO setpoint, inoculum OD_{600}, pre- and post-induction pH setpoints, temperature, aeration and the lengths of the glycerol and methanol fed-batch phases were kept approximately the same as at the smaller scale. The agitation rates were controlled by the system to maintain the DO setpoint. The glycerol batch phase was shorter compared to that seen at the smaller scale.

Parameter	250mL Dasgip® scale	First 30L Biostat® Cplus fermentation
OD_{600} of inoculum for fermenter inoculation (AU)	6-15	7
Inoculum volume (L)	0.01	1
Media and media volume	Fermentation basal salts medium (100mL)	Fermentation basal salts medium (10L)
DO setpoint (%)	30	30
pH pre-induction	5.0	5.0
Temperature (°C)	30	30
Agitation (rpm)	400-1200 (cascade control)	300-800 (cascade control)
Aeration (vvm)	0.5-6.0 (cascade control)	0.5 (cascade control)
Length of glycerol batch phase (hrs)	18-24	14.5
Length of glycerol fed-batch phase (hrs)	4	4
Length of methanol fed-batch phase (hrs)	~6	5
pH post-induction	6.5	6.5
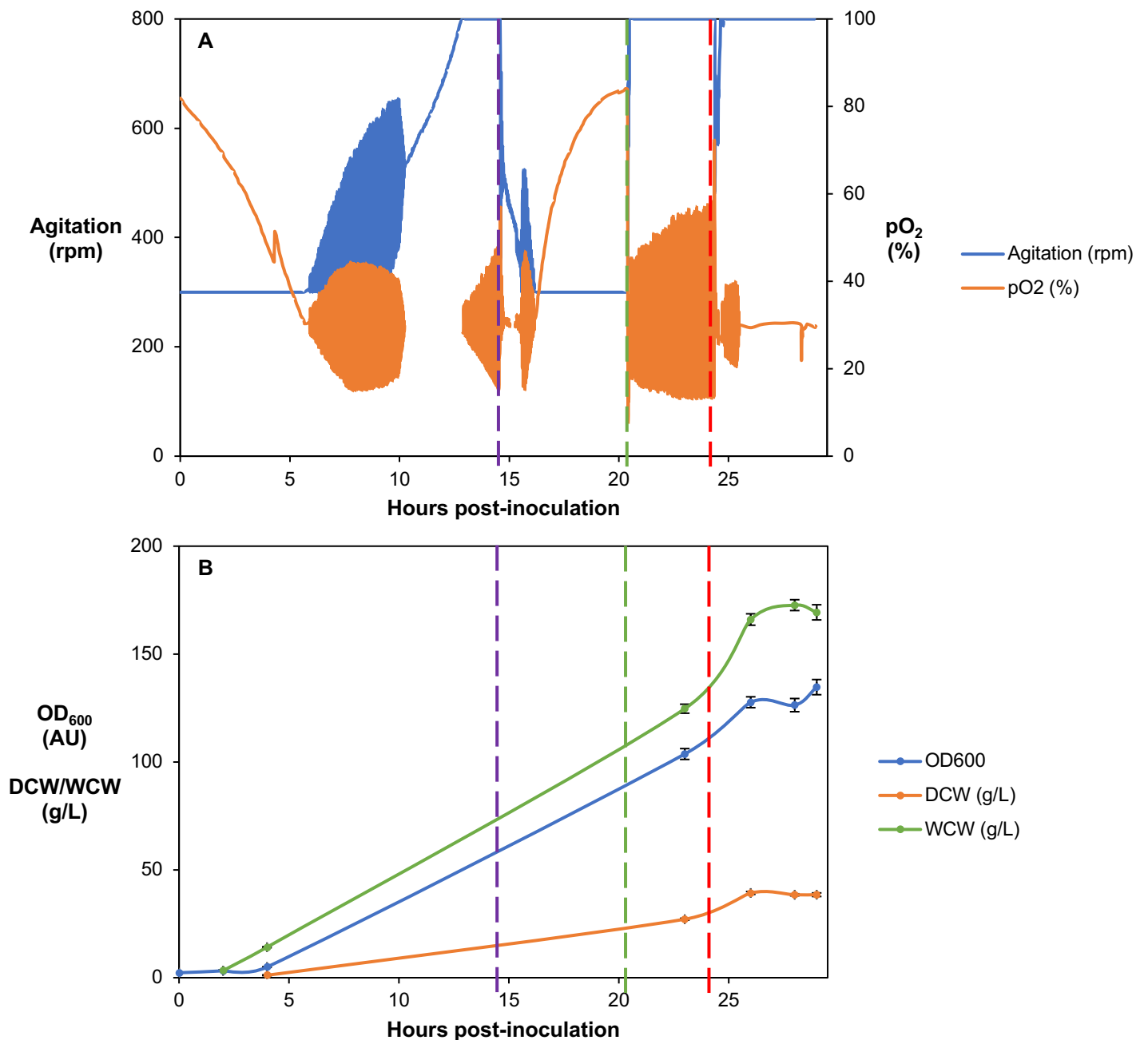
Figure 4.14 – A) fermentation trace and **B)** growth plot (n = 3) for the first fermentation of *P. pastoris* GlycoSwitch™ SuperMan5-10 to produce Man5 in the 30L Biostat® Cplus bioreactor. The glycerol batch phase lasted 14.5 hours (magenta dashed line), after which there was a ~6 hour starvation phase. The glycerol fed-batch phase lasted ~4 hours and then the methanol fed-batch phase commenced manually (red dashed line) and lasted for ~5 hours.

A starvation period occurred at the end of the glycerol batch phase. This is due to the glycerol batch phase being much shorter than anticipated (timings based on smaller scale fermentation) and feeding being switched over manually. When starvation periods had occurred in smaller scale fermentations, the cells had recovered and gone on to make product

(see Figure 4.13). As cell growth in this fermentation seemed to recover to similar levels seen at small scale, it was decided that the run could proceed.
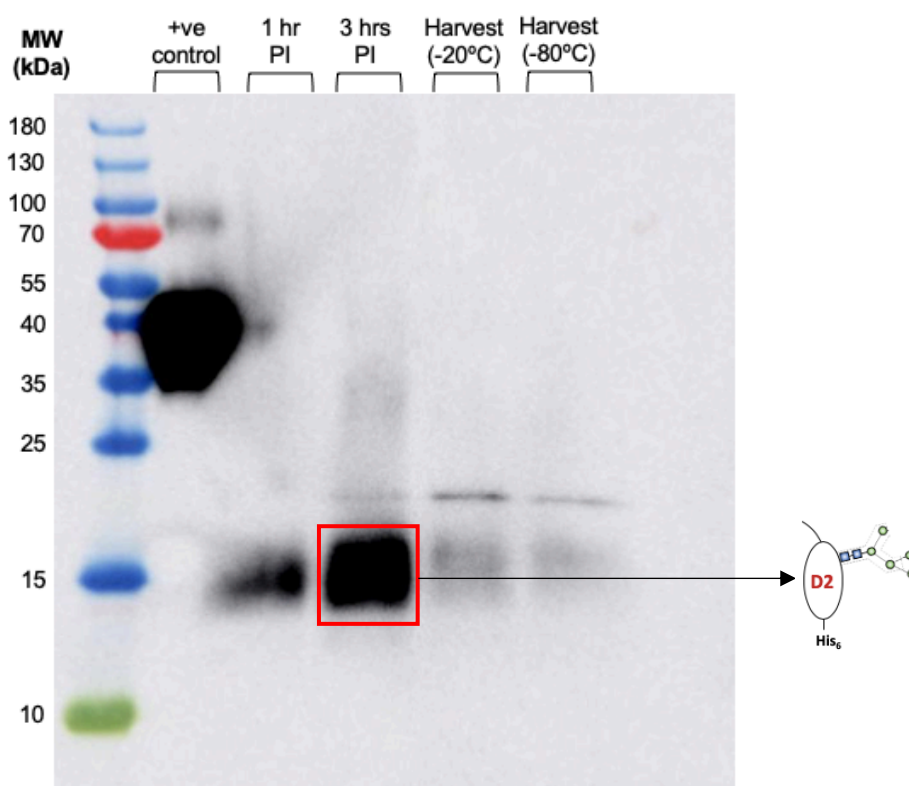
Figure 4.15 – Western blot analysis of 1 hour, 3 hours and 5 hours (harvest) post induction (PI). This gel was run under reducing conditions. Product can be seen at 3 hours PI, but very little is seen in the harvest at 5 hours PI. The primary antibody used was an anti-His-tag antibody and no secondary antibody was used. The positive control was His-tagged refFcγRIIIa.

To investigate whether the storage conditions were having any impact on product degradation, some harvest was stored at -20°C and some was stored at -80°C. It was anticipated that there would be more degradation, if any, in the sample that was stored at -20°C than at -80°C, although the opposite appeared to be the case according to Figure 4.15. However, the harvest that was stored at -20°C reached the storage conditions earlier than the harvest that was stored at -80°C, so it is possible that degradation was occurring during the harvesting period itself. It was therefore decided that the following strategies would be employed for the next large-scale fermentation; a 3-hour methanol fed-batch phase, the addition of protease inhibitors during harvesting, and the harvest would be cooled more quickly during and prior to centrifugation to slow down the activity of any proteases.
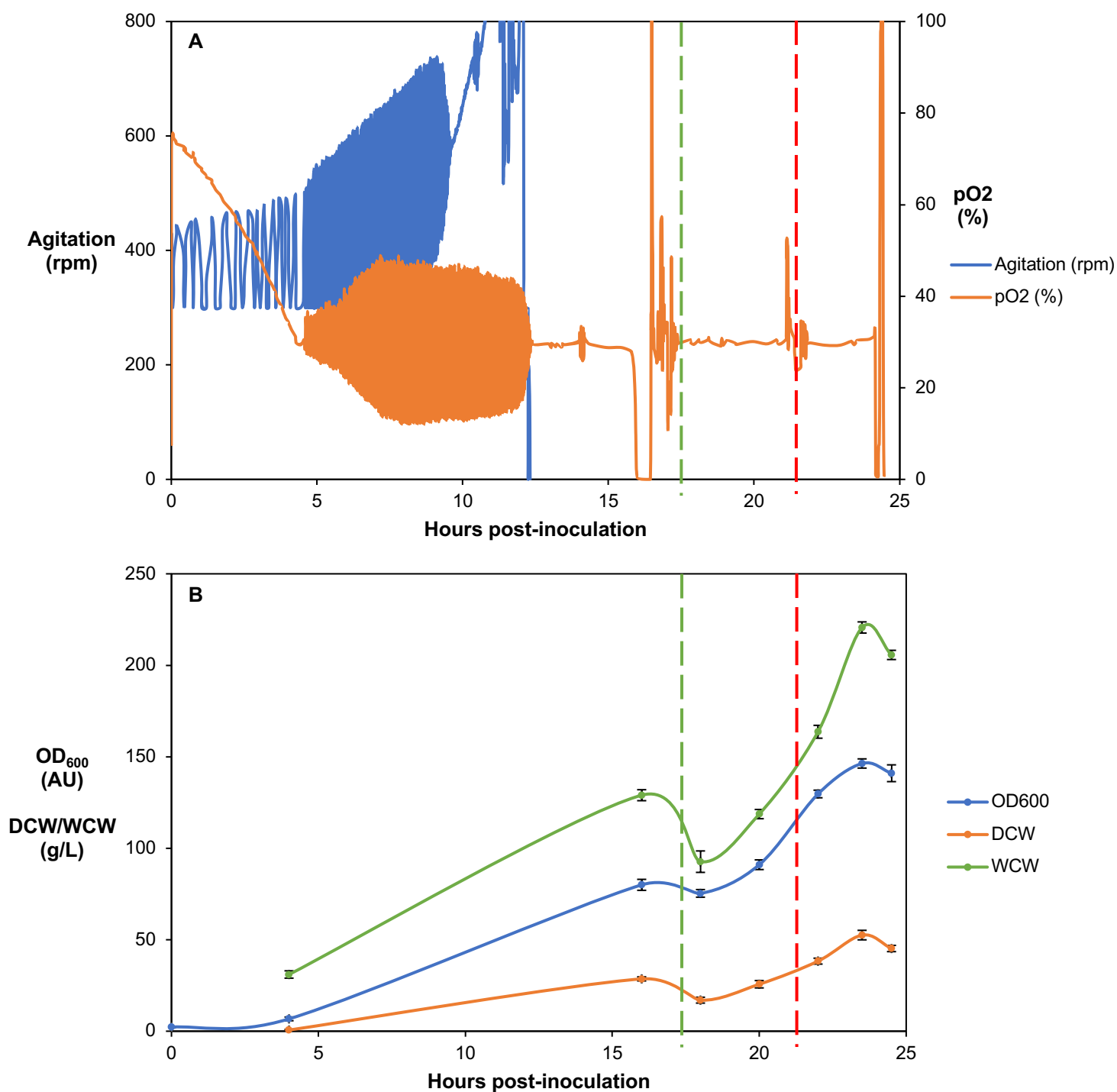
Figure 4.16 – A) fermentation trace and **B)** growth plot (n = 3) from the second large-scale fermentation growing *P. pastoris* GlycoSwitch™ SuperMan5-10 to produce Man5 using the 30L Biostat® Cplus bioreactor. The green dashed line represents the start of the 4-hour glycerol fed-batch phase and the red dashed line represents the start of the 3-hour methanol fed-batch phase. Agitation measurements failed after ~12 hours post-inoculation, although the impeller was still functioning so the run proceeded.

There was a brief starvation phase before the glycerol fed-batch phase, which is reflected in the growth plot as seen by the reduction in growth at ~18 hours post-inoculation, however cell

growth recovered. The agitation readings failed at ~12 hours post-inoculation, however the impeller was visibly functioning and the cells were still growing so the run proceeded.
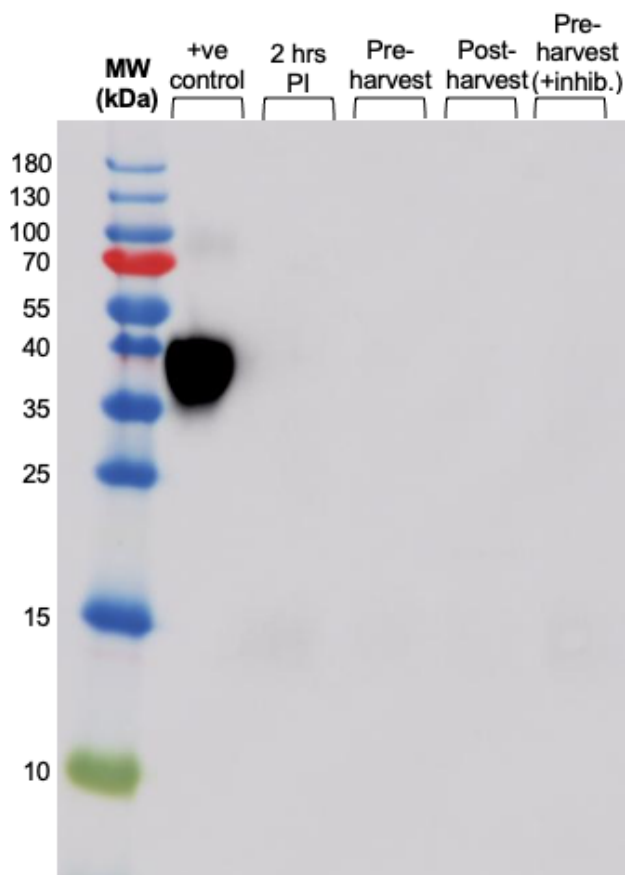
Figure 4.17 – Western blot analysis of samples from 2 and 3 (harvest) hours PI, including samples before and after harvest to monitor any progressive degradation over the harvesting period, and a sample pre-harvest with added protease inhibitors. However, no product was seen. The primary antibody used was an anti-His-tag antibody and no secondary antibody was used. The positive control was His-tagged refFcγRIIIa.

A zymogram was carried out to analyse and compare the protease activity in samples from shake flasks and small- and large-scale fermentations producing Man5 using GlycoSwitch® SuperMan5-10. Zymography is an analytical technique used to detect the presence of enzymatic activity and can therefore be used to detect proteolytic activity in samples. Samples are run across an electrophoretic SDS gel with embedded protein substrates and any proteases in the samples degrade the substrates within the gel. Upon staining, the molecular weight of the proteases in the sample can be identified.
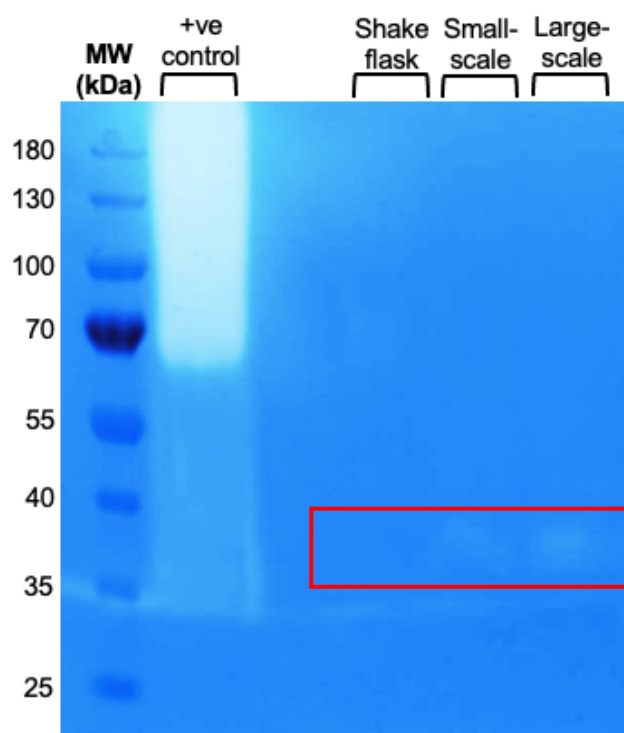
Figure 4.18 – zymogram analysis of shake flask and small- and large-scale fermentation harvest samples producing Man5 using GlycoSwitch® SuperMan5-10, a protease-deficient strain (*PEP4⁻*, *SUB2⁻*). In the shake flask, there was very minimal to no protease activity detected. The positive control was thermolysin (34.6kDa, some dimerisation). In the small-scale fermentation harvest, a very low signal is detected, and in the large-scale fermentation harvest, a low signal is detected, although it is slightly higher than what is detected in the small-scale harvest sample. The signal was detected at around 38kDa (highlighted in red).

Figure 4.18 shows that there is almost no proteolytic activity in the shake flask sample, a small amount of proteolytic activity in the small-scale fermentation and a slightly higher signal in the large-scale fermentation sample at ~38kDa. This reflects how the rate of degradation increases with scale.

4.3 Conclusion

Initially, it was decided that fermentation would be a good way to produce a large amount of the FcγR ligands for analytical and binding studies, and potentially for immobilisation to a chromatographic resin. However, the lack of reproducibility seen in both the small- and large-scale fermentations along with the proteolytic degradation issues meant that establishing a reliable protocol was very challenging. Strategies to mitigate the degradation were employed but did not make a notable difference to product yield. Zymogram analysis confirmed some proteolytic activity that increased with increasing scale, even in a protease-deficient strain of

P. pastoris. It was decided that production would revert to shake flask culture in order to make enough of the ligands for binding studies and analysis.

Chapter 5 – Shake Flask Production, Purification and Analysis of FcγR Ligands

5.1 Introduction

Small-scale production of recombinant proteins is often carried out in shake flask cultures. Shake flasks are easier to manage and run in parallel compared to stirred-tank bioreactors and are therefore commonly used for characterisation and optimisation studies for the production of recombinant proteins before scale-up. However, there is far less in-line monitoring of shake flask cultures compared to cultures grown in bioreactors, and there is limited control of some variables such as pH and dissolved oxygen content (Link & Weuster-Botz, 2011). This can affect the quality of recombinant proteins produced during shake flask cultures and means that optimisation of the process is often required. In this work, the refinement of the shake flask protocol to produce the FcγR ligands was an iterative process, with a significant amount of work going into determining the causes of issues such as a lack of expression, protein aggregation and more.

In Chapter 4, attempts to produce the ligands using fermentation were described. Given the degradation issues encountered during fermentation, it was decided that we would revert to shake flask production in order to generate enough of the FcγR ligands for binding studies and characterisation using mass spectrometry. This chapter will detail the refinement of the shake flask culture protocol used to produce the FcγR ligands, the His-tag affinity purification process, analysis and characterisation of the ligands and sample preparation for binding studies. Issues arose with protein aggregation during the shake flask cultures, and these issues were rectified by growing the cultures to different cell densities at various growth phases and adding antifoam to prevent the formation of an air-liquid interface as a result of foaming. The His-tag affinity purification was effective and the chromatograms are analysed in this section. The mass spectrometry data was used to confirm that the proteins being produced by the *P. pastoris* expression systems were of the correct primary structure and also had the expected glycosylation, i.e. that the FcγRIIIa D2 Man5 (Man5) had *N*-linked glycosylation of the Man5-Man10 structure at the expected site and a reduced amount of hypermannosylation compared to FcγRIIIa D2 Man9 (Man9).

5.2 Results

This section primarily details the results from the shake flask culture studies, His-tag affinity purification and mass spectrometry analysis.

5.2.1 Shake Flask Production

All production in shake flasks was carried out using Mut^+ *P. pastoris* expression systems as these were protease-deficient strains. The original shake flask protocol used was based on the protocol provided by Invitrogen™ in their document '*Pichia* Expression Kit' (publication number: MAN0000012, revision: A.0, page 61). However, some alterations to this protocol were made based on observations and protein analysis.

5.2.1.1 Protein Aggregation Mitigation

P. pastoris has not been widely reported to be prone to yield aggregated product during recombinant protein production, particularly in shake flask cultures. However, methanol toxicity during recombinant protein production in *P. pastoris* is known to have negative effects on cell growth (Fischer et al., 2019; Hu et al., 2020) and could therefore contribute to issues with recombinant protein production such as degradation and aggregation. Additionally, foaming of the cell culture liquid during recombinant protein production can cause protein aggregation due to the introduction of an air-liquid interface (Duerkop et al., 2018). During the optimisation of the cell culture process, issues with protein aggregation were encountered.
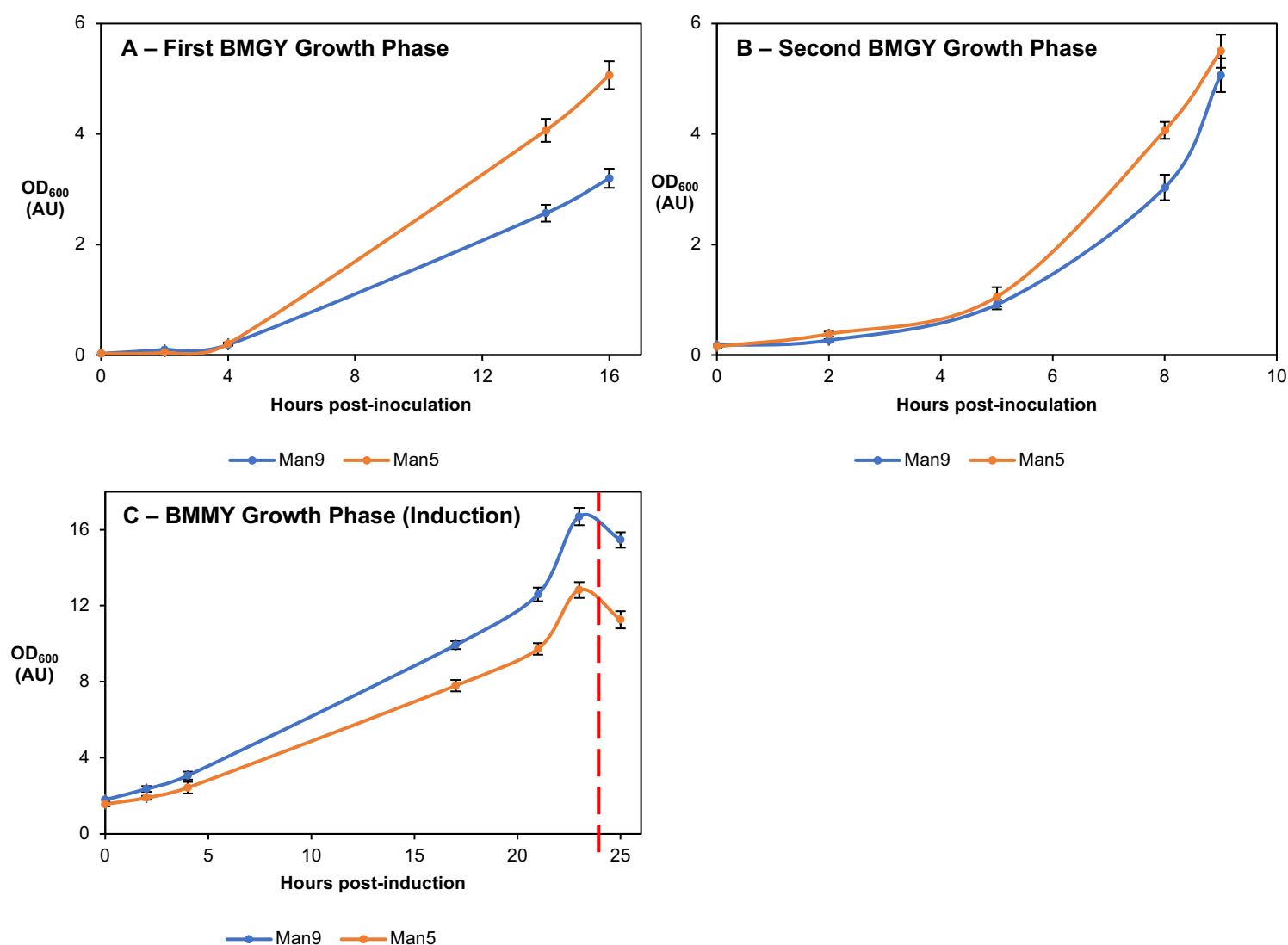
Figure 5.1 – growth curves for the production of Man9 using Mut$^+$ Bg25 *P. pastoris* and Man5 using GlycoSwitch™ SuperMan5-10 (n = 3). The Western blot of this harvest is shown in Figure 5.2. **A)** Growth curve of the cultures in the first BMGY growth phase, which inoculated 0.5mL of each glycerol cell stock (OD$_{600}$ ~11AU) into 1L sterile, baffled shake flasks containing 100mL BMGY at 30°C, 220rpm. Once OD$_{600}$ 2-6AU had been reached, 5mL of these cultures were used to inoculate 2L sterile, baffled shake flasks containing 200mL BMGY for **B)** the second BMGY growth phase. These cultures were also grown at 30°C, 220rpm. **C)** Once the cell densities reached OD$_{600}$ ~5AU, induction took place and the BMMY growth phase commenced. This involved resuspending the centrifuged cell pellet in 100mL BMMY and inoculating 1L sterile, baffled shake flasks containing 190mL of BMMY with 10mL of this resuspended cell pellet. The red dashed line indicates methanol addition to a final concentration of 0.5% at 24 hours post-induction.
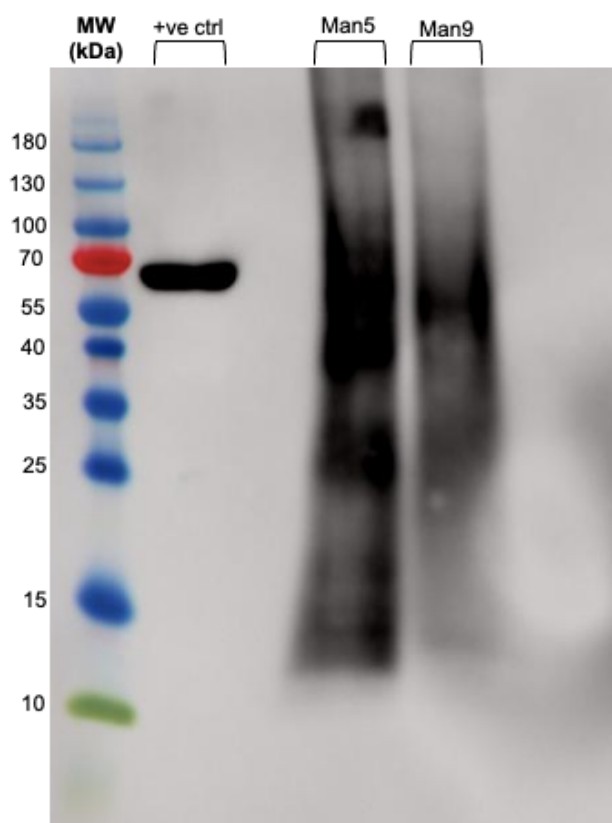
Figure 5.2 – Western blot analysis of harvest from growth curves shown in Figure 5.1, run under reducing conditions. The expected bands are ~14kDa for Man5 and ~25kDa for Man9. However, there is a significant amount of smearing and higher molecular weight bands than expected in both sample lanes, indicating aggregation. The antibody used was Bio-Techne polyHis HRP mAb clone AD.1.1.10, an anti-His antibody.

During methanol induction, the culture growing in BMGY is centrifuged and the cell pellet is resuspended in BMMY media, which contains methanol as the carbon source. The Invitrogen™ guidance specifies an OD_{600} of 2-6AU should be reached in the second BMGY growth phase before methanol induction. In addition, the guidance specifies that the OD_{600} at the start of methanol induction should be ~1AU. For the cell culture shown in Figure 5.1, the OD_{600} at the end of the second BMGY growth phase was ~5AU and the OD_{600} at the start of the methanol induction phase was ~1.5AU. However, this cell culture, along with other cultures that had been grown and reached similar OD_{600} levels at these phases, all gave rise to harvest which had significant levels of aggregation (see Figure 5.2). In addition, some foaming of cultures was seen, which introduces an air-liquid interface and may have contributed towards protein aggregation.

Table 5.1 – OD_{600} values of cultures that produced aggregated and non-aggregated protein at the end of the glycerol batch phase and at the start of the methanol induction phase. The OD_{600} of the harvest that produced aggregated protein at the end of the second BMGY growth phase was ~10-fold lower than the culture producing non-aggregated protein. The OD_{600} at the start of the BMMY growth phase for the harvest that produced the aggregated protein was lower than the non-aggregated protein.

	OD_{600} at end of second BMGY growth phase (AU)	OD_{600} at start of BMMY growth phase/induction (AU)
Aggregated protein in harvest	2-6	0.2-1.5
Non-aggregated protein in harvest	18-59	2.5-5.3

The data in Table 5.1 shows two findings. The first is that a higher OD_{600} at the start of the BMMY growth phase (induction) is associated with less aggregated protein compared to a lower OD_{600} at the start of this phase, which could be a result of a higher cell density culture undergoing less cell death due to methanol toxicity than a lower cell density culture. This could result in reduced cell stress and therefore less aggregated protein. However, the most significant difference in OD_{600} values between cultures producing aggregated and non-aggregated protein is the OD_{600} at the end of the second BMGY growth phase. It could be that harvesting cells that are in a healthier state and a more established phase of growth and inducing to a higher OD_{600} at the start of the BMMY growth phase results in reduced cell stress. Again, by having a culture containing more cells that are in a better condition, the proportion of cells in the culture that die off due to methanol toxicity during induction could be reduced, resulting in a healthier culture during induction and protein of an improved quality being produced. Therefore, in subsequent cultures following this finding, cells were grown to a greater OD_{600} value at the end of the second BMGY growth phase and the OD_{600} at the start of the induction was also increased.

In addition to the changes made to the cell densities achieved during the second BMGY growth phase and the start of the BMMY growth phase, antifoam was added at a concentration of 0.05mL per L cell culture to the shake flasks at the start of the induction phase. The finalised cell culture production protocol and growth curves to produce the FcγR ligands are shown in the following section.

5.2.1.2 Shake Flask Culture Protocol Establishment

As mentioned, the original shake flask protocol used was based on the Invitrogen™ protocol '*Pichia* Expression Kit' (publication number: MAN0000012, revision: A.0, pages 61). However,

some alterations to this protocol were made based on observations and protein analysis. The changes to this protocol that were made are detailed in Table 5.2.

Table 5.2 – alterations made to the Invitrogen™ protocol to establish the FcγR shake flask production protocol. The main alterations that were made were the cell densities reached at the end of the second BMGY growth phase and at the start of the BMMY growth phase. The media and flask volumes were scaled up linearly 4x and the agitation rate was reduced compared to the Invitrogen™ guidelines.

Parameter	Invitrogen™ Guidelines	FcγR Shake Flask Culture Protocol
Media and flask volumes first BMGY growth phase	25mL media 250mL shake flask	100mL media 1L shake flask
Temperature BMGY growth phases (°C)	28-30	28
Agitation rate BMGY growth phases (rpm)	250-300	180
OD_{600} end of second BMGY growth phase (AU)	2-6	≥18
OD_{600} start of BMMY growth phase (AU)	1	2.5-5
Temperature BMMY growth phase (°C)	28-30	30

The protocol was similar to the Invitrogen™ protocol, however some changes were made. Two BMGY growth phases were used, as specified in the guidance. For the first BMGY growth phase, the shake flask and media volume was scaled up 4x, as the cultures had already been grown successfully in 1L shake flasks containing 100mL of media from glycerol stocks to produce the fermentation inoculum. The ratio of media to flask volume was kept constant at 1:10 for the first BMGY growth phase. The ratio of media to flask volume in the BMMY growth phase was 1:5. Optimal growth and subsequent recombinant protein expression was found to be achieved by growing the cultures at 28°C at a lower agitation rate than specified in the guidance during the BMGY growth phases. Conversely, improved protein production was seen during the BMMY growth phase by increasing the temperature to 30°C. The most notable differences between the Invitrogen™ guidance and the established FcγR shake flask production protocol were the cell densities reached at the end of the second BMGY growth phase and at the start of the BMMY growth phase.
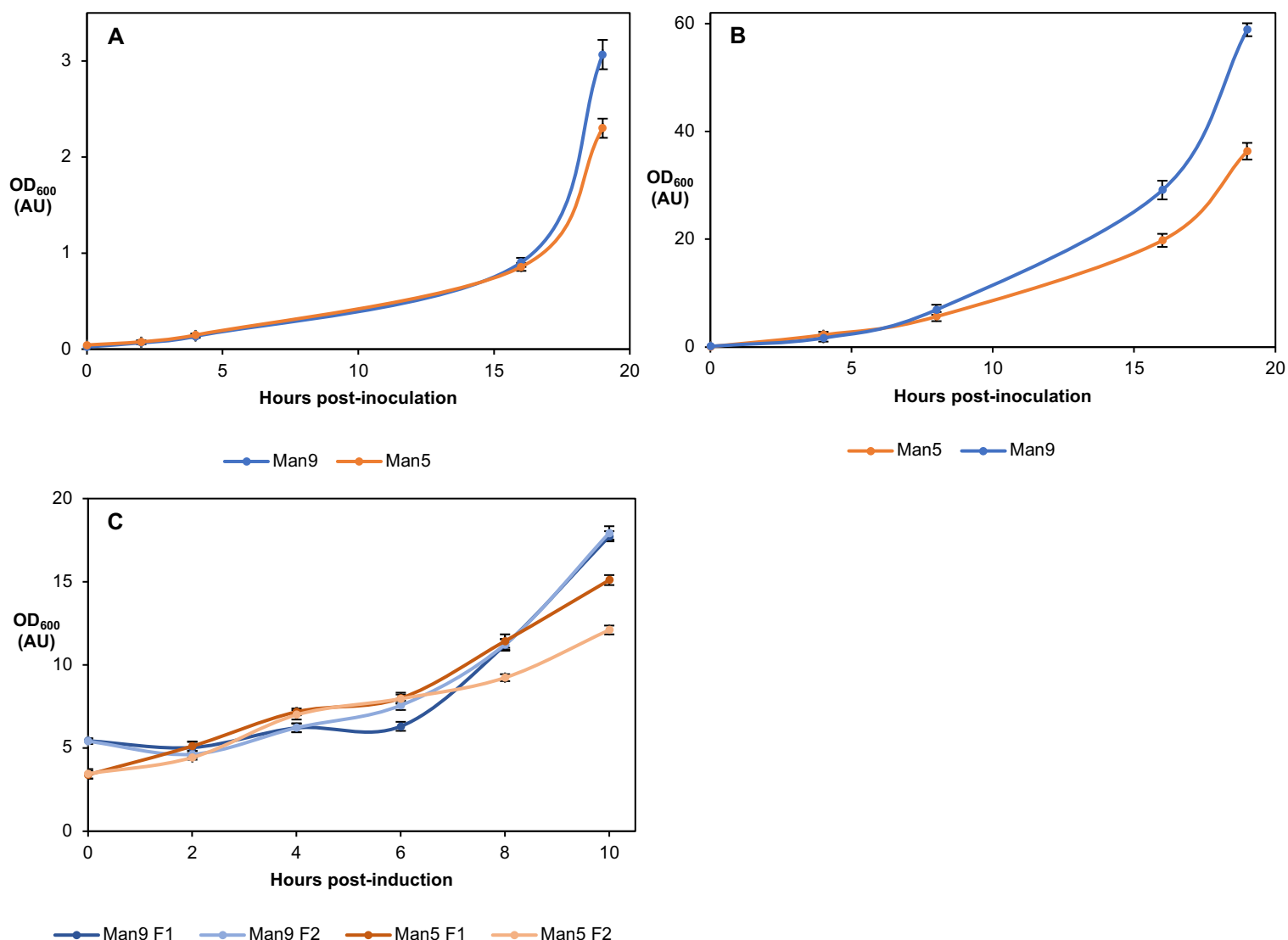
Figure 5.3 – growth curves for the production of Man9 using Mut$^+$ Bg25 *P. pastoris* and Man5 using GlycoSwitch™ SuperMan5-10 (n = 3). **A)** The first BMGY growth phase, which inoculated 0.5mL of each glycerol cell stock (OD$_{600}$ ~11AU) into 1L sterile, baffled shake flasks containing 100mL BMGY. Cultures were grown at 28°C, 180rpm until OD$_{600}$ ~2-3AU was reached. **B)** The second BMGY growth phase, which inoculated 5mL of the cultures from the first BMGY growth phase into 1L sterile, baffled shake flasks containing 200mL BMGY. These were grown at 28°C, 180rpm for 19 hours, at which point the OD$_{600}$ had reached 18AU for the Man5-producing culture and 59 for the Man9-producing culture. **C)** Induction took place by centrifuging the cultures from the second BMGY growth phase and resuspending the cell pellet in 100mL BMMY (F1 = flask 1, F2 = flask 2). For the Man5-producing culture, 20mL of this resuspension was added to 1L sterile, baffled shake flasks containing 180mL of BMMY, and for the Man9-producing culture, 10mL of the resuspension was added to flasks containing 190mL of BMMY. The cultures were grown at 30°C, 150rpm until OD$_{600}$ ~11-18AU was reached, which occurred at 10 hours post-induction. Antifoam was added to Man9 F1 and Man5 F1 at a concentration of 0.05mL/L.

From previous shake flask studies, the optimal cell density at which to harvest seemed to be OD_{600} ~11-18AU. The shake flask harvest for which the growth curves are shown in Figure 5.3 were analysed in a timecourse study using a Western blot; this is shown in Figure 5.4.
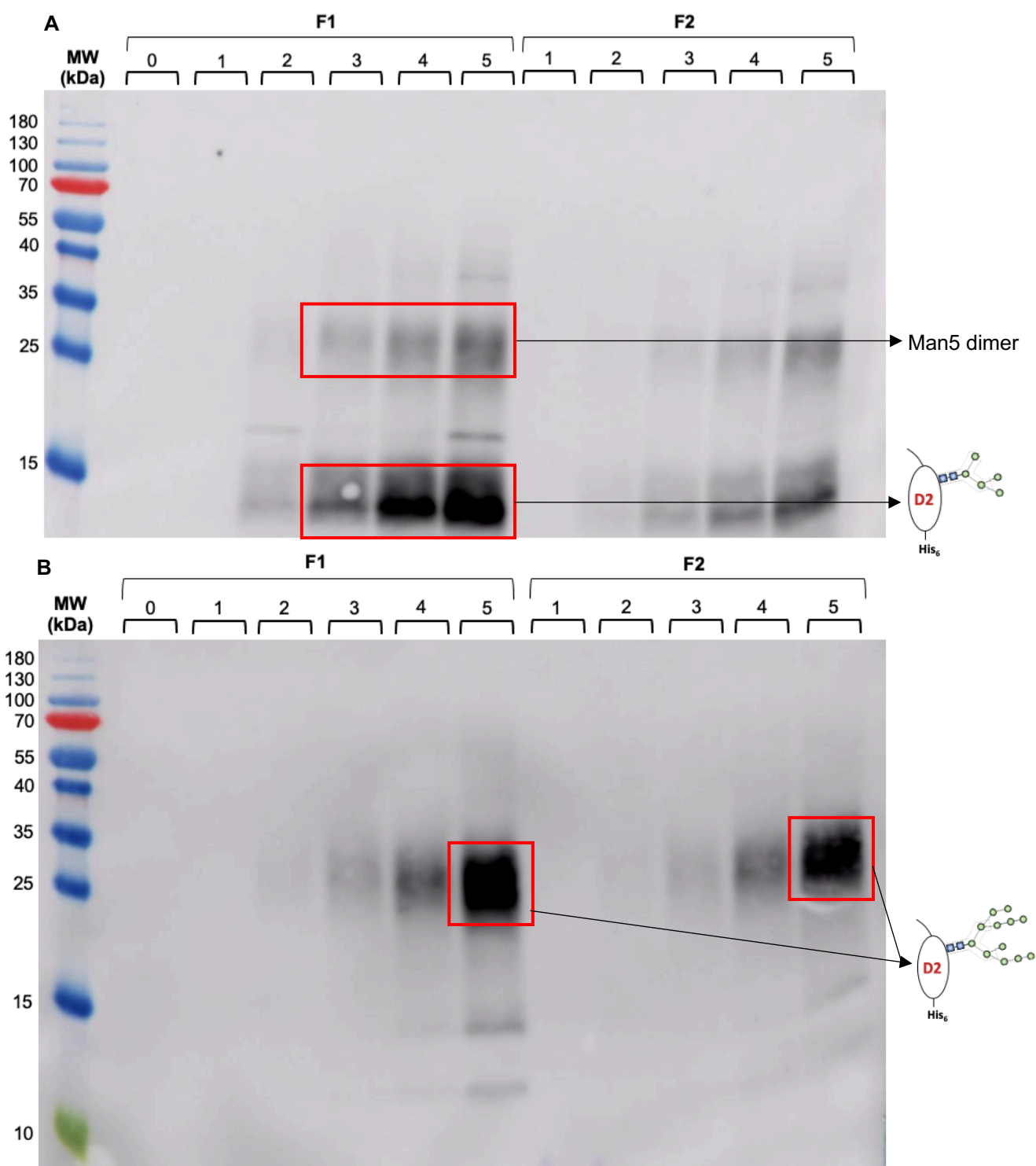
Figure 5.4 – Western blot analysis of the shake flask culture producing **A)** Man5 and **B)** Man9 (growth curves shown in Figure 5.3). The gel was carried out under reducing conditions. The labelling 0-5 of the sample lanes refers to the timepoints at which the samples were taken. 0 = point of induction, 1 = 2 hours post-induction (PI), 2 = 4 hours PI, 3 = 6 hours PI, 4 = 8 hours PI 5 = harvest (10 hours PI). Antifoam was added to both F1 flasks but not to the F2 flasks. The bands of the expected molecular weights for Man5 and Man9 are labelled and the antibody used was anti-His antibody.

Figure 5.4 shows significantly less aggregation compared to Figure 5.2. The main differences between these harvests include the differences in OD_{600} at the end of the second BMGY growth phase and at the start of the BMMY growth phase, the reduction in agitation rate and the addition of antifoam. The addition of antifoam to both F1 flasks does seem to have improved expression, very slightly for Man9 and more noticeably for Man5. However, this improved expression for Man5 F1 could also be attributed to the higher cell density achieved in this culture compared to Man5 F2 (see Figure 5.3C). The finalised FcγR ligand cell culture production protocol is given in Section 2.4.

The reasoning behind why the bands on the Western blots for Man5 and Man9 show at the molecular weights that they do is explained in Section 5.2.3.3 using the mass spectrometry data which details the glycomic profile of the FcγR ligands.

5.2.2 His-Tag Affinity Purification

As mentioned, the FcγR ligands possess a 6xHis tag, allowing for His-tag affinity purification using Ni-NTA chromatography. In this section, chromatograms from the purification of the FcγR ligands are shown.
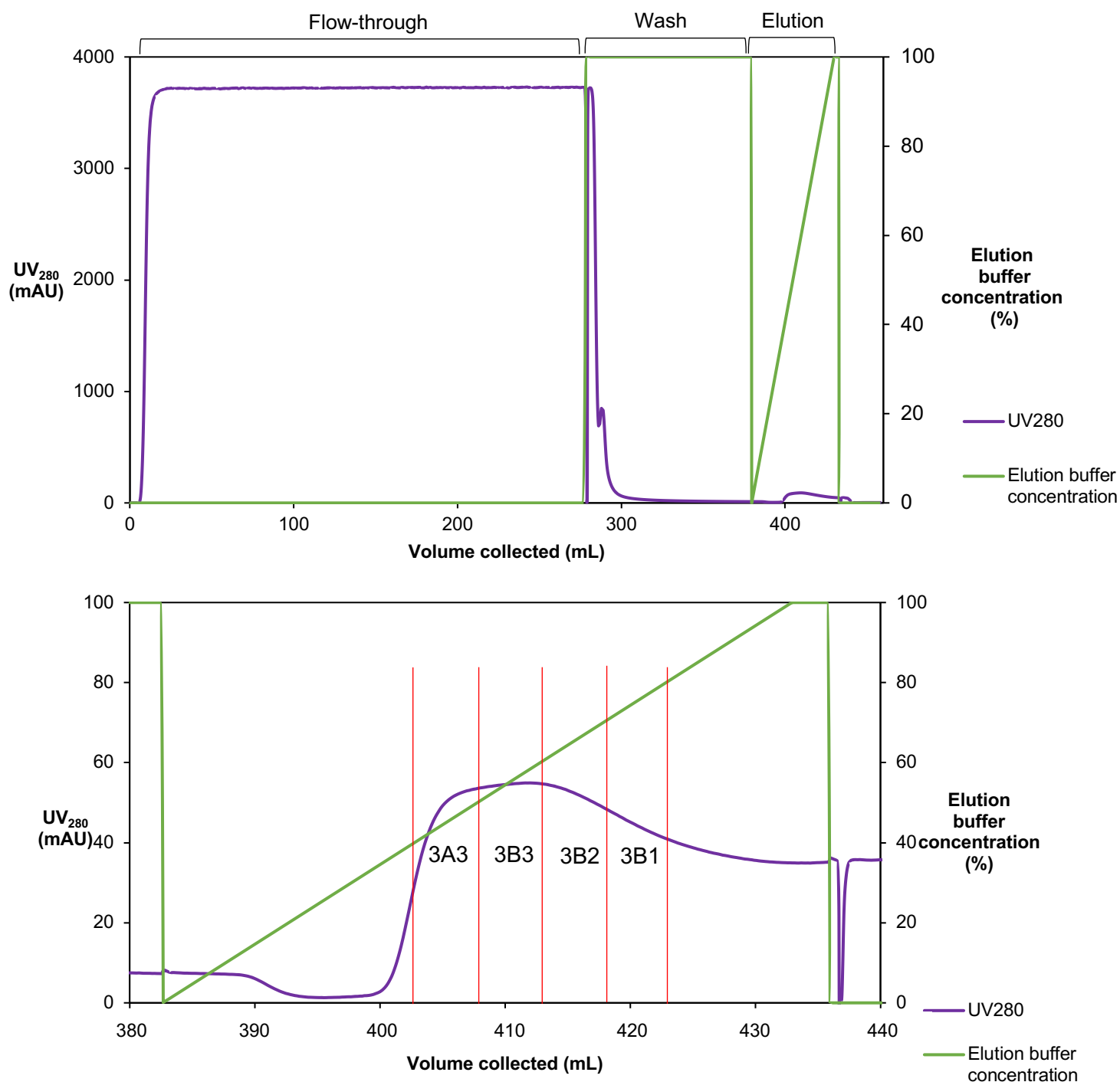
Figure 5.5 – **A)** purification of ~280mL of filtered Man5 shake flask culture harvest (run 1, R1) using a 5mL HisPur™ Ni-NTA column from ThermoFisher Scientific™ on an ÄKTA avant™ 150 purification system. The separation was carried out in bind-elute mode. Shake flask harvest was thawed in a room temperature water bath and pH-adjusted to pH 7.2-7.8 to allow for interaction with the Ni²⁺ on the stationary phase. The column was first equilibrated with 10CV equilibration buffer (50mM sodium phosphate 10mM imidazole), which was not collected. The sample was kept on ice and loaded via a sample pump until all available sample had been loaded. The wash phase was carried out with 20CV of 50mM sodium phosphate 20mM imidazole. The elution was carried out using a gradient of 4-100% elution buffer (50mM sodium phosphate 300mM imidazole). The flow rate was 5mL/min throughout the

separation. **B)** the elution phase only of this separation. Fractions 3A3, 3B3, 3B2 and 3B1 were analysed in the Western blot shown in Figure 5.7A.
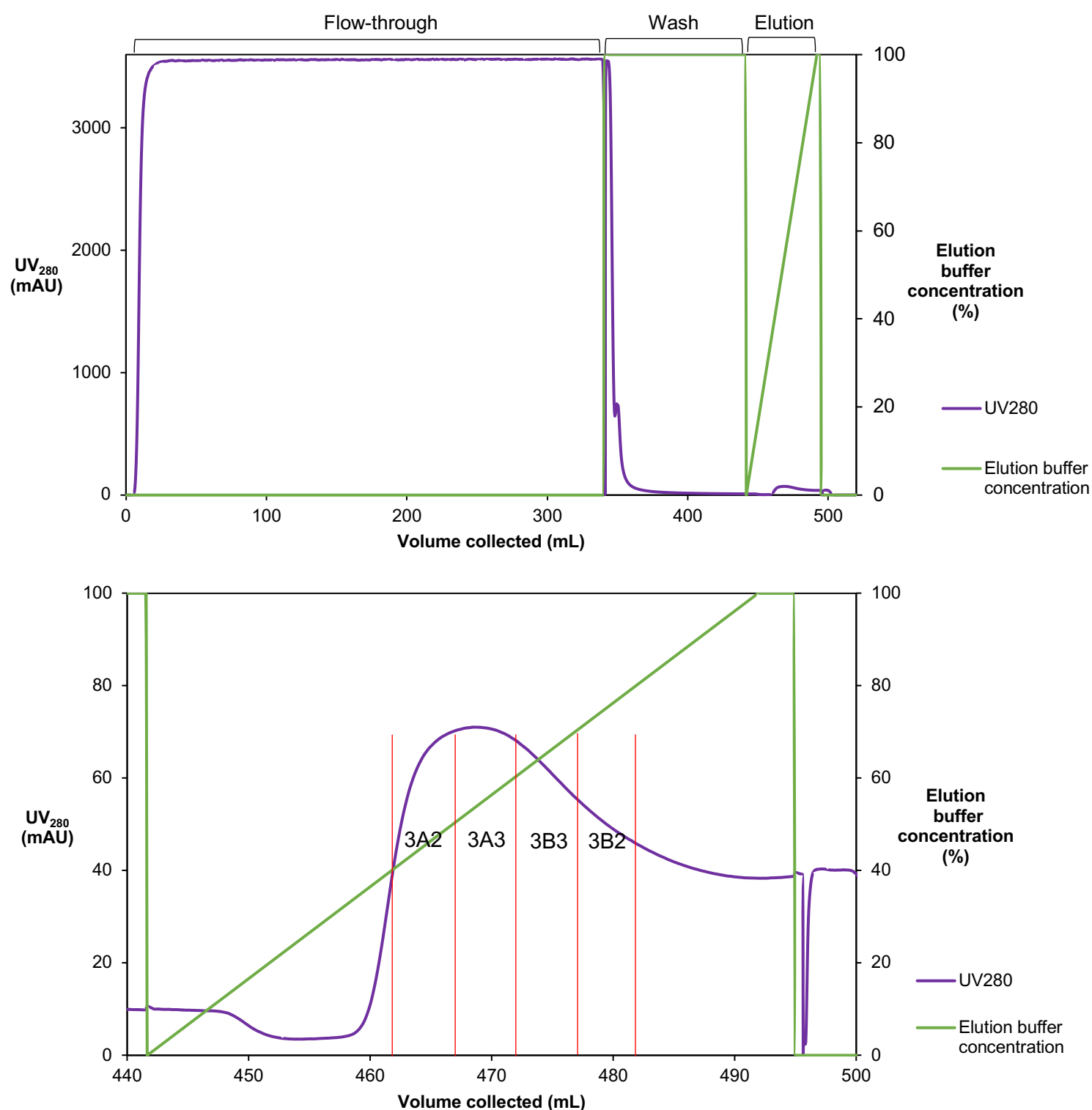
Figure 5.6 – **A)** purification of ~330mL of filtered Man9 shake flask culture harvest (run 1, R1). The same conditions and parameters set out in the figure legend of Figure 5.5 were used for this

separation, although a separate 5mL Ni-NTA column was used to avoid cross-contamination of Man5 and Man9 constructs. **B)** the elution phase only of this separation. Fractions 3A2, 3A3, 3B3 and 3B2 were analysed in the Western blot shown in Figure 5.7B.

Figures 5.5 and 5.6 show the flow-through (load), wash and elution phases of the separation of the filtered shake flask culture harvests producing Man5 and Man9, respectively. The A_{280} during the flow-through phases is high, at ~3500-3700mAU. This is likely due to the host cell proteins (HCPs) and possibly some lysed dead cells, along with media components, such as yeast and peptone which absorb at 280nm. At the start of the wash phases, there is what appears to be some peak splitting or shouldering. This could be a loosely-bound impurity eluting from the column at the very start of the wash phase before the remaining flow-through has eluted from the column. The elution peaks have an A_{280} of ~70-90mAU at the highest point of the peaks. The peaks themselves have significant broadening and also showing a large degree of tailing. Due to the broad and tailing peaks that were shown on the chromatogram, the elution fractions were analysed by Western blot analysis to detect where within the elution peaks the proteins are eluting. These Western blots are shown below.
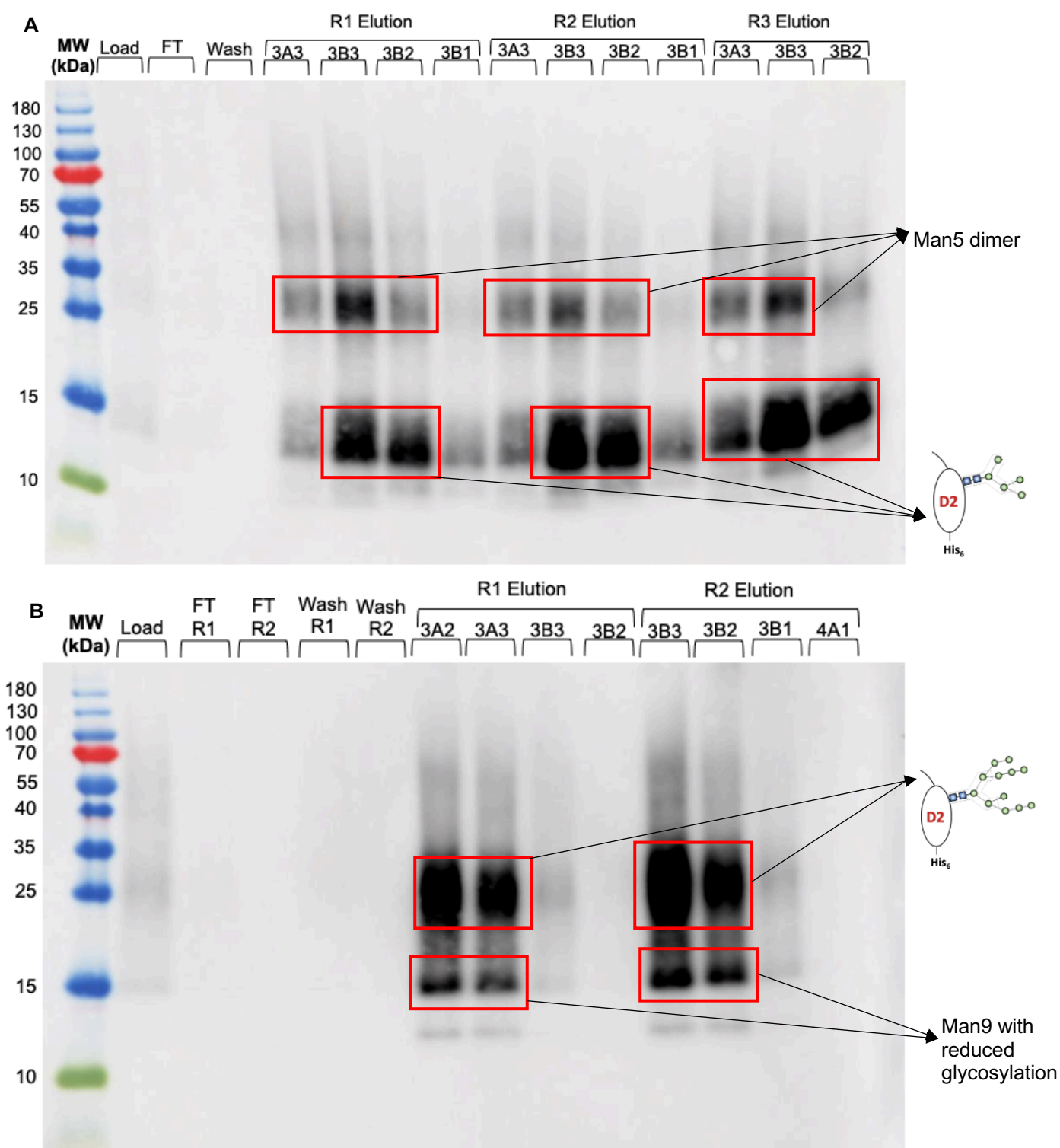
Figure 5.7 – Western blot analysis of the purification of **A)** Man5 cell culture harvest and **B)** Man9 cell culture harvest, both using His-tag affinity chromatography as described previously. The gels were run under reducing conditions. R1, R2 etc refers to separate purifications of the same harvest. For the Man5 Western blot (A), the flow-through (FT) and wash fractions were from R1. 3A2, 3A3 etc. refers to the position and labelling of the fraction in the fraction collector. The bands of the expected molecular weights for Man5 and Man9 are labelled and the antibody used was anti-His antibody.

Figure 5.7 shows that the bind-elute His-tag affinity separation was working as expected. For both blots, the load sample lanes have a much lower signal than the elution fraction sample lanes, showing the concentrative effect of the separation process as well as the purification. The FT and wash fractions exhibit no or very minimal signal, meaning that the His-tags on the FcγR ligands are binding the column effectively and the high A_{280} reading seen in the chromatograms in Figures 5.5 and 5.6 is therefore highly likely to be a result of HCPs and other impurities that absorb at 280nm rather than the His-tagged protein.

The fractions which showed the highest signal intensity in the Western blots were processed for subsequent binding studies. This processing included dialysis into a lower salt buffer to remove the imidazole and concentration of the samples, which is described in the following section as well as Section 2.8.5.

5.2.3 FcγR Ligand Sample Analysis

After the chromatography step, the FcγR ligands were solubilised in the imidazole elution buffer. These high-salt conditions would prevent binding of the FcγR ligands to antibody, so the samples required dialysis to remove the imidazole and reduce the salt concentration for subsequent binding studies. In addition to the salt concentration being too high for further studies, even after the concentration of the FcγR ligand samples during the chromatography step the sample concentrations still tended to be in the region of ~15-20μg/mL. As this would not be practical for mass spectrometry analysis, the samples required concentration as well as dialysis. This section details how the FcγR ligand samples were processed and subsequently analysed prior to binding studies being carried out.

5.2.3.1 Dialysis, Sample Concentration and Quantification

The 2mL elution fractions that detected Man9 or Man5 according to Western blot analysis were pooled (a maximum of 3 samples were pooled per ligand construct). These samples were dialysed into Biacore running buffer, 1X PBS-P$^+$, according to the Float-A-Lyzer® protocol described in Section 2.8.5.

Once the FcγR ligand samples had been dialysed, they were then concentrated. This was carried out using the Pall Microsep™ Advance Spin Filters (5mL, 3K MWCO) using the protocol described in Section 2.8.5. The retentate from the spin filters was collected and the concentration was quantified using a NanoDrop™ One Spectrophotometer.

Table 5.3 – NanoDrop™ A_{280} and $\frac{A_{260}}{A_{280}}$ measurements of dialysed and concentrated Man9 and Man5 samples which were used for subsequent binding studies. PBS-P⁺ was used as the blank and three separate 2μL samples were taken from the Man9 and Man5 stock for each measurement. The mean A_{280} and $\frac{A_{260}}{A_{280}}$ values were calculated for each ligand construct stock solution.

FcγR Ligand Construct	Measurement	A_{280} (AU)	$\frac{A_{260}}{A_{280}}$
Man9	1	0.15	0.73
	2	0.18	0.76
	3	0.15	0.76
	Mean	**0.16**	**0.75**
Man5	1	0.21	0.85
	2	0.24	0.73
	3	0.24	0.71
	Mean	**0.23**	**0.73**

An $\frac{A_{260}}{A_{280}}$ value of ~0.6 indicates a pure protein sample (DeNovix, 2019). The $\frac{A_{260}}{A_{280}}$ values for the FcγR ligand stock solutions are ~0.75, which indicates there was some nucleic acid material present in the samples, however this was not considered to be significant enough to purify the material again due to the additional product loss this would cause. The A_{280} measurement was used for calculating the sample concentrations (see Section 2.8.5 for calculations), which were found to be 0.081mg/mL for the Man9 sample and 0.12mg/mL for the Man5 sample to 2 decimal places.

5.2.3.2 Deglycosylation of Man5

In order to prepare the FcγRIIIa D2 ligand construct, an aliquot of the Man5 sample was deglycosylated. Previously, PNGase F had been used to attempt to deglycosylate another FcγR ligand construct that has not been tested in this work, called FcγR Mut. FcγR Mut consisted of the dual-domain FcγRIIIa with the same single *N*-glycosylation site that is present on Man5 and Man9, and the protein was also expressed in *P. pastoris*. Initial mass spectrometry studies used PNGase F to attempt deglycosylation of this construct, but it was found to be unsuccessful (see Figure 5.8A). Endo H was then successfully used to deglycosylate FcγR Mut, so this enzyme was also used to deglycosylate Man5 in this project.

PNGase F is an effective and common enzyme used for the removal of high-mannose, hybrid and complex *N*-linked glycans from glycoproteins. PNGase F cleaves between an Asn residue and the innermost GlcNAc of an *N*-glycan attached to this residue (New England Biolabs®,

'PNGase F'). A possible explanation for the PNGase F not working could be steric hindrance, meaning the enzyme cannot access the $\beta 1,N$ bond between the nitrogen on the Asn residue and the innermost GlcNAc on the glycan when the protein is in its native state. Endo H, however, cleaves the $\beta 1,4$ linkage between the two GlcNAc residues within the chitobiose core of N-linked glycans, leaving one GlcNAc still attached to the protein and releasing the rest of the N-glycan. Endo H is specific for high-mannose and hybrid glycans, and does not cleave complex glycans (Rao, Guan & Van Roey, 1995). Man5 was incubated with Endo H according to the protocol given in Section 2.9.2.
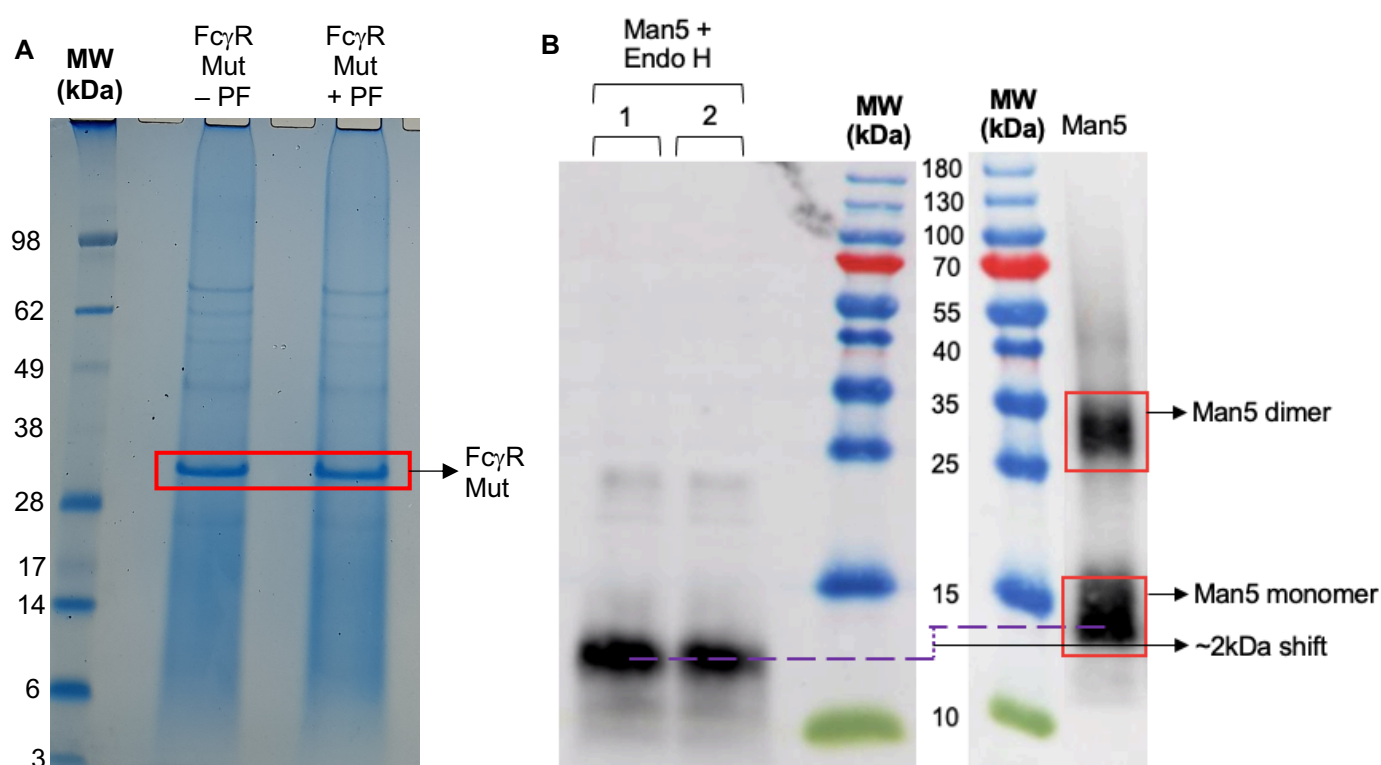
Figure 5.8 – **A)** reduced SDS-PAGE gel of FcγR Mut with and without PNGase F (PF). The protocol for PNGase F incubation can be found in Section 2.9.2. FcγR Mut is present at ~32kDa. There is no band shift indicating deglycosylation from the sample that had been incubated with PNGase F, indicating that the deglycosylation was not effective. Image obtained and provided by Dr. Anja Krueger, Imperial College London. **B)** Western blot analysis of Man5 and Man5 with Endo H (repeats 1 and 2 labelled as 1 and 2). All samples were run under reducing conditions and the antibody used was anti-His antibody.

Endo H worked effectively as we can see from the molecular weight band shift in Figure 5.8B. In Figure 5.18, we can see that the predominant N-glycan structure at the single site on Man5 is of the Man8 structure. One mannose residue has a molecular weight of 162Da, so one Man8 glycan has a molecular weight of 1.3kDa. Whilst not all glycans are of this structure, it had the highest intensity according to Figure 5.18, indicating that it is the most common

structure and is therefore the most logical structure to use in molecular weight calculations. The peptide alone is 11.4kDa, which gives a total molecular weight of the peptide and Man8 at one site of 12.7kDa. Man5 is present at ~14kDa on a Western blot, which is consistent with the peptide, the single *N*-glycan plus some possible *O*-linked glycosylation. The band on Figure 5.8B from Man5 after incubation with Endo H is present at ~12kDa, which is approximately equal to the molecular weight of the peptide backbone plus some possible *O*-linked glycosylation which is not cleaved by Endo H.

5.2.3.3 Mass Spectrometry

Mass spectrometry analysis was used to analyse and confirm the proteomic and glycomic profiles of FcγRIIIa D2 Man9 and Man5. Samples were analysed using matrix-assisted laser desorption/ionisation-time-of-flight (MALDI-TOF) and tandem mass spectrometry (MALDI-TOF/TOF) to analyse the glycomic profile of the ligands. In addition, electrospray ionisation-liquid chromatography-mass spectrometry (ESI-LC-MS) was used for proteomic and glycoproteomic data analysis via peptide mapping. All analysis was carried out and all figures and tables were produced by Dr. Anja Krueger, Imperial College London. Dr. Krueger also helped significantly in the writing of this section.

The first FcγR construct that was analysed was refFcγRIIIa, which has up to 5 glycosylation sites. On this construct, the most important *N*-glycan site to identify was N164 (see Sequence 2, Section 3.5), which translates to N76 in the FcγR ligand sequence. The *N*-glycan at N164 directly interacts with IgG1 and was the only *N*-glycan that we had kept from the WT FcγRIIIa on the Man5 and Man9 constructs. The glycoproteomic analysis to confirm that *N*-glycosylation was present at N164 evolved to be a challenging task, as this site was very close to another *N*-linked site on refFcγRIIIa and was also close to sites which possessed *O*-linked glycans. Additionally, there was a significant degree of microheterogeneity at the *N*-linked sites (see Figure 5.9), increasing the complexity of the analysis further. Initial analysis of FcγR Mut also indicated *O*-glycosylation was present within the region containing the *N*-glycan. This was later confirmed with Glu-C digestion (see Appendix 9.2).
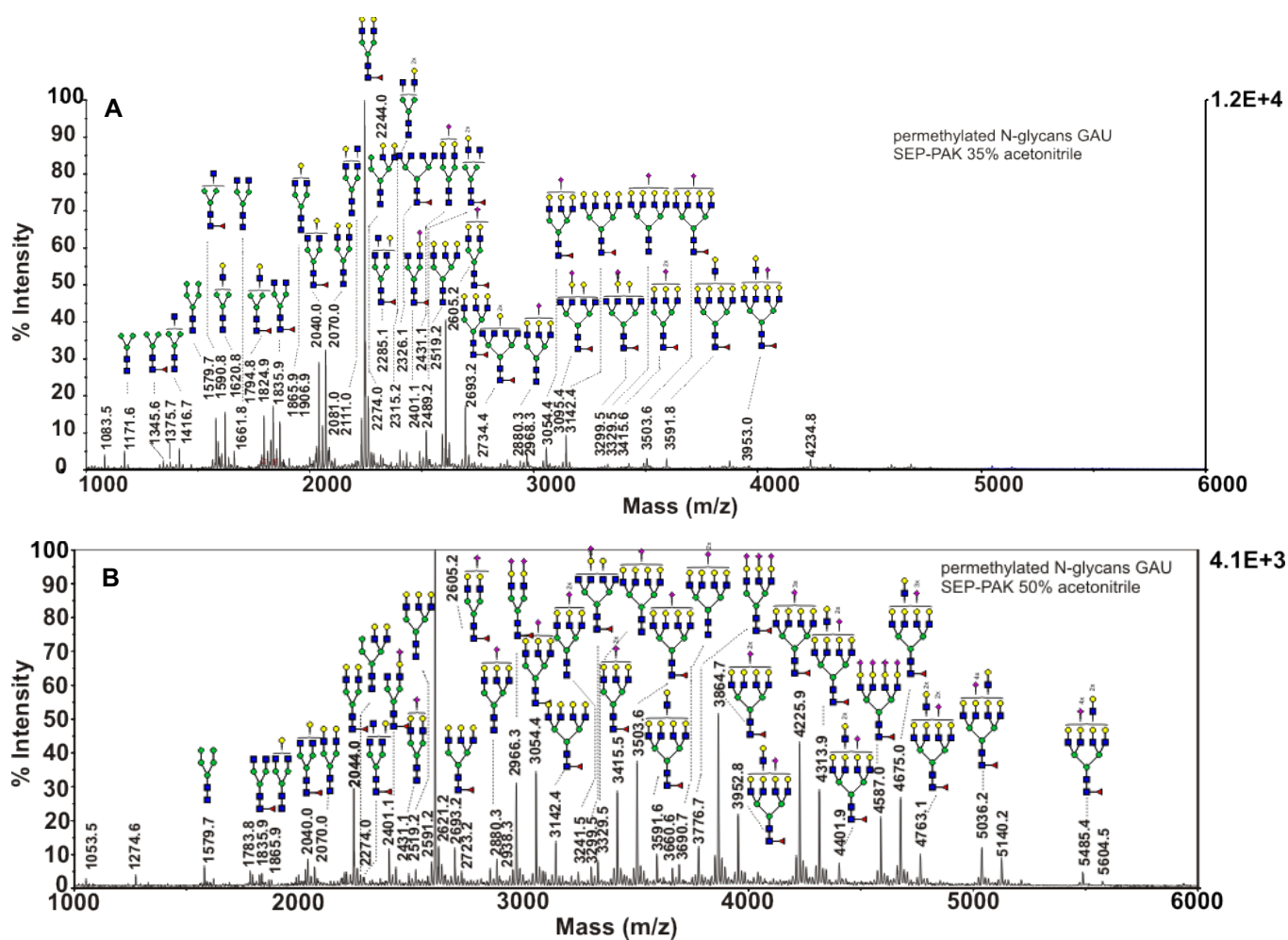
Figure 5.9 – MALDI-TOF MS spectrum of permethylated *N*-glycans from refFcγRIIIa after solid phase extraction using Sep-Pak® C18 using **A)** 35% acetonitrile and **B)** 50% acetonitrile. 35 structures were found.
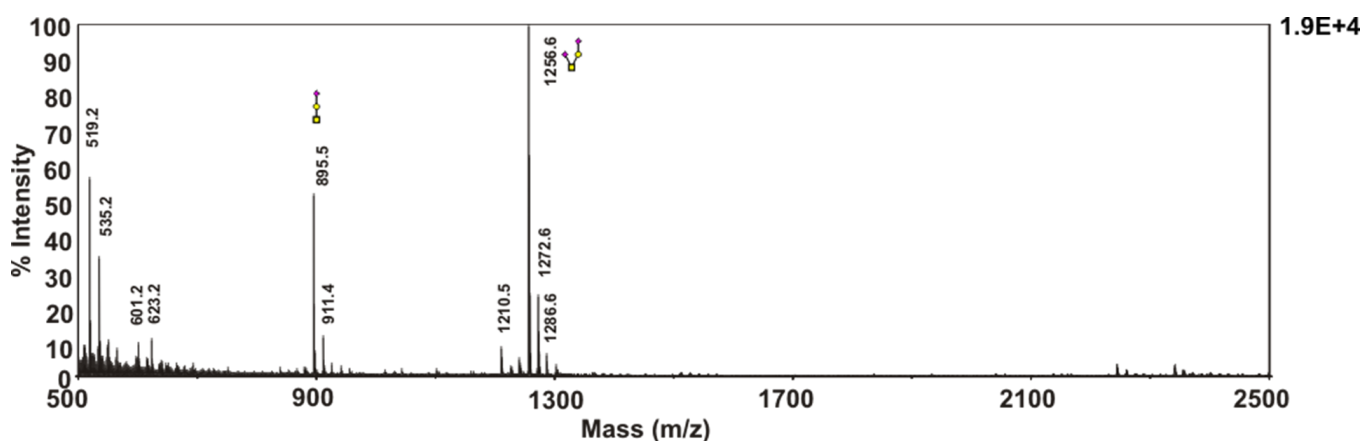
Figure 5.10 – MALDI-TOF MS spectrum of permethylated *O*-glycans after Sep-Pak® purification of refFcγRIIIa. 2 core *O*-glycan structures were found.

Once the MS protocol had been defined and the *N*- and *O*-glycans of refFcγRIIIa had been profiled, the glycomics of Man9 were profiled using the same protocol.

Man9

Based on experience analysing refFcγRIIIa, Man9 was peptide-mapped with 3 individual sequencing grade proteases in individual digests using trypsin, chymotrypsin and Glu-C (see Figure 5.11). Distinct proteases ensured different cleavage sites within the glycoprotein and therefore improved the likelihood of success in detecting the glycopeptide. Glu-C was used to identify the site containing the His-tag, which had been difficult to identify in previous work with FcγR Mut.

Peptide mapping of Man 9

Trypsin digestion: sequence coverage: 69.7%, 69/99 AA

| 1 to 50: | HIGWLLLQAP | RWVFKEEDPI | HLRCHSWKNT | ALHKVTYLQN | GKGRKYFHHN |
| 51 to 99: | SDFYIPKATL | KDSGSYFCRG | LVGSK**N**VSSE | TVQITITQGG | GSHHHHHHC |

Chymotrypsin digestion: sequence coverage: 67.7%, 67/99 AA

| 1 to 50: | HIGWLLLQAP | RWVFKEEDPI | HLRCHSWKNT | ALHKVTYLQN | GKGRKYFHHN |
| 51 to 99: | SDFYIPKATL | KDSGSYFCRG | LVGSK**N**VSSE | TVQITITQGG | GSHHHHHHC |

Glu-C digestion: sequence coverage: 19.2%, 19/99 AA

| 1 to 50: | HIGWLLLQAP | RWVFKEEDPI | HLRCHSWKNT | ALHKVTYLQN | GKGRKYFHHN |
| 51 to 99: | SDFYIPKATL | KDSGSYFCRG | LVGSK**N**VSSE | TVQITITQGG | GSHHHHHHC |

Figure 5.11 – peptide mapping of Man9. Individual protein sequence coverages of the proteases trypsin, chymotrypsin and Glu-C were used to cleave Man9 and confirm the primary structure.

In order to isolate the most challenging region within the glycoprotein containing the *N*-glycan at N76 involved in IgG1 binding (G70 to E80), a combined digestion of chymotrypsin and Glu-C was used.

FcgR3a D2 single domain mono-*N*-glycosylated: total sequence coverage: 80.9%, 80/99 AA

1 to 50:	HIGWLLLQAP	RWVFKEEDPI	HLRCHSWKNT	ALHKVTYLQN	GKGRKYFHHN
51 to 99:	SDFYIPKATL	KDSGSYFCRG	LVGSK**N**VSSE	TVQITITQGG	GSHHHHHHC

via targeted MS/MS
Glu-C, Chymotrypsin, Endo Hf

Figure 5.12 – sequence coverage of Man9 achieved by digesting the protein with Glu-C, chymotrypsin and Endo Hf.

The glycopeptide was then digested with Endo Hf to remove the *N*-glycan, leaving a GlcNAc residue which is detected as HexNAc. This was analysed using ESI-LC-MS and a fast data-dependent acquisition (fast DDA) approach to confirm that the *N*-glycan is present on the N76 as expected.
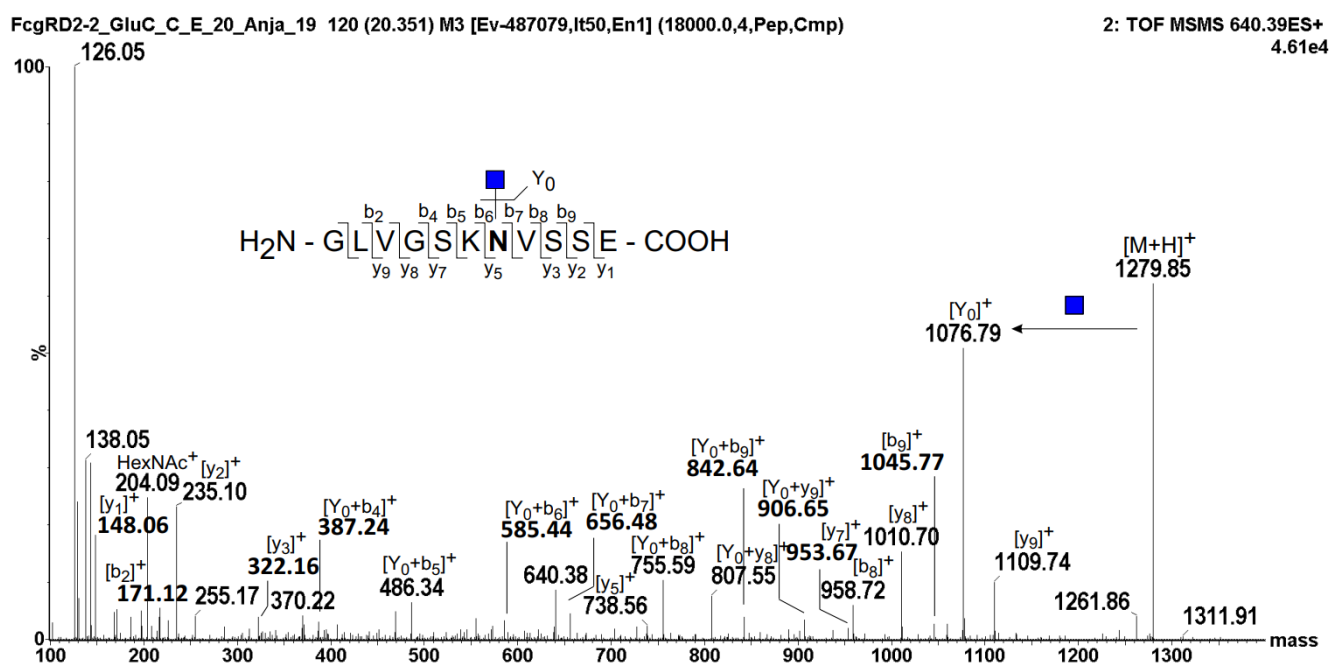
Figure 5.13 – ESI-LC-MS fast DDA MS/MS spectrum of the single glycosylation site with 1 HexNAc attached after Endo Hf digestion of Man9, proving that the correct glycopeptide had been identified.

This MS/MS analysis confirmed that the glycan was present at the N76 site as expected. Next, the glycomic profile of Man9 was analysed.
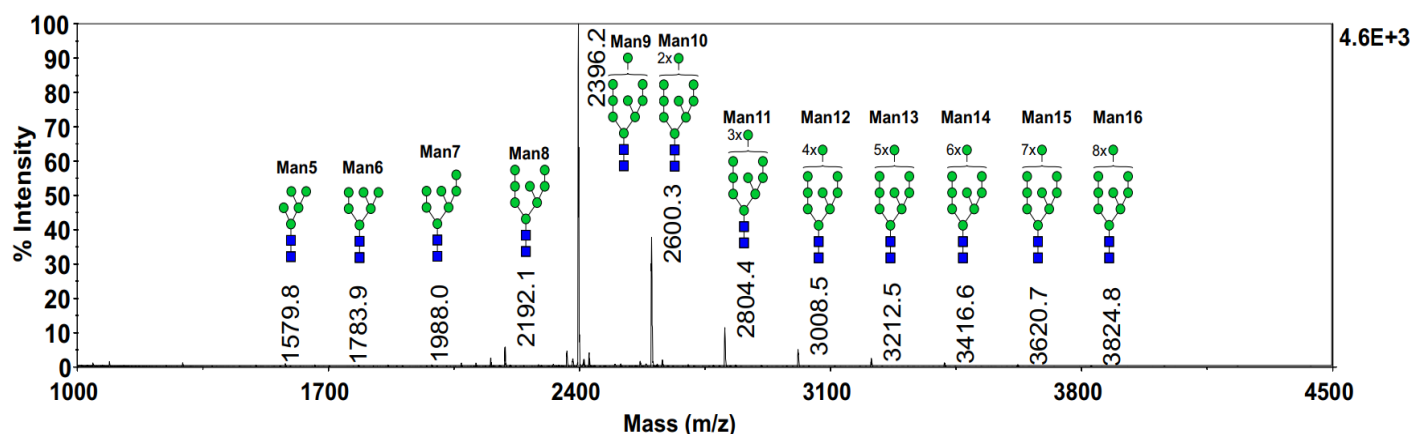
Figure 5.14 – MALDI-TOF MS spectrum of permethylated *N*-glycans after Sep-Pak® purification of FcγRIIIa D2 Man9. 16 structures were found, with the most prevalent structure being Man9.

By comparing signal intensities in Figure 5.14, it can be concluded that the predominant *N*-glycan structure found at N76 of Man9 is of the Man9 structure. There is also a large degree of hypermannosylation on the ligand construct, with glycans branching up to Man16 at this site.
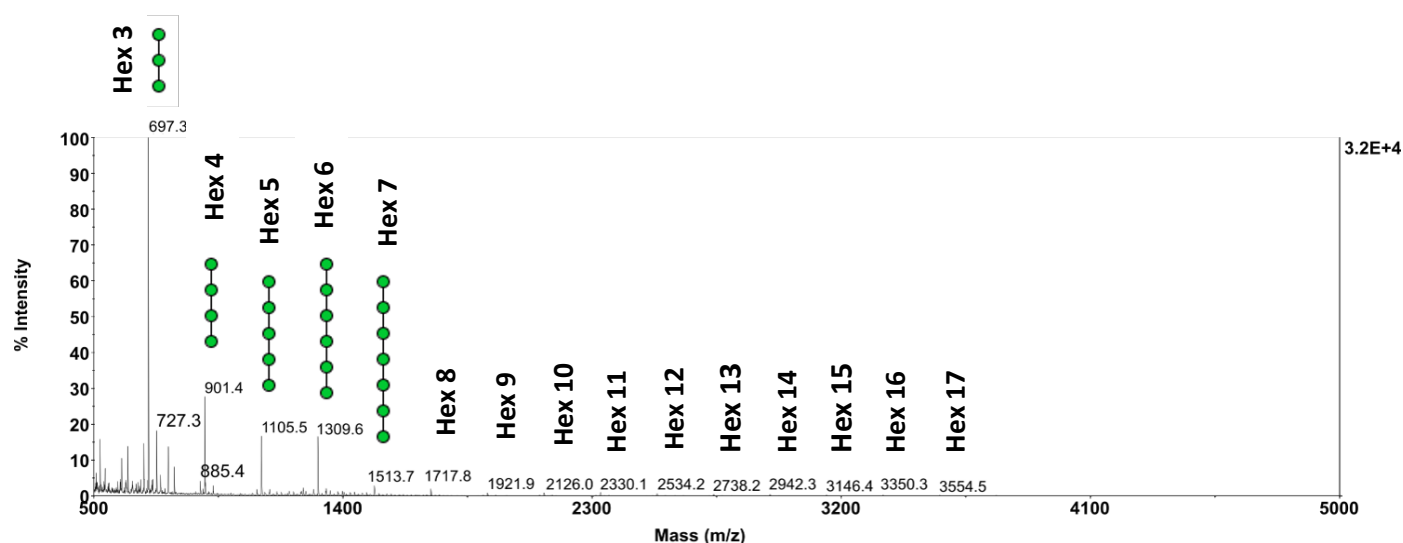
Figure 5.15 – MALDI-TOF MS spectrum of permethylated *O*-glycans after Sep-Pak® purification of FcγRIIIa D2 Man9. 17 structures were found, with the most prevalent structure being hexose 3 (Man3).

This glycomic profiling explained why Man9 runs at a much higher molecular weight than Man5 during Western blot analysis. The protein has one *N*-glycan site, and at this site structures up to Man16 were found. If we assume an 'average' glycan structure at this site of Man10, this gives a mass for the *N*-linked Man9 of 13kDa. If we then include *O*-linked glycans, which could be present at a minimum of 6 sites (see Table 5.4) and assume an 'average' glycan structure at each site of Hex6 (Man6), this gives a total protein molecular weight of 18.8kDa. Man9

tends to show as a band at ~24kDa on a Western blot, but is very possible that there are more than 6 *O*-glycan sites on Man9, which would explain why the band shows at a higher molecular weight than 18.8kDa on a Western blot.

In Figure 5.15, the monosaccharides on the spectrum are labelled as Hex. This is because during MS, only the hexose (Hex) residue is detected, but the isomer that is present (glucose, galactose or mannose) cannot be discerned. However, we know that *P. pastoris N-* and *O*-glycans are high-mannose structures, and in particular that *O*-glycans in *P. pastoris* are made up of mannoses (Nett et al., 2013). Therefore, we can assume that all hexoses detected in the glycomic analysis of Man9 are mannose residues.

Table 5.4 – table of likely and confirmed glycosylation sites on Man9.

Peptide	Amino acids	Glycosylation type	Confirmed	Possible or confirmed site(s)
C(CM)HSWKNTALHK	24-34	*O*-linked	No	S26, T30 (possible)
NTALHKVTYLQNGK	29-42	*O*-linked	No	T30, T36 (possible)
KYFHHNSDFYIPK	45-57	*O*-linked	Yes	S51 (possible)
ALTKDSGSYFC(CM)R	58-69	*O*-linked	Yes	T60, S63, S65 (possible)
GLVGSKNVSSE	70-80	*N*-linked	Yes	N76 (confirmed)
TVQITITQGGGSHHHHHHC(CM)	81-99	*O*-linked	Yes	T81, T85, T87, S92 (possible)

1 to 50:	HIGWLLLQAP	RWVFKEEDPI	HLRCH**S**WKN**T**	ALHKV**T**YLQN	GKGRKYFHHN
51 to 99:	**S**DFYIPKA**T**L	KD**S**G**S**YFCRG	LVGSK**NVSS**E	**T**VQI**T**I**T**QGG	G**S**HHHHHHC

Figure 5.16 – summary of potential *N-* and *O*-linked glycosylation sites on Man9. The amino acid that is confirmed to be glycosylated is N76, with the other serine and threonine sites highlighted in grey being possibly *O*-glycosylated.

In conclusion, all proteomic and glycoproteomic analysis, including peptide mapping and the ESI-LC-MS spectrum, confirmed total sequence coverage of Man9 and confirmed the *N*-glycan site to be N76, which was as expected. Next, Man5 was profiled.

Man5

As the analysis of the FcγRIIIa-based constructs so far had been challenging and had taken several months to achieve, some time had been taken away from the Man5 analysis. Therefore, only the proteomic, glycoproteomic and *N*-glycan profiles of Man5 were analysed. As Man9 and Man5 are very similar proteins, parameters and approaches used in the Man9 analysis were also used to analyse Man5.

Peptide mapping of Man 5

Trypsin digestion: sequence coverage: 94.4% 94/99 AA

1 to 50:   HIGWLLLQAP RWVFKEEDPI HLRCHSWKNT ALHKVTYLQN GKGRKYFHHN

51 to 99:   SDFYIPKATL KDSGSYFCRG LVGSK**N**VSSE TVQITITQGG GSHHHHHHC

Chymotrypsin digestion: sequence coverage: 78.8% 78/99 AA

1 to 50:   HIGWLLLQAP RWVFKEEDPI HLRCHSWKNT ALHKVTYLQN GKGRKYFHHN

51 to 99:   SDFYIPKATL KDSGSYFCRG LVGSK**N**VSSE TVQITITQGG GSHHHHHHC

Figure 5.17 – peptide mapping of Man5. The full sequence was identified and the N76 glycosylation site is highlighted.

In the peptide mapping of Man5, full sequence coverage was achieved using trypsin and chymotrypsin. Glu-C digestion was not necessary as the glycans were less diverse and the His-tag was identified in the trypsin digest.
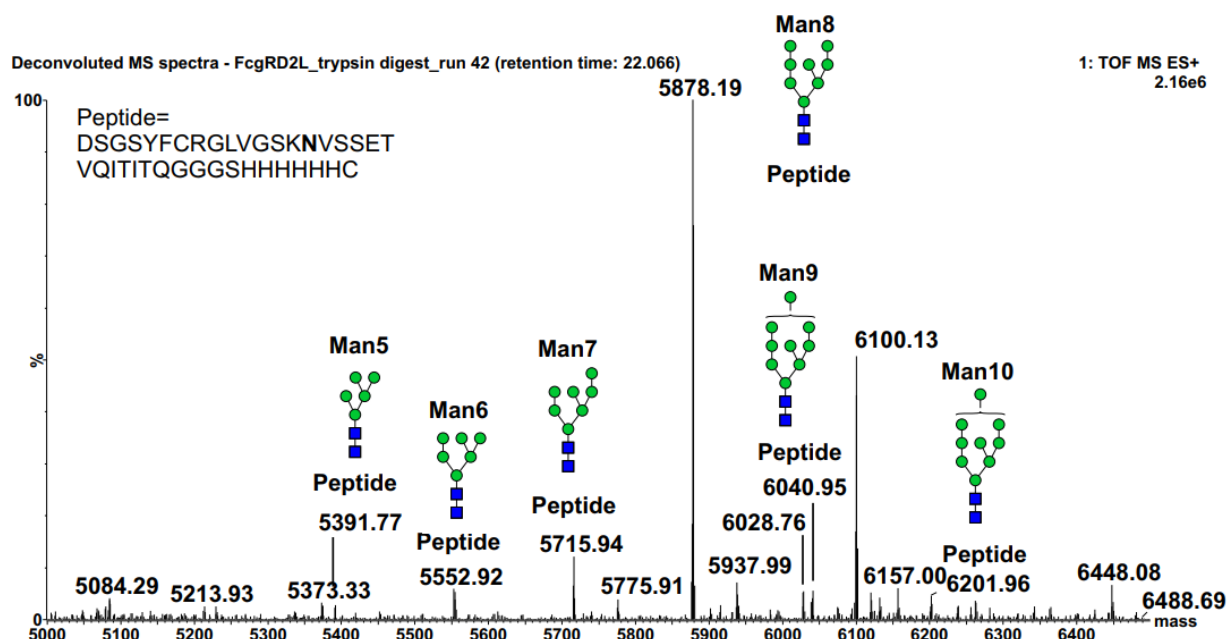
Figure 5.18 – glycoproteomic deconvoluted MS/MS spectrum showing *N*-glycan fragmentations found on Man5 at the N76 site. Glycans up to Man10 were seen, with Man8 being the predominant structure.

As mentioned previously, Man5 was expressed in the GlycoSwitch™ SuperMan5-10 strain, which only yields high-mannose glycans up to Man10. According to the spectrum of Man5 shown in Figure 5.18, the predominant *N*-glycan structure on Man5 is Man8, which is consistent with the expression system in which it was produced. This analysis confirmed that Man5 has a reduced degree of mannosylation at the single *N*-glycan site compared to the

Man9 construct. Glycoproteomic analysis confirming that this glycan was present at N76 is given in Figure 5.18.

5.3 Conclusion

In this chapter, the shake flask culture protocol for the production of the FcγR ligands was detailed, along with how issues associated with protein aggregation were mitigated. By growing cells to higher cell densities at the end of the second BMGY growth phase and inducing to a higher OD_{600} at the start of the BMMY growth phase, protein aggregation appeared to be minimised. The purification of the ligands using His-tag affinity chromatography was successful, and the Man9 and Man5 samples were processed by dialysis to remove the imidazole from the elution buffer and were concentrated using spin filters for subsequent analysis, including mass spectrometry analysis and binding studies (see Chapter 6). Mass spectrometry analysis confirmed the primary structure of both Man9 and Man5 from enzymatic digests using trypsin, chymotrypsin, Glu-C and combined digestions. Glycomic analysis confirmed Man9 has a higher degree of mannosylation at the *N*-linked site on N76 compared to Man5, and *O*-glycosylation was also confirmed to be present on Man9, with possible and confirmed sites of this glycosylation also provided.

Chapter 6 – Measuring FcγR Ligand Affinities for IgG1 Glycovariants

6.1 Introduction

There are a variety of different techniques that can be used to detect and quantify the interactions between proteins. A well-established method is SPR, and one of the most widely-used instruments that employs SPR to detect protein-protein interactions is the Biacore™. The Biacore™ is capable of measuring interactions between molecules with a huge range of sizes, from small molecules to viruses, over a wide concentration and affinity range. Binding experiments using this instrument do not require labelling of the binding partners and the data obtained can be used to provide affinity constants for interactions, as well as giving an idea about how specific the interactions are (Helmerhorst et al., 2012). There are different types of Biacore™ instruments and a variety of chip types are available, including custom-made chips, meaning that a set-up can be found for almost any interaction to be studied. SPR is widely used in drug discovery for characterising binding between drugs and their target. In the context of this work, the Biacore™ was used for chromatographic affinity ligand development.

The work leading up to this chapter has focused on the design and production of the FcγR ligands, including fermentation, the finalised shake flask culture protocol, His-tag affinity purification and various protein analysis techniques to confirm the primary sequence and glycomic profile of the ligands. This chapter details the work carried out to assess whether the FcγR affinity ligands bind IgG1 and possess different affinities for IgG1 glycovariants.

To test whether the FcγR ligands possessed the same differential affinity for fucosylated and afucosylated IgG1 as FcγRIIIa, two glycovariants of trastuzumab (fucosylated and afucosylated) were purchased. However, after the trastuzumab samples proved challenging to immobilise, we moved on to working with tocilizumab, an alternative IgG1. For the kinetics/affinity assays in this work, tocilizumab glycovariants were immobilised to CM5 chips using EDC/NHS chemistry and the FcγR ligands were passed across the chip surfaces as the analytes. This is a similar format to other work which has tested the affinity of various FcγRs for antibodies (Wang & Chen, 2022) and allowed for higher throughput testing of the FcγR ligands. In this chapter, the results of the attempted immobilisation of trastuzumab, the preparation of a low-fucose sample of tocilizumab and the sensorgrams of the kinetics/affinity analyses of refFcγRIIIa and the FcγR ligands with tocilizumab glycovariants are shown, along with affinity data for these interactions.

There was a choice between immobilising the antibody constructs or the FcγR constructs to the sensor chip surfaces. The first set of experiments aimed to measure the interaction of the FcγR constructs with glycosylated and deglycosylated tocilizumab, i.e. only two antibody constructs. As there were four FcγR constructs (refFcγRIIIa, FcγRIIIa D2 Man9, FcγRIIIa D2 Man5 and FcγRIIIa D2) to test, it was decided that the antibodies would be immobilised to two separate chips and the FcγR constructs would be used as the analytes to enable for faster ligand screening. Later on in the project, the low-fucose tocilizumab construct was used for affinity testing, so again this antibody glycovariant was immobilised to a CM5 chip and the FcγR constructs were used as the analytes for higher throughput screening.

In the first results section, the techniques trialled for the immobilisation of glycovariants of trastuzumab and tocilizumab are detailed. In the second results section, the interactions of the FcγR constructs with glycosylated and deglycosylated tocilizumab are described. In the final results section, the preparation of a low-fucose sample of tocilizumab and the interaction of the FcγR constructs with this sample is shown.

6.2 Results – Antibody Immobilisation Techniques for Affinity Analysis

As mentioned, both fucosylated and afucosylated samples of trastuzumab were purchased for testing against the FcγR ligands. Trastuzumab is thought to use ADCC as one of its effector functions (Mandó et al., 2021), making it an ideal choice for use in these experiments. The most common strategy for immobilisation and the one which is often the best starting point when immobilising a protein is EDC/NHS chemistry, which for Biacore™ studies involves immobilising the protein to a CM5 sensor chip via lysine side chains on the protein. Despite many different conditions being trialled, primarily involving the pH and salt concentration of the sample buffer, the immobilisation of both glycovariants of trastuzumab to a CM5 chip using EDC/NHS chemistry was unsuccessful. Other immobilisation strategies shown in Table 6.1 were therefore attempted, with the results of these approaches shown in the following sections. For the sake of clarity, where the term 'fucosylated trastuzumab' is used, it refers to a sample of heterogeneously-glycosylated trastuzumab which has been produced in a CHO cell line and purified using Protein A chromatography; i.e., it does not consist of only fucosylated trastuzumab, but has a far greater degree of fucosylation compared to afucosylated trastuzumab. In general, IgG tend to have 1.3-19.3% afucosylated glycans in their Fc region (Pučić et al., 2011). The term 'afucosylated trastuzumab' refers to a sample of trastuzumab which was produced in CHO using GlymaxX® technology, which can result in the production of 98% afucosylated antibody (von Horsten et al., 2010).

Table 6.1 – comparison of different immobilisation techniques used in this work. Due to the transient nature of the interaction between antibody (ligand) and immobilisation binding partners Protein L and HER2, these techniques were tested for trastuzumab immobilisation but were not utilised as approaches for binding assays. Green represents an advantage, orange a minor disadvantage and red a critical disadvantage.

	Antibody Immobilisation Technique				
	EDC/NHS	**Streptavidin-biotin**	**Protein L**	**HER2**	**Click Chemistry**
Strength of immobilisation	Very high	High	Weak	Weak	Very high
Baseline drift after immobilisation	No	No	Yes	Yes	No
Optimal orientation for analyte binding	Unknown	Unknown	Yes	Yes	Unknown
Ease of procedure	Relatively easy	Moderate	Relatively easy	Moderate	Moderate
Cost	Relatively low	Relatively high	Moderate	Relatively high	Moderate
Effect on analyte binding	Moderate-low	Moderate-low	Low	Low	Moderate-low

6.2.1 Streptavidin-Biotin

This immobilisation technique exploits the high-affinity interaction between streptavidin (SA) and biotin. This interaction is the strongest non-covalent interaction known ($K_D = 10^{-15}$M) (Jain & Cheng, 2017) and is therefore convenient for Biacore™ studies as it can withstand relatively harsh regeneration conditions and does not cause baseline drift.

Immobilisation of a protein to an SA chip requires the protein for immobilisation to be conjugated to biotin. This can be done using different chemistries. The most common is using EDC/NHS chemistry which adds biotin to lysine residues on the protein, and another method often used is tagging via cysteine residues on the protein using thiol chemistry. In this work, both of these methods were attempted using fucosylated trastuzumab to see if there was a difference or improvement in conjugation using one chemistry compared to the other.
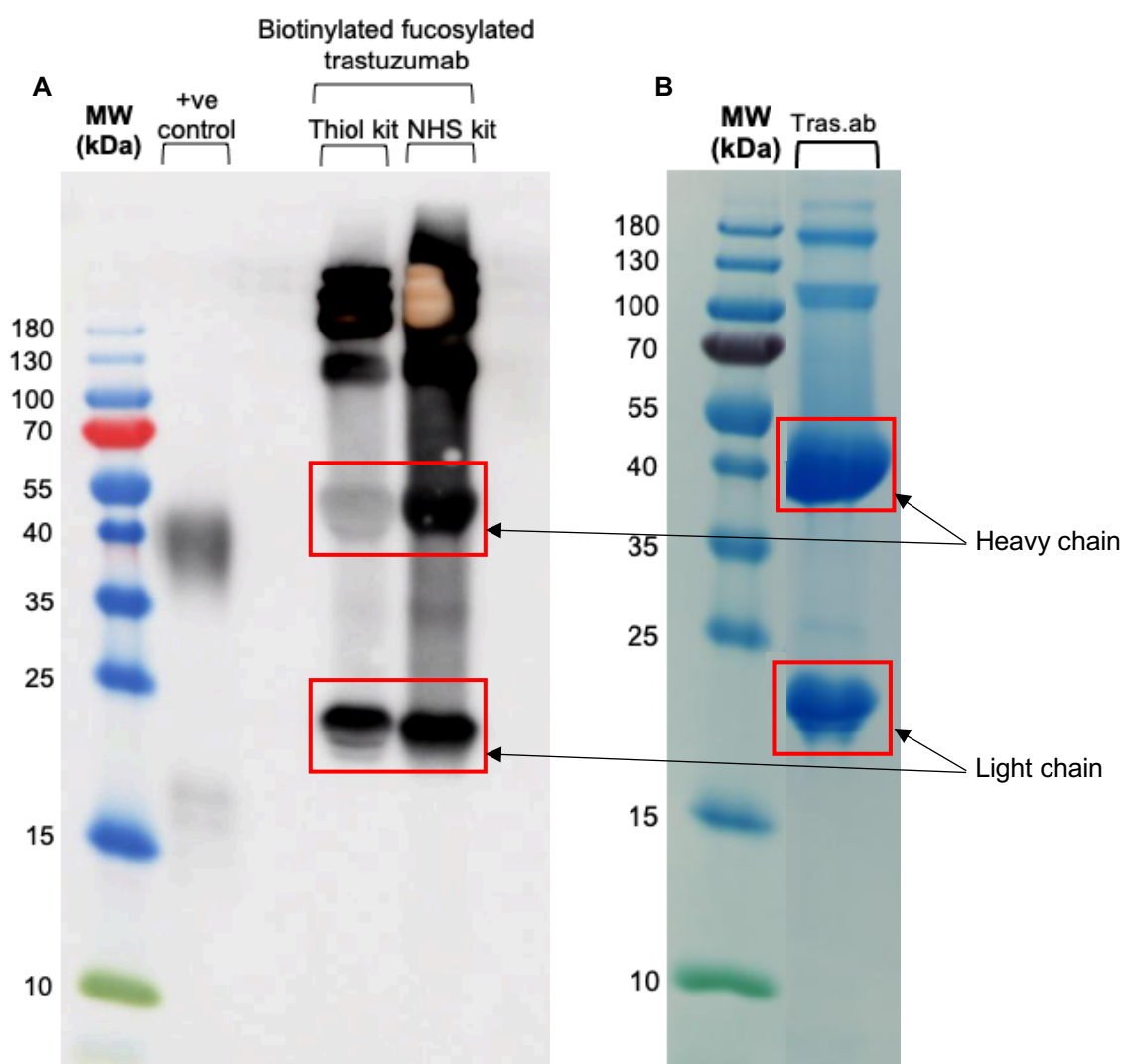
Figure 6.1 – A) Western blot confirming biotinylation of fucosylated trastuzumab using both thiol- and NHS-coupling kits. The positive control used was biotinylated refFcγRIIIa and the gel was run under reducing conditions. To probe for biotin tagging, SA directly conjugated to HRP was used. Using both linkage types, there was labelling seen of what is likely to be individual light chains (~23kDa). The NHS kit also showed likely biotinylation of the heavy chain (~50kDa), as well as the whole antibody at ~140-150kDa and higher molecular weight derivatives at molecular weights at or above 180kDa, which could be aggregates. The thiol kit also showed biotinylation of the whole antibody construct and higher molecular weight derivatives, although no or very little biotinylation of the heavy chain; an explanation for this is given in the paragraph below. **B)** SDS-PAGE image of the same trastuzumab sample not conjugated to biotin. A similar pattern of bands can be seen on both the Western blot and the gel at ~23kDa, ~50kDa, ~120kDa and ~170kDa, with another band at a slightly higher molecular weight than the ladder can accurately measure.

The biotinylation of trastuzumab worked and showed a strong signal, indicating a high level of conjugation, i.e. a high number of biotin molecules per molecule of antibody. For the thiol conjugation, there was very little to no conjugation of the heavy chains (~50kDa). This could

be because the cysteines in the heavy chain primary sequence are all involved in disulfide bridges holding the chains together, and these are broken during reduction in order for biotin tagging to take place. The breaking of these chains is likely to give rise to bands at a very similar molecular weight to the light chain, which would explain the lack of visible band at ~50kDa for the thiol kit. Overall, the NHS kit showed a higher intensity on the resulting image, indicating an overall higher level of biotinylation using the NHS kit compared to the thiol kit (see Figure 6.1). This could be due to the much greater number of lysines in the trastuzumab primary sequence compared to the number of free cysteines.

```
EVQLVESGGG  LVQPGGSLRL  SCAASGFNIK  DTYIHWVRQA  PGKGLEWVAR
IYPTNGYTRY  ADSVKGRFTI  SADTSKNTAY  LQMNSLRAED  TAVYYCSRWG
GDGFYAMDYW  GQGTLVTVSS  ASTKGPSVFP  LAPSSKSTSG  GTAALGCLVK
DYFPEPVTVS  WNSGALTSGV  HTFPAVLQSS  GLYSLSSVVT  VPSSSLGTQT
YICNVNHKPS  NTKVDKKVEP  KSCDKTHTCP  PCPAPELLGG  PSVFLFPPKP
KDTLMISRTP  EVTCVVVDVS  HEDPEVKFNW  YVDGVEVHNA  KTKPREEQYN
STYRVVSVLT  VLHQDWLNGK  EYKCKVSNKA  LPAPIEKTIS  KAKGQPREPQ
VYTLPPSREE  MTKNQVSLTC  LVKGFYPSDI  AVEWESNGQP  ENNYKTTPPV
LDSDGSFFLY  SKLTVDKSRW  QQGNVFSCSV  MHEALHNHYT  QKSLSLSPG
```

Sequence 4 – trastuzumab heavy chain sequence. Lysines are highlighted in blue, cysteines in red. There are 29 lysines and 11 cysteines in the above sequence, illustrating how there is much more opportunity for conjugation of biotin using the NHS kit compared to the thiol kit.

```
DIQMTQSPSS  LSASVGDRVT  ITCRASQDVN  TAVAWYQQKP  GKAPKLLIYS
ASFLYSGVPS  RFSGSRSGTD  FTLTISSLQP  EDFATYYCQQ  HYTTPPTFGQ
GTKVEIKRTV  AAPSVFIFPP  SDEQLKSGTA  SVVCLLNNFY  PREAKVQWKV
DNALQSGNSQ  ESVTEQDSKD  STYSLSSTLT  LSKADYEKHK  VYACEVTHQG
LSSPVTKSFN  RGEC
```

Sequence 5 – trastuzumab light chain sequence. Lysines are highlighted in blue, cysteines in red. There are 13 lysines and 5 cysteines in the above sequence, again illustrating how there is much more opportunity for conjugation of biotin using the NHS kit compared to the thiol kit.

From the above Western blot and sequence analyses, it is clear that biotinylation of trastuzumab via either lysine or cysteine side chains may not be the most suitable method of immobilisation for subsequent FcγR ligand binding. The high signal levels on the SA Western blot using both kits indicate a high degree of conjugation, with a higher signal using the NHS

kit; this is likely due to the higher number of lysines compared to cysteines in the primary sequence. This means there is probably a high number of biotin molecules per molecule of antibody, which could perturb affinity for the FcγR ligands; subsequent kinetics/affinity assays with refFcγRIIIa did indeed show no or very minimal binding of this protein to immobilised biotinylated trastuzumab. It may be possible to optimise the conjugation protocol to allow for a lower level of conjugation, which could be done using a lower molar excess of biotin, although this may be difficult to control and quantify. There may also be lysine residues in the FcγRIIIa-trastuzumab binding site in the Fc region of trastuzumab, and if these are tagged it would create steric hindrance and hinder binding of the antibody to refFcγRIIIa or the FcγR ligands. Biotinylation using the thiol kit is not a viable option due to the cysteines in the primary sequence all being involved in either intra- or interchain disulfide bridges, meaning that the antibody must be reduced into an incomplete structure for biotinylation to take place. This would not be a reliable or accurate assay for these binding studies as the aim is to investigate the interaction between the FcγR ligands and complete antibody rather than individual chains. This immobilisation method was therefore not used for the kinetics/affinity assays with the FcγR ligands.

6.2.2 Protein L

Protein L is a 76kDa bacterial surface protein first isolated from *Peptostreptococcus magnus*. It selectively binds the V_L chains in the Fab region of all classes of immunoglobulins (Akerström & Björck, 1989). By immobilising via the Fab region using Protein L, the Fc region should theoretically be available for FcγR ligand binding. This is not a permanent immobilisation method like EDC/NHS, streptavidin-biotin or click chemistry and can therefore result in baseline drift during an SPR assay.

Chips with Protein L pre-immobilised via EDC/NHS chemistry are commercially available. Tocilizumab was used as a test IgG1 to establish whether the baseline drift would be too significant before using up our more limited supply of fucosylated and afucosylated trastuzumab. Tocilizumab was injected onto the surface of a Protein L chip which had been equilibrated in 1X PBS-P$^+$ running buffer.
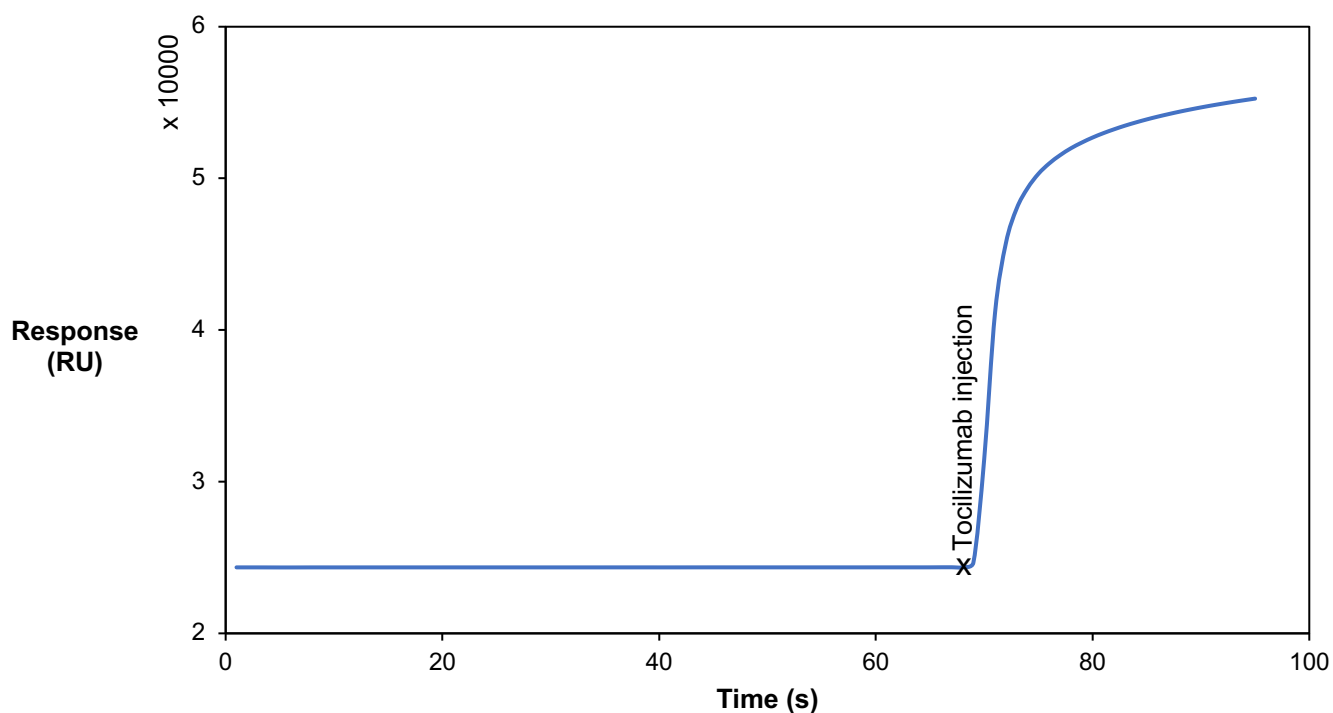
Figure 6.2 – injection of 27μM tocilizumab onto the Protein L chip surface (Fc 2). The baseline was ~24,350RU and the length of the tocilizumab pulse was 25 seconds, after which the response went up to 55,260RU. This gives an initial capture level of ~31,000RU.

The initial capture level is very high at ~31,000RU. This is due to the high concentration of tocilizumab sample that was injected (27μM). It was anticipated that tocilizumab would dissociate from the chip, so a higher than desired initial capture level was first achieved. A ~1-hour wash using running buffer was then used to wash off loosely-bound antibody and establish whether a baseline drift was noticeable (see Figure 6.3).
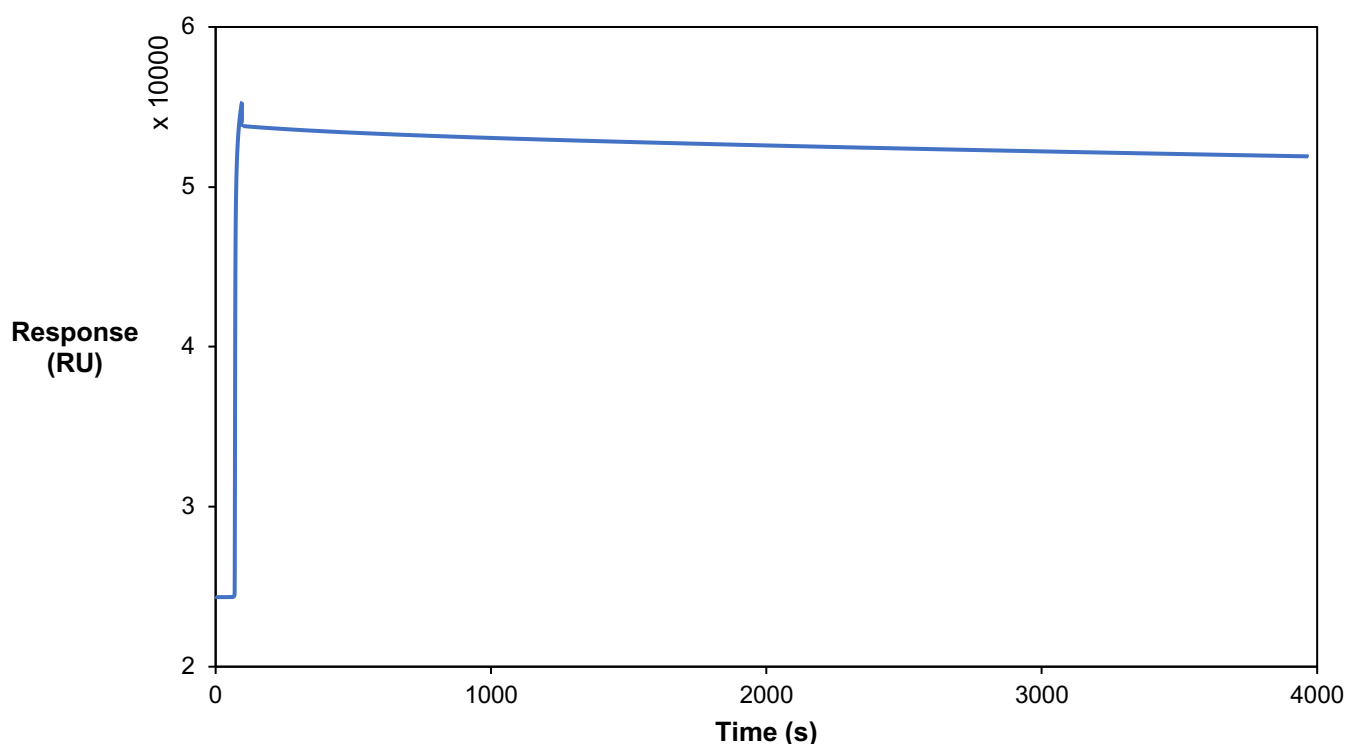
Figure 6.3 – immobilisation of tocilizumab and subsequent wash to remove loosely-bound ligand. Baseline drift is visible; the response on Fc 2 just after the tocilizumab injection is 53,809RU, and after the ~1-hour (66.1 minute) wash the response was 51,881RU.

The response consistently decreased throughout the duration of the 1-hour wash. It was decided that this baseline drift was too significant to continue with the kinetics/affinity assay, as after multiple rounds of regeneration too much antibody would have dissociated from the chip and subsequent kinetic analysis would not be accurate. It is possible to chemically cross-link an interaction with reagents such as DMSO, although this can perturb binding affinity and could also therefore distort the kinetic/affinity analysis. There was also an option to re-immobilise after each concentration cycle, but even within each ~20-minute cycle there likely would have been a notable degree of baseline drift.

6.2.3 Human Epidermal Growth Factor Receptor 2

Human epidermal growth factor receptor 2 (HER2) is the cognate receptor for trastuzumab, binding in the Fab region (see Figure 6.4). The Fab region of trastuzumab binds the HER2 extracellular domain (HER2 ECD) with a K_D of 2-5nM (Lakayan et al., 2018). The strategy was to immobilise HER2 ECD to the surface of a CM5 chip via EDC/NHS chemistry and then capture trastuzumab to the HER2 ECD on the surface of the chip. This would again not be a permanent immobilisation method, but our plan was to either carry out regeneration scouting and monitor the baseline to see whether a regeneration solution could be found which could

remove the analyte (FcγR ligand) from the trastuzumab but would not remove the trastuzumab from the HER2, or to explore the option of re-immobilising the trastuzumab after each cycle.
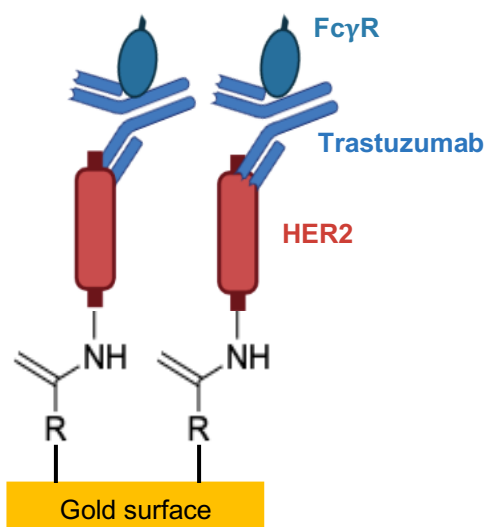
Figure 6.4 – depiction of HER2-trastuzumab immobilisation strategy. The HER2 ECD is immobilised via EDC/NHS chemistry to a CM5 chip. The trastuzumab is then captured to the immobilised HER2 ECD. The FcγR ligands would be injected over the chip surface and would theoretically bind the captured trastuzumab.

Firstly, HER2 ECD was immobilised to a CM5 chip (see Figure 6.8) using EDC/NHS chemistry (see Figure 6.5).
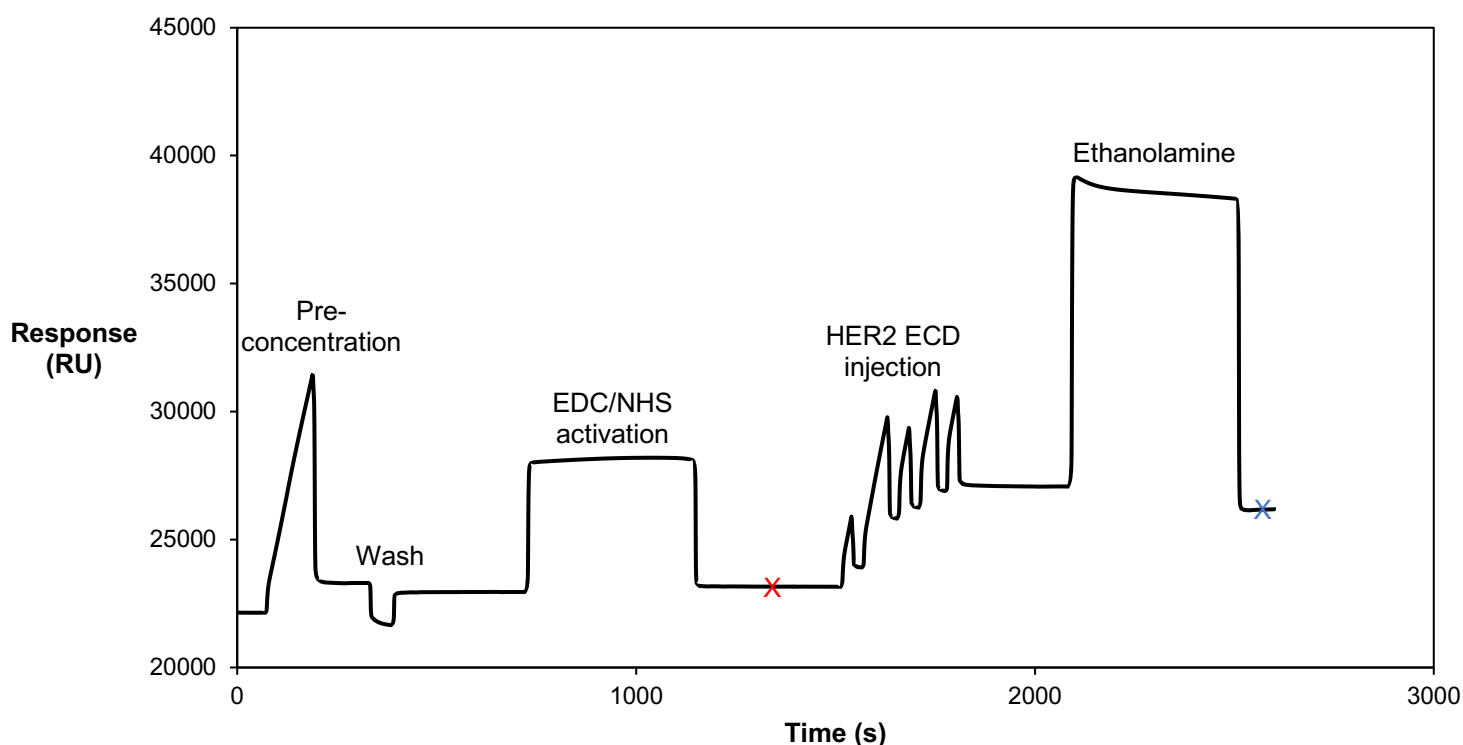
Figure 6.5 – EDC/NHS immobilisation of 0.98μM HER2 ECD to the Fc 2 channel of a CM5 chip. More details about this procedure can be found in Section 2.9.1.1. The wash step was carried out with 50mM sodium hydroxide. The final immobilised protein level is given by subtracting the response level at the red cross from the response level at the blue cross. The immobilised HER2 ECD level was ~3200RU.

Figure 6.5 shows that the EDC/NHS immobilisation of HER2 ECD was successful, achieving an immobilised ligand level of ~3000RU. The next step was to capture trastuzumab to the HER2 ECD on the chip surface and see how well it bound.

A 20μM sample of afucosylated trastuzumab was injected over the surface of the HER2 ECD-immobilised chip surface.
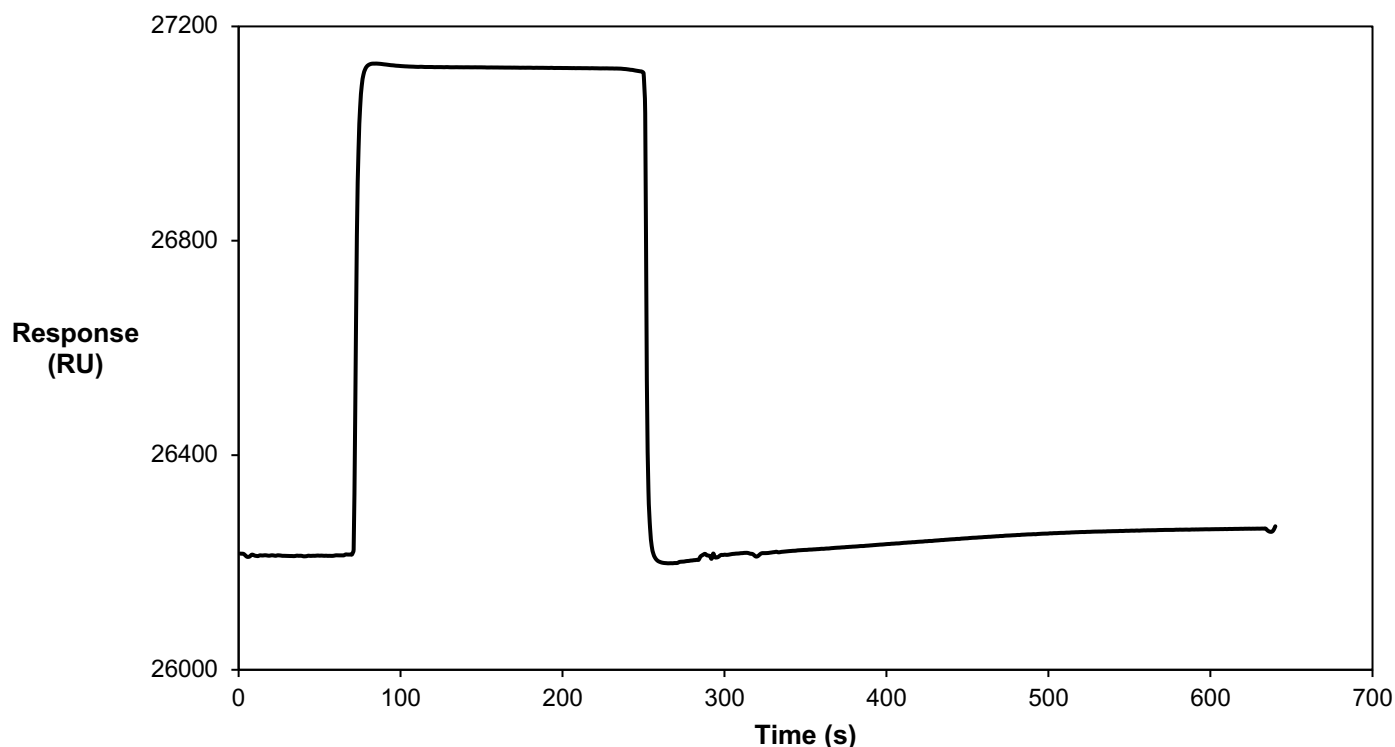
Figure 6.6 – injection of 20μM afucosylated trastuzumab over the HER2-immobilised CM5 chip. Afucosylated trastuzumab was injected over the chip surface at a flow rate of 5μL/min for 180s. The baseline before sample injection was 26,213RU, during injection it was 27,124RU, and after injection the response level returned to approximately baseline level (26,263RU).

There was an increase in response level after the trastuzumab was injected from 26,123RU to 27,124RU, which is an increase of ~900RU. However, once the injection was stopped, the response level stabilised after several minutes at approximately baseline value (26,263RU). This meant that the running buffer itself was enough to cause the trastuzumab to dissociate from the HER2 ECD, or the association was not particularly strong in the first place. This outcome meant that this would not be a suitable immobilisation set-up for the kinetics/affinity assays investigating the FcγR ligand affinity for IgG1.

6.2.4 Click Chemistry

Strain-promoted azide-alkyne cycloaddition (SPAAC), also known as copper-free click chemistry, involves a strained cyclooctyne and an organic azide. It is the most commonly-utilised metal-free click transformation in biochemistry due to its high specificity, lack of by-product formation and suitability for *in cellulo* and *in vivo* contexts (Bird et al., 2021). In the context of Biacore™ experiments, click chemistry immobilisation usually involves conjugating the protein to be immobilised to a cyclooctyne which can then be injected over an azide chip. The click chemistry reaction should occur between the cyclooctyne on the protein to be immobilised and the azide on the chip, resulting in permanent immobilisation of the protein.

The cyclooctyne used in this work was bicyclo[6.1.0]nonyne (BCN). Both fucosylated and afucosylated trastuzumab were used for BCN conjugation experiments. 20μM trastuzumab samples were conjugated with 5, 10 and 15 molar equivalents of BCN (see Section 2.9.1.5 for full protocol). To evaluate the success of the conjugation step, polyethylene glycol-trapping (PEG-trapping) was used. The samples were incubated with PEGylated azide and these were then run on an SDS-PAGE gel. In theory, if the antibody has been successfully conjugated to BCN, these will 'click' with the azide portion of the PEGylated azide. Successful PEGylation of the BCN-antibody conjugate results in laddering on an SDS-PAGE gel (see Figure 6.7B).
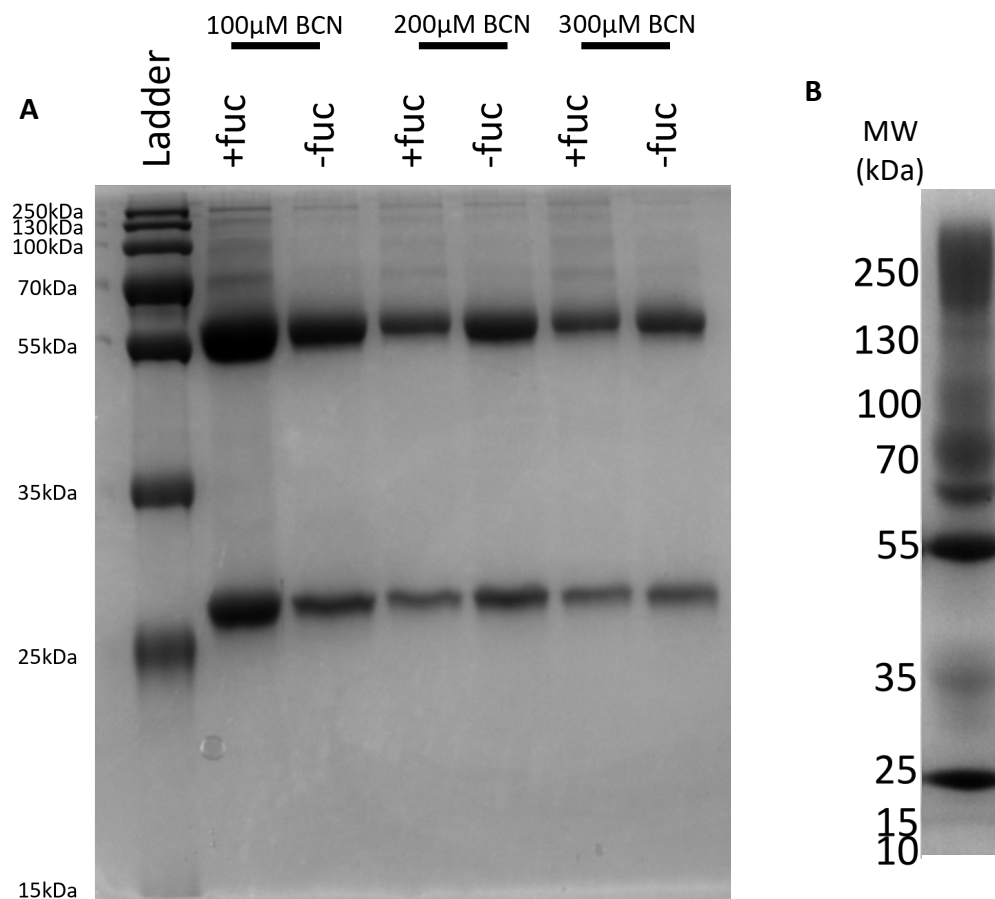
Figure 6.7 – **A)** PEG-trapping gel of the result of attempted conjugation of fucosylated and afucosylated trastuzumab with the cyclooctyne BCN. **B)** Example of how successfully-conjugated BCN-trastuzumab normally runs on a PEG-trapping gel (image provided by Dr. David Beal, University of Kent).

Figure 6.7B shows what trastuzumab successfully conjugated to BCN looks like on an SDS-PAGE PEG-trapping gel, and Figure 6.7A shows the result of our conjugation experiment. As there is minimal laddering seen in Figure 6.7A, we can conclude that there was very little to no conjugation of trastuzumab with BCN. This could be due to the ester hydrolysing, or the molar equivalents of BCN used being incorrect. As a result, immobilisation to an azide chip was not possible due to this lack of conjugation.

6.2.5 EDC/NHS Immobilisation of Tocilizumab

As the immobilisation techniques described in this section so far had not been successful for the immobilisation of trastuzumab, including EDC/NHS, an alternative antibody (tocilizumab) was trialled.

Tocilizumab is a humanised IgG1 antibody that targets the interleukin-6 (IL-6) receptor. The Fc portion of the antibody interacts with FcγRIIIa (Jiménez Morales et al., 2019), making it a suitable antibody to use in our binding studies. Our sample of tocilizumab had been produced in a CHO expression system, meaning it would be heterogeneously glycosylated. For our

binding studies, it would therefore be necessary to derive glycovariant samples from this tocilizumab sample, namely a sample possessing no *N*-linked glycosylation (deglycosylated tocilizumab) and a sample with minimal or no fucosylation (low-fucose tocilizumab). For the sake of clarity, the term 'tocilizumab' used throughout this section will refer to a sample of natively- or heterogeneously-glycosylated tocilizumab (predominantly fucosylated).

EDC/NHS is the most common and well-established immobilisation method, primarily due to its relative ease and its covalent, and therefore permanent, conjugation. This means no or very little ligand dissociation, which is highly favourable in SPR studies. This method does not result in uniformly-oriented immobilised protein, although this does not normally cause issues in binding experiments. A figure explaining the chemistry behind EDC/NHS immobilisation is shown (see Figure 6.8).
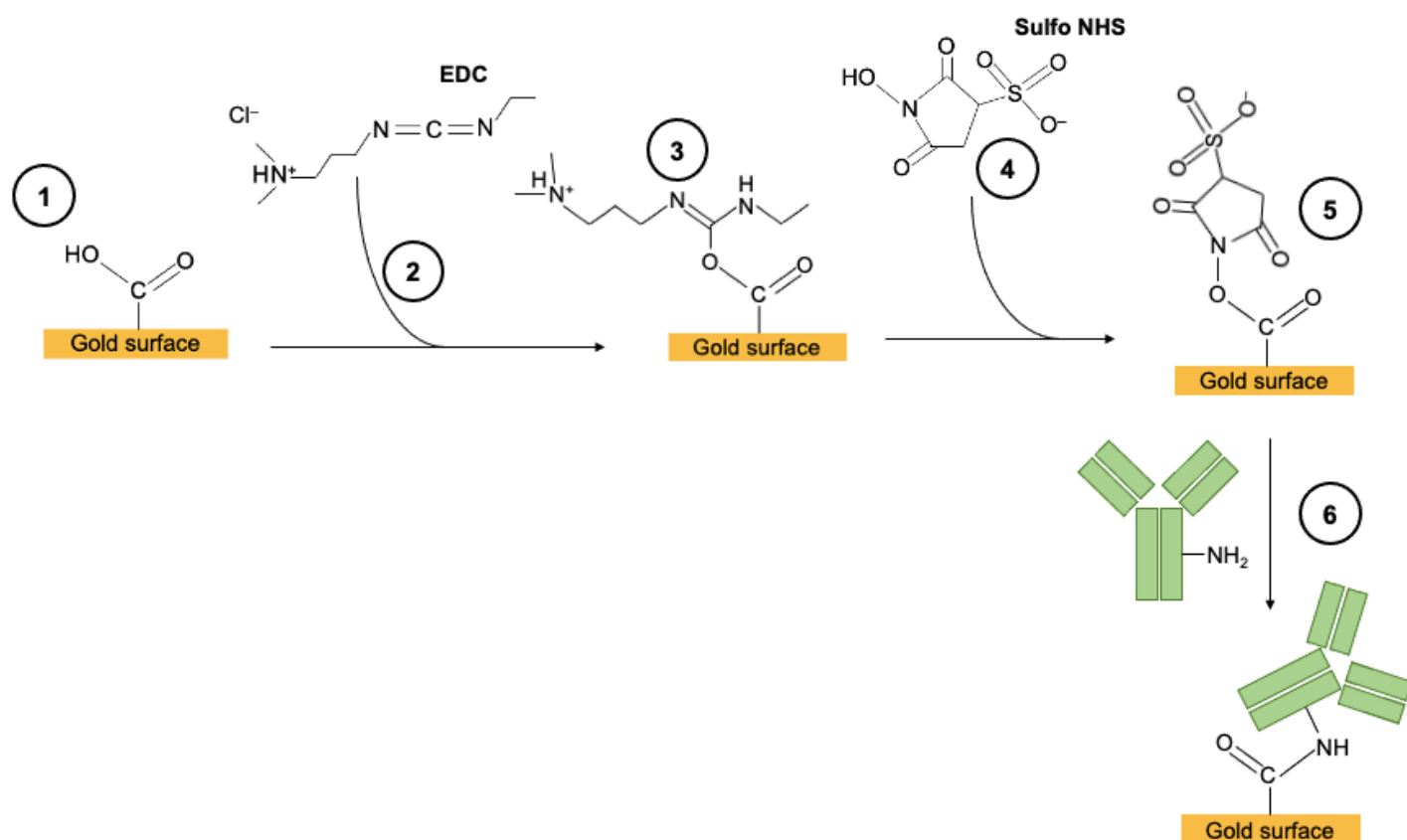
Figure 6.8 – EDC/NHS immobilisation chemistry. 1) The CM5 chip surface has long dextran chains (not shown) with carboxyl groups at the terminus of these chains. The chip itself normally consists of a gold surface. 2) The compound EDC is added, which activates the carboxyl groups in the presence of chloride ions to form 3) an unstable reactive O-acyl isourea ester intermediate. 4) NHS is then introduced, in this case sulfo-NHS, which reacts with the O-acyl isourea intermediate to form a 5) semi-stable amine-reactive NHS-ester. 6) The tocilizumab antibody to be immobilised is then injected onto the chip, and the -NH$_2$ groups on lysine side chains react with the amine-reactive NHS-ester to conjugate the antibody to the chip through an amide linkage. Figure adapted from Figure 1 of Bart, J.,

Tiggelaar, R., Yang, M., Schlautmann, S., et al. (2009) Room-temperature intermediate layer bonding for microfluidic devices. *Lab on a Chip*.

The EDC/NHS immobilisation traces for tocilizumab and deglycosylated tocilizumab, which produced the surfaces used in the kinetic/affinity assays with refFcγRIIIa and the FcγR ligands, are shown below.
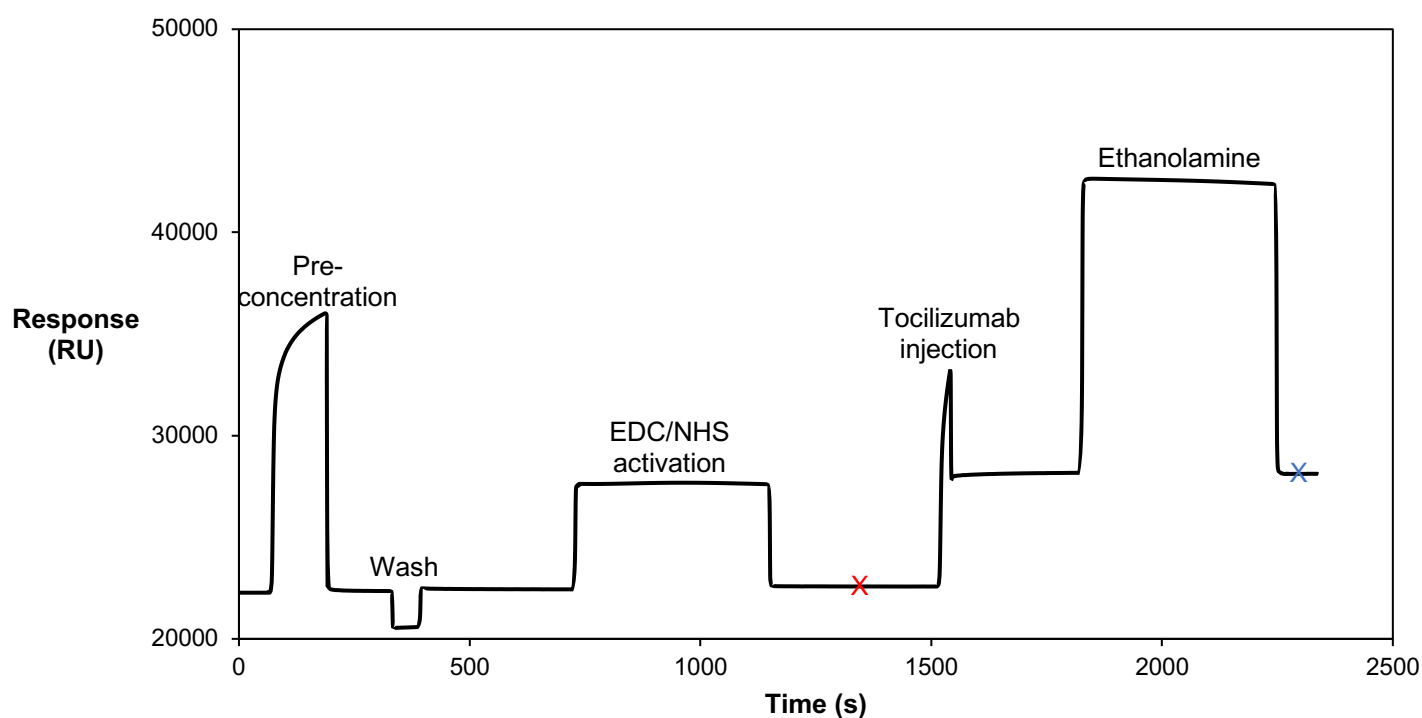
Figure 6.9 – EDC/NHS immobilisation of 27μM tocilizumab to a CM5 chip. More details about this procedure can be found in Section 2.9.1.1. The wash step was carried out with 50mM sodium hydroxide. The final immobilised protein level is given by subtracting the response level at the red cross from the response level at the blue cross. The immobilised tocilizumab level was ~5500RU.

In order for EDC/NHS immobilisation to a CM5 chip to work, the protein to be immobilised must be solubilised in a buffer which is at least 1.5 pH units below the protein's pI. This ensures that the lysine residues are protonated and allows the EDC/NHS reaction and immobilisation to take place. After some optimisation of the pH conditions of this buffer, immobilisation of tocilizumab was achieved. It was found that the optimal buffer pH for EDC/NHS immobilisation of the antibody was pH 6.5.

It has been widely reported that the removal of the *N*-glycan in the Fc region of IgG1 results in the abolishment of binding of IgG1 to FcγRIIIa (Geuijen et al., 2017; Hanson & Barb, 2015). In order to test if our binding of refFcγRIIIa and our FcγR ligands to tocilizumab was a genuine result, it was decided that we would also deglycosylate tocilizumab and investigate the interactions of refFcγRIIIa and the FcγR ligands with this protein. Tocilizumab was deglycosylated using the enzyme PNGase F (see Section 2.9.2) and also immobilised to a CM5 Biacore™ sensor chip.
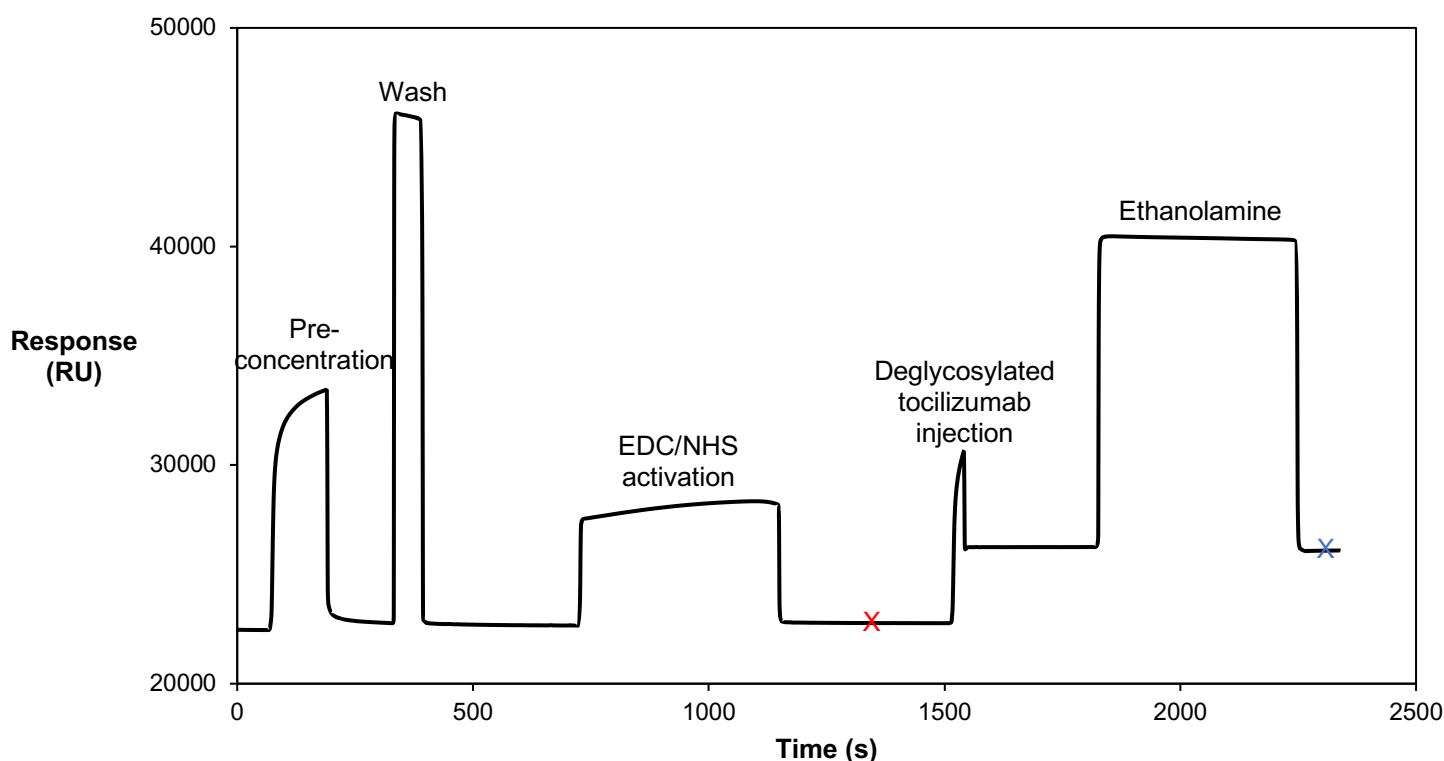
Figure 6.10 – EDC/NHS immobilisation of 27μM deglycosylated tocilizumab to a CM5 chip. The wash step was carried out with 10mM sodium acetate pH 3.5. The immobilised deglycosylated tocilizumab level was ~3300RU.

It was estimated that an immobilised antibody level of upwards of 1500RU would have been more than enough for the kinetics/affinity assays with refFcγRIIIa and the FcγR ligands. The immobilisation levels achieved using tocilizumab and deglycosylated tocilizumab are within a similar range and were both achieved using one sample injection. Although the PNGase F was not removed from the deglycosylated tocilizumab sample prior to immobilisation, the amount present in the sample that would have been injected over the chip surface would have been negligible, so there were no concerns about immobilising more PNGase F than tocilizumab to the chip surface and affecting subsequent kinetics/affinity analyses.

6.2.6 Summary of Antibody Immobilisation Techniques

This section showed how a variety of different immobilisation techniques were attempted for the immobilisation of trastuzumab. EDC/NHS immobilisation is usually the first choice due to it being one of the most well-established and reliable immobilisation strategies, but when this was unsuccessful other techniques were trialled. Streptavidin-biotin is the next most widely-used immobilisation technique, but the biotinylation process proved to be less successful than was hoped and would not have been suitable for our experiments. Both the Protein L and HER2 strategies did not result in permanent immobilisation, which would have created issues with baseline drift during the kinetics/affinity assays, and the click chemistry strategy was unsuccessful due to the BCN conjugation experiments not working. Therefore, we moved on to using an alternative IgG1, tocilizumab, which immobilised successfully using EDC/NHS. The affinity data using glycovariants of this antibody and the FcγR constructs are presented in the following sections.

6.3 Results – Interaction of FcγR Ligands with Glycosylated and Deglycosylated Tocilizumab

As mentioned, the binding data was obtained using glycovariants of tocilizumab immobilised to CM5 chips using EDC/NHS chemistry and the FcγR ligands were injected over the chip surfaces. Equation 4 shown in the following section was used to plot steady state response values against analyte concentration to derive K_D values for each interaction, as well as providing a standard error for these values and some statistical analysis. These values were obtained using the Biacore™ Evaluation Software and the K_D values were used for comparison between the FcγR constructs. All binding was assumed to be 1:1 (antibody:FcγR). The resulting sensorgrams and the derived K_D values for each interaction are given below.

6.3.1 Interaction of FcγRs with Tocilizumab

Firstly, the binding of refFcγRIIIa to immobilised tocilizumab was tested. This was to establish whether the assay set-up was working as expected and would also give some idea as to what analyte concentrations should be used when testing the affinity of the FcγR ligands for tocilizumab. Literature values state that the K_D for the FcγRIIIa-158F (low-affinity variant) interaction with IgG1 is in the micromolar range (Hayes et al., 2016; Li et al., 2007; Wang & Chen, 2022) and depends on many factors, such as the method used (e.g. SPR, isothermal titration calorimetry etc.), the experimental set-up and the type of IgG1 used.

All model fitting curves for the positive binding interactions seen are shown in Appendix 9.7.
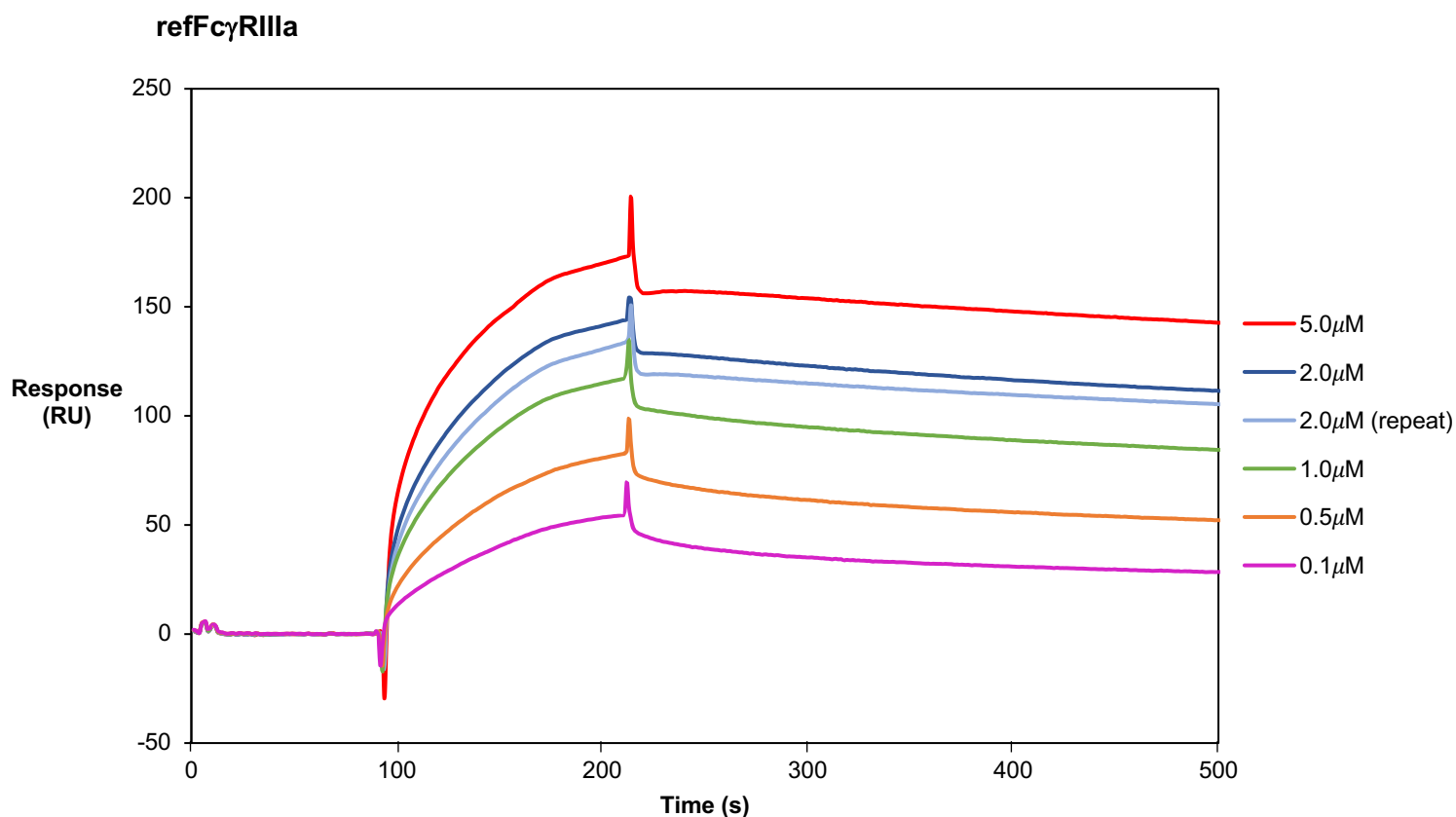
refFcγRIIIa

Figure 6.11 – sensorgram of refFcγRIIIa (analyte) against tocilizumab immobilised to a CM5 chip. The immobilised tocilizumab level was ~5500RU. Analyte concentrations of 0.1-5.0μM were used, which were initially based on approximate expected K_D values and then optimised and established through concentration scouting. The 2μM analyte concentration was repeated. The running buffer used was PBS-P$^+$.

The K_D was obtained using the Affinity – Steady State 1:1 model in the Biacore™ Evaluation Software (Biacore™ X100 Handbook BR-1008-10 Edition AB, Cytiva™, Appendix D). This model assumes a 1:1 interaction and calculates K_D from a plot of steady state binding values (R_{eq}) against analyte concentration (C). The equation includes an offset for the bulk refractive index contributions (RI), which is assumed to be the same for all samples:

$$R_{eq} = \frac{C\,R_{max}}{K_D + C} + RI \ (4)$$

where R_{eq} = steady state binding level (RU)

C = analyte concentration (μM)

R_{max} = analyte binding capacity of the surface (RU)

K_D = dissociation constant (μM)

RI = bulk refractive index contribution (RU)
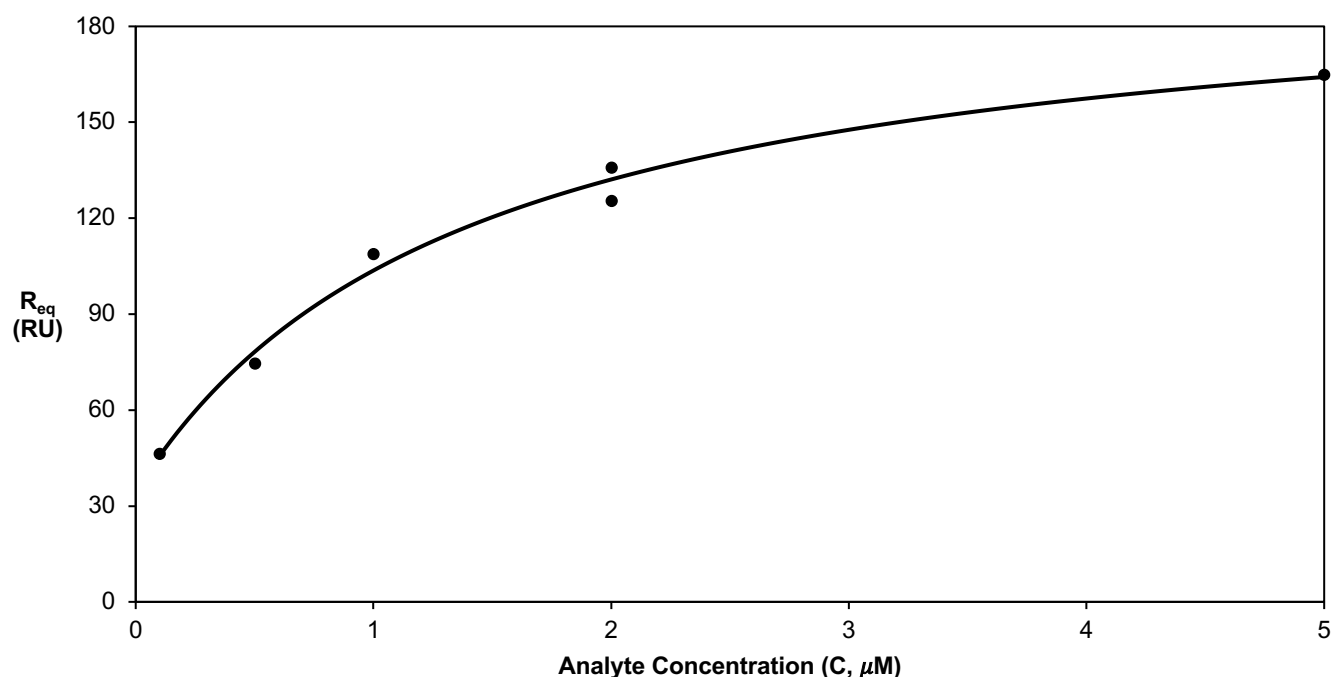
Figure 6.12 – steady state plot for the interaction of refFcγRIIIa and tocilizumab. n = 6. Steady state binding levels R_{eq} are plotted against analyte concentration C and a fit was generated by the Biacore™ Evaluation Software, which is represented by the trendline. K_D is derived from this plot using equation 4. The K_D derived from this interaction was 1.40μM.

Table 6.2 – values of K_D, standard error (SE) of K_D, R_{max} and Chi^2 reported by the Biacore™ Evaluation Software for the interaction of refFcγRIIIa with tocilizumab.

refFcγRIIIa-tocilizumab	
K_D (μM)	1.40
SE of K_D (±μM)	0.39
R_{max} (RU)	166
Chi^2	33.4

The K_D derived by the Biacore™ Evaluation Software for the interaction of refFcγRIIIa with tocilizumab was 1.40μM. Ideally, the Chi^2 statistic would be <10% of R_{max}, however our value of Chi^2 is greater than this significance level at ~20% of R_{max}. As mentioned, the K_D value was expected to be within the micromolar range, which our derived value of 1.40μM is, and this value is also within the range tested experimentally. The R_{max} seems reasonable, which is the R_{eq} value at which the steady state plot is expected to plateau, and when the standard error (SE) is added or subtracted from the K_D the value is still within the expected micromolar range. We therefore concluded from this that the experimental assay was working as expected;

158

despite the statistical analysis suggesting that the exact K_D value provided of 1.40μM may not be accurate, the value we obtained was within the expected range. We decided that the same experimental set-up could be applied to the FcγR ligands.

FcγRIIIa D2 Man9
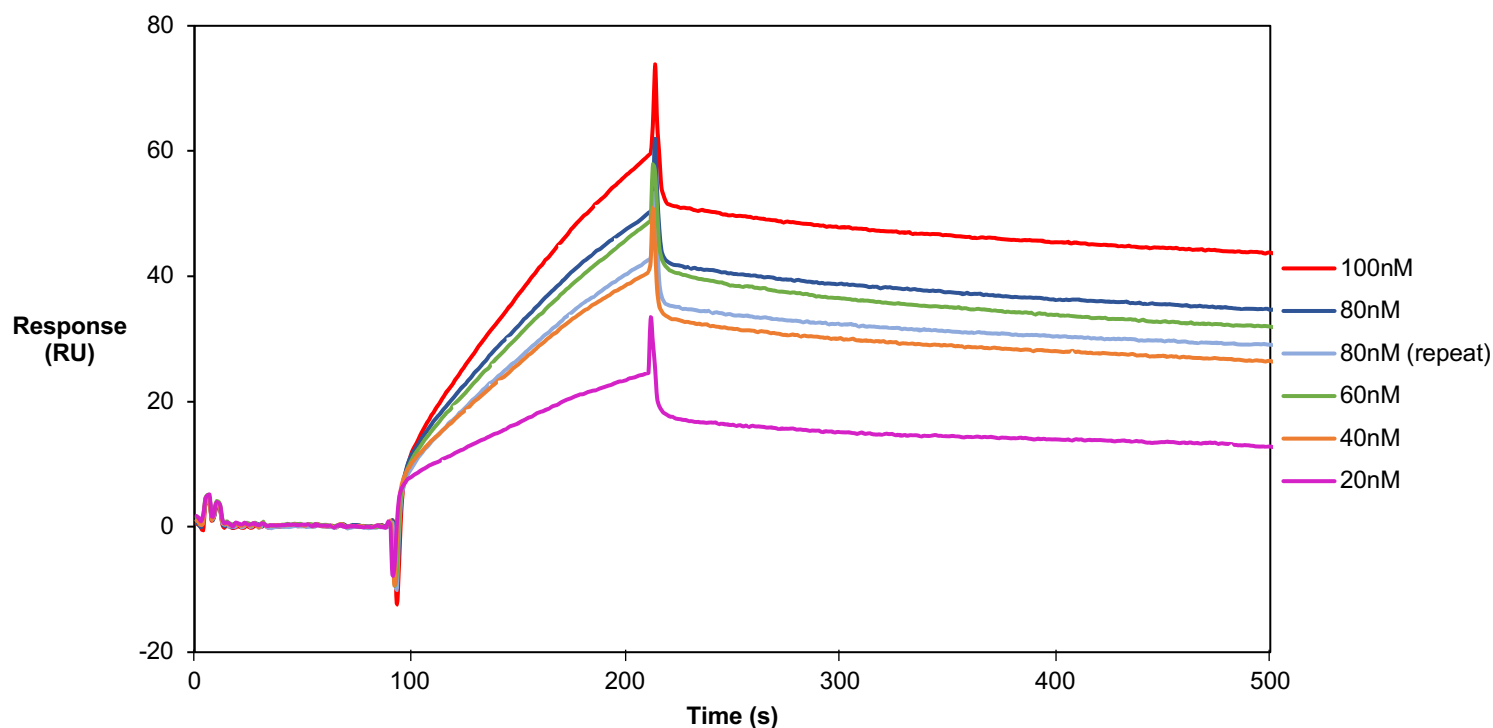
Figure 6.13 – sensorgram of Man9 (analyte) against tocilizumab immobilised to a CM5 chip. The immobilised tocilizumab level was ~5500RU; the same chip was used as for the refFcγRIIIa assay. Analyte concentrations of 20-100nM were used; initially the same concentrations as established by the refFcγRIIIa assay were used, and these were then refined based on concentration scouting. The 80nM analyte concentration was repeated. The running buffer used was PBS-P⁺.

Initially, the same analyte concentrations (0.1-5.0μM) used for the refFcγRIIIa-tocilizumab assay were used for the Man9-tocilizumab assay. However, the gradient of the curves seemed high and the Evaluation Software was struggling to find a model to fit the data. Concentration scouting was carried out, and eventually the concentration range of 20-100nM (0.02-0.10μM) was decided upon. The response level of Man9 was lower than that of refFcγRIIIa, with the response being ~60RU at the highest concentration of Man9 compared to ~160RU at the highest concentration of refFcγRIIIa. This is assumed to be a result of Man9 being a smaller molecule than refFcγRIIIa, therefore generating a lower response.
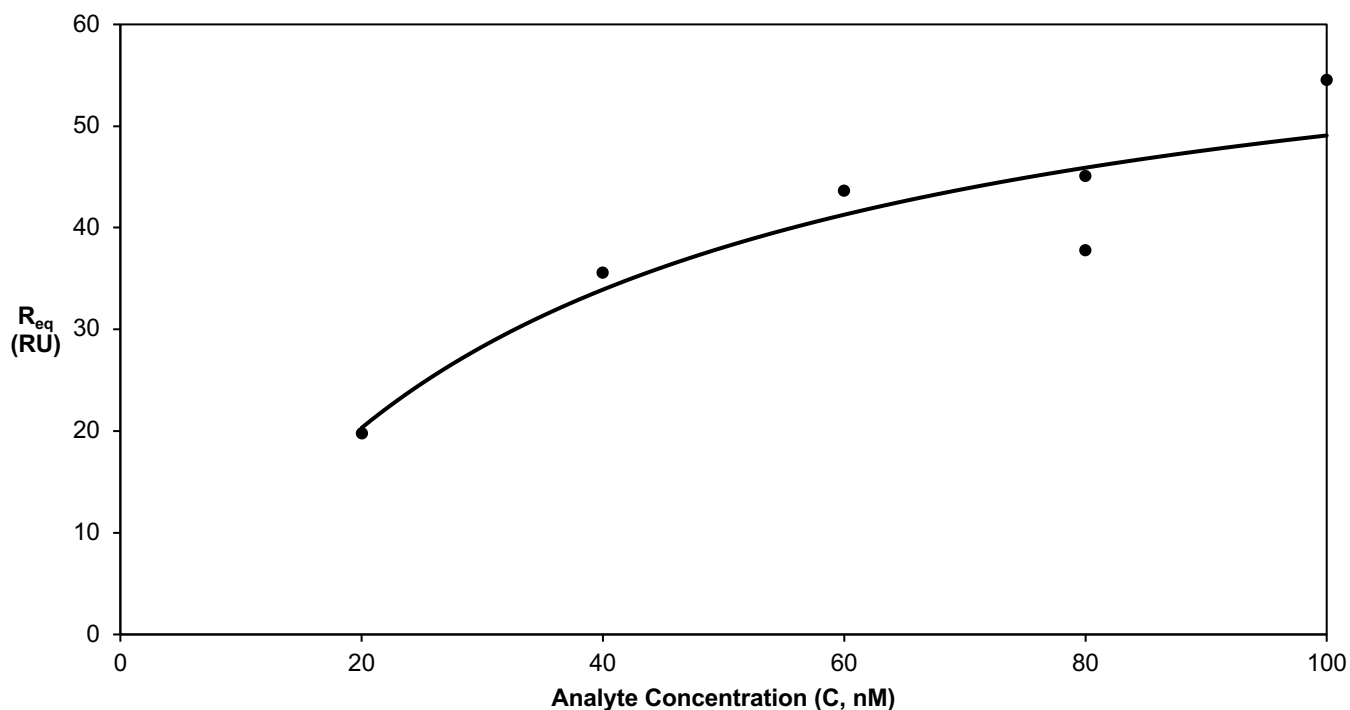
Figure 6.14 – steady state plot for the interaction of Man9 and tocilizumab. n = 6. Steady state binding levels R_{eq} are plotted against analyte concentration C and a fit was generated by the Biacore™ Evaluation Software, which is represented by the trendline. The K_D derived from this interaction was 30nM.

Table 6.3 – values of K_D, SE of K_D, R_{max} and Chi^2 reported by the Biacore™ Evaluation Software for the interaction of Man9 with tocilizumab.

FcγRIIIa D2 Man9-tocilizumab	
K_D (nM)	30
SE of K_D ($\pm$nM)	60
R_{max} (RU)	79.3
Chi^2	34.8

The derived K_D value given by the Biacore™ Evaluation Software for the Man9-tocilizumab interaction was 30nM, which is approximately a 100-fold reduction in K_D compared to the refFcγRIIIa-tocilizumab interaction and is in the nanomolar range. However, the standard error of K_D is large at 60nM, larger even than the value of K_D itself, and the Chi^2 statistic is considerably greater than 10% of R_{max} at ~44%. The K_D value is within the range of analyte concentrations tested, but only just. This value of K_D therefore may not be completely reliable, but there is an indication that Man9 is binding tocilizumab with possibly a lower K_D than refFcγRIIIa, meaning there could be tighter binding of Man9 compared to refFcγRIIIa with tocilizumab.

FcγRIIIa D2 Man5

Figure 6.15 – sensorgram of Man5 (analyte) against tocilizumab immobilised to a CM5 chip. The immobilised tocilizumab level was ~5500RU; the same chip was used as for the refFcγRIIIa and Man9 assays. Analyte concentrations of 20-100nM were used. The 60nM analyte concentration was repeated. The running buffer used was PBS-P⁺.
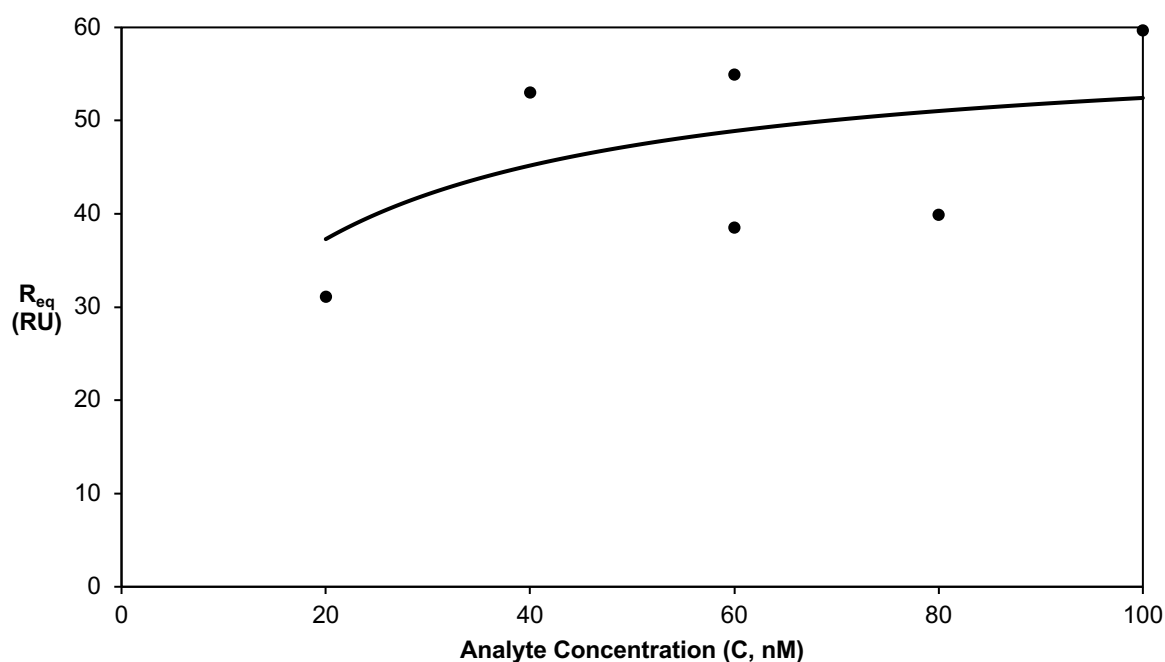
Figure 6.16 – steady state plot for the interaction of Man5 and tocilizumab. n = 6. Steady state binding levels R_{eq} are plotted against analyte concentration C and a fit was generated by the Biacore™ Evaluation Software, which is represented by the trendline. The K_D derived from this interaction was 20nM.

Table 6.4 – values of K_D, SE of K_D, R_{max} and Chi^2 reported by the Biacore™ Evaluation Software for the interaction of Man5 with tocilizumab.

FcγRIIIa D2 Man5-tocilizumab	
K_D (nM)	20
SE of K_D ($\pm$nM)	20
R_{max} (RU)	60.3
Chi^2	140

The derived K_D value given by the Biacore™ Evaluation Software for the Man5-tocilizumab interaction was 20nM, which is approximately a 100-fold reduction in K_D compared to refFcγRIIIa. This value is in the nanomolar range and is very similar to the value obtained for the Man9-tocilizumab interaction. However, the standard error of K_D is large at 20nM and the Chi^2 statistic is even higher than the R_{max} value itself. By looking at the steady state plot in Figure 6.16, we can see that the model is not a particularly good fit for the dataset. Therefore, we can conclude that this value of K_D is also not reliable, but the sensorgrams again indicate that Man5 is binding tocilizumab with possibly a stronger affinity than refFcγRIIIa and a similar affinity to that of Man9.

FcγRIIIa D2
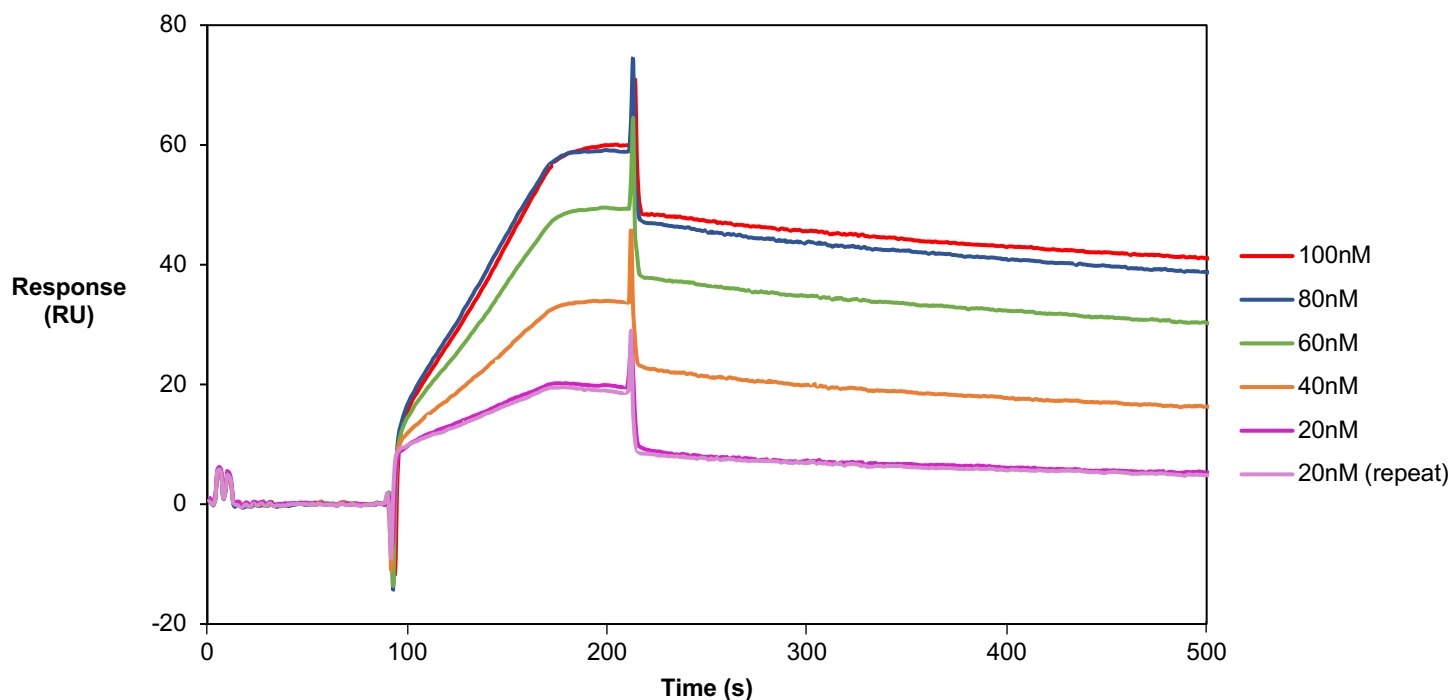
Figure 6.17 – sensorgram of FcγRIIIa D2 (analyte) against tocilizumab immobilised to a CM5 chip. The immobilised tocilizumab level was ~5500RU; the same chip was used as for the refFcγRIIIa, Man9 and Man5 assays. Analyte concentrations of 20-100nM were used. The 20nM analyte concentration was repeated. The running buffer used was PBS-P$^+$.

The sensorgram in Figure 6.17 shows almost a 'two-phase binding' effect. There is an initial, almost linear increase in response for the first ~70-80 seconds of the association phase, followed by a plateau-type phase for the remainder of the association. This could either be a result of the way in which the FcγRIIIa D2 binds tocilizumab, or it could be an experimental artifact.
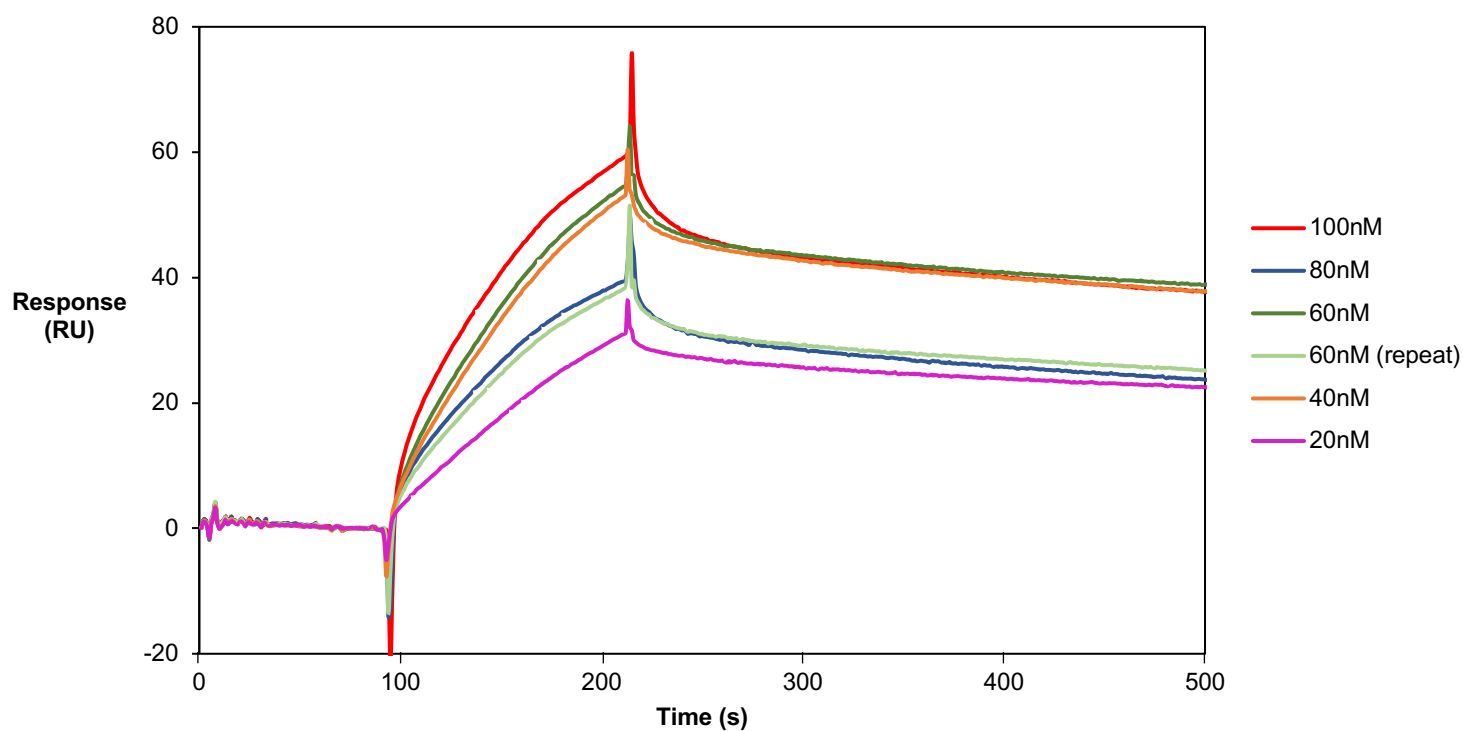
163
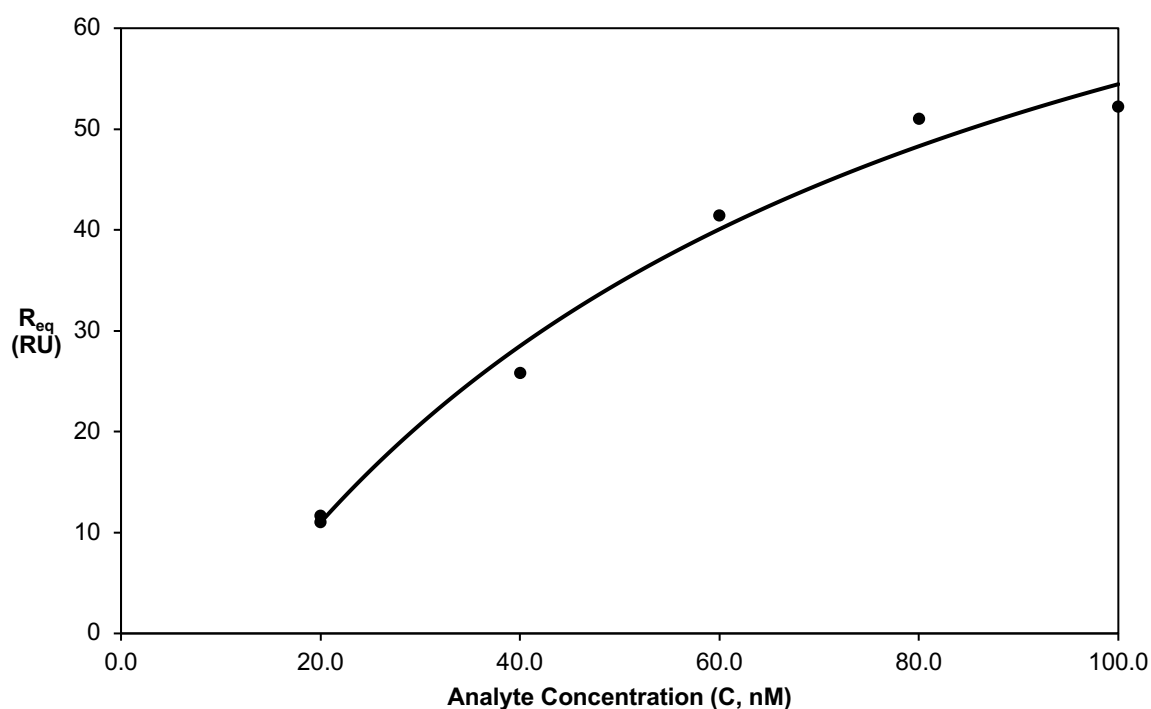
Figure 6.18 – steady state plot for the interaction of FcγRIIIa D2 and tocilizumab. n = 6. Steady state binding levels R_{eq} are plotted against analyte concentration C and a fit was generated by the Biacore™ Evaluation Software, which is represented by the trendline. The K_D derived from this interaction was 60nM.

Table 6.5 – values of K_D, SE of K_D, R_{max} and Chi^2 reported by the Biacore™ Evaluation Software for the interaction of FcγRIIIa D2 with tocilizumab.

FcγRIIIa D2-tocilizumab	
K_D (nM)	60
SE of K_D ($\pm$nM)	40
R_{max} (RU)	115.5
Chi^2	7.20

The derived K_D value given by the Biacore™ Evaluation Software for the FcγRIIIa D2-tocilizumab interaction was 60nM, which is again approximately a 100-fold reduction in K_D compared to the refFcγRIIIa-tocilizumab interaction and is in the nanomolar range. The standard error of K_D is relatively large at 40nM, but the Chi^2 statistic is below the 10% significance level, meaning that statistically this value should be reliable. By looking at the steady state plot in Figure 6.18, we can see that the R_{eq} model fits the data well. However, the R_{max} is higher than what might be expected at 115.5RU; the values of R_{max} for Man9 and Man5 were 79.3RU and 60.3RU respectively, and the response levels are all similar at ~60RU for the highest analyte concentration. This may be a result of the 'two-phase binding' effect seen

on the sensorgrams, resulting in the model fitting the initial 'phase' of the binding but not the second plateau-type phase. If the R_{max} is lower in reality, it would change the fit, which could give a slightly different K_D and a different Chi^2 statistic. However, the first portion of the data fits well, and the K_D is within a very similar range to the K_D values derived for both the Man9 and Man5 interactions with tocilizumab. We can therefore conclude that this is a reliable indication of the strength of the affinity between FcγRIIIa D2 and tocilizumab.

Table 6.6 – summary of derived K_D values along with SEs for the interaction of the FcγR constructs with tocilizumab. The K_D values for refFcγRIIIa and FcγRIIIa D2 are assumed to be reliable, whilst the values for Man9 and Man5 are approximate indications of K_D (nanomolar affinity). The grey represents the reference value (K_D of refFcγRIIIa-tocilizumab interaction) and the blue indicates an increase in affinity compared to the reference value. Micromolar units are used for consistency.

Tocilizumab	K_D (μM)	SE of K_D (±μM)
refFcγRIIIa	1.40	0.39
Man9	0.03 ↑↑	0.06
Man5	0.02 ↑↑	0.02
FcγRIIIa D2	0.06 ↑↑	0.04

6.3.2 Interaction of FcγRs with Deglycosylated Tocilizumab

Tocilizumab was deglycosylated using PNGase F (see Section 2.9.2) and immobilised to a CM5 chip (see Figure 6.10) to a response level of ~3300RU. The same analyte concentrations were used as for the tocilizumab kinetics/affinity assays. The expected result was that there would be no binding response observed for the interactions of refFcγRIIIa nor the FcγR ligands with deglycosylated tocilizumab.
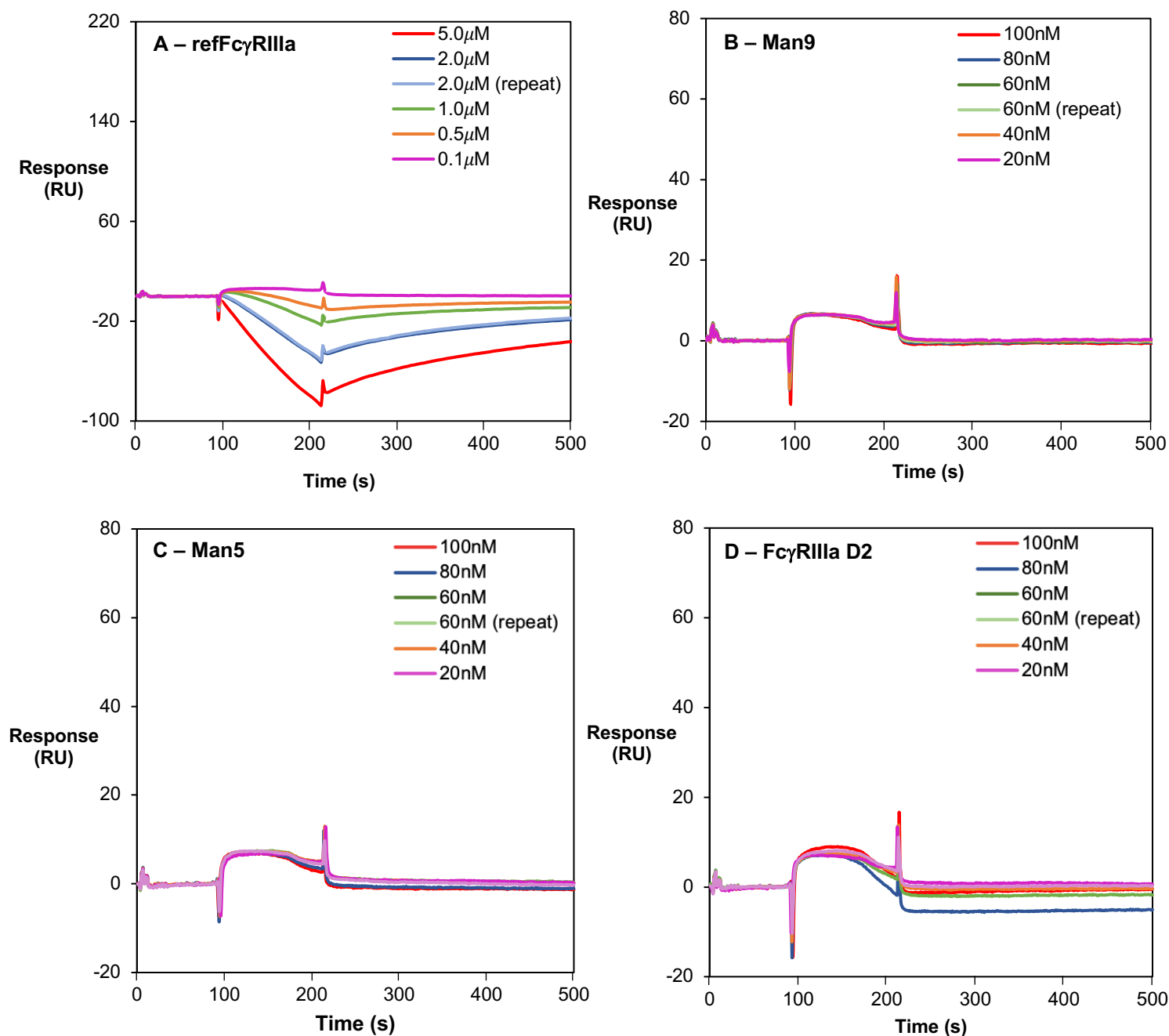
Figure 6.19 – sensorgrams of **A)** refFcγRIIIa **B)** Man9 **C)** Man5 and **D)** FcγRIIIa D2 against deglycosylated tocilizumab immobilised to a CM5 chip. The immobilised deglycosylated tocilizumab level was ~3300RU and the same chip was used for all assays. Analyte concentrations of 0.1-5.0μM were used for refFcγRIIIa and 20-100nM was used for Man9, Man5 and FcγRIIIa D2. The running buffer used was PBS-P⁺.

Firstly, refFcγRIIIa was tested against the deglycosylated tocilizumab chip as a reference to ensure that the chip/assay was working as expected. This sensorgram yielded a response below the baseline (see Figure 6.19A). This is often a result of the analyte having a greater affinity or association with the Fc 1 reference channel, meaning that the reference-subtracted

values which are used to generate the sensorgram end up being negative values. This could have been the result of some non-specific binding with the surface. In Appendix 9.3, the responses from Fc 1 and Fc 2 are shown for this interaction, including the responses from Fc 1 and Fc 2 of the refFcγRIIIa-tocilizumab interaction for the avoidance of doubt that the assay was working as expected. In Figures 6.19B, C and D, there is a very low response level (<10RU) and there is no concentration-dependent increase in response. This is indicative of no binding to the immobilised deglycosylated tocilizumab, which is the expected result. These results indicated that our FcγR ligands are beginning to behave in a similar way to refFcγRIIIa, despite some quite significant structural differences between refFcγRIIIa and the FcγR ligands.

Table 6.7 – summary table of K_D values obtained from interactions studied thus far, their standard errors, R_{max} and chi^2 values. As mentioned, these values are only an indication of the affinity range, i.e. micromolar, nanomolar. The grey represents the reference value (K_D of refFcγRIIIa-tocilizumab interaction) and the blue indicates an increase in affinity compared to the reference value. Micromolar units are used for consistency.

	Tocilizumab				Deglycosylated tocilizumab	
	K_D (μM)	SE of K_D ($\pm\mu$M)	R_{max} (RU)	Chi^2	K_D (μM)	SE of K_D ($\pm\mu$M)
refFcγRIIIa	1.40	0.39	166	33.4	N/A	N/A
Man9	0.03 ↑↑	0.06	79.3	34.8	N/A	N/A
Man5	0.02 ↑↑	0.02	60.3	140	N/A	N/A
FcγRIIIa D2	0.06 ↑↑	0.04	115.5	7.20	N/A	N/A

Next, the final set of experiments took place, which involved testing the affinity of refFcγRIIIa and the FcγR ligands for low-fucose tocilizumab. Before this, a sample of low-fucose tocilizumab was prepared.

6.4 Results – Interaction of FcγR Ligands with Low-Fucose Tocilizumab

Tocilizumab proved to immobilise successfully to a CM5 chip using EDC/NHS chemistry (see Figure 6.9). Once this had been established, the next challenge was to prepare the afucosylated or low-fucose glycovariant of tocilizumab that was needed to test the binding affinity of refFcγRIIIa and the FcγR ligands for these glycovariants. This was needed to answer the original research question of whether or not our engineered FcγR ligands possessed the same differential affinity for fucosylated and afucosylated IgG1 as FcγRIIIa.

6.4.1 Preparation of Low-Fucose Tocilizumab

There were two main strategies that could have been employed to generate a sample of tocilizumab with no or reduced fucosylation. One of these was enzymatic remodelling. There is no known fucosidase that will remove only an $\alpha 1,6$ fucose linked to a core GlcNAc on an *N*-linked glycan, leaving the rest of the glycan intact. Therefore, enzymatic remodelling to generate an afucosylated sample of tocilizumab would first involve removing the entire glycan, which could be done using either PNGase F or Endo H. The glycan without the fucose could then be built back onto the protein enzymatically using a variety of glycosyltransferases and substrates. This option would involve a number of steps, each of which would be likely to require optimisation and troubleshooting, so this option was not attempted first. Instead, the second strategy was attempted, which involved using the commercially available Glycap-3A™ column from Zepteon™, an FcγRIIIa-immobilised column, to separate fucosylated and afucosylated tocilizumab.

The Glycap-3A™ resin is immobilised with FcγRIIIa which was expressed in HEK-293 cells and then immobilised to agarose beads using EDC/NHS chemistry. This FcγRIIIa column binds afucosylated IgG1 more readily than fucosylated IgG1 and is capable of enriching for afucosylated IgG1 species by 60-70% compared to the load, depending on the antibody (Bolton, Ackerman & Boesch, 2013). Our strategy involved loading the FcγRIIIa column with tocilizumab and carrying out a chromatographic separation, which would theoretically give an elution pool which is enriched for afucosylated tocilizumab. This elution pool would then be immobilised to a CM5 chip and used to evaluate the binding affinity of refFcγRIIIa and the FcγR ligands to afucosylation-enriched (low-fucose) tocilizumab. The load and elution from the separation were also analysed using mass spectrometry to confirm that the load was enriched for afucosylated glycoforms (see Figure 6.22). It is worth mentioning that only one side of the Fc region needs to be afucosylated to bind the column, so in the elution pool there could be some antibody molecules which have one fucosylated *N*-glycan on one side of the Fc region and the *N*-glycan on the other side could be afucosylated.
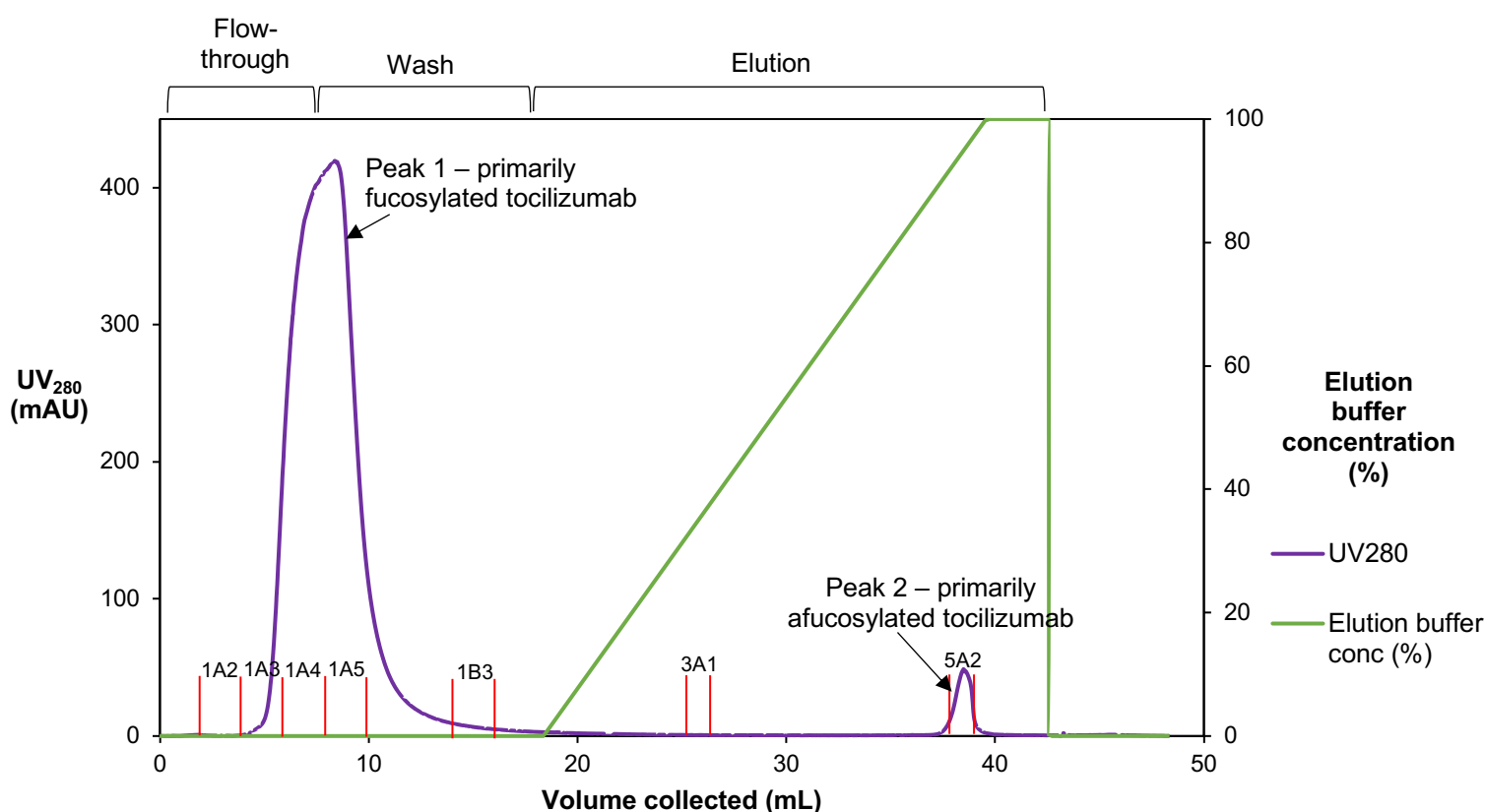
Figure 6.20 – chromatogram of the separation of 5.5mL of tocilizumab using an FcγRIIIa column, the Glycap-3A™ resin from Zepteon™ (6mg total tocilizumab in load). The separation was carried out on an ÄKTA avant™ 150 purification system and operated in bind-elute mode. Tocilizumab stock (4mg/mL) was diluted with equilibration buffer, PBS, to make up the final load sample concentration of 1.1mg/mL. The column was equilibrated with 10CV of PBS, which was not collected, before sample was applied to the column via a sample pump. The column was then washed with 20CV of PBS and the elution was carried out in a gradient of 4-100% elution buffer, which was 100mM glycine pH 3.2 and was mixed with PBS to create the gradient over 20CV. The flow rate was 0.5mL/min throughout the separation. Flow-through, wash and elution fractions are labelled and were analysed on an SDS-PAGE gel (see Figure 6.21).

Figure 6.20 shows the chromatogram resulting from the separation of 1.1mg/mL (6mg total) tocilizumab using the FcγRIIIa column. A total of 5.5mL of sample was loaded onto the column at a flow rate of 0.5mL/min. Whilst the flow-through was not characterised using mass spectrometry, it is expected that peak 1 would contain a larger proportion of fucosylated glycoforms compared to the load. Fraction 5A2 (peak 2) eluted at ~92% elution buffer and was immobilised to a CM5 chip. Due to the low pH of the elution buffer, neutralisation buffer was added to the later tubes in the fraction collector that were predicted to contain the elution fractions prior to the separation (see Section 2.7.2). Both the load and some of fraction 5A2 were analysed using mass spectrometry (see Figure 6.22).
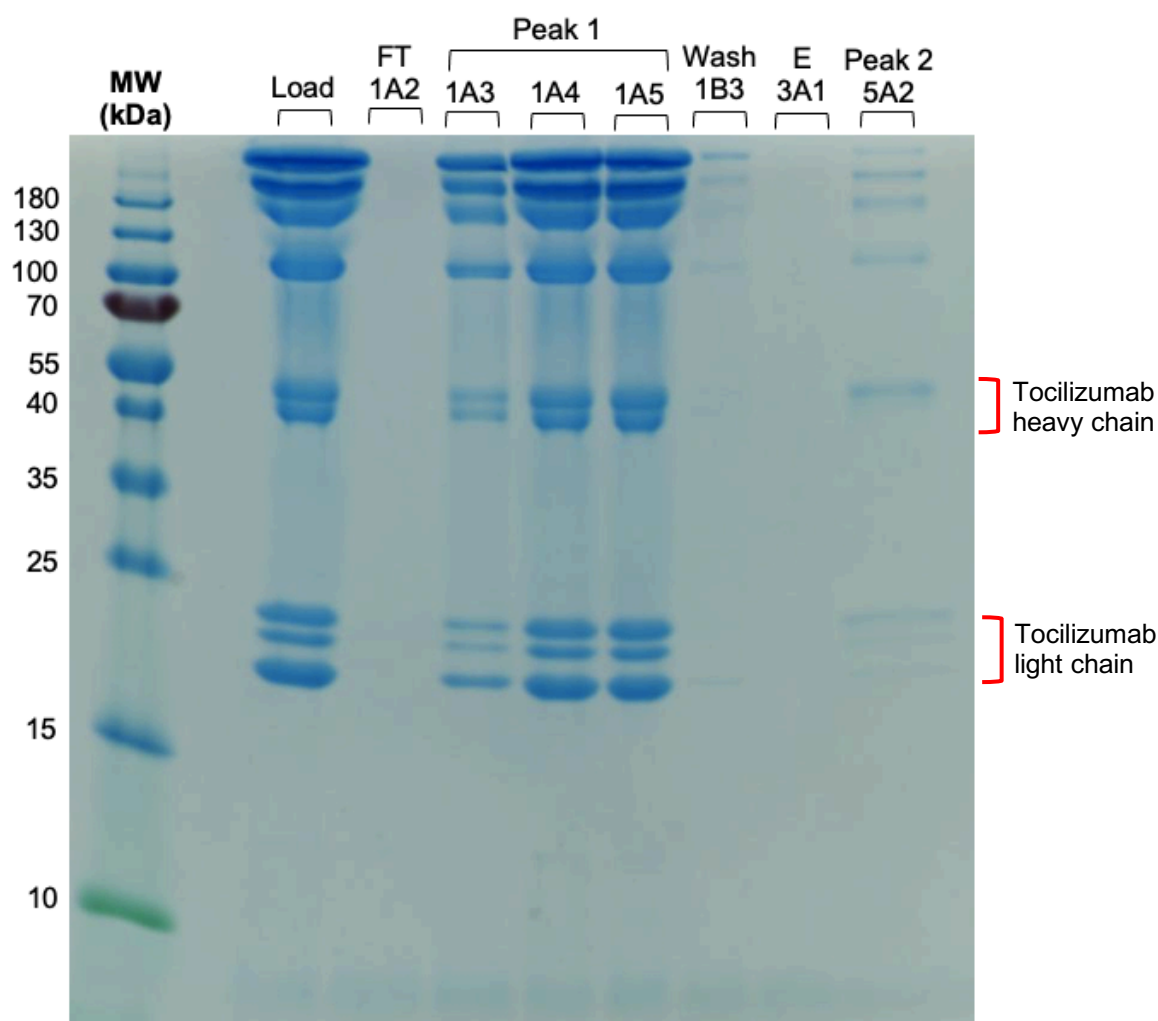
Figure 6.21 – SDS-PAGE analysis of the tocilizumab separation depicted by the chromatogram in Figure 6.20. The fractions and peaks 1 and 2 shown in this gel image are labelled on Figure 6.19. FT = flow-through, E = elution phase (but not where the peak is). This gel was run under reducing conditions.

The relative signal intensities in Figure 6.21 reflect the comparatively large amount of antibody in peak 1 (predominantly fucosylated) compared to peak 2 (enriched for afucosylated tocilizumab). The exact proportion of afucosylated species in tocilizumab is not known, although it is known that there are 'low levels' of afucosylated species in typical samples (Sheppard et al., 2017). A study of human plasma IgG showed that levels of afucosylation vary between 1.3-19.3% (Pučić et al., 2011), so it is likely that the proportion of afucosylated tocilizumab is within this region. The peak ratio in Figure 6.20 suggests that afucosylation levels are in the region of ~3% but are likely to be slightly less (peak 1 area = ~97%, peak 2 area = ~3%) (see Appendix 9.4 for calculation).
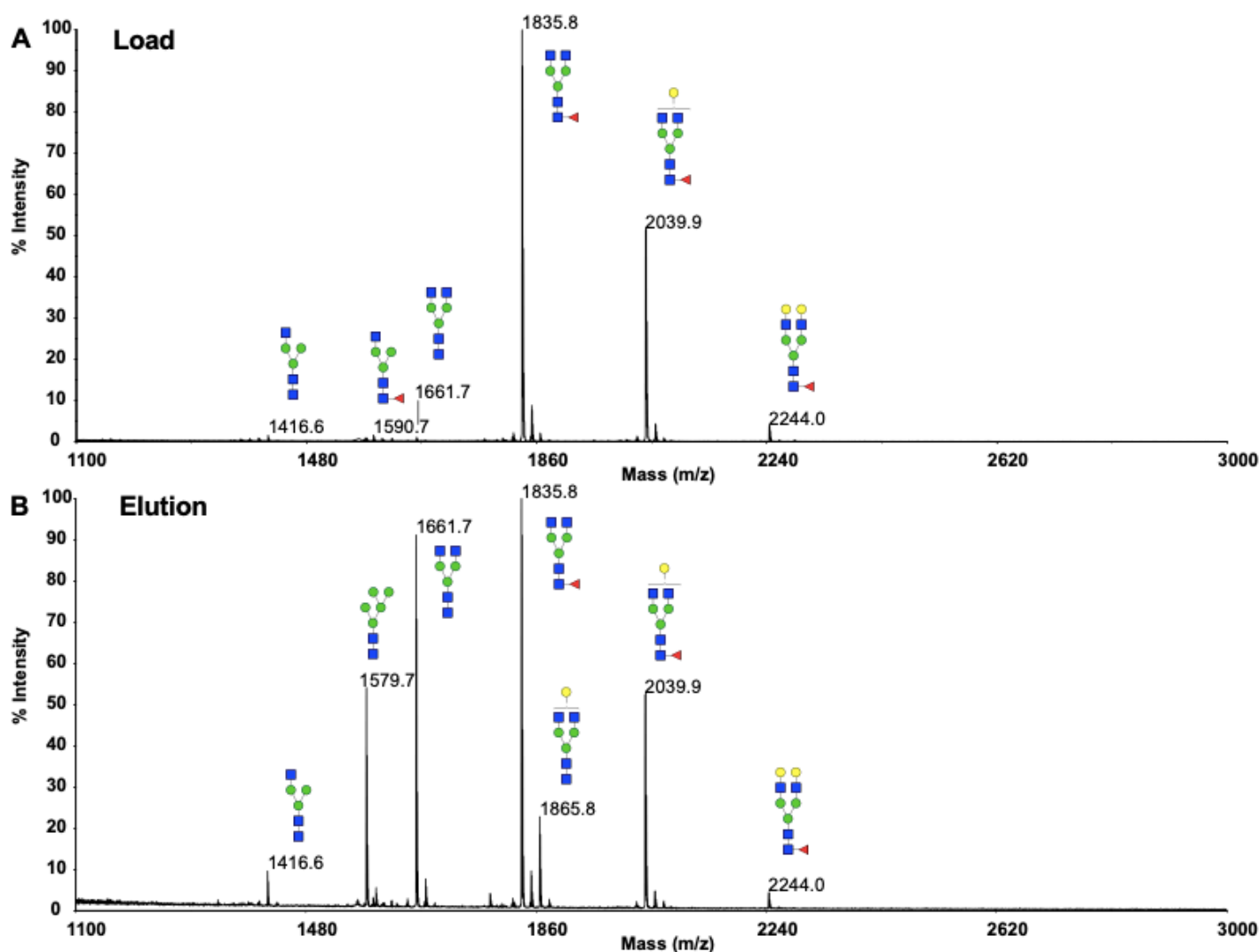
Figure 6.22 – mass spectrometry glycomic analysis of **A)** tocilizumab loaded onto the FcγRIIIa column and **B)** elution fraction 5A2 (peak 2) from the separation depicted by the chromatogram in Figure 6.20.

Figure 6.22 shows that in the elution fraction 5A2, the peaks at m/z ratios of 1579.7, 1661.7 and 1865.8 are enriched, which represent afucosylated glycans. A relative quantification graph showing percentage enrichment for each peak is provided in Appendix 9.5. This confirms that the elution and therefore the sample immobilised to the CM5 chip is enriched for afucosylated tocilizumab.

6.4.2 EDC/NHS Immobilisation of Low-Fucose Tocilizumab

Using the same protocol as for the other two tocilizumab glycovariants, low-fucose tocilizumab was immobilised to a CM5 Biacore™ sensor chip.
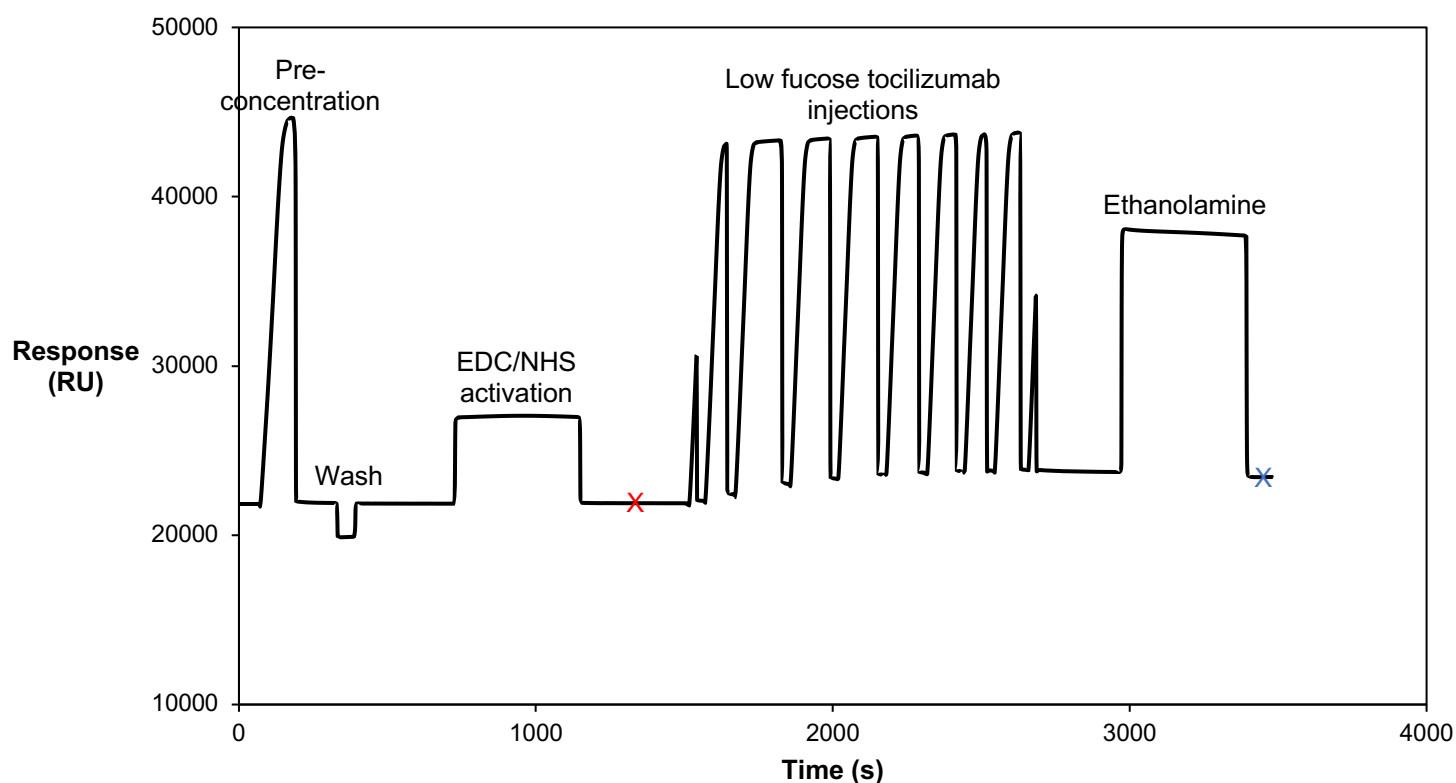
Figure 6.23 – EDC/NHS immobilisation of 0.17μM low-fucose tocilizumab to a CM5 chip. The wash step was carried out with 50mM sodium hydroxide. The immobilised low-fucose tocilizumab level was ~1600RU.

The low-fucose tocilizumab sample had a much lower concentration compared to the tocilizumab and deglycosylated tocilizumab samples. This meant that more protein injections were required to achieve an immobilised ligand level of at least 1500RU.

6.4.3 Interaction of FcγR Ligands with Low-Fucose Tocilizumab

The previous SPR experiments had shown that the FcγR ligands had some binding capabilities similar to that of refFcγRIIIa in that they bound tocilizumab and did not appear to bind deglycosylated tocilizumab. The data suggested that the FcγR ligands may have a stronger affinity for tocilizumab than refFcγRIIIa (nanomolar affinity compared to micromolar). The aim of the next set of experiments was to establish whether the FcγR ligands also possessed the same differential affinity for fucosylated and afucosylated IgG1 as refFcγRIIIa, i.e. a higher affinity for afucosylated compared to fucosylated IgG1.

Firstly, the assay was carried out using refFcγRIIIa against immobilised low-fucose tocilizumab. The sample of low-fucose tocilizumab was prepared as described in Section 6.4.1 and immobilised to a CM5 chip to an immobilisation level of ~1600RU (see Figure 6.22). The

same concentrations that were used for the previous two refFcγRIIIa kinetics/affinity assays were used for the assay with low-fucose tocilizumab.
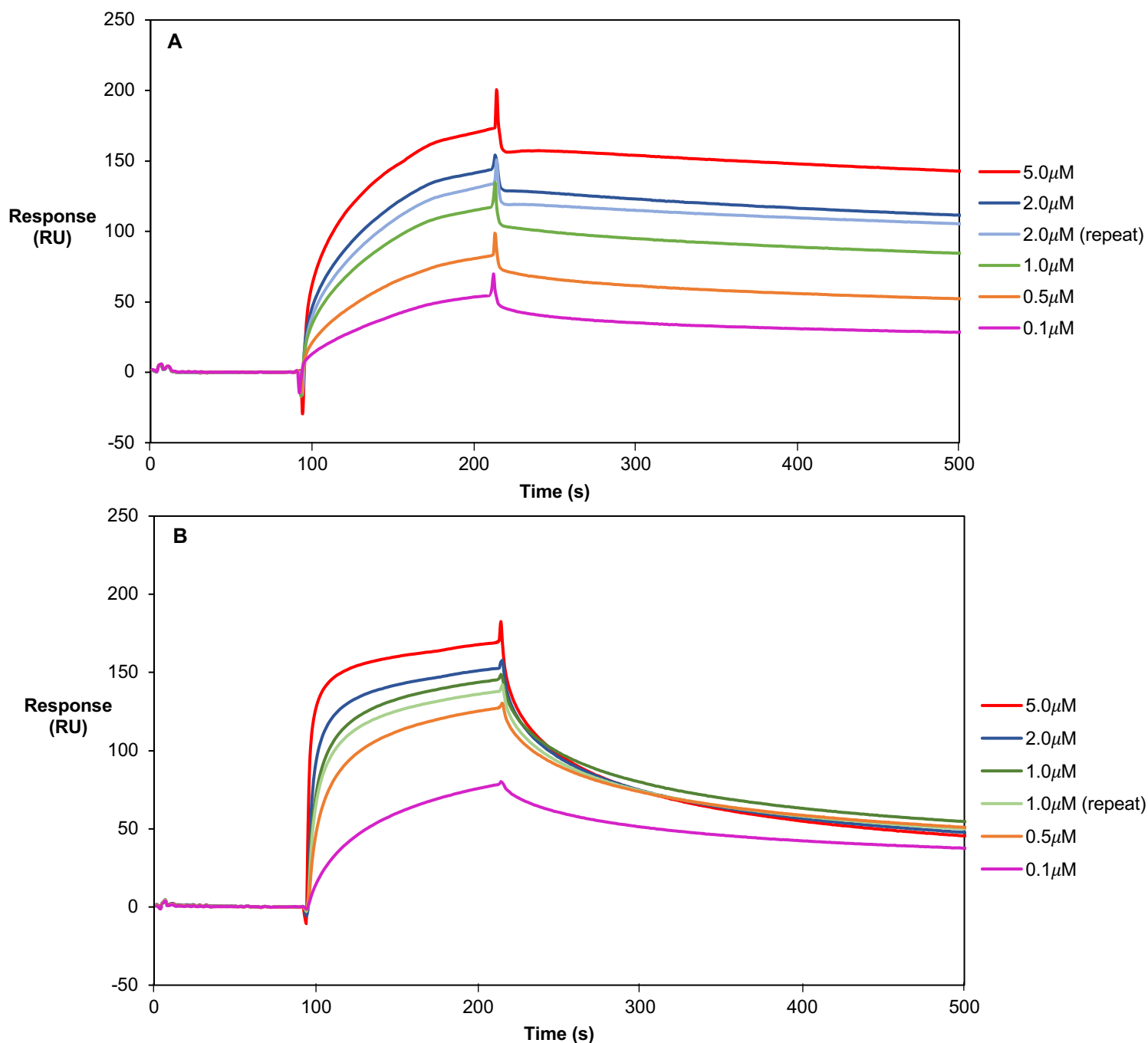
Figure 6.24 – sensorgrams of **A)** refFcγRIIIa against tocilizumab and **B)** refFcγRIIIa against low-fucose tocilizumab immobilised to a CM5 chip. The immobilised tocilizumab level was ~5500RU and the immobilised low-fucose tocilizumab level was ~1600RU. Analyte concentrations of 0.1-5.0μM were used for both assays. The 2.0μM analyte concentration was repeated for the tocilizumab assay and the 1.0μM analyte concentration was repeated for the low-fucose tocilizumab assay. The running buffer used was PBS-P⁺.

Figure 6.24 shows the sensorgrams arising from the interaction of refFcγRIIIa with tocilizumab (also Figure 6.11) and the interaction of refFcγRIIIa with low-fucose tocilizumab. The response level in Figure 6.24A is similar to that in Figure 6.24B, with the highest analyte concentration reaching ~160RU for each assay. The association phase on the curve is steeper in Figure 6.24B compared to Figure 6.24A, indicating a stronger association of refFcγRIIIa to low-fucose tocilizumab compared to tocilizumab.
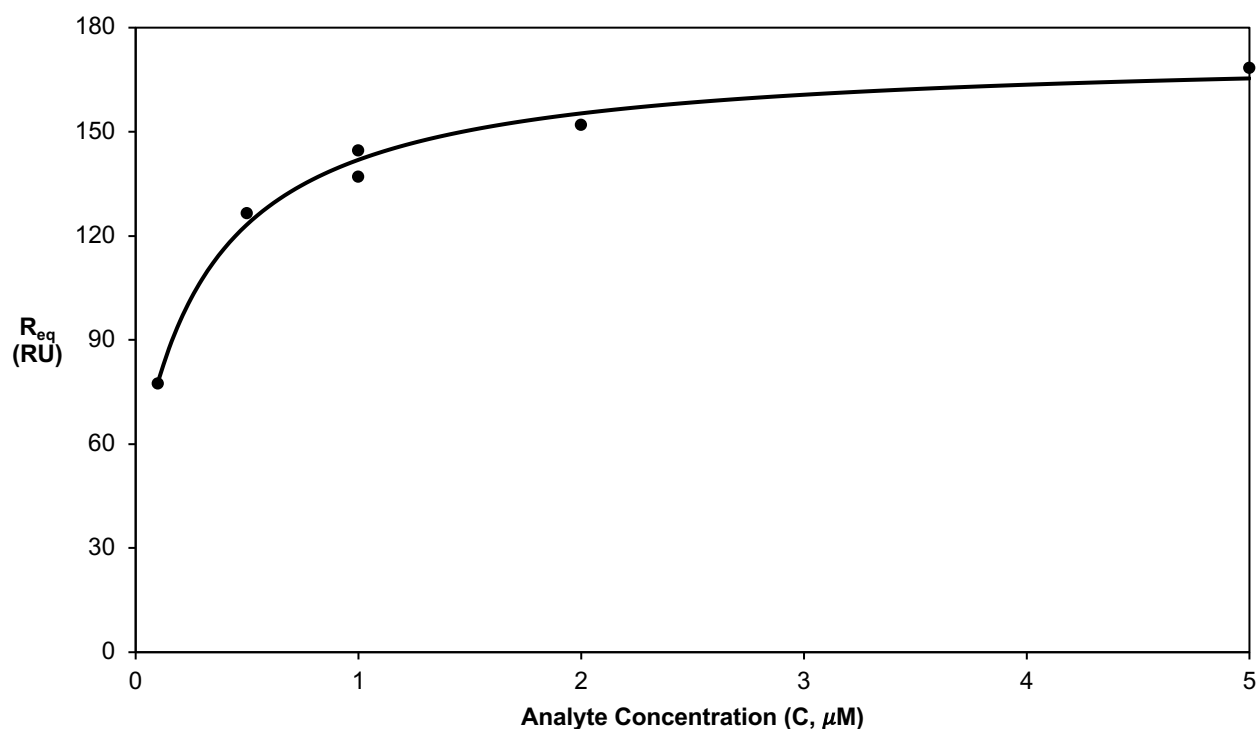
Figure 6.25 – steady state plot for the interaction of refFcγRIIIa and low-fucose tocilizumab. Steady state binding levels R_{eq} are plotted against analyte concentration C and a fit was generated by the Biacore™ Evaluation Software, which is represented by the trendline. The K_D derived from this interaction was 0.34μM.

Table 6.8 – values of K_D, SE of K_D, R_{max} and Chi^2 reported by the Biacore™ Evaluation Software for the interaction of refFcγRIIIa with low-fucose tocilizumab.

refFcγRIIIa-low-fucose tocilizumab	
K_D (μM)	0.34
SE of K_D ($\pm\mu$M)	0.10
R_{max} (RU)	173.4
Chi^2	20.5

The K_D derived by the Evaluation Software for the interaction of refFcγRIIIa with low-fucose tocilizumab was 0.34μM, which is a ~4-fold reduction in affinity compared to the interaction of

refFcγRIIIa with tocilizumab. In the literature, the K_D can be anywhere between 1.2-40-fold lower for the interaction of FcγRIIIa with afucosylated IgG1 compared to fucosylated IgG1 (Braster et al., 2021; Larsen et al., 2021). The K_D can also depend on a variety of factors, including the glycosylation profile of the FcγRIIIa and the IgG1 (aside from fucose levels of IgG1, e.g. galactose and mannose levels), the type of IgG1 used and the experimental set-up used. Our value of ~4-fold tighter binding between refFcγRIIIa and low-fucose tocilizumab compared to refFcγRIIIa and tocilizumab is therefore credible. The Chi^2 statistic is slightly greater than the 10% significance level at 11.5% of R_{max}, but the R_{max} itself seems reasonable and the R_{eq} model appears to fit the dataset well. The derived K_D value is therefore likely to be a reliable indication of the actual affinity of this interaction. As there is a reduction in K_D within the expected range compared to the refFcγRIIIa-tocilizumab interaction, we decided that the chip and assay could be used for testing with the FcγR ligands.

A – Man9-tocilizumab

| 100nM |
| 80nM |
| 80nM (repeat) |
| 60nM |
| 40nM |
| 20nM |

B – Man9-low-fucose tocilizumab

| 100nM |
| 80nM |
| 60nM |
| 40nM |
| 40nM (repeat) |
| 20nM |

C – Man5-tocilizumab

| 100nM |
| 80nM |
| 60nM |
| 60nM (repeat) |
| 40nM |
| 20nM |

D – Man5-low-fucose tocilizumab

| 100nM |
| 80nM |
| 60nM |
| 60nM (repeat) |
| 40nM |
| 20nM |
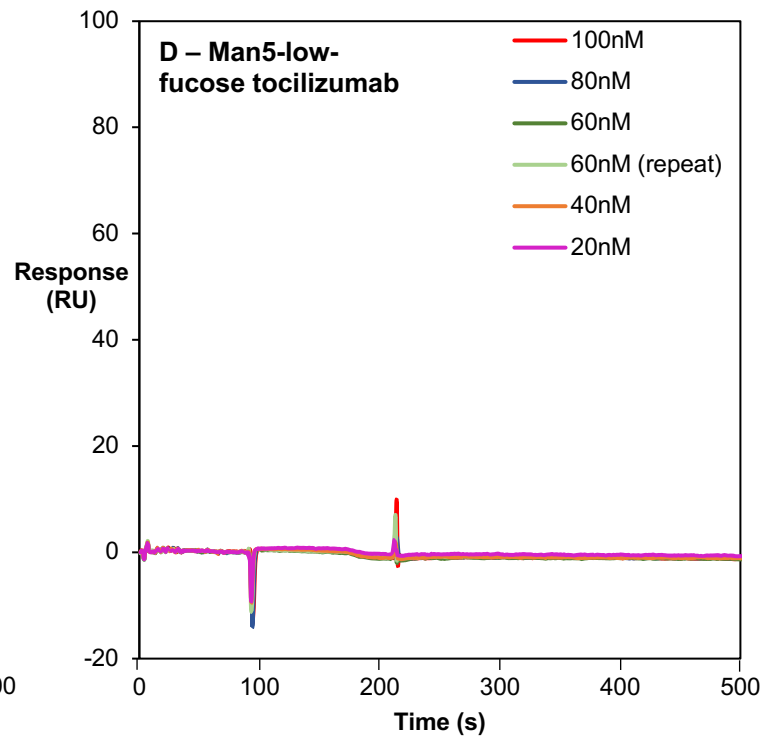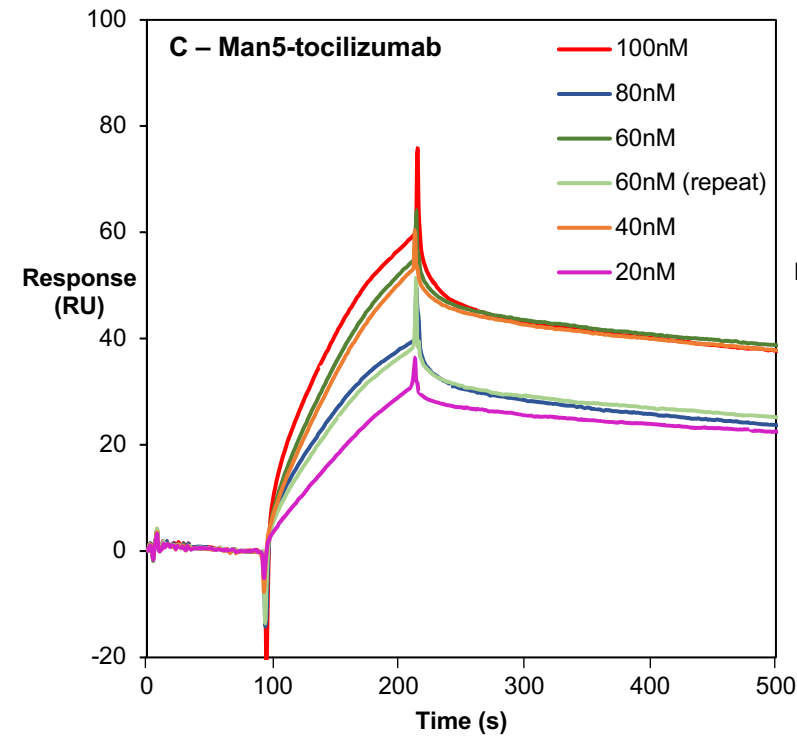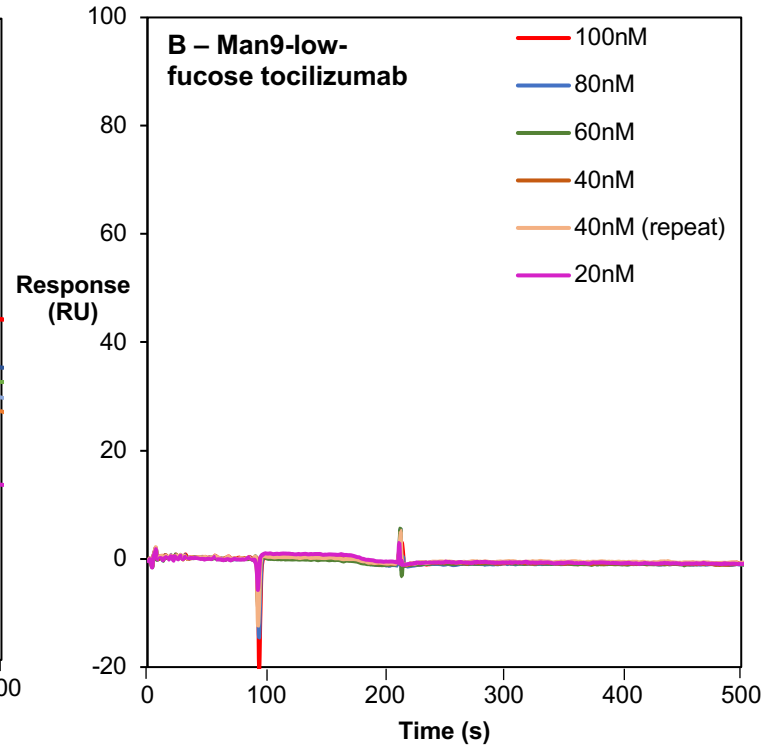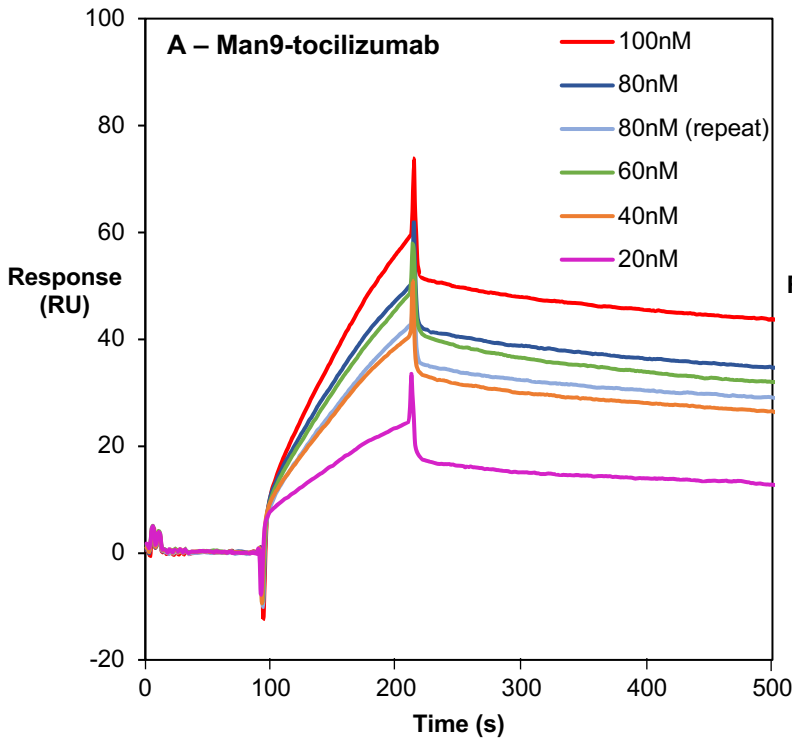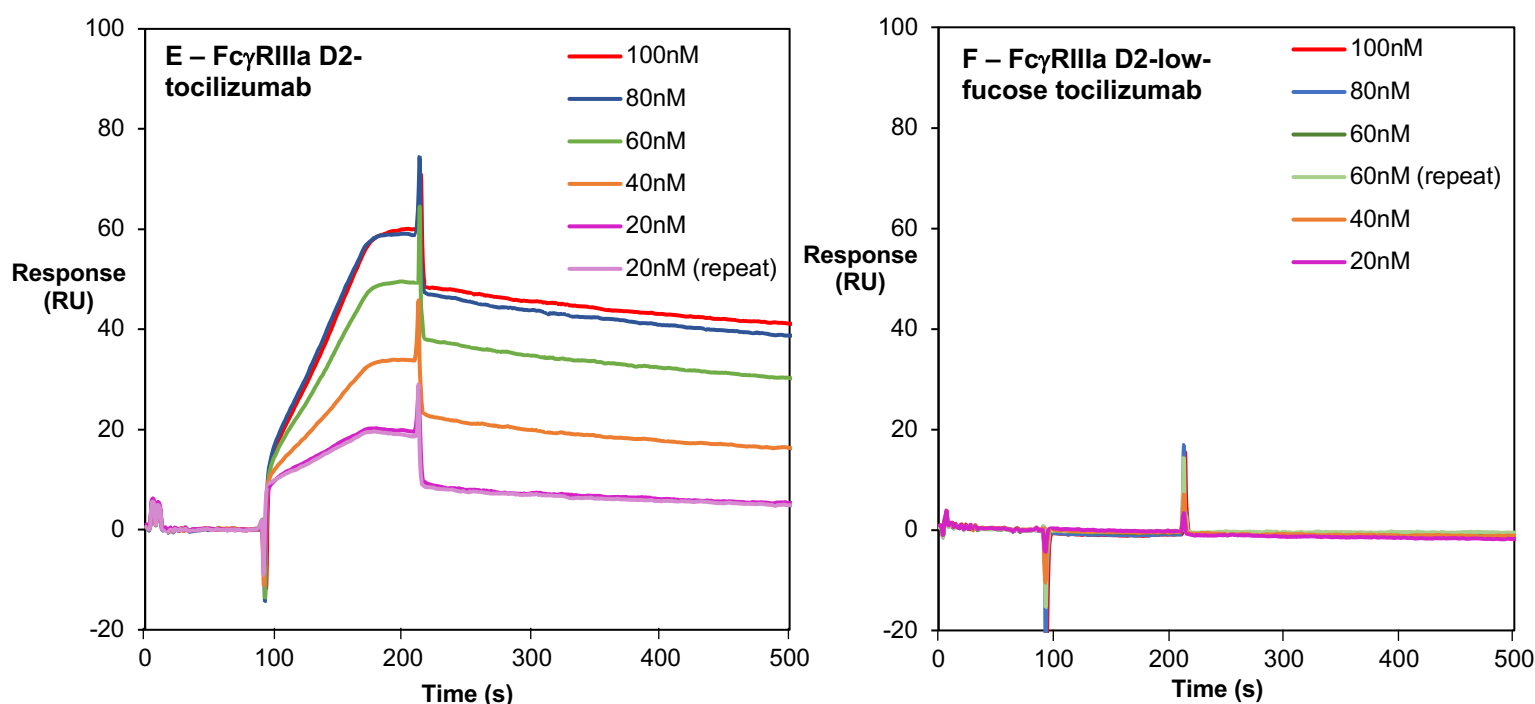
Figure 6.26 – sensorgrams of **A)** Man9-tocilizumab **B)** Man9-low-fucose tocilizumab **C)** Man5-tocilizumab **D)** Man5-low-fucose tocilizumab **E)** FcγRIIIa D2-tocilizumab and **F)** FcγRIIIa D2-low-fucose tocilizumab. The immobilised tocilizumab level was ~5500RU and the immobilised low-fucose tocilizumab level was ~1600RU. Analyte concentrations of 20-100nM were used. The running buffer used was PBS-P$^+$ and all sensor chips were CM5.

Surprisingly, the sensorgrams in Figure 6.26 show that there was no interaction between any of the FcγR ligands and low-fucose tocilizumab.

6.5 Conclusion

Unexpectedly, the FcγR ligands appeared to not bind the low-fucose tocilizumab chip at all. The assays using the low-fucose tocilizumab chip were repeated numerous times with refFcγRIIIa and the FcγR ligands, with very similar results being obtained each time (see Appendix 9.6). These results suggest that the differential affinity of our FcγR ligands for fucosylated and afucosylated IgG1 could be the opposite way around to FcγRIIIa, with the FcγR ligands binding fucosylated IgG1 and not binding afucosylated IgG1. In fact, there is an indication that the FcγR ligands bind fucosylated IgG1 more tightly than refFcγRIIIa does, which could be at least partially attributed to the removal of the *N*-linked glycan at Asn45 on the D1 domain of FcγRIIIa; it is known that this Asn45 glycosylation site has an inhibitory effect on IgG1 binding by causing steric hindrance (Mizushima et al., 2011; Yagi et al., 2018).

Additionally, our refFcγRIIIa was the low-affinity variant (F158), whilst the FcγR ligands possessed a valine at the equivalent site which confers the high-affinity variant in WT FcγRIIIa.

Whilst the switch in affinity of the FcγR ligands for fucosylated and afucosylated IgG1 was an unexpected result, the mass spectrometry analysis of the FcγR ligands confirmed that our ligands have undergone some significant structural changes of both the primary structure and the glycosylation profile, which is highly likely to have altered the tertiary structure of the proteins quite significantly. This may well have altered the binding characteristics of the FcγR ligands compared to FcγRIIIa.

As mentioned, the FcγRIIIa column used to prepare the low-fucose IgG1 sample also binds IgG which only has one afucosylated *N*-glycan out of the two *N*-glycans in the Fc region. As these two glycans are in fairly close proximity (see Figure 6.27), it could be the case that some of these species with only one afucosylated glycan also prevent binding of the FcγR ligands due to these changes in structure compared to the FcγRIIIa. In addition, Figure 6.26 shows structural differences in the D1 domain of FcγRIIIa in complex with afucosylated compared to fucosylated IgG1, highlighting how the dual-domain structure of the protein may have more of an influence on its differential affinity for FcγRIIIa than previously thought.
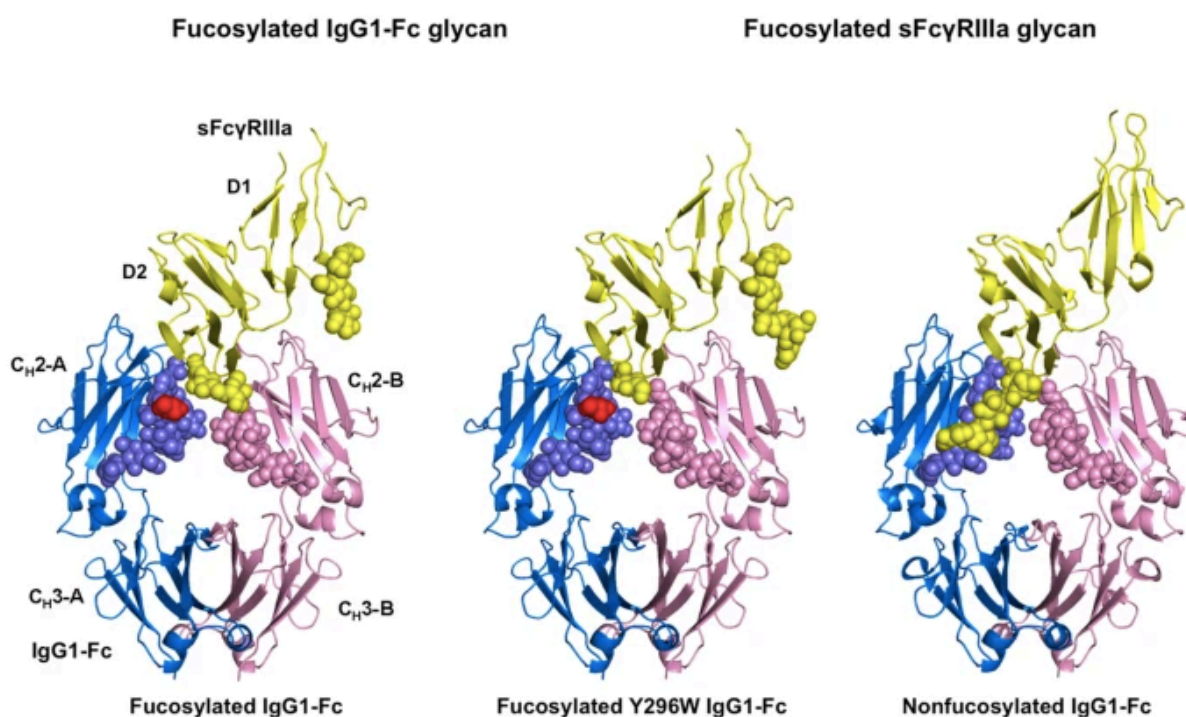
Figure 6.27 – crystal structures of fucosylated and afucosylated IgG1 in complex with a soluble form of FcγRIIIa (sFcγRIIIa). The fucose is highlighted in red and the glycans are represented as spheres. sFcγRIIIa is represented in yellow and the two IgG1 Fc chains are represented in pink and blue. Taken

from Figure 1b of Sakae, Y., Satoh, T., Yagi, H., Yanaka, S., et al. (2017) Conformational effects of *N*-glycan core fucosylation of immunoglobulin G Fc region on its interaction with Fcγ receptor IIIa. *Scientific Reports*.

The mass spectrometry analysis also showed potentially quite a significant degree of *O*-linked glycosylation on the FcγR ligands. This *O*-linked glycosylation is not present on FcγRIIIa and is also not present as the same type of glycan structure, as FcγRIIIa is produced in mammalian expression systems and is complexly-glycosylated whereas our FcγR ligands possess high-mannose glycans. This *O*-linked glycosylation would not have been removed by Endo H when digesting Man5 to make FcγRIIIa D2 and could have an impact on the 3D structure and affinity of the FcγR ligands for IgG1 glycovariants.

Table 6.9 – summary table of dissociation constants, SEs, R_{max} and chi^2 values for all interactions studied. As mentioned, these values are only an indication of the affinity range, i.e. micromolar, nanomolar. The grey represents the reference value (K_D of refFcγRIIIa-tocilizumab interaction) and the blue indicates an increase in affinity compared to the reference value, with darker blue indicating a greater increase in affinity (a greater degree of reduction in K_D). Micromolar concentrations are used for consistency.

	Tocilizumab				Low-fucose tocilizumab				Deglycosylated tocilizumab	
	K_D (μM)	SE of K_D (±μM)	R_{max} (RU)	Chi^2	K_D (μM)	SE of K_D (±μM)	R_{max} (RU)	Chi^2	K_D (μM)	SE of K_D (±μM)
refFcγRIIIa	1.40	0.39	166	33.4	0.34 ↑	0.10	173.4	20.5	N/A	N/A
Man9	0.03 ↑↑	0.06	79.3	34.8	N/A	N/A	N/A	N/A	N/A	N/A
Man5	0.02 ↑↑	0.02	60.3	140	N/A	N/A	N/A	N/A	N/A	N/A
FcγRIIIa D2	0.06 ↑↑	0.04	115.5	7.20	N/A	N/A	N/A	N/A	N/A	N/A

Chapter 7 – Conclusions and Future Work

7.1 Review of Thesis Aims and Objectives

In Section 1.5, the thesis aims and objectives were detailed. These included the design, production, analysis and testing of the FcγR ligands for different IgG1 glycovariants. In this section, the conclusions from each results chapter in this thesis will be discussed in more detail and used to review the initial thesis aims and objectives. The implications that the experimental outcomes have on both the use of the current generation of ligands and future generations of engineered FcγR ligands will also be considered.

7.1.1 FcγR Ligand Design and Construction

The affinity ligand design was based on the native FcγRIIIa, a protein which naturally possesses a stronger affinity for afucosylated compared to fucosylated IgG1. This protein exists as a dual-domain protein, with both domains existing extracellularly and anchored to the immune cell membrane using an α-chain connected to the D2 domain (IgG1-binding domain). There is also an associated FcγR transmembrane domain which contains the ITAM signalling motif, which elicits cellular biochemical cascades after a binding event to the extracellular D2 domain takes place. The dual-domain (D1 and D2) portion of the FcγRIIIa contains up to five *N*-linked glycosylation sites, and as the receptor exists in mammalian (human) systems this glycosylation type is complex (see Figures 3.1 and 3.6).

Major structural changes were made to the FcγRIIIa to generate the engineered FcγRIIIa D2 Man9, FcγRIIIa D2 Man5 and FcγRIIIa D2 ligand constructs. The primary structure was engineered so that only the D2 domain of the FcγRIIIa existed; there was no connecting D1 domain, no α-chain anchoring the D2 domain to a cell membrane, and no associated transmembrane FcγR chain. Some amino acid residues were also changed, such as the N83 residue which is normally attached to the second glycan on the D2 domain (see Sequence 3, Section 3.5). In addition, the glycomic profile of the ligands was changed; not only do the three *N*-glycan sites on the D1 domain not exist in our FcγR ligands, but one of the two sites on the D2 domain was eliminated so that the D2 domain was only monoglycosylated with the *N*-glycan that is thought to be directly involved in IgG1 binding and differentiation between fucosylated and afucosylated IgG1. The type of glycosylation was also changed compared to WT FcγRIIIa as the ligands were produced in a yeast expression system rather than a mammalian system, resulting in high-mannose type glycosylation rather than complex-type glycosylation. Mass spectrometry analysis also detected some *O*-linked glycosylation on our FcγR ligands which would not have been present on WT FcγRIIIa. These substantial changes

were made in order to reduce the cost and complexity of producing FcγRIIIa-based ligands in a mammalian expression system and to remove some of the heterogeneity and complexity associated with a relatively large and highly-glycosylated protein-based affinity ligand. These changes were also made to reduce the ligands' hydrodynamic radii and improve the ligand density and therefore separation efficiency of a column immobilised with FcγR ligands compared to FcγRIIIa, whilst hopefully retaining the ability of the ligands to separate fucosylated and afucosylated IgG1.

7.1.2 FcγR Ligand Production, Purification and Analysis

Initially, the aim was to produce a large amount of the FcγR ligand constructs (~10mg each) so that there would be enough material for mass spectrometry analysis, SPR binding studies and potentially immobilisation to a chromatographic resin should that stage of the work have been reached. We therefore started with using fermentation to produce the ligands in an attempt to generate a large amount of material.

Issues arose primarily regarding proteolytic degradation in the bioreactors. Mitigation strategies were employed to reduce this effect, including adding casamino acids, using a mixed sorbitol/methanol co-feed and shortening the induction period. Success was seen in some cases by shortening the induction period, but the lack of reproducibility in the results meant that a consistent and reliable process could not be established and production reverted to shake flask cultures. After some optimisation and refinement, including troubleshooting after some cultures produced aggregated protein, a reproducible shake flask protocol was established and batches of FcγRIIIa Man9 and Man5 were produced. FcγRIIIa D2 was produced by enzymatically digesting Man5 with the deglycosylase Endo H to remove the majority of the *N*-linked glycan, leaving only a single GlcNAc residue and *O*-linked glycosylation. Western blot analysis using an anti-His-tag antibody was successfully used to detect and analyse Man9, Man5 and FcγRIIIa D2.

Man9 was detected at ~25kDa, Man5 at ~14kDa, and FcγRIIIa D2 at ~12kDa by Western blot analysis. As all three ligand constructs have the same primary structure, the discrepancies in band weights are attributed to changes in both *N*- and *O*-linked glycosylation. Mass spectrometry analysis confirmed that Man9 possesses a slightly greater degree of *N*-glycosylation, and this ligand is also assumed to have a greater degree of *O*-glycosylation than Man5, which would account for discrepancies in apparent molecular weights. The ~2kDa shift of Man5 from ~14kDa to the ~12kDa band seen for FcγRIIIa D2 is approximately consistent with the removal of the single *N*-glycan on Man5. Mass spectrometry analysis also

confirmed the expected primary structure of both Man9 and Man5 using trypsin, chymotrypsin and Glu-C enzymatic digestions.

The FcγR ligands were purified using His-tag affinity chromatography, which was successful. The chromatograms exhibited some peak broadening and tailing, which meant that a Western blot was again used to detect which elution fractions contained the highest concentration of product. These fractions were dialysed into PBS-P$^+$ buffer before being concentrated. Purity levels were measured using the $\frac{A_{260}}{A_{280}}$ ratio, which was found to be ~0.75, and the samples were then used for SPR binding studies.

7.1.3 Measuring FcγR Ligand Affinities for IgG1 Glycovariants

Different fucosylation models of trastuzumab were obtained for the testing of the FcγR ligand affinities for different IgG1 glycovariants. However, when this antibody proved difficult to immobilise, by way of EDC/NHS and otherwise, we moved on to using a different IgG1, tocilizumab.

Tocilizumab was successfully immobilised using EDC/NHS chemistry, providing a chip that could be used for testing the affinities of refFcγRIIIa and subsequently the FcγR ligands for IgG1. Once it had been established that refFcγRIIIa bound the tocilizumab chip with a K_D within the expected micromolar range (1.4μM), the chip was used to test the affinities of our engineered FcγR ligands. The assays with Man9, Man5 and FcγRIIIa D2 also gave positive results and indicated that the binding of the FcγR ligands to fucosylated tocilizumab could be tighter than the refFcγRIIIa binding to this IgG1 glycoform, giving K_D values in the nanomolar range for the FcγR ligand-tocilizumab interactions (20-60nM).

We then required a deglycosylated variant of tocilizumab. The purpose of the deglycosylated tocilizumab assay was to help confirm that the tocilizumab result had been reliable, as it is known that removal of *N*-glycans from the Fc region of IgG1 abolishes binding to the FcγRIIIa (Geuijen et al., 2017, Hanson & Barb, 2015). The assay investigating the binding between deglycosylated tocilizumab and both refFcγRIIIa and the FcγR ligands had the expected result, showing no binding of the refFcγRIIIa or the FcγR ligands to deglycosylated tocilizumab. Consequently, attention was turned towards investigating whether the FcγR ligands possessed the same differential affinity for fucosylated and afucosylated IgG1 as FcγRIIIa, i.e. a stronger affinity for afucosylated or low-fucose tocilizumab compared to our heterogeneously-glycosylated tocilizumab sample.

A sample of low-fucose tocilizumab was prepared using an FcγRIIIa column, which predominantly binds afucosylated antibody, and carrying out a separation of tocilizumab. For our separation using this column, we obtained a flow-through which was expected to mainly consist of fucosylated tocilizumab and an elution which was confirmed by mass spectrometry to be enriched for afucosylated tocilizumab compared to the load. The elution peak was dialysed into a low-salt sodium acetate buffer and this sample of low-fucose tocilizumab was immobilised to a carboxymethylated dextran SPR sensor chip using EDC/NHS chemistry.

The expected result was that both the refFcγRIIIa and the FcγR ligands would bind the low-fucose tocilizumab chip and the derived K_D values for these interactions would be lower than the K_D values obtained for the corresponding interactions of each ligand with tocilizumab. Firstly, refFcγRIIIa was tested against the low-fucose tocilizumab chip. This gave the expected result and a K_D value of 0.34μM, ~4-fold lower than the interaction of refFcγRIIIa with tocilizumab. We therefore proceeded with testing the FcγR ligands' affinity for the low-fucose tocilizumab chip. Unexpectedly, the Man9, Man5 and FcγRIIIa D2 all showed no affinity for the low-fucose chip, suggesting that the FcγR ligands had the opposite affinity for fucosylated and afucosylated IgG1 compared to refFcγRIIIa.

As summarised in Section 7.1.1, extensive changes have been made to both the protein structure and the glycosylation profile of the FcγR ligands compared to WT FcγRIIIa. These considerable changes will have undoubtedly caused alterations in the 3D structure of the FcγR ligands compared to FcγRIIIa, and it is likely that these changes, both proteomic and glycomic, are what has caused the alterations in affinities of the FcγR ligands for fucosylated and afucosylated IgG1 compared to FcγRIIIa. These results also suggest that our current understanding of the FcγRIIIa-IgG1 interaction and the differentiation between fucosylated and afucosylated forms may be incomplete, and it may be a combination of both domains and the *N*-glycans which mediates this differential affinity.

In terms of ligand functionality, these results mean that instead of an FcγR ligand-immobilised column operating in bind-elute mode as the FcγRIIIa column does, it would operate in flow-through mode; the afucosylated IgG1 would flow through the column and the fucosylated would bind. This could have advantages including no harsh elution conditions for the afucosylated (often more desirable) antibody glycoform, which can cause damage and protein aggregation, and the afucosylated antibody could also be separated more quickly in flow-through mode compared to going through an elution phase, as is required when using an FcγRIIIa column. It would also mean that the column would need a greater capacity than the

FcγRIIIa column, as the FcγR ligand column would bind the more prevalent glycovariant. However, the FcγR ligands have already been designed with an increased capacity in mind, as described in Chapter 3. Additionally, from the K_D values derived by the Biacore™ Evaluation Software, there is an indication that the FcγR ligands could bind fucosylated IgG1 more strongly than our model of FcγRIIIa, which could mean that the FcγR ligands have a greater difference in affinity between fucosylated and afucosylated IgG1 compared to refFcγRIIIa. This would mean a more effective separation of the two glycovariants using the FcγR ligands compared to FcγRIIIa.

In the thesis aims and objectives, it was stated that the aims of the project were to develop FcγRIIIa-based affinity ligands for the separation of fucosylated and afucosylated IgG1. The objectives were to make these ligands smaller, less complex and cheaper to produce and scale-up than FcγRIIIa. These objectives have largely been achieved; the apparent molecular weight and mass spectrometry analysis have confirmed that the ligands are smaller and that the *N*-glycosylation is slightly less complex and more homogenous than FcγRIIIa. In addition, the aim was to produce one construct, Man5, with reduced hypermannosylation compared to Man9, which was also accomplished. Expression in *P. pastoris* was achieved and has been cheaper than mammalian cell culture, although scale-up was challenging and requires further optimisation. The thesis aims also stated that the binding interactions of the FcγR ligands with IgG1, deglycosylated IgG1 and afucosylated or reductively-fucosylated IgG1 would be investigated, which was completed in this work. As not enough material was generated for resin immobilisation, this part of the project was not carried out, making this an obvious next step for future work.

7.2 Recommendations for Future Work

There is ample opportunity for further study and engineering of FcγRIIIa-based ligands. This work has elucidated further understanding about the fundamental knowledge of the interaction between FcγRIIIa and IgG1 and what may govern FcγRIIIa's ability to bind afucosylated IgG1 more tightly than fucosylated IgG1. In addition to this, there is also much more research that can be done into designing and engineering future FcγR ligands, which could follow a similar path to how Protein A was refined and developed. Based on this, there are two aspects to future work in this area; the more academic aspect, which would be based on investigating the FcγRIIIa-IgG1 interaction further, and the more application-focussed side of the work which would involve the development of future FcγRIIIa-based affinity ligands for the separation of fucosylated and afucosylated IgG1.

7.2.1 Further Investigation of the FcγRIIIa-IgG1 Interaction

In this section, the more academic side of the future work is explored, which pertains to further exploration of the FcγRIIIa-IgG1 interaction. The research described in this thesis has shown that there may be more to learn about the role of the FcγRIIIa dual-domain structure and *N*-glycan pattern and how these may interact with each other to discern the receptor's binding characteristics and overall functionality.

It has been established that deglycosylated dual domain FcγRIIIa binds IgG1 but does not differentiate between fucosylated and afucosylated IgG1 (Kiyoshi et al., 2018). We also know from the work in this thesis that single domain monoglycosylated (Asn76) high-mannose FcγRIIIa likely has a higher affinity for fucosylated IgG1 than afucosylated IgG1 and does not appear to bind afucosylated IgG1 at all. To investigate what combination of protein domains and glycans are important for differentiating between fucosylated and afucosylated IgG1, as well as whether glycosylation type affects this affinity, more FcγRIIIa constructs would need to be generated. These could include dual domain FcγRIIIa with one *N*-glycan site knocked out at a time, dual domain FcγRIIIa with two *N*-glycan sites knocked out at a time and so on. In addition, the D2 single domain FcγRIIIa, although it has not yet been successfully expressed up until this work, could be expressed with both one and two *N*-glycans present. These could all be expressed in a mammalian expression system as well as a yeast system, for example *P. pastoris*, to investigate the effect of different types of FcγRIIIa glycosylation on IgG1 glycovariant affinity. Furthermore, the effect of these alterations on the affinity for other IgG1 glycovariants could be investigated, such as different galactosylation levels on the Fc *N*-glycan. Although it is acknowledged that this would be expensive and time-consuming work, it could have a huge impact on our current biological understanding of the FcγRIIIa-IgG1 interaction and could perhaps even have implications on future mAb development as well as FcγR-based affinity ligand development.

7.2.2 Future FcγR Ligand Constructs

The following sections are geared more towards the application-based aspect of the future work. The results in this project have shown that the isolated D2 domain with one single *N*-glycosylation site exhibits very different binding properties compared to FcγRIIIa. This could mean that the combination of the D1 and D2 domains as well as the *N*-glycans could all work together to mediate and differentiate between fucosylated and afucosylated IgG1 in a way that has not yet been fully explored. A fairly logical step in the engineering and development of future FcγRIIIa-based affinity ligand constructs would be to isolate the binding site on the D2 only, although considering our results in this work this may also give some unexpected binding

results. However, it would still be an interesting investigation and may shed more light on how the FcγRIIIa differentiates between fucosylated and afucosylated IgG1.

Our FcγR ligands were not stable below pH 6.0. This is not favourable for a chromatographic separation where the bound species must be eluted using low pH conditions, as the FcγR ligands would denature and the column would no longer be usable. It would therefore be useful to engineer pH stability into the ligands. There are computer-based tools which are available for predicting the effect of single point mutations on protein pH stability, such as AlphaFold, which could be used as a starting point in this development.

7.2.3 Optimisation of Fermentation to Produce FcγR Ligands

Rectifying the issues with the fermentation process and developing a more reproducible protocol would be key to the commercial viability and scale-up of the FcγR ligand manufacturing process. It has been reported that reducing the pH to ~3.5-4.0 during fermentation reduces proteolytic activity in *P. pastoris* fermentations (Velez-Suberbie et al., 2020). However, due to the FcγR ligands not being stable below pH 6.0, this strategy was not an option. It would therefore be useful from a manufacturing point of view to improve the stability of the FcγR ligands at low pH conditions, as well as from a ligand functionality standpoint as described in Section 7.2.2. As for the work described in Section 7.2.1, it is acknowledged that this work would be time-consuming and expensive.

7.2.4 Future Binding Studies for FcγR Ligand-IgG1 Glycovariant Interactions

As the obtained binding results were unexpected, it would be beneficial to use other types of IgG1 to confirm the results are reliable. As the trastuzumab was difficult to immobilise, alternative instruments using in-solution techniques could be used to investigate the binding affinity of FcγRIIIa and the FcγR ligands for the different fucosylated forms of trastuzumab. Such instruments could include a MicroCal ITC instrument from Malvern Panalytical™ which uses isothermal titration calorimetry, the Refeyn™ OneMP instrument which uses mass photometry, or the NanoTemper™ Monolith X which uses spectral shift technology.

Chapter 8 – References

Aghamohseni, H., Ohadi, K., Spearman, M., Krahn, N., et al. (2014) Effects of nutrient levels and average culture pH on the glycosylation pattern of camelid-humanized monoclonal antibody. *Journal of Biotechnology*. [Online] 186, 98–109. Available from: https://doi.org/10.1016/j.jbiotec.2014.05.024.

Akerström, B. & Björck, L. (1989) Protein L: an immunoglobulin light chain-binding bacterial protein. Characterization of binding and physicochemical properties. *The Journal of Biological Chemistry*. 264 (33), 19740–19746.

Alberts, B., Johnson, A., Lewis, J., Raff, M., et al. (2002) *Molecular Biology of the Cell*. 4th edition. New York, Garland Science.

St. Amand, M.M., Radhakrishnan, D., Robinson, A.S. & Ogunnaike, B.A. (2014) Identification of manipulated variables for a glycosylation control strategy. *Biotechnology and Bioengineering*. [Online] 111 (10), 1957–1970. Available from: https://doi.org/10.1002/bit.25251.

Amiah, M.A., Ouattara, A., Okou, D.T., N'Guetta, S.-P.A., et al. (2020) Polymorphisms in Fc gamma receptors and susceptibility to malaria in an endemic population. *Frontiers in Immunology*. [Online] 11. Available from: https://doi.org/10.3389/fimmu.2020.561142.

Anthony, R.M., Nimmerjahn, F., Ashline, D.J., Reinhold, V.N., et al. (2008) Recapitulation of IVIg anti-inflammatory activity with a recombinant IgG Fc. *Science (New York, N.Y.)*. [Online] 320 (5874), 373–376. Available from: https://doi.org/10.1126/science.1154315.

Bart, J., Tiggelaar, R., Yang, M., Schlautmann, S., et al. (2009) Room-temperature intermediate layer bonding for microfluidic devices. *Lab on a Chip*. [Online] 9 (24), 3481–3488. Available from: https://doi.org/10.1039/B914270C.

Bas, M., Terrier, A., Jacque, E., Dehenne, A., et al. (2019) Fc sialylation prolongs serum half-life of therapeutic antibodies. *Journal of Immunology (Baltimore, Md. : 1950)*. [Online] 202 (5), 1582–1594. Available from: https://doi.org/10.4049/jimmunol.1800896.

von Behring, E. & Kitasato, S. (1890) On the development of diptheria immunity and tetanus immunity in animals. *German Weekly Medical Journal*. (Translated from German by native speaker).

Bill, R.M. (2015) Recombinant protein subunit vaccine synthesis in microbes: a role for yeast? *The Journal of Pharmacy and Pharmacology*. [Online] 67 (3), 319–328. Available from: https://doi.org/10.1111/jphp.12353.

BioSpace (2019) ProBioGen™ Licenses GlymaxX® Technology to Bayer. BioSpace. [Online] Available from:
https://www.biospace.com/article/probiogen-licenses-glymaxx-technology-to-bayer/.

Bird, R.E., Lemmel, S.A., Yu, X. & Zhou, Q.A. (2021) Bioorthogonal chemistry and its

applications. *Bioconjugate Chemistry*. [Online] 32 (12), 2457–2479. Available from: https://doi.org10.1021/acs.bioconjchem.1c00461.

Boesch, A.W., Kappel, J.H., Mahan, A.E., Chu, T.H., et al. (2018) Enrichment of high affinity subclasses and glycoforms from serum-derived IgG using FcγRs as affinity ligands. *Biotechnology and Bioengineering*. [Online] 115 (5), 1265–1278. Available from: https://doi.org/10.1002/bit.26545.

Bolton, G.R., Ackerman, M.E. & Boesch, A.W. (2013) Separation of nonfucosylated antibodies with immobilized FcgRIII receptors. *American Institute of Chemical Engineers*. [Online] Available from: https://doi.org/10.1002/btpr.1717.

Bolton, G.R. & Mehta, K.K. (2016) The role of more than 40 years of improvement in protein A chromatography in the growth of the therapeutic antibody industry. *Biotechnology Progress*. [Online] 32 (5), 1193–1202. Available from: https://doi.org/10.1002/btpr.2324.

Boune, S., Hu, P., Epstein, A.L. & Khawli, L.A. (2020) Principles of *N*-linked glycosylation variations of IgG-based therapeutics: pharmacokinetic and functional considerations. *Antibodies*. [Online] 9 (2). Available from: https://doi.org/10.3390/antib9020022.

Braster, R., Bögels, M., Benonisson, H., Wuhrer, M., et al. (2021) Afucosylated IgG targets FcγRIV for enhanced tumor therapy in mice. *Cancers*. [Online] 13 (10). Available from: https://doi.org/10.3390/cancers13102372.

Brückner, C., Lehmann, C., Dudziak, D. & Nimmerjahn, F. (2017) Sweet SIGNs: IgG glycosylation leads the way in IVIg-mediated resolution of inflammation. *International Immunology*. [Online] 29 (11), 499–509. Available from: https://doi.org/10.1093/intimm/dxx053.

Çalık, P., Bozkurt, B., Zerze, G.H., İnankur, B., et al. (2013) Effect of co-substrate sorbitol different feeding strategies on human growth hormone production by recombinant *Pichia pastoris*. *Journal of Chemical Technology & Biotechnology*. [Online] 88 (9), 1631–1640. Available from: https://doi.org/10.1002/jctb.4011.

Carillo, S., Pérez-Robles, R., Jakes, C., Ribeiro da Silva, M., et al. (2020) Comparing different domains of analysis for the characterisation of *N*-glycans on monoclonal antibodies. *Journal of Pharmaceutical Analysis*. [Online] 10 (1), 23–34. Available from: https://doi.org/10.1016/j.jpha.2019.11.008.

Chen, S., Lu, C., Gu, H., Mehta, A., et al. (2012) Aleuria Aurantia Lectin (AAL)-reactive immunoglobulin G rapidly appears in sera of animals following antigen exposure. *PLoS One*. [Online] 7 (9), e44422. Available from: https://doi.org/10.1371/journal.pone.0044422.

Choi, B.-K., Bobrowicz, P., Davidson, R.C., Hamilton, S.R., et al. (2003) Use of combinatorial genetic libraries to humanize *N*-linked glycosylation in the yeast *Pichia pastoris*. *Proceedings of the National Academy of Sciences*. [Online] 100 (9), 5022–5027.

Available from: https://doi.org/10.1073/pnas.0931263100.

Chung, C.-Y., Wang, Q., Yang, S., Yin, B., et al. (2017) Integrated genome and protein editing swaps α-2,6 sialylation for α-2,3 sialic acid on recombinant antibodies from CHO. *Biotechnology Journal*. [Online] 12 (2). Available from: https://doi.org/10.1002/biot.201600502.

Clare, J.J., Romanes, M.A., Rayment, F.B., Rowedder, J.E., et al. (1991) Production of mouse epidermal growth factor in yeast: high-level secretion using *Pichia pastoris* strains containing multiple gene copies. *Gene*. [Online] 105 (2), 205–212. Available from: https://doi.org/10.1016/0378-1119(91)90152-2.

Cregg, J. (2022) *The Pichia System*. [Online] 2022. Available from: https://pichia.com/science-center/james-m-cregg-ph-d/.

Cuatrecasas, P., Wilchek, M. & Anfinsen, C.B. (1968) Selective enzyme purification by affinity chromatography. *Proceedings of the National Academy of Sciences of the United States of America*. [Online] 61 (2), 636–643. Available from: https://doi.org/10.1073/pnas.61.2.636.

DeNovix (2019) *Technical Note 130 Purity Ratios Explained*. [Online] 2019. Available from: https://www.denovix.com/tn-130-purity-ratios-explained.

Duerkop, M., Berger, E., Dürauer, A. & Jungbauer, A. (2018) Impact of cavitation, high shear stress and air/liquid interfaces on protein aggregation. *Biotechnology Journal*. [Online] 13 (7), e1800062. Available from: https://doi.org/10.1002/biot.201800062.

Dunkelberger, J.R. & Song, W.-C. (2010) Complement and its role in innate and adaptive immune responses. *Cell Research*. [Online] 20 (1), 34–50. Available from: https://doi.org/10.1038/cr.2009.139.

Edelman, G.M. (1959) Dissociation of γ-globulin. *Journal of the American Chemical Society*. [Online] 81 (12), 3155–3156. Available from: https://doi.org/10.1021/ja01521a071.

Edwards, E., Livanos, M., Krueger, A., Dell, A., et al. (2022) Strategies to control therapeutic antibody glycosylation during bioprocessing: synthesis and separation. *Biotechnology and Bioengineering*. [Online] Available from: https://doi.org/10.1002/bit.28066.

EMA (1999) ICH Topic Q6B Specifications: Test Procedures and Acceptance Criteria for Biotechnological/Biological Products. [Online] Available from: https://www.ema.europa.eu/en/ich-q6b-specifications-test-procedures-acceptance-criteria-biotechnological-biological-products.

Evans, J.B. & Syed, B.A. (2014) Next-generation antibodies. *Nature Reviews Drug Discovery*. Available from: https://doi.org/10.1038/nrd4255.

Falconer, D.J., Subedi, G.P., Marcella, A.M. & Barb, A.W. (2018) Antibody fucosylation lowers the FcγRIIIa/CD16a affinity by limiting the conformations sampled by the N162-glycan. *ACS Chemical Biology*. [Online] 13 (8), 2179–2189. Available from:

https://doi.org/10.1021/acschembio.8b00342.

Ferrara, C., Brünker, P., Suter, T., Moser, S., et al. (2006) Modulation of therapeutic antibody effector functions by glycosylation engineering: influence of Golgi enzyme localization domain and co-expression of heterologous β1, 4-*N*-acetylglucosaminyltransferase III and Golgi α-mannosidase II. *Biotechnology and Bioengineering*. [Online] 93 (5), 851–861. Available from: https://doi.org/10.1002/bit.20777.

Ferrara, C., Grau, S., Jäger, C., Sondermann, P., et al. (2011) Unique carbohydrate-carbohydrate interactions are required for high affinity binding between FcgammaRIII and antibodies lacking core fucose. *Proceedings of the National Academy of Sciences of the United States of America*. [Online] 108 (31), 12669–12674. Available from: https://doi.org/10.1073/pnas.1108455108.

Ferrara, C., Stuart, F., Sondermann, P., Brünker, P., et al. (2006) The carbohydrate at FcγRIIIa Asn-162: an element required for high affinity binding to non-fucosylated IgG glycoforms. *Journal of Biological Chemistry*. [Online] 281 (8), 5032–5036. Available from: https://doi.org/10.1074/jbc.M510171200.

Fischer, J.E., Hatzl, A.-M., Weninger, A., Schmid, C., et al. (2019) Methanol independent expression by *Pichia pastoris* employing de-repression technologies. *JoVE*. [Online] (143), e58589. Available from: https://doi.org/10.3791/58589.

Forsgren, A. & Sjöquist, J. (1966) Protein A. *The Journal of Immunology*. [Online] 97 (6), 822 LP – 827. Available from: http://www.jimmunol.org/content/97/6/822.abstract.

Freeman, C.L. & Sehn, L.H. (2018) A tale of two antibodies: obinutuzumab versus rituximab. *British Journal of Haematology*. [Online] 182 (1), 29–45. Available from: https://doi.org/10.1111/bjh.15232.

Freimoser–Grundschober, A., Rueger, P., Fingas, F., Sondermann, P., et al. (2020) FcγRIIIa chromatography to enrich afucosylated glycoforms and assess the potency of glycoengineered therapeutic antibodies. *Journal of Chromatography A*. [Online] 1610, 460554. Available from: https://doi.org/10.1016/j.chroma.2019.460554.

Gagneux, P. & Varki, A. (1999) Evolutionary considerations in relating oligosaccharide diversity to biological function. *Glycobiology*. [Online] 9 (8), 747–755. Available from: https://doi.org/10.1093/glycob/9.8.747.

Gawlitzek, M., Estacio, M., Fürch, T. & Kiss, R. (2009) Identification of cell culture conditions to control *N*-glycosylation site occupancy of recombinant glycoproteins expressed in CHO cells. *Biotechnology and Bioengineering*. [Online] 103 (6), 1164–1175. Available from: https://doi.org/10.1002/bit.22348.

Geuijen, K.P.M., Oppers-Tiemissen, C., Egging, D.F., Simons, P.J., et al. (2017) Rapid screening of IgG quality attributes - effects on Fc receptor binding. *FEBS Open Bio*.

[Online] 7 (10), 1557–1574. Available from: https://doi.org/10.1002/2211-5463.12283.

Goetze, A.M., Liu, Y.D., Zhang, Z., Shah, B., et al. (2011) High-mannose glycans on the Fc region of therapeutic IgG antibodies increase serum clearance in humans. *Glycobiology*. [Online] 21 (7), 949–959. Available from: https://doi.org/10.1093/glycob/cwr027.

Gómez Román, V.R., Murray, J.C. & Weiner, L.M. (2014) *Chapter 1 - Antibody-Dependent Cellular Cytotoxicity (ADCC)*. In: Margaret E Ackerman & Falk B T - Antibody Fc Nimmerjahn (eds.). [Online] Boston, Academic Press. pp. 1–27. Available from: https://doi.org/10.1016/B978-0-12-394802-1.00001-7.

GrandViewResearch.com (2021) Monoclonal Antibodies Market Size, Share & Trends Analysis Report By Source Type (Chimeric, Murine, Humanized, Human), By Production Type (In Vivo, In Vitro), By Application, By End-use, By Region, And Segment Forecasts, 2023 - 2030. [Online] Available from:

https://www.grandviewresearch.com/industry-analysis/monoclonal-antibodies-market.

Gulich, S., Uhlen, M. & Hober, S. (2000) Protein engineering of an IgG-binding domain allows milder elution conditions during affinity chromatography. *Journal of Biotechnology*. [Online] 76 (2–3), 233–244. Available from:

https://doi.org/10.1016/s0168-1656(99)00197-2.

Hage, D.S., Anguizola, J.A., Bi, C., Li, R., et al. (2012) Pharmaceutical and biomedical applications of affinity chromatography: recent trends and developments. *Journal of Pharmaceutical and Biomedical Analysis*. [Online] 69, 93–105. Available from: https://doi.org/10.1016/j.jpba.2012.01.004.

Hanson, Q.M. & Barb, A.W. (2015) A perspective on the structure and receptor binding properties of immunoglobulin G Fc. *Biochemistry*. [Online] 54 (19), 2931–2942. Available from: https://doi.org/10.1021/acs.biochem.5b00299.

Hayes, J., Wormald, M.R., Rudd, P. & Davey, G. (2016) Fc gamma receptors: glycobiology and therapeutic prospects. *Dovepress*. [Online] Available from: https://doi.org/10.2147/JIR.S121233.

Helmerhorst, E., Chandler, D.J., Nussio, M. & Mamotte, C.D. (2012) Real-time and label-free bio-sensing of molecular interactions by surface plasmon resonance: a laboratory medicine perspective. *The Clinical Biochemist: Reviews*. 33 (4), 161–173.

Hjelm, H., Hjelm, K. & Sjöquist, J. (1972) Protein A from *Staphylococcus aureus*: its isolation by affinity chromatography and its use as an immunosorbent for isolation of immunoglobulins. *FEBS Letters*. [Online] 28 (1), 73–76. Available from: https://doi.org/10.1016/0014-5793(72)80680-X.

Hober, S., Nord, K. & Linhult, M. (2007) Protein A chromatography for antibody purification. *Journal of Chromatography B*. [Online] 848 (1), 40–47. Available from: https://doi.org/10.1016/j.jchromb.2006.09.030.

von Horsten, H.H., Ogorek, C., Blanchard, V., Demmler, C., et al. (2010) Production of non-fucosylated antibodies by co-expression of heterologous GDP-6-deoxy-d-lyxo-4-hexulose reductase. *Glycobiology.* [Online] 20 (12), 1607–1618. Available from: https://doi.org/10.1093/glycob/cwq109.

Hossler, P., Khattak, S.F. & Li, Z.J. (2009) Optimal and consistent protein glycosylation in mammalian cell culture. *Glycobiology.* [Online] 19 (9), 936–949. Available from: https://doi.org/10.1093/glycob/cwp079.

Hu, R., Lan, D., Cui, R., Hong, H., et al. (2020) Controlling methanol feeding for recombinant protein production by *Pichia pastoris* under oxidation stress in fed-batch fermentation. *Applied Biochemistry and Biotechnology.* [Online] Available from: https://doi.org/10.21203/rs.3.rs-85999/v1.

Hurum, D.C. & Rohrer, J.S. (2011) Five-minute glycoprotein sialic acid determination by high-performance anion exchange chromatography with pulsed amperometric detection. *Analytical Biochemistry.* [Online] 419 (1), 67–69. Available from: https://doi.org/10.1016/j.ab.2011.08.002.

Inbar, D., Hochman, J. & Givol, D. (1972) Localization of antibody-combining sites within the variable portions of heavy and light chains. *Proceedings of the National Academy of Sciences of the United States of America*. [Online] 69 (9), 2659–2662. Available from: https://doi.org/10.1073/pnas.69.9.2659.

Isoda, Y., Yagi, H., Satoh, T., Shibata-Koyama, M., et al. (2015) Importance of the side chain at position 296 of antibody Fc in interactions with FcγRIIIa and other Fcγ receptors. *PLoS One.* [Online] 10 (10), e0140120. Available from: https://doi.org/10.1371/journal.pone.0140120.

Iwamoto, M., Sekiguchi, Y., Nakamura, K., Kawaguchi, Y., et al. (2018) Generation of efficient mutants of endoglycosidase from *Streptococcus pyogenes* and their application in a novel one-pot transglycosylation reaction for antibody modification. *PLoS One.* [Online] 13 (2), e0193534. Available from: https://doi.org/10.1371/journal.pone.0193534.

Jain, A. & Cheng, K. (2017) The principles and applications of avidin-based nanoparticles in drug delivery and diagnosis. *Journal of Controlled Release: Official Journal of the Controlled Release Society.* [Online] 245, 27–40. Available from: https://doi.org/10.1016/j.jconrel.2016.11.016.

Janeway Jr., C.A., Travers, P., Walport, M. & Shlomchik, M.J. (2001) *Immunobiology: The Immune System in Health and Disease*. 5th edition. [Online] New York, Garland Science. Available from: https://www.ncbi.nlm.nih.gov/books/NBK27144/.

Janson, J.-C. & Jönsson, J.Å. (2011) Introduction to Chromatography. In: Jan-Christer Janson (ed.). *Protein Purification: Principles, High Resolution Methods and Applications*. 3rd edition. John Wiley & Sons, Ltd.

Jensen, K. (1958) A normally-occurring *Staphylococcus* antibody in human serum. *Acta Pathologica Microbiologica Scandinavica*. [Online] 44 (4), 421–428. Available from: https://doi.org/10.1111/j.1699-0463.1958.tb01093.x.

Jiménez Morales, A., Maldonado-Montoro, M., Martínez de la Plata, J.E., Pérez Ramírez, C., et al. (2019) FcgR2a/FcgR3a gene polymorphisms and clinical variables as predictors of response to tocilizumab and rituximab in patients with rheumatoid arthritis. *The Journal of Clinical Pharmacology*. [Online] 59 (4), 517–531. Available from: https://doi.org/10.1002/jcph.1341.

Jolles, S., Sewell, W.A.C. & Misbah, S.A. (2005) Clinical uses of intravenous immunoglobulin. *Clinical and Experimental Immunology*. [Online] 142 (1), 1–11. Available from: https://doi.org/10.1111/j.1365-2249.2005.02834.x.

Junker, F., Gordon, J. & Qureshi, O. (2020) Fc gamma receptors and their role in antigen uptake, presentation, and T cell activation. *Frontiers in Immunology*. [Online] 11, 1393. Available from: https://doi.org/10.3389/fimmu.2020.01393.

Kanda, Y., Imai-Nishiya, H., Kuni-Kamochi, R., Mori, K., et al. (2007) Establishment of a GDP-mannose 4,6-dehydratase (GMD) knockout host cell line: a new strategy for generating completely non-fucosylated recombinant therapeutics. *Journal of Biotechnology*. [Online] 130 (3), 300–310. Available from: https://doi.org/10.1016/j.jbiotec.2007.04.025.

Kang, S., Zhang, Z., Richardson, J., Shah, B., et al. (2015) Metabolic markers associated with high mannose glycan levels of therapeutic recombinant monoclonal antibodies. *Journal of Biotechnology*. [Online] 203, 22–31. Available from: https://doi.org/10.1016/j.jbiotec.2015.03.002.

Karbalaei, M., Rezaee, S.A. & Farsiani, H. (2020) *Pichia pastoris*: a highly successful expression system for optimal synthesis of heterologous proteins. *Journal of Cellular Physiology*. [Online] 235 (9), 5867–5881. Available from: https://doi.org/10.1002/jcp.29583.

Käsermann, F., Boerema, D.J., Rüegsegger, M., Hofmann, A., et al. (2012) Analysis and functional consequences of increased Fab-sialylation of intravenous immunoglobulin (IVIg) after lectin fractionation. *PLoS One*. [Online] 7 (6), e37243. Available from: https://doi.org/10.1371/journal.pone.0037243.

Keogh, D., Thompson, R., Larragy, R., McMahon, K., et al. (2014) Generating novel recombinant prokaryotic lectins with altered carbohydrate binding properties through mutagenesis of the PA-IL protein from *Pseudomonas aeruginosa*. *Biochimica et Biophysica Acta (BBA) - General Subjects*. [Online] 1840 (6), 2091–2104. Available from: https://doi.org/10.1016/j.bbagen.2014.01.020.

Kiyoshi, M., Caaveiro, J.M.M., Tada, M., Tamura, H., et al. (2018) Assessing the heterogeneity of the Fc-glycan of a therapeutic antibody using an engineered FcγRIIIa-immobilized

column. *Scientific Reports*. [Online] 8 (1), 3955. Available from: https://doi.org/10.1038/s41598-018-22199-8.

Köhler, G. & Milstein, C. (1975) Continuous cultures of fused cells secreting antibody of predefined specificity. *Nature*. [Online] 256 (5517), 495–497. Available from: https://doi.org/10.1038/256495a0.

Kurogochi, M., Mori, M., Osumi, K., Tojino, M., et al. (2015) Glycoengineered monoclonal antibodies with homogeneous glycan (M3, G0, G2, and A2) using a chemoenzymatic approach have different affinities for FcγRIIIa and variable antibody-dependent cellular cytotoxicity activities. *PLoS One*. [Online] 10 (7), e0132848. Available from: https://doi.org/10.1371/journal.pone.0132848.

Łacki, K.M. & Riske, F.J. (2019) Affinity chromatography: an enabling technology for large-scale bioprocessing. *Biotechnology Journal*. [Online] Available from: https://doi.org/10.1002/biot.201800397.

Lakayan, D., Haselberg, R., Gahoual, R., Somsen, G.W., et al. (2018) Affinity profiling of monoclonal antibody and antibody-drug-conjugate preparations by coupled liquid chromatography-surface plasmon resonance biosensing. *Analytical and Bioanalytical Chemistry*. [Online] 410 (30), 7837–7848. Available from: https://doi.org/10.1007/s00216-018-1414-y.

Larsen, M.D., Lopez-Perez, M., Dickson, E.K., Ampomah, P., et al. (2021) Afucosylated *Plasmodium falciparum*-specific IgG is induced by infection but not by subunit vaccination. *Nature Communications*. [Online] 12 (1), 5838. Available from: https://doi.org/10.1038/s41467-021-26118-w.

Laukens, B., Visscher, C. De & Callewaert, N. (2015) Engineering yeast for producing human glycoproteins: where are we now? *Future Microbiology*. [Online] 10 (1), 21–34. Available from: https://doi.org/10.2217/fmb.14.104.

Lee, M.-H., Hsu, T.-L., Lin, J.-J., Lin, Y.-J., et al. (2020) Constructing a human complex type *N*-linked glycosylation pathway in *Kluyveromyces marxianus*. *PLoS One*. [Online] 15 (5), e0233492. Available from: https://doi.org/10.1371/journal.pone.0233492.

Li, J., Hsu, H.-C., Mountz, J.D. & Allen, J.G. (2018) Unmasking fucosylation: from cell adhesion to immune system regulation and diseases. *Cell Chemical Biology*. [Online] 25 (5), 499–512. Available from: https://doi.org/10.1016/j.chembiol.2018.02.005.

Li, P., Jiang, N., Nagarajan, S., Wohlhueter, R., et al. (2007) Affinity and kinetic analysis of Fc gamma Receptor IIIa (CD16a) binding to IgG ligands. *Journal of Biological Chemistry*. [Online] 282 (9), 6210–6221. Available from: https://doi.org/10.1074/jbc.M609064200.

Li, T., Li, C., Quan, D.N., Bentley, W.E., et al. (2018) Site-specific immobilization of endoglycosidases for streamlined chemoenzymatic glycan remodeling of antibodies. *Carbohydrate Research*. [Online] 458–459, 77–84. Available from:

https://doi.org/10.1016/j.carres.2018.02.007.

Li, X., Ptacek, T.S., Brown, E.E. & Edberg, J.C. (2009) Fc gamma receptors: structure, function and role as genetic risk factors in SLE. *Genes and Immunity*. [Online] 10 (5), 380–389. Available from: https://doi.org/10.1038/gene.2009.35.

Link, H. & Weuster-Botz, D. (2011) *2.11 - Medium Formulation and Development*. In: Murray B T - Comprehensive Biotechnology (Second Edition) Moo-Young (ed.). [Online] Burlington, Academic Press. pp. 119–134. Available from: https://doi.org/10.1016/B978-0-08-088504-9.00092-1.

Lippold, S., Nicolardi, S., Domínguez-Vega, E., Heidenreich, A.-K., et al. (2019) Glycoform-resolved FcγRIIIa affinity chromatography–mass spectrometry. *MAbs*. [Online] 11 (7), 1191–1196. Available from: https://doi.org/10.1080/19420862.2019.1636602.

List, K., Høyer-Hansen, G., Rønne, E., Danø, K., et al. (1999) Different mechanisms are involved in the antibody mediated inhibition of ligand binding to the urokinase receptor: a study based on biosensor technology. *Journal of Immunological Methods*. [Online] 222 (1), 125–133. Available from: https://doi.org/10.1016/S0022-1759(98)00189-6.

Liu, J., Wang, Y., Xiong, E., Hong, R., et al. (2019) Role of the IgM Fc receptor in immunity and tolerance. *Frontiers in Immunology*. [Online] 10 p.529. Available from: https://www.frontiersin.org/article/10.3389/fimmu.2019.00529.

Liu, W.-C., Gong, T., Wang, Q.-H., Liang, X., et al. (2016) Scaling-up fermentation of *Pichia pastoris* to demonstration-scale using new methanol-feeding strategy and increased air pressure instead of pure oxygen supplement. *Scientific Reports*. [Online] 6 (1), 18439. Available from: https://doi.org/10.1038/srep18439.

Lloyd, K.O. (1970) The preparation of two insoluble forms of the phytohemagglutinin, concanavalin A, and their interactions with polysaccharides and glycoproteins. *Archives of Biochemistry and Biophysics*. [Online] 137 (2), 460–468. Available from: https://doi.org/10.1016/0003-9861(70)90463-7.

Loebrich, S., Clark, E., Ladd, K., Takahashi, S., et al. (2019) Comprehensive manipulation of glycosylation profiles across development scales. *MAbs*. [Online] 11 (2), 335–349. Available from: https://doi.org/10.1080/19420862.2018.1527665.

Lu, R.-M., Hwang, Y.-C., Liu, I.-J., Lee, C.-C., et al. (2020) Development of therapeutic antibodies for the treatment of diseases. *Journal of Biomedical Science*. [Online] 27 (1), 1. Available from: https://doi.org/10.1186/s12929-019-0592-z.

Manabe, S., Yamaguchi, Y., Abe, J., Matsumoto, K., et al. (2018) Acceptor range of endo-β-*N*-acetylglucosaminidase mutant endo-CC N180H: from monosaccharide to antibody. *Royal Society Open Science*. [Online] 5 (5), 171521. Available from: https://doi.org/10.1098/rsos.171521.

Mandó, P., Rivero, S.G., Rizzo, M.M., Pinkasz, M., et al. (2021) Targeting ADCC: a different

approach to HER2 breast cancer in the immunotherapy era. *Breast (Edinburgh, Scotland)*. [Online] 60, 15–25. Available from: https://doi.org/10.1016/j.breast.2021.08.007.

Marshall, M.J.E., Stopforth, R.J. & Cragg, M.S. (2017) Therapeutic antibodies: what have we learnt from targeting CD20 and where are we going? *Frontiers in Immunology*. [Online] 8. Available from: https://doi.org/10.3389/fimmu.2017.01245.

Meinwald, Y.C., Stimson, E.R. & Scheraga, H.A. (1986) Deamidation of the asparaginyl-glycyl sequence. *International Journal of Peptide and Protein Research*. [Online] 28 (1), 79–84. Available from: https://doi.org/10.1111/j.1399-3011.1986.tb03231.x.

Mizushima, T., Yagi, H., Takemoto, E., Shibata-Koyama, M., et al. (2011) Structural basis for improved efficacy of therapeutic antibodies on defucosylation of their Fc glycans. *Genes to Cells: Devoted to Molecular & Cellular Mechanisms*. [Online] 16 (11), 1071–1080. Available from: https://doi.org/10.1111/j.1365-2443.2011.01552.x.

Narhi, L., Arakawa, T., Aoki, K., Elmore, R., et al. (1991) The effect of carbohydrate on the structure and stability of erythropoietin. *The Journal of Biological Chemistry*. 266 34, 23022–23026.

Neelamegham, S., Aoki-Kinoshita, K., Bolton, E., Frank, M., et al. (2019) Updates to the Symbol Nomenclature for Glycans guidelines. *Glycobiology*. [Online] 29 (9), 620–624. Available from: https://doi.org/10.1093/glycob/cwz045.

Nett, J.H., Cook, W.J., Chen, M.-T., Davidson, R.C., et al. (2013) Characterization of the *Pichia pastoris* protein-*O*-mannosyltransferase gene family. *PLoS One*. [Online] 8 (7), e68325. Available from: https://doi.org/10.1371/journal.pone.0068325.

O'Connor, B.F., Monaghan, D. & Cawley, J. (2017) *Lectin Affinity Chromatography (LAC) BT - Protein Chromatography: Methods and Protocols*. In: Dermot Walls & Sinéad T Loughran (eds.). [Online] New York, NY, Springer New York. pp. 411–420. Available from: https://doi.org/10.1007/978-1-4939-6412-3_23.

Oregioni, A., Stieglitz, B., Kelly, G., Rittinger, K., et al. (2017) Determination of the pKa of the N-terminal amino group of ubiquitin by NMR. *Scientific Reports*. [Online] 7, 43748. Available from: https://doi.org/10.1038/srep43748.

Pacis, E., Yu, M., Autsen, J., Bayer, R., et al. (2011) Effects of cell culture conditions on antibody *N*-linked glycosylation - what affects high mannose 5 glycoforms? *Biotechnology and Bioengineering*. [Online] 108 (10), 2348–2358. Available from: https://doi.org/10.1002/bit.23200.

Pekarsky, A., Veiter, L., Rajamanickam, V., Herwig, C., et al. (2018) Production of a recombinant peroxidase in different glyco-engineered *Pichia pastoris* strains: a morphological and physiological comparison. *Microbial Cell Factories*. [Online] 17 (1), 183. Available from: https://doi.org/10.1186/s12934-018-1032-6.

Peschke, B., Keller, C.W., Weber, P., Quast, I., et al. (2017) Fc-galactosylation of human immunoglobulin gamma isotypes improves C1q binding and enhances complement-dependent cytotoxicity. *Frontiers in Immunology*. [Online] 8, 646. Available from: https://doi.org/10.3389/fimmu.2017.00646.

Petricevic, B., Laengle, J., Singer, J., Sachet, M., et al. (2013) Trastuzumab mediates antibody-dependent cell-mediated cytotoxicity and phagocytosis to the same extent in both adjuvant and metastatic HER2/neu breast cancer patients. *Journal of Translational Medicine*. [Online] 11, 307. Available from: https://doi.org/10.1186/1479-5876-11-307.

Porter, R.R. (1959) The hydrolysis of rabbit γ-globulin and antibodies with crystalline papain. *The Biochemical Journal*. [Online] 73 (1), 119–126. Available from: https://doi.org/10.1042/bj0730119.

Pučić, M., Knežević, A., Vidič, J., Adamczyk, B., et al. (2011) High throughput isolation and glycosylation analysis of IgG – variability and heritability of the IgG glycome in three isolated human populations. *Molecular & Cellular Proteomics*. [Online] 10 (10), M111.010090. Available from: https://doi.org/10.1074/mcp.M111.010090.

Rameez, S., Gowtham, Y.K., Nayar, G. & Mostafa, S.S. (2021) Modulation of high mannose levels in *N*-linked glycosylation through cell culture process conditions to increase antibody-dependent cell-mediated cytotoxicity activity for an antibody biosimilar. *Biotechnology Progress*. [Online] e3176. Available from: https://doi.org/10.1002/btpr.3176.

Ramos de la Peña, A.M., González-Valdez, J. & Aguilar, O. (2019) Protein A chromatography: challenges and progress in the purification of monoclonal antibodies. *Journal of Separation Science*. [Online] 42. Available from: https://doi.org/10.1002/jssc.201800963.

Rao, V., Guan, C. & Van Roey, P. (1995) Crystal structure of endo-β-*N*-acetylglucosaminidase H at 1.9Ä resolution: active-site geometry and substrate recognition. *Structure (London, England: 1993)*. [Online] 3 (5), 449–457. Available from: https://doi.org/10.1016/s0969-2126(01)00178-2.

Reichert, J.M. (2023) Antibody therapeutics approved or in regulatory review in the EU or US. 2023. *The Antibody Society*. [Online] Available from: https://www.antibodysociety.org/resources/approved-antibodies/.

Rohrer, J.S. (2000) Analyzing sialic acids using high-performance anion-exchange chromatography with pulsed amperometric detection. *Analytical Biochemistry*. [Online] 283 (1), 3–9. Available from: https://doi.org/10.1006/abio.2000.4643.

Rosales, C. & Uribe-Querol, E. (2017) Phagocytosis: a fundamental process in immunity. *BioMed Research International*. [Online] 2017, 9042851. Available from: https://doi.org/10.1155/2017/9042851.

Sakae, Y., Satoh, T., Yagi, H., Yanaka, S., et al. (2017) Conformational effects of *N*-glycan core fucosylation of immunoglobulin G Fc region on its interaction with Fcγ receptor IIIa. *Scientific Reports*. [Online] 7 (1), 13780. Available from: https://doi.org/10.1038/s41598-017-13845-8.

Schroeder, H.W.J. & Cavacini, L. (2010) Structure and function of immunoglobulins. *The Journal of Allergy and Clinical Immunology*. [Online] 125 (2 Suppl 2), S41-52. Available from: https://doi.org/10.1016/j.jaci.2009.09.046.

Schwab, I., Mihai, S., Seeling, M., Kasperkiewicz, M., et al. (2014) Broad requirement for terminal sialic acid residues and FcγRIIB for the preventive and therapeutic activity of intravenous immunoglobulins *in vivo*. *European Journal of Immunology*. [Online] 44 (5), 1444–1453. Available from: https://doi.org/10.1002/eji.201344230.

Seo, Y., Ishii, Y., Ochiai, H., Fukuda, K., et al. (2014) Cetuximab-mediated ADCC activity is correlated with the cell surface expression level of EGFR but not with the KRAS/BRAF mutational status in colorectal cancer. *Oncology Reports*. [Online] 31 (5), 2115–2122. Available from: https://doi.org/10.3892/or.2014.3077.

Sheppard, M., Laskou, F., Stapleton, P.P., Hadavi, S., et al. (2017) Tocilizumab (Actemra). *Human Vaccines & Immunotherapeutics*. [Online] 13 (9), 1972–1988. Available from: https://doi.org/10.1080/21645515.2017.1316909.

Shields, R.L., Lai, J., Keck, R., O'Connell, L.Y., et al. (2002) Lack of fucose on human IgG1 *N*-linked oligosaccharide improves binding to human Fc gamma RIII and antibody-dependent cellular toxicity. *The Journal of Biological Chemistry*. [Online] 277 (30), 26733–26740. Available from: https://doi.org/10.1074/jbc.M202069200.

Shinkawa, T., Nakamura, K., Yamane, N., Shoji-Hosaka, E., et al. (2003) The absence of fucose but not the presence of galactose or bisecting *N*-acetylglucosamine of human IgG1 complex-type oligosaccharides shows the critical role of enhancing antibody-dependent cellular cytotoxicity. *The Journal of Biological Chemistry*. [Online] 278 (5), 3466–3473. Available from: https://doi.org/10.1074/jbc.M210665200.

Sinha, J., Plantz, B.A., Inan, M. & Meagher, M.M. (2005) Causes of proteolytic degradation of secreted recombinant proteins produced in methylotrophic yeast *Pichia pastoris*: case study with recombinant ovine interferon-tau. *Biotechnology and Bioengineering*. [Online] 89 (1), 102–112. Available from: https://doi.org/10.1002/bit.20318.

Sjögren, J., Lood, R. & Nägeli, A. (2020) On enzymatic remodeling of IgG glycosylation; unique tools with broad applications. *Glycobiology*. [Online] 30 (4), 254–267. Available from: https://doi.org/10.1093/glycob/cwz085.

Strohl, W.R. & Strohl, L.M. (2012) - Therapeutic antibody classes. In: *Woodhead Publishing Series in Biomedicine*. [Online] Woodhead Publishing. pp. 197–595. Available from: https://doi.org/10.1533/9781908818096.197.

Subedi, G.P. & Barb, A.W. (2018) CD16a with oligomannose-type *N*-glycans is the only "low-affinity" Fcγ receptor that binds the IgG crystallizable fragment with high affinity *in vitro*. *Journal of Biological Chemistry*. [Online] 293 (43), 16842–16850. Available from: https://doi.org/10.1074/jbc.RA118.004998.

Thomson, C.A. (2016) *IgG Structure and Function*. In: Michael J H B T - Encyclopedia of Immunobiology Ratcliffe (ed.). [Online] Oxford, Academic Press. pp. 15–22. Available from: https://doi.org/10.1016/B978-0-12-374279-7.05002-5.

Velez-Suberbie, M.L., Morris, S.A., Kaur, K., Hickey, J.M., et al. (2020) Holistic process development to mitigate proteolysis of a subunit rotavirus vaccine candidate produced in *Pichia pastoris* by means of an acid pH pulse during fed-batch fermentation. *Biotechnology Progress*. [Online] 36 (3), e2966. Available from: https://doi.org/10.1002/btpr.2966.

Villacrés, C., Tayi, V.S. & Butler, M. (2021) Strategic feeding of NS0 and CHO cell cultures to control glycan profiles and immunogenic epitopes of monoclonal antibodies. *Journal of Biotechnology*. [Online] 333, 49–62. Available from: https://doi.org/10.1016/j.jbiotec.2021.04.005.

Villiger, T.K., Roulet, A., Périlleux, A., Stettler, M., et al. (2016) Controlling the time evolution of mAb *N*-linked glycosylation, part I: microbioreactor experiments. *Biotechnology Progress*. [Online] 32 (5), 1123–1134. Available from: https://doi.org/10.1002/btpr.2305.

Wang, W. & Chen, Q. (2022) Antigen improves binding of IgGs to FcγRs in SPR analysis. *Analytical Biochemistry*. [Online] 640, 114411. Available from: https://doi.org/10.1016/j.ab.2021.114411.

Wildt, S. & Gerngross, T.U. (2005) The humanization of *N*-glycosylation pathways in yeast. *Nature Reviews Microbiology*. [Online] 3 (2), 119–128. Available from: https://doi.org/10.1038/nrmicro1087.

Xie, C.B., Jane-Wit, D. & Pober, J.S. (2020) Complement membrane attack complex: new roles, mechanisms of action, and therapeutic targets. *The American Journal of Pathology*. [Online] 190 (6), 1138–1150. Available from: https://doi.org/10.1016/j.ajpath.2020.02.006.

Yagi, H., Takakura, D., Roumenina, L.T., Fridman, W.H., et al. (2018) Site-specific *N*-glycosylation analysis of soluble Fcγ receptor IIIb in human serum. *Scientific Reports*. [Online] 8 (1), 2719. Available from: https://doi.org/10.1038/s41598-018-21145-y.

Yang, Q. & Wang, L.-X. (2017) Chemoenzymatic glycan remodeling of natural and recombinant glycoproteins. *Methods in Enzymology*. [Online] 597, 265–281. Available from: https://doi.org/10.1016/bs.mie.2017.06.006.

Yin, B., Wang, Q., Chung, C.-Y., Bhattacharya, R., et al. (2017) A novel sugar analog enhances sialic acid production and biotherapeutic sialylation in CHO cells.

Biotechnology and Bioengineering. [Online] 114 (8), 1899–1902. Available from: https://doi.org/10.1002/bit.26291.

Yu, M., Brown, D., Reed, C., Chung, S., et al. (2012) Production, characterization, and pharmacokinetic properties of antibodies with *N*-linked mannose-5 glycans. *MAbs*. [Online] 4 (4), 475–487. Available from: https://doi.org/10.4161/mabs.20737.

Yu, X., Marshall, M.J.E., Cragg, M.S. & Crispin, M. (2017) Improving antibody-based cancer therapeutics through glycan engineering. *BioDrugs*. [Online] 31 (3), 151–166. Available from: https://doi.org/10.1007/s40259-017-0223-8.

Zahavi, D., AlDeghaither, D., O'Connell, A. & Weiner, L.M. (2018) Enhancing antibody-dependent cell-mediated cytotoxicity: a strategy for improving antibody-based immunotherapy. *Antibody Therapeutics*. [Online] 1 (1), 7–12. Available from: https://doi.org/10.1093/abt/tby002.

Zaroff, S. & Tan, G. (2019) Hybridoma technology: the preferred method for monoclonal antibody generation for *in vivo* applications. *BioTechniques*. [Online] 67 (3), 90–92. Available from: https://doi.org/10.2144/btn-2019-0054.

Zhang, Q., Joubert, M.K., Polozova, A., De Guzman, R., et al. (2020) Glycan engineering reveals interrelated effects of terminal galactose and core fucose on antibody-dependent cell-mediated cytotoxicity. *Biotechnology Progress*. [Online] 36 (6), e3045. Available from: https://doi.org/10.1002/btpr.3045.

Zhang, Y., Liu, R. & Wu, X. (2007) The proteolytic systems and heterologous proteins degradation in the methylotrophic yeast *Pichia pastoris*. *Annals of Microbiology*. [Online] 57 (4), 553. Available from: https://doi.org/10.1007/BF03175354.

Zhou, Q., Shankara, S., Roy, A., Qiu, H., et al. (2008) Development of a simple and rapid method for producing non-fucosylated oligomannose containing antibodies with increased effector function. *Biotechnology and Bioengineering*. [Online] 99 (3), 652–665. Available from: https://doi.org/10.1002/bit.21598.

Zhou, S. & Wang, L. (2019) Unraveling the structural and chemical features of biological short hydrogen bonds. *Chemical Science*. [Online] 10 (33), 7734–7745. Available from: https://doi.org/10.1039/C9SC01496A.

Zimmermann, M., Ehret, J., Kolmar, H. & Zimmer, A. (2019) Impact of acetylated and non-acetylated fucose analogues on IgG glycosylation. *Antibodies*. [Online] 8 (1). Available from: https://doi.org/10.3390/antib8010009.

Chapter 9 – Appendix

9.1 Plasmid Maps
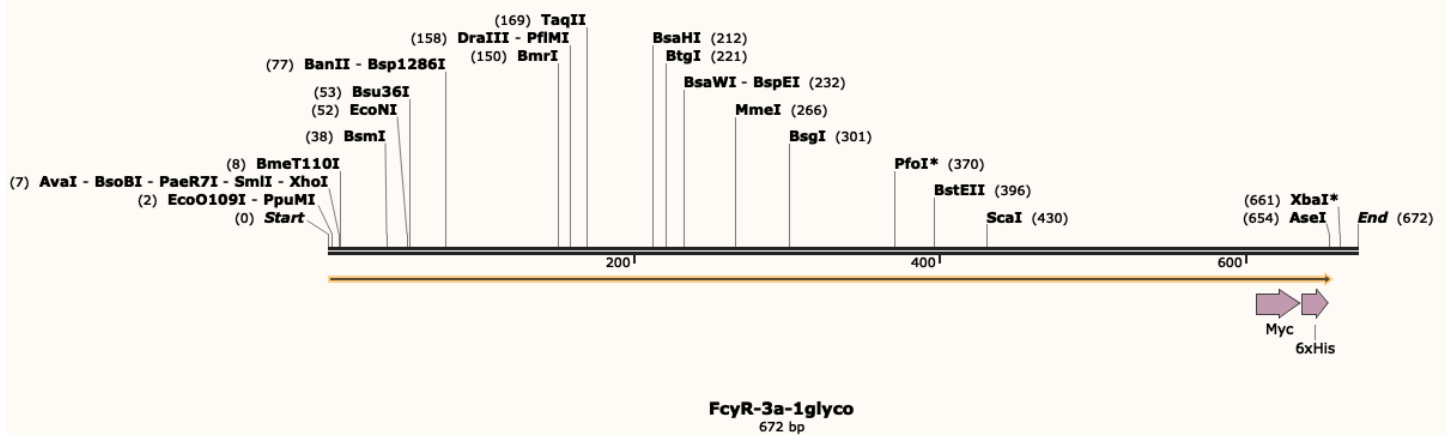
Figure 9.1 – linearised map of the gene for all FcγR ligand constructs with restriction enzyme sites labelled. Created using SnapGene® software.
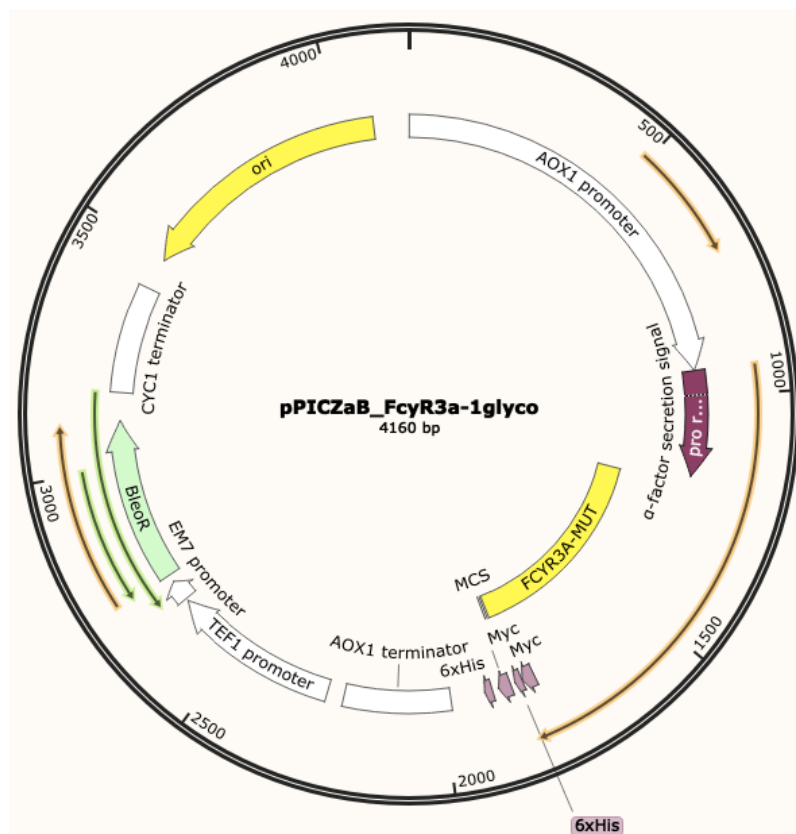

Figure 9.2 – map of the pPICZαB plasmid containing the gene for the FcγR ligands to create the final vector. The plasmid was linearised using PmeI. Restriction sites used: XhoI and XbaI. This construct was ordered as a gene block from Integrated DNA Technologies (IDT). Image created using SnapGene® software.

9.2 Glycoproteomic Analysis of FcγR Mut
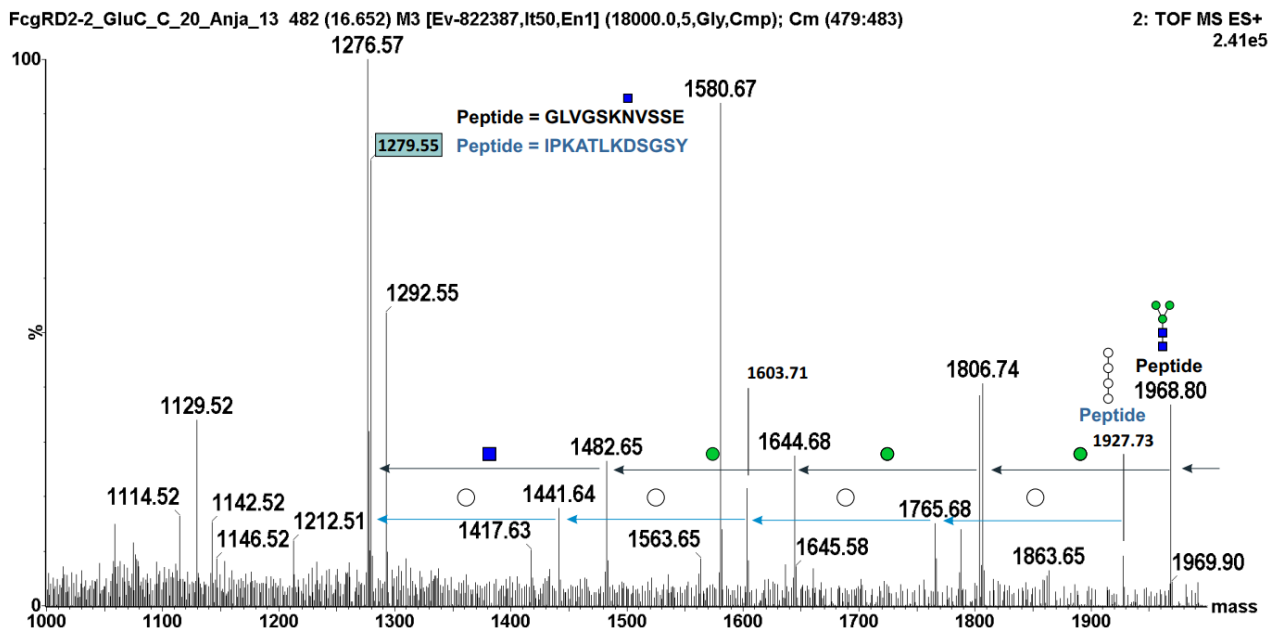
Figure 9.3 – deconvoluted ESI-LC-MS/MS spectrum showing that the region of FcγR Mut that contained the single *N*-glycan also contained *O*-glycosylation.

9.3 Individual SPR Channel Responses
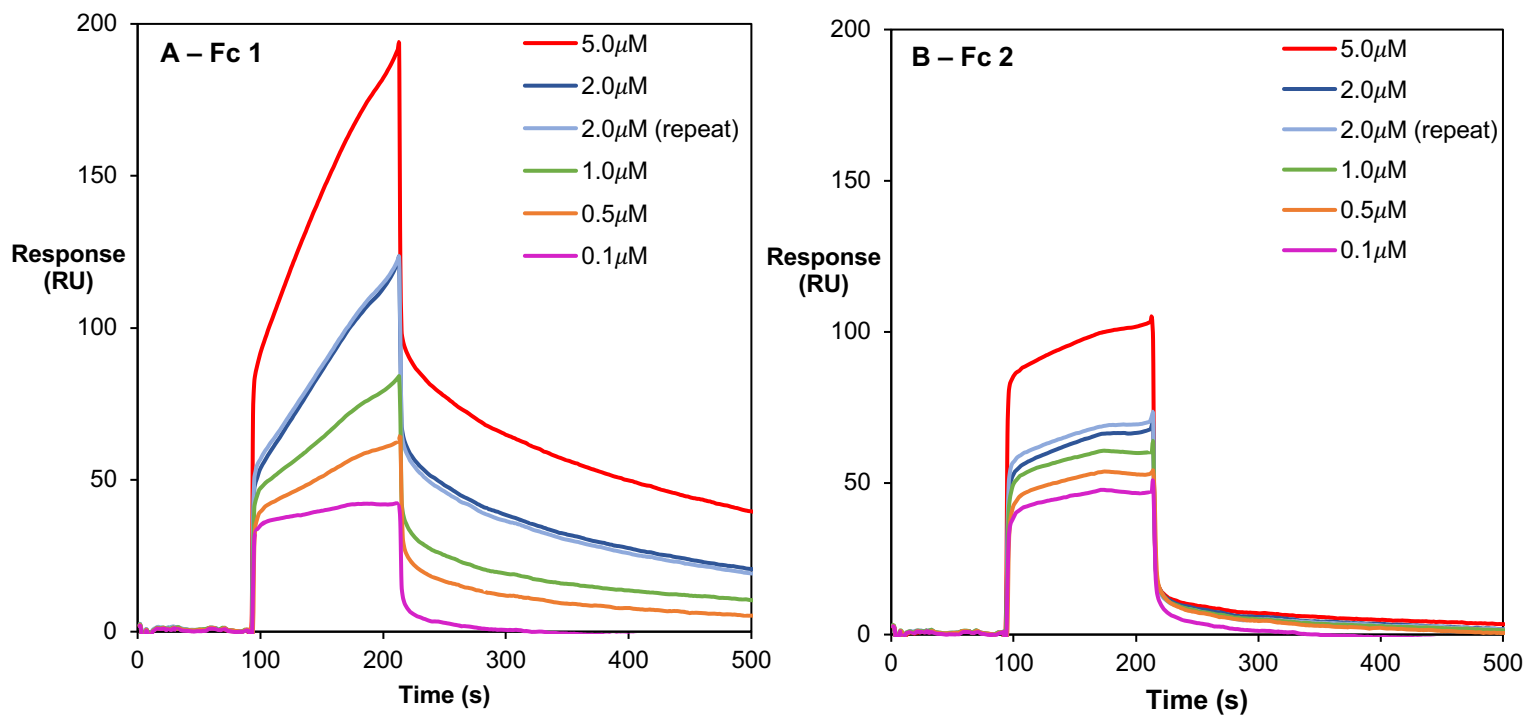
Figure 9.4 – individual channel responses of Fc 1 and Fc 2 of the refFcγRIIIa-deglycosylated tocilizumab interaction.
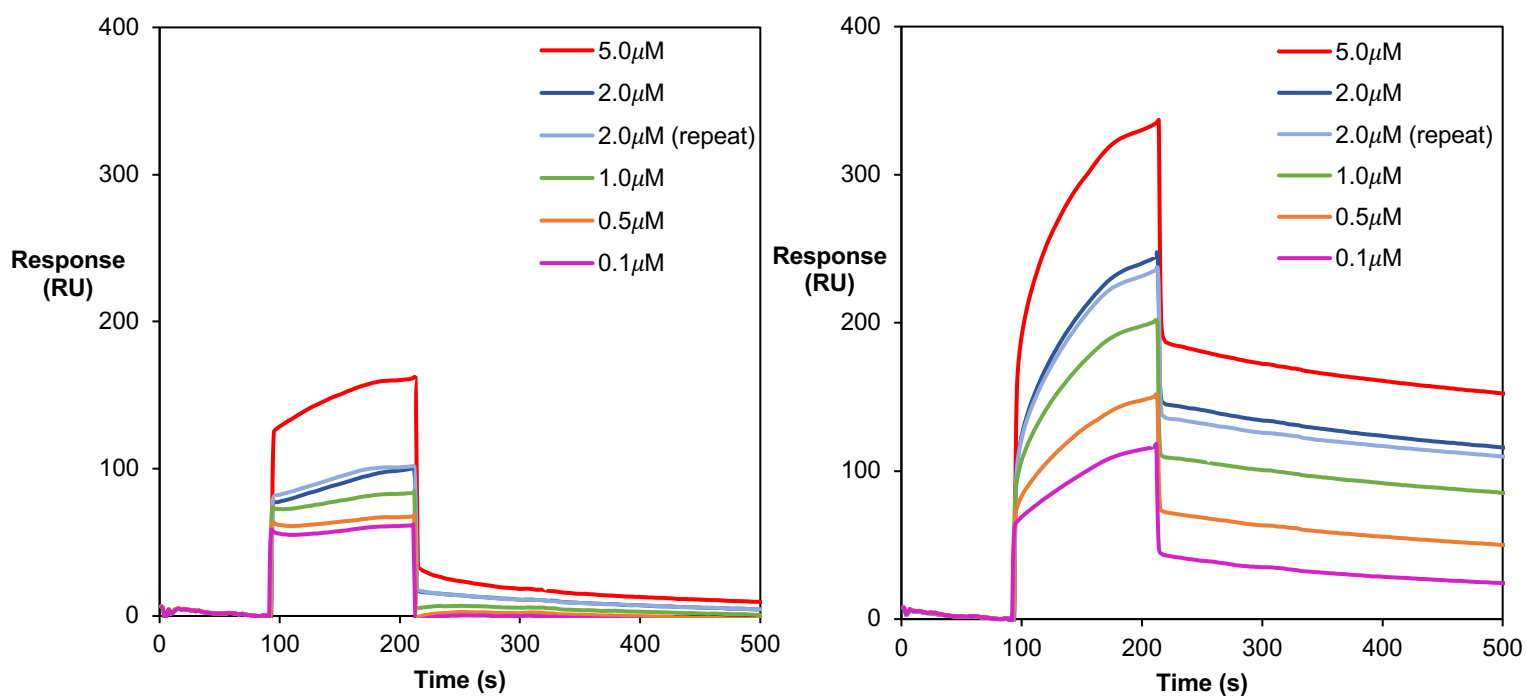
Figure 9.5 – individual channel responses of Fc 1 and Fc 2 of the refFcγRIIIa-tocilizumab interaction.

9.4 Peak Ratio Calculations for FcγRIIIa Separation of Tocilizumab

These calculations refer to the peaks in Figure 6.20. The trapezium method was used with multiple trapezia, which were between 0.001-0.002 units in width. The area of each trapezium was calculated using the following equation:

$$T_A = \frac{a+b}{2} \times h \ (4)$$

where T_A = trapezium area

a = y-value at first x-value

b = y-value at second x-value

h = difference in x-values (trapezium width)

Each of these trapezia areas were summed to give the total area of each peak.

Table 9.1 – peak 1 area, peak 2 area and total area under chromatogram. Percentages were calculated from these values. All calculations were completed using Microsoft® Excel.

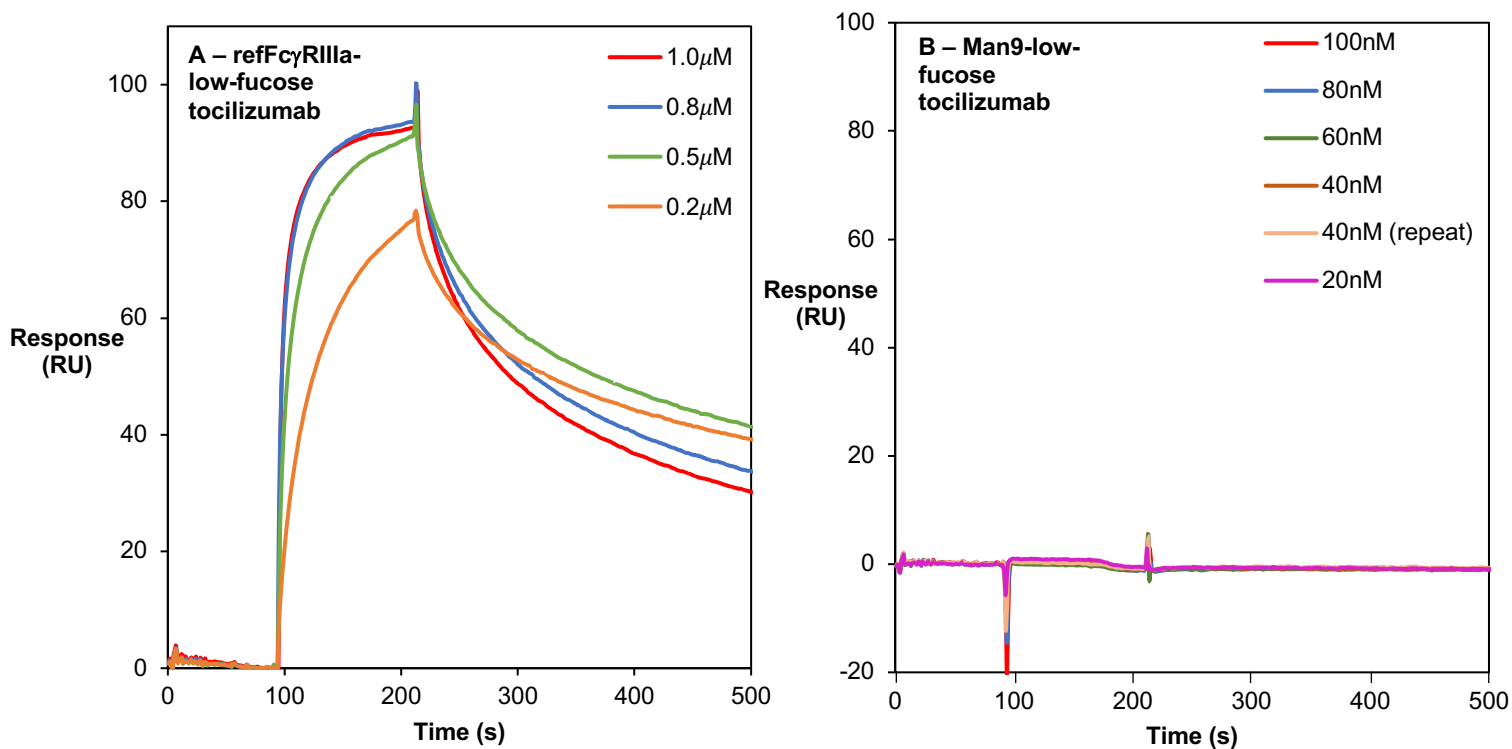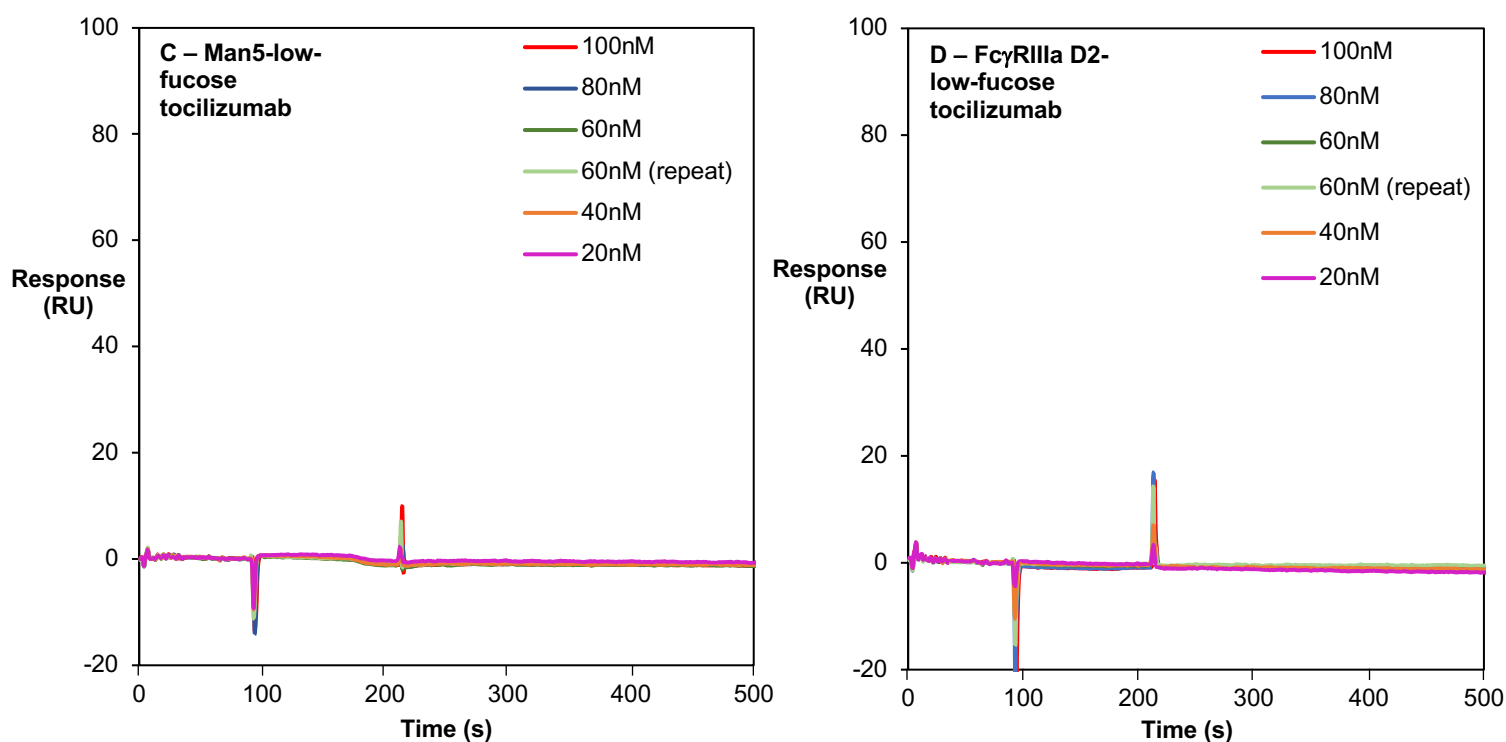| Peak 1 area	Peak 2 area	Total area under chromatogram
1583.78	46.05	1629.83

9.5 Relative Quantification of Afucosylated Tocilizumab
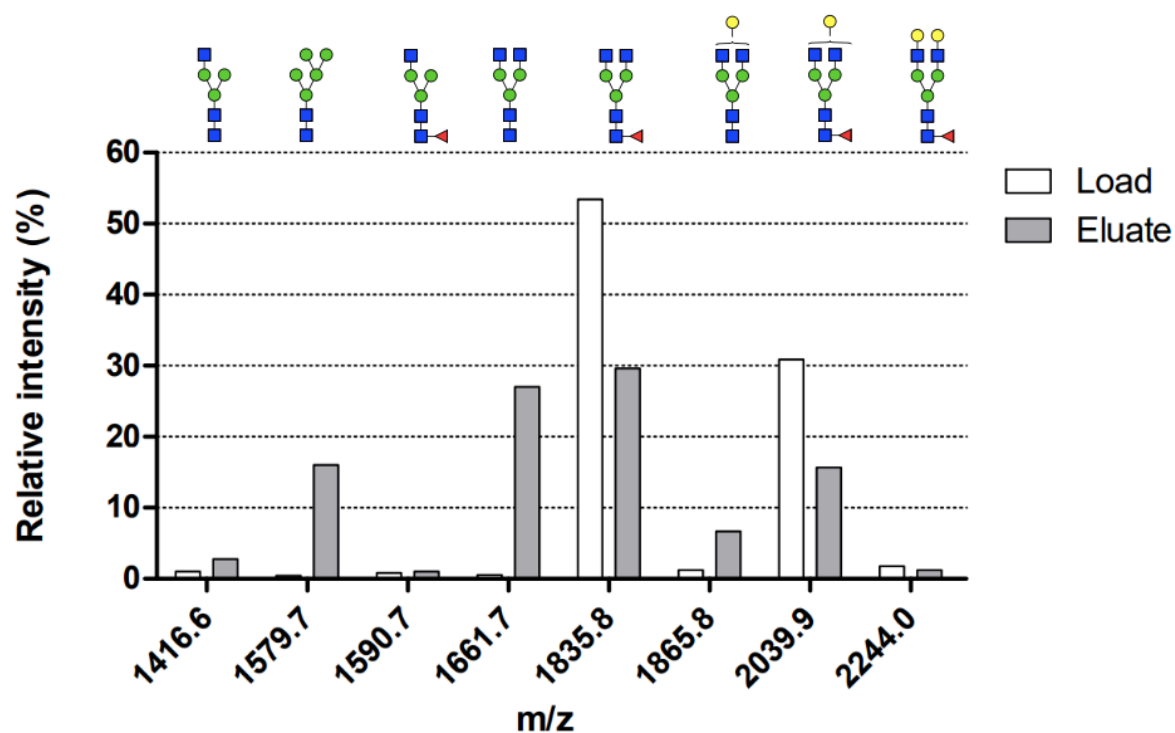
Figure 9.6 – relative quantification of each glycan species found in the load and eluate of tocilizumab from the FcγRIIIa-column separation.
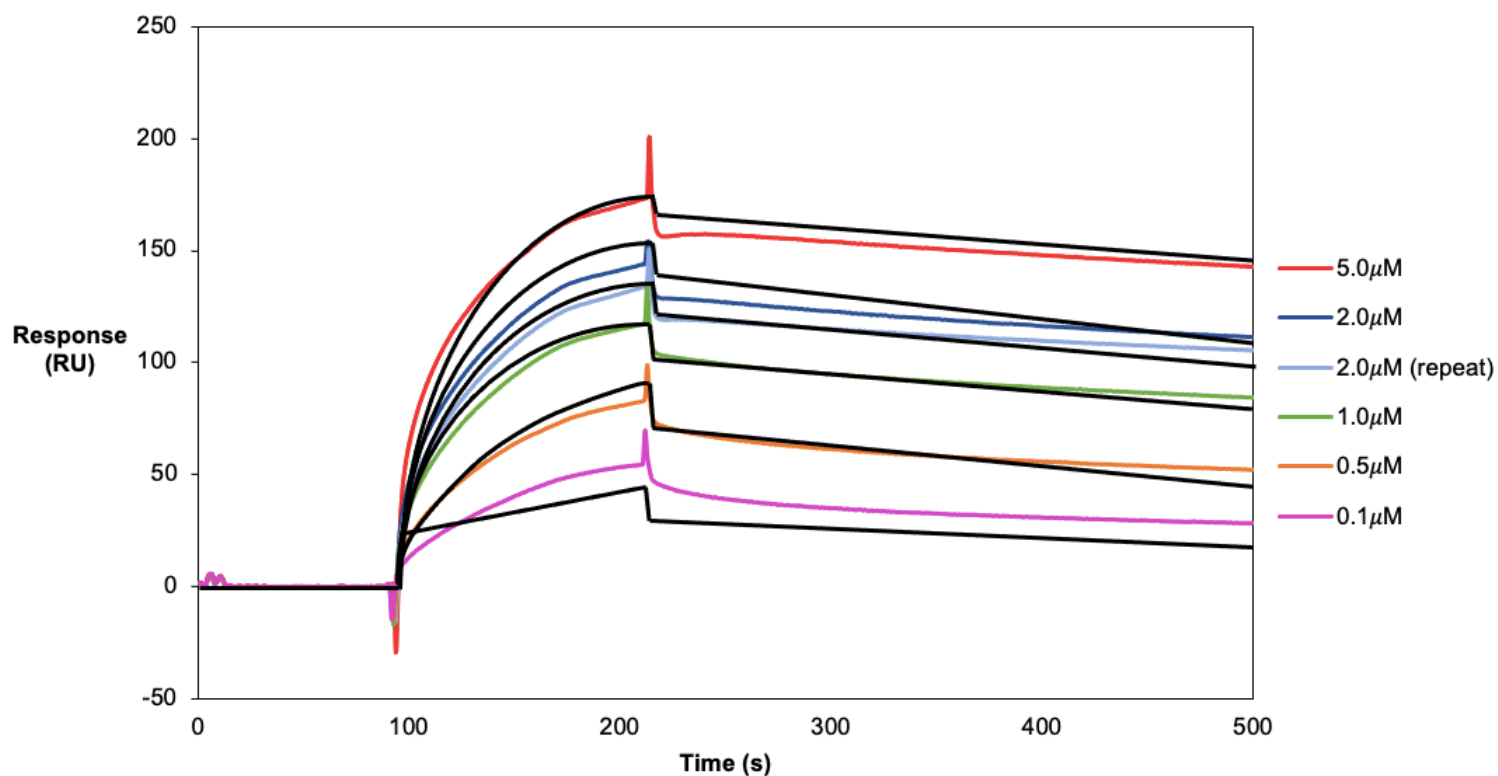
## 9.6 Low-Fucose Tocilizumab SPR Kinetics/Affinity Assay Repeats

Figure 9.7 – repeat SPR kinetic/affinity assays of **A)** refFcγRIIIa, **B)** Man9, **C)** Man5 and **D)** FcγRIIIa D2 against low-fucose tocilizumab, using the same chip (~1600RU) and protocol as for the assays described in Section 6.4.3.
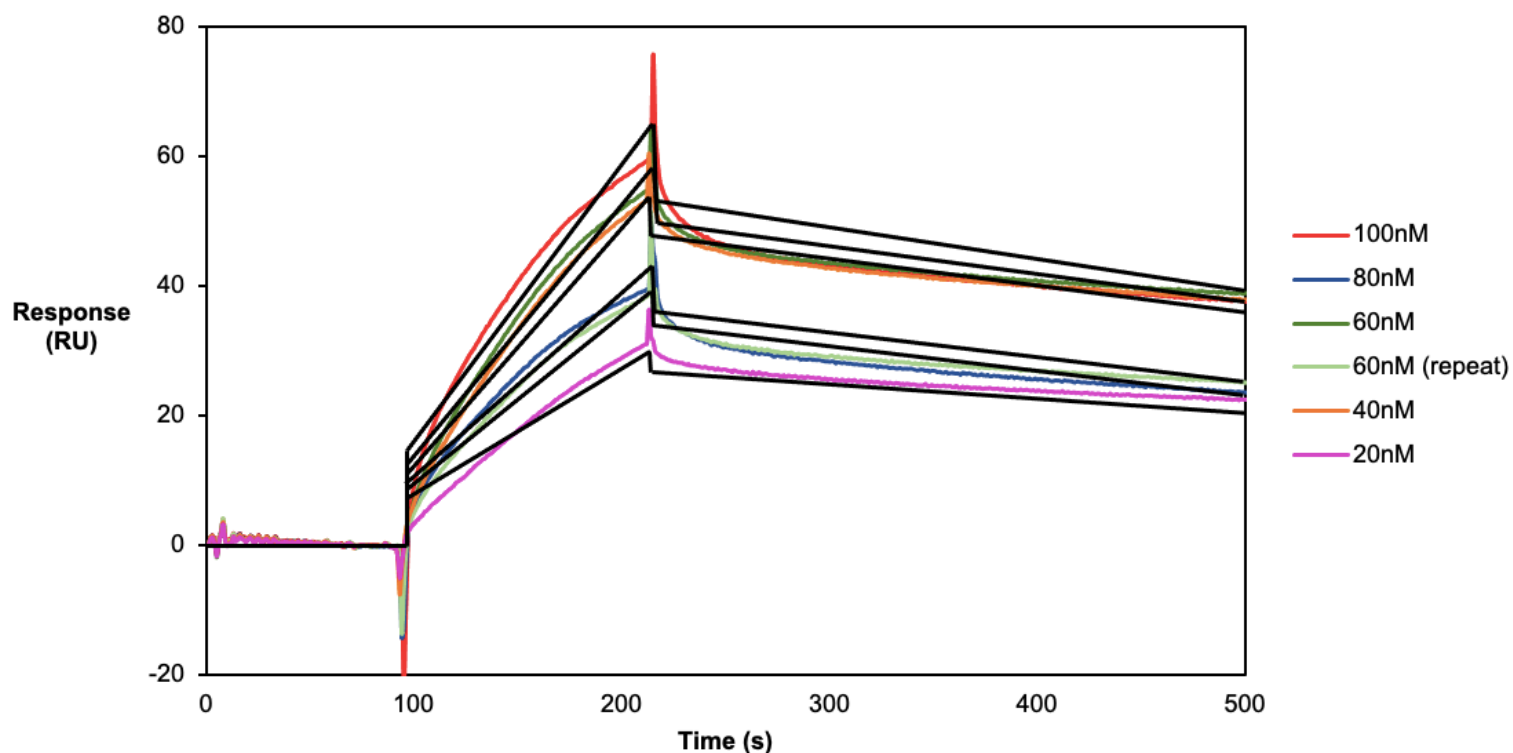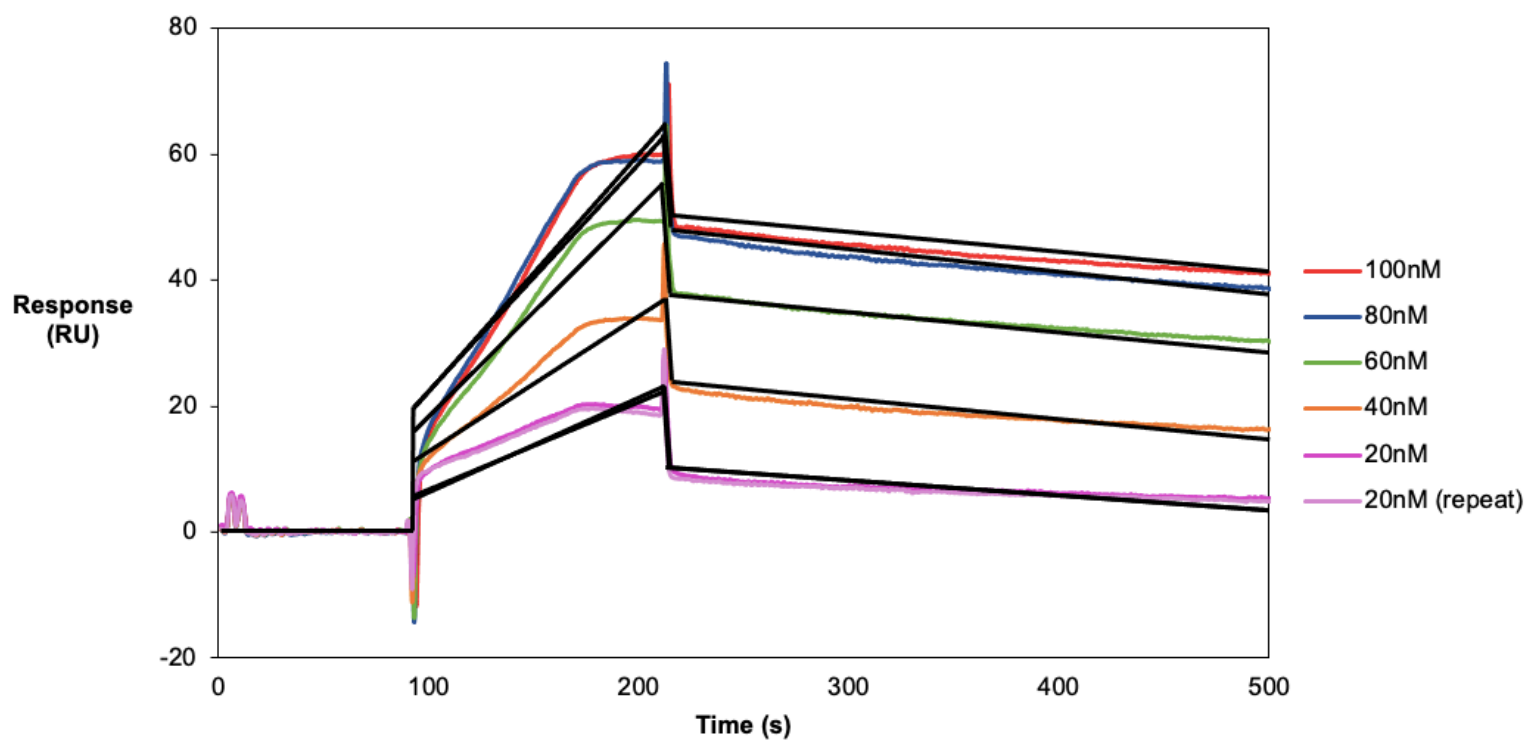
9.7 Model Fitting of SPR Data

Figure 9.8 – fitted curves generated by the Biacore Evaluation Software for the tocilizumab-refFcγRIIIa interaction, overlayed onto the sensorgram for this interaction (Figure 6.11).
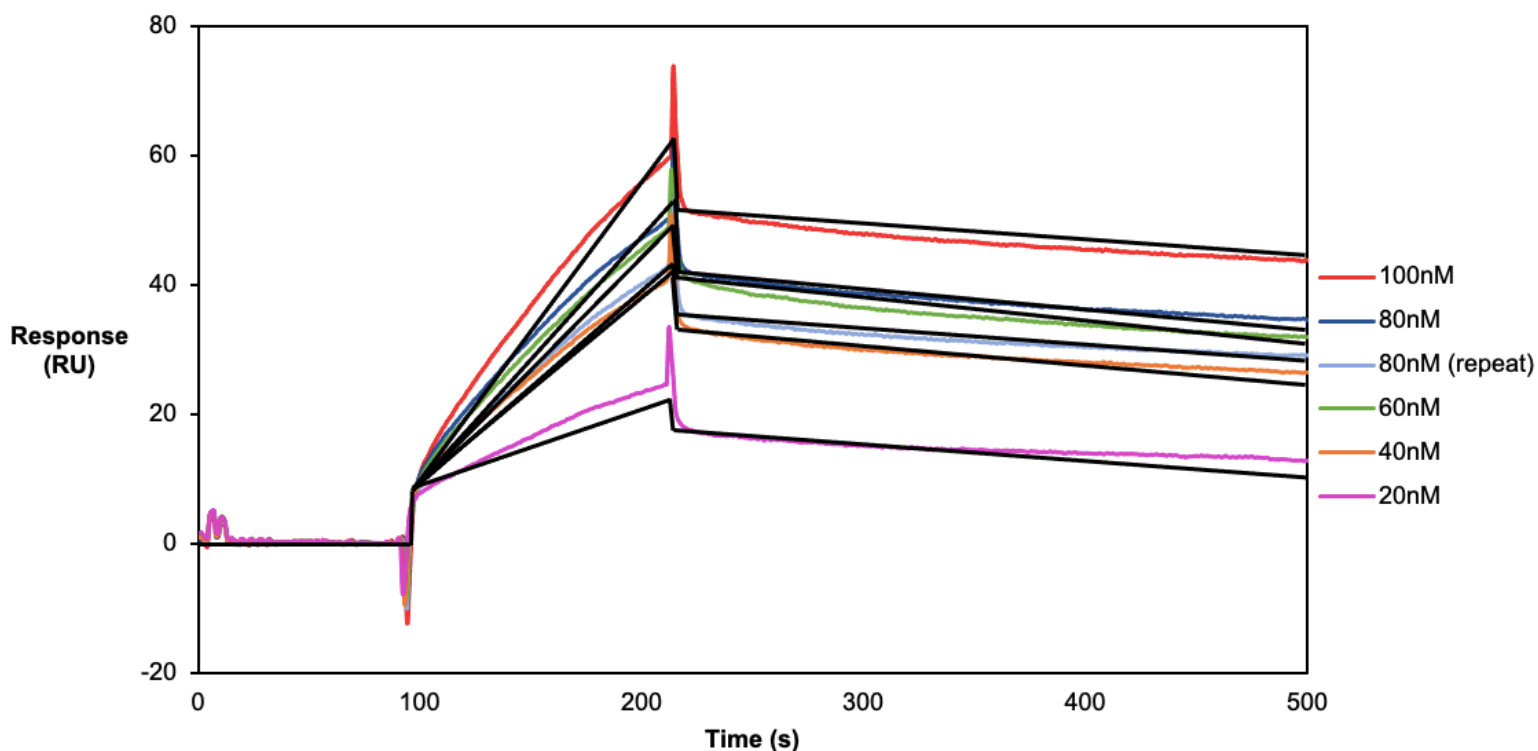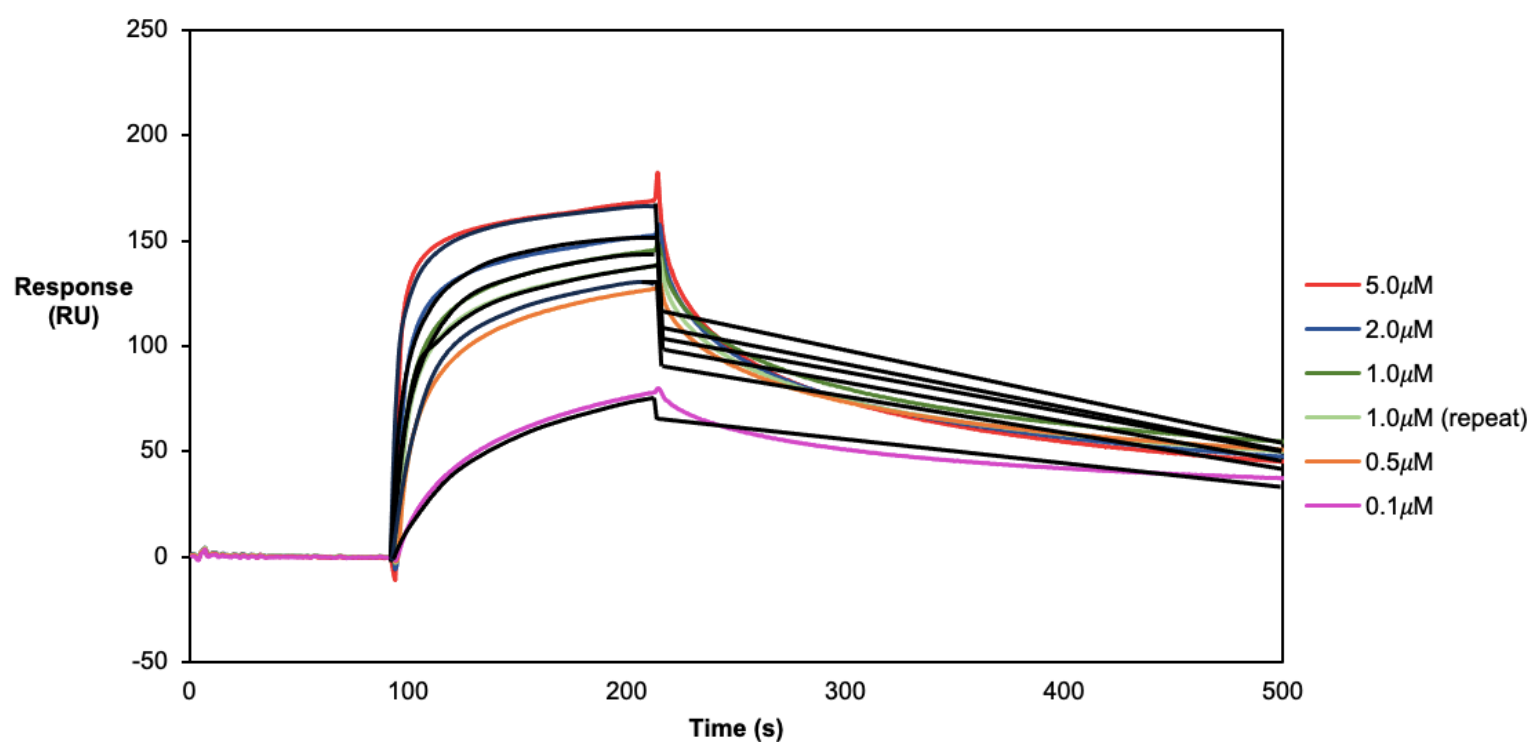

Figure 9.9 – fitted curves generated by the Biacore Evaluation Software for the tocilizumab-Man9 interaction, overlayed onto the sensorgram for this interaction (Figure 6.13).

Figure 9.10 – fitted curves generated by the Biacore Evaluation Software for the tocilizumab-Man5 interaction, overlayed onto the sensorgram for this interaction (Figure 6.15).

Figure 9.11 – fitted curves generated by the Biacore Evaluation Software for the tocilizumab-FcγRIIIa D2 interaction, overlayed onto the sensorgram for this interaction (Figure 6.17).

Figure 9.12 – fitted curves generated by the Biacore Evaluation Software for the afucosylated tocilizumab-refFcγRIIIa D2 interaction, overlayed onto the sensorgram for this interaction (Figure 6.24B).